1985

Part I: The Quadratic Pade Method For Calculating Local Densities Of States Part Ii: Classical Stochasticity And Ionisation In A Square Potential Well Driven By An Oscillating Laser Field

Ilan Lippa Mayer

CANADIAN THESES ON MICROFICHE

THÈSES CANADIENNES SUR MICROFICHE

National Library of Canada
Collections Development Branch

Canadian Theses on
Microfiche Service

Ottawa, Canada
K1A 0N4

Bibliothèque nationale du Canada
Direction du développement des collections

Service des thèses canadiennes
sur microfiche

NOTICE

The quality of this microfiche is heavily dependent upon the quality of the original thesis submitted for microfilming. Every effort has been made to ensure the highest quality of reproduction possible.

If pages are missing, contact the university which granted the degree.

Some pages may have indistinct print especially if the original pages were typed with a poor typewriter ribbon or if the university sent us an inferior photocopy.

Previously copyrighted materials (journal articles, published tests, etc.) are not filmed.

Reproduction in full or in part of this film is governed by the Canadian Copyright Act, R.S.C. 1970, c. C-30. Please read the authorization forms which accompany this thesis.

AVIS

La qualité de cette microfiche dépend grandement de la qualité de la thèse soumise au microfilmage. Nous avons tout fait pour assurer une qualité supérieure de reproduction.

S'il manque des pages, veuillez communiquer avec l'université qui a conféré le grade.

La qualité d'impression de certaines pages peut laisser à désirer, surtout si les pages originales ont été dactylographiées à l'aide d'un ruban usé ou si l'université nous a fait parvenir une photocopie de qualité inférieure.

Les documents qui font déjà l'objet d'un droit d'auteur (articles de revue, examens publiés, etc.) ne sont pas microfilmés.

La reproduction, même partielle, de ce microfilm est soumise à la Loi canadienne sur le droit d'auteur, SRC 1970, c. C-30. Veuillez prendre connaissance des formules d'autorisation qui accompagnent cette thèse.

THIS DISSERTATION
HAS BEEN MICROFILMED
EXACTLY AS RECEIVED

LA THÈSE A ÉTÉ
MICROFILMÉE TELLE QUE
NOUS L'AVONS REÇUE

Canada

NL 339 (r. 86/09)

PART I

THE QUADRATIC PADÉ METHOD FOR CALCULATING LOCAL DENSITIES OF STATES

PART II

CLASSICAL STOCHASTICITY AND IONISATION IN A SQUARE POTENTIAL WELL DRIVEN BY AN OSCILLATING LASER FIELD

by

Ilan Lippa Mayer

Department of Physics

Submitted in partial fulfilment
of the requirements for the degree of
Doctor of Philosophy

Faculty of Graduate Studies
The University of Western Ontario
London, Ontario
August, 1985

Dedicated to my parents

Abstract

Part I

A new method of calculating local densities of states from the moments of the Hamiltonian by means of a three polynomial Hermite-Padé approximant is developed and studied. In this method a finite number of moments of the Hamiltonian at a given lattice site are first calculated. The quadratic Padé approximant, which is a special case of the Hermite-Padé approximant, is then used to obtain an approximation for the local Green function from the available moments. The local density of states is then obtained from the imaginary part of the local Green function.

The new method was tested on several cases, which included some regular lattices, a regular binary alloy, the semi-infinite simple cubic lattice, and a realistic model for the valence band of silicon. The results have been compared with those obtained by using other methods, and a way for improving the convergence of the quadratic Padé results has been devised.

The new method produces fairly accurate results in most parts of the energy band(s) if the number of singularity points in the band(s) is small. The accuracy obtained is comparable to or better than that of other methods of similar generality and complexity. The accuracy, however, decreases near some of the singularity points themselves.

Part II

A square potential well can be experimentally fabricated in a

semiconductor crystal by means of heteroepitaxial crystal growth techniques. This structure is used in quantum well lasers. By irradiating the crystal with a driving laser beam the quantum well laser can be made tunable. In such a situation one has electrons inside a square potential well driven by an oscillating laser field. The intenaity of the driving laser may not exceed a certain limit, otherwise the elcetrons will ionise, i.e. move out from the well and into the conduction band.

When the number of quantum energy levels is fairly large, the behaviour of the electrons in the laser driven potential well can be studied by means of classical dynamics. The presence of the oscillating laser field causes the motion of the electrons to become stochastic, i.e. random-like in character, and through this stochastic motion they can escape from the well into the conduction band.

The onset of stochasticity has been studied by looking at the solution to the classical equations of motion in action-angle space. The ionisation process has been studied by solving the equations of motion for an ensemble of particles in momentum-position space. The dependence of the ionisation rate on the frequency and intensity of the driving laser field has been studied for square wells of different dimensions.

The classical ionisation rate has been found to bear the characteristics of a multiphoton ionisation process, i.e. a power law dependence on the intensity of the driving laser. The power law coefficient has been found to be fairly close to the quantum mechanical estimate in the high frequency region. This unusual behaviour has been explained as the effect of the higher harmo-

nics of the oscillating square potential well, as seen by the electron in the high frequency region.

Finally, an experimental study of this physical system has been suggested, in which the classical predictions of this study can be tested.

Acknowledgements

I would like to express my gratitude to Professor B. Y. Tong for his constant guidance and instructive advice throughout the research work I have carried out for my thesis. I would also like to express my gratitude to Dr. L. C. M. Miranda for his guidance and assistance throughout the work I have carried out for the second part of my thesis.

I would like to thank Professor G. S. Rose, the Chairman of the Physics Department, for making available the facility of the department for me to carry out my research work.

I wish to thank Professor J. Nuttall for his continuing interest and involvement in my work and for his helpful advice. I also wish to thank Dr. S. D. Rosner and Dr. S. P. Goldman for their interest in my work as advisory committee members.

I thank Dr. K. Aashamar for the use of his multiple-precision arithmetic code GENPREC, which was of great help to me in the computational work for the first part of my thesis.

This work has been supported in part by a grant to professor B. Y. Tong from the National Research Council of Canada. Financial assistance in the form of Teaching Assistantships and Research Assistantships is gratefully acknowledged.

Table of contents

List of tables

pulse duration for 100 periods of the oscillating laser field is 3.5ps.

List of figures

Figure 7 - page 79

The density of states for the face centred cubic lattice, with the self-energy of the lattice sites set at 4V, as obtained from the order N=16 quadratic Padé approximant. The exact results are represented by dashed lines. V is the nearest neighbour interaction energy.

Figure 8 - page 81

The local density of states for the regular binary alloy on the simple cubic lattice, with site energies E_1=-V and E_2=V, for a site with self-energy E_1, as obtained from the order N=16 quadratic Padé approximant. The exact results are represented by dashed lines. V is the nearest neighbour interaction energy.

Figure 9 - page 82

The density of states for the regular binary alloy on the simple cubic lattice, with site energies E_1=-V and E_2=V, as obtained from the order N=16 quadratic Padé approximant. The exact results are represented by dashed lines. V is the nearest neighbour interaction energy.

Figure 10 - page 83

The local density of states for a site located at the surface of the semi-infinite simple cubic lattice, as obtained from the order N=16 quadratic Padé approximant. V is the nearest neighbour interaction energy.

Figure 11 - page 84

The local density of states for a site located one layer away from the surface of the semi-infinite simple cubic lattice, as obtained from the order N=16 quadratic Padé approximant. V is the nearest neighbour interaction energy.

Figure 12 - page 85

The local density of states for a site located two layers away from the surface of the semi-infinite simple cubic lattice, as obtained from the order N=16 quadratic Padé approximant. V is the nearest neighbour interaction energy.

Figure 13 - page 86

The local density of states for a site located three layers away from the surface of the semi-infinite simple cubic lattice, as

obtained from the order N=16 quadratic Padé approximant. V is the nearest neighbour interaction energy.

Figure 14 - page 89

The weighted delta-functions for the square lattice, as obtained from the order N=25 Padé approximant (equivalent to the continued fraction truncated at N=25). The position of each line on the energy axis indicates the position of a delta-function, and the length indicates the corresponding weight. V is the nearest neighbour interaction energy.

Figure 15 - page 90

The weighted delta-functions for the diamond lattice, as obtained from the order N=25 Padé approximant (equivalent to the continued fraction truncated at N=25). The position of each line on the energy axis indicates the position of a delta-function, and the length indicates the corresponding weight. V is the nearest neighbour interaction energy.

Figure 16 - page 91

The density of states for the square lattice in histogram representation, as obtained from the order N=25 Padé approximant (equivalent to the continued fraction truncated at N=25). V is the nearest neighbour interaction energy.

Figure 17 - page 92

The density of states for the diamond lattice in histogram representation, as obtained from the order N=25 Padé approximant (equivalent to the continued fraction truncated at N=25). V is the nearest neighbour interaction energy.

Figure 18 - page 96

The density of states for the square lattice, as obtained from the continued fraction truncated at N=25, when the quadratic termination scheme is used. V is the nearest neighbour interaction energy.

Figure 19 - page 97

The density of states for the simple cubic lattice, as obtained from the continued fraction truncated at N=25, when the quadratic termination scheme is used. V is the nearest neighbour interaction energy.

Figure 20 - page 98

The density of states for the body centred cubic lattice, as obtained from the continued fraction truncated at N=25, when the quadratic termination scheme is used. V is the nearest neighbour interaction energy.

Figure 21 - page 99

The density of states for the face centred cubic lattice, with the self-energies of the lattice sites set at 4V, as obtained from the continued fraction truncated at N=25, when the quadratic termination scheme is used. V is the nearest neighbour interaction energy.

Figure 22 - page 100

The density of states for the diamond lattice, as obtained from the continued fraction truncated at N=25, when the quadratic termination scheme is used. V is the nearest neighbour interaction energy.

Figure 23 - page 104

The local density of states for the regular binary alloy on the simple cubic lattice, with site energies E_1=-V and E_2=V, for a site with self-energy E_1, in histogram representation, as obtained from the order N=25 Padé approximant (equivalent to the continued fraction truncated at N=25). V is the nearest neighbour interaction energy.

Figure 24 - page 106

The local density of states for the regular binary alloy on the simple cubic lattice, with site energies E_1=-V and E_2=V, for a site with self-energy E_1, as obtained from the continued fraction truncated at N=25, when the quadratic termination scheme is used. V is the nearest neighbour interaction energy.

Figure 25 - page 108

The local density of states for a site located at the surface of the semi-infinite simple cubic lattice, as obtained from the continued fraction truncated at N=25, when the quadratic termination scheme is used. V is the nearest neighbour interaction energy.

Figure 26 - page 109

The local density of states for a site located one layer away from the surface of the semi-infinite simple cubic lattice, as obtained from the continued fraction truncated at N=25, when the quadratic termination scheme is used. V is the nearest neighbour interaction energy.

Figure 27 - page 110

The local density of states for a site located two layers away from the surface of the semi-infinite simple cubic lattice, as obtained from the continued fraction truncated at N=25, when the quadratic termination scheme is used. V is the nearest neighbour interaction energy.

Figure 28 - page 111

The local density of states for a site located three layers away from the surface of the semi-infinite simple cubic lattice, as obtained from the continued fraction truncated at N=25, when the quadratic termination scheme is used. V is the nearest neighbour interaction energy.

Figure 29 - page 123

A section of the diamond lattice, used as the basis for the bonds model for silicon. O denotes the bond of origin, used as reference. A denotes a nearest neighbour bond. B denotes a second nearest neighbour bond oriented at 60° to the bond of origin. C denotes a second nearest neighbour bond oriented at 180° to the bond of origin.

Figure 30 - page 126

The density of states for the valence band of silicon, as obtained from the order N=11 quadratic Padé approximant.

Figure 31 - page 127

The density of states for the valence band of silicon, as obtained from the order N=12 quadratic Pade approximant.

Figure 32 - page 132

The density of states for the valence band of silicon, as obtained from the enhanced version of the quadratic Padé method, using orders 9, 10, and 11 of the quadratic Padé approximant.

Figure 40 - page 145

The zeroes of the polynomials $p_j^{(n)}(E)$, j=1,2,3, and $R^{(n)}(E)$, for the order N=16 quadratic Padé approximant, in the case of the body centred cubic lattice. The nearest neighbour interaction energy is equal to 1.

Figure 41 - page 146

The zeroes of the polynomials $p_j^{(n)}(E)$, j=1,2,3, and $R^{(n)}(E)$, for the order N=16 quadratic Padé approximant, in the case of the face centred cubic lattice. The nearest neighbour interaction energy is equal to 1, and the self-energy of the lattice sites is equal to 4.

Figure 42 - page 147

The zeroes of the polynomials $p_j^{(n)}(E)$, j=1,2,3, and $R^{(n)}(E)$, for the order N=16 quadratic Padé approximant, in the case of the diamond lattice. The nearest neighbour interaction energy is equal to 1.

Figure 43 - page 149

The zeroes of the polynomials $p_j^{(n)}(E)$, j=1,2,3, and $R^{(n)}(E)$, for the order N=16 quadratic Padé approximant, in the case of the regular binary alloy on the simple cubic lattice. The nearest neighbour interaction energy is equal to 1. The site energies are E_1=-1 and E_2=1, and these results are for a site with self-energy E_1.

Figure 44 - page 150

The zeroes of the polynomials $p_j^{(n)}(E)$, j=1,2,3, and $R^{(n)}(E)$, for the order N=16 quadratic Padé approximant, in the case of the semi-infinite simple cubic lattice. The nearest neighbour interaction energy is equal to 1, and these results are for a site located at the surface.

Figure 45 - page 151

The zeroes of the polynomials $p_j^{(n)}(E)$, j=1,2,3, and $R^{(n)}(E)$, for the order N=16 quadratic Padé approximant, in the case of the semi-infinite simple cubic lattice. The nearest neighbour interaction energy is equal to 1, and these results are for a site located one layer away from the surface.

Figure 46 - page 152

The zeroes of the polynomials $p_j^{(n)}(E)$, j=1,2,3, and $R^{(n)}(E)$, for the order N=16 quadratic Pade approximant, in the case of the semi-infinite simple cubic lattice. The nearest neighbour interaction energy is equal to 1, and these results are for a site located two layers away from the surface.

Figure 47 - page 153

The zeroes of the polynomials $p_j^{(n)}(E)$, j=1,2,3, and $R^{(n)}(E)$, for the order N=16 quadratic Padé approximant, in the case of the semi-infinite simple cubic lattice. The nearest neighbour interaction energy is equal to 1, and these results are for a site located three layers away from the surface.

Figure 48 - page 154

The zeroes of the polynomials $p_j^{(n)}(E)$, j=1,2,3, and $R^{(n)}(E)$, for the order N=11 quadratic Pade approximant, in the case of the bonds model for the valence band of silicon. The energy is given in units of eV.

Figure 49 - page 155

The zeroes of the polynomials $p_j^{(n)}(E)$, j=1,2,3, and $R^{(n)}(E)$, for the order N=12 quadratic Pade approximant, in the case of the bonds model for the valence band of silicon. The energy is given in units of eV.

Figure 50 - page 186

Schematic diagram of a tunable laser with a square well potential in a semiconductor. The ground level in the square well is populated with electrons from the valence band (the arrow "A"). The driving laser (with intensity I and frequency ω) causes this ground level to shift. The recombination process (the arrow "B") occurs from there back to the valence band, and produces the tunable laser beam. It is tunable, because the amount of shifting (of the ground level) depends on the intensity of the driving laser, and thus the wavelength of the tunable laser beam depends on it as well.

Figure 51 - page 199

A section of action-angle space with several tori in the case of the square well potential with 4 energy levels (N=4), with the laser frequency parameter Ω=1.0 and the field strength parameter λ=0.0050 (these parameters are defined in section 9.c). With no laser field (no perturbation) present, all the tori would have

been horizontal straight lines. Because of the perturbation the tori are distorted. The one at the bottom has been destroyed, as motion in this region has already become stochastic. The torus above it and the third torus from the top are resonant, and therefore they are significantly distorted (forming "island chains"), whereas the remaining tori, which are not resonant, are only slightly distorted.

Figure 52 - page 225

The resonances n=1, n=3, and n=5 for the square well with N=4 levels, perturbed by a laser field with frequency parameter η=1.0 and field strength parameter λ=0.0052. The resonances appear as "island chains". The n^{th} resonance has n "islands" in it.

Figure 53 - page 226

The resonances n=1, n=3, and n=5 for the square well with N=4 levels, perturbed by a laser field with frequency parameter η=1.0 and field strength parameter λ=0.0054. The resonances n=1 and n=3 still appear as "island chains", but the resonance n=5 has already become stochastic.

Figure 54 - page 239

The compensated energy (in units of $\hbar^2/2Md^2$) as a function of time (in units of the period of the oscillating laser field) for a particle which does not ionise, in the case of the N=12 level well with η=19.0 and λ=4.5. The horizontal line at $144\pi^2$ denotes the ionisation threshold $E_C=V_0$.

Figure 55 - page 240

The compensated energy (in units of $\hbar^2/2Md^2$) as a function of time (in units of the period of the oscillating laser field) for a particle which does ionise, in the case of the N=12 level well with η=19.0 and λ=4.5. The horizontal line at $144\pi^2$ denotes the ionisation threshold $E_C=V_0$.

Figure 56 - page 241

The ionisation probability P (in percents) as a function of time (in units of the period of the oscillating laser field) for an ensemble of 100 particles in the N=12 level well with η=19.0 and λ=4.5.

Figure 57 - page 242

The ionisation probability P (in percents) as a function of time

(in units of the period of the oscillating laser field) for an ensemble of 100 particles in the N=12 level well with η=19.0 and λ=6.5.

Figure 58 - page 244

The ionisation rate W as a function of the laser field strength parameter λ for a N=12 level well. The straight lines indicate a $W \alpha \lambda^{2\nu}$ behaviour. For η=9.5 the value of ν is 2.2, and for η=30.0 it is 1.2.

Figure 59 - page 247

The power law exponent ν as a function of the frequency parameter η for the N=4 level well. The straight solid line corresponds to the quantum expression for ν as a function of η.

Figure 60 - page 248

The power law exponent ν as a function of the frequency parameter η for the N=8 level well. The straight solid line corresponds to the quantum expression for ν as a function of η.

Figure 61 - page 249

The power law exponent ν as a function of the frequency parameter η for the N=10 level well. The straight solid line corresponds to the quantum expression for ν as a function of η.

Figure 62 - page 250

The power law exponent ν as a function of the frequency parameter η for the N=12 level well. The straight solid line corresponds to the quantum expression for ν as a function of η.

Part I

The quadratic Pade method for calculating local densities of states

Chapter 1

General review of density of states calculations

1.a. General introduction

We consider ourselves in this work with a lattice - a collection of atoms, of one or several types, each located at a certain position (site) $\vec{r}$. This lattice can have either a regular or an irregular structure, depending on the types of atoms it contains and their locations.

Each atom has one or more electrons, each at a certain energy level. When the atoms come together to form the lattice, they interact with each other. As a result these energy levels split, and a spectrum of quasi-continuous energy bands is formed (a genuine continuum is obtained only when the lattice becomes infinite).

We are interested in this work in the density of states - the number of electron states per unit energy (a precise definition will be given in the next section). If the lattice is regular, then the density of states is the same for all the sites $\vec{r}$. Otherwise the density of states is different at each site, and therefore the local density of states for the various sites has to be considered instead.

The local density of states can be readily obtained from the local Green function of the lattice (see section 1.b for further explanation). The latter can be obtained in the form of a power series (in $1/E$, where E is the energy) from the Hamiltonian of the lattice. The coefficients in this power series are known as the moments of the Hamiltonian (section 1.d). In practice only a

finite number of terms in this power series expansion can be calculated.

In this part of the thesis we discuss a method that we have developed, namely the quadratic Padé method, for obtaining an approximation for the local density of states from the finite number of available moments, i.e. available terms in the above mentioned power series expansion.

In the following sections of this chapter we discuss the general physical background in further detail. This includes a discussion of the density of states and its relation to the lattice Green function, a survey of methods used for calculating the (local) density of states, and a discussion of the moments of the Hamiltonian and their application to density of states calculations.

In chapter 2 we discuss the quadratic Padé approximant, upon which our method is based, and present an efficient method for its calculation by means of a recurrence relation.

In chapter 3 we discuss the application of the quadratic Padé approximant to the calculation of density of states, i.e. the essence of our method. We survey the methods used for calculating the moments of the Hamiltonian, and explain how an approximation for the local density of states can be obtained from a finite number of these moments by means of the quadratic Padé approximant.

In chapter 4 we discuss other methods for calculating the local density of states, which are based, either explicitly or implicitly, on the use of the moments of the Hamiltonian. First

we discuss the continued fraction method. Then we show its relation to the ordinary Padé approximant, which, like the quadratic Padé approximant, can be calculated directly from the moments. Finally we discuss the method of modified moments.

In chapter 5 we present and discuss results obtained by using the quadratic Padé method. First we show how we have obtained the moments of the Hamiltonian for various regular and nearly regular lattices. Then we present the results for the local density of states for these lattices, as obtained by using the quadratic Pade method. We compare these results with the results for the same lattices, as obtained by using the continued fraction method. We also compare them with the exact results, wherever possible. Then we discuss a more realistic case, namely the valence band of silicon. We show how the moments are calculated, present our results, present an improved version of the quadratic Padé method, and finally present our improved results, which we then compare with the results obtained by other methods.

In chapter 6 we present a discussion of the accuracy of the results obtained with the quadratic Padé method. We see its relation to the singularities of the density of states function, and to the distribution of the zeroes of the quadratic Padé polynomials. Finally, based on this discussion, we note the applicability and limitations of our new method.

1.b. Density of states - the basic concepts

The local density of states $\rho(\vec{r},E)$ is defined as follows. $\rho(\vec{r},E)dE$ is the number of electron states located at $\vec{r}$ in the energy interval between E and E+dE, where dE is infinitesimally small. It is usually normalised so as to have

$$\int_{-\infty}^{\infty}\rho(\vec{r},E)dE=1. \qquad (1.b.1)$$

The density of states $\rho(E)$ is obtained by averaging the local density of states $\rho(\vec{r},E)$ over all the sites $\vec{r}$. In a regular lattice, where all the lattice sites are equivalent, the local density of states $\rho(\vec{r},E)$ and the density of states $\rho(E)$ are identical.

The density of states is closely related to the band structure, i.e. the behaviour of the energy E as a function of the wave vector $\vec{k}$. If Ω denotes the volume of the crystal, then the density of states is given by (Callaway 1964)

$$\rho(E)=[\Omega/(2\pi)^3](d/dE)(\int d^3\vec{k}), \qquad (1.b.2)$$

where the integration is carried out over the volume of $\vec{k}$-space bounded by the surface of constant energy E.

Expression (1.b.2) can be rewritten in the form

$$\rho(E)=[\Omega/(2\pi)^3]\int|\vec{\nabla}_{\vec{k}}(E)|^{-1}ds, \qquad (1.b.3)$$

where ds is an element of area, and the integration is carried out over the surface of constant energy E.

From expression (1.b.3) we can see, that the density of states function $\rho(E)$ may have singularity points, if the integration

includes values of $\vec{k}$ where $|\vec{\nabla}_{\vec{k}}(E)|=0$. Such points are known as critical points, and they occur when $E(\vec{k})$ has a minimum, a maximum, or a saddle point. This subject has first been studied by Morse (1938), and later by Van Hove (1953), and such singularity points have become to be known as Van Hove singularities.

In inhomogeneous systems, where the local density of states $\rho(\vec{r},E)$ is of importance for itself, it can be obtained from the relation (Heine 1980)

$$\rho(\vec{r},E)=\sum_{E_{\vec{k}}} |\psi_{\vec{k}}(\vec{r})|^2\delta(E-E_{\vec{k}}), \qquad (1.b.4)$$

where $E_{\vec{k}}$ is the energy value for a given $\vec{k}$, and $\psi_{\vec{k}}$ is the corresponding wave function. The integration is carried out over the relevant parts of $\vec{k}$-space.

The local density of states is closely related to the local Green function (Economou 1979). The local Green function for a site $\vec{r}$ is given by

$$G(\vec{r},E)=\langle\vec{r}|(E-H)^{-1}|\vec{r}\rangle, \qquad (1.b.5)$$

where H is the Hamiltonian for the lattice in question. The branch cuts of $G(\vec{r},E)$ correspond to the continuous energy spectrum, whereas the poles of $G(\vec{r},E)$ correspond to the discrete spectrum.

The local density of states refers to the continuous spectrum, and is obtained from the local Green function by

$$\rho(\vec{r},E)=(2\pi i)^{-1}\lim_{\varepsilon\to 0^+}[G(\vec{r},E+i\varepsilon)-G(\vec{r},E-i\varepsilon)]. \qquad (1.b.6)$$

Conversely, the local Green function is obtained from the local density of states by

$$G(\vec{r},E)=\lim_{\varepsilon\to 0^+}\left(\int_{-\infty}^{\infty}[\rho(\vec{r},\lambda)/(E+i\varepsilon-\lambda)]d\lambda\right). \qquad (1.b.7)$$

The local Green function can also be expressed in the form

$$G(\vec{r},E)=\sum_{E_{\vec{k}}}|\psi_{\vec{k}}(\vec{r})|^2/(E-E_{\vec{k}}), \qquad (1.b.8)$$

where the summation is a formal one, and is carried out over the entire spectrum, discrete as well as continuous. This expression is easily obtained from expression (1.b.4) for the corresponding local density of states by means of expression (1.b.7).

The density of states function is of considerable interest, as it can be experimentally measured, either directly or indirectly, and then compared with the results of the theoretical calculations. This way, for example, the validity of a theoretical model may be checked.

1.c. Calculation of density of states - a survey of the methods used

A large number of methods for calculating the local density of states and the density of states is available, and we shall present here a brief survey of some of those.

We have seen in the previous section, that the density of states is closely related to the band structure. The subject of band structure calculations is well developed, and an assortment of methods for carrying out the calculation is available (Callaway 1964). From the results of a band structure calculation, the density of states can be obtained with considerable accuracy.

This method for density of states calculation has two main drawbacks. The first drawback is the large magnitude of the calculations and computations involved in this kind of work. The second drawback is, that this method is mainly suitable for regular lattices in the bulk, where one can make full use of the periodicity of the lattice. In the case of a regular lattice near the surface, or an irregular lattice, other methods may be needed to carry out the calculation. In such cases the density of states depends on the location, and thus the local density of states usually is the physical quantity of interest.

One way for obtaining the local density of states is the direct diagonalisation of the Hamiltonian (Choo et al 1974, Tong et al 1974, Tong and Choo 1976). A finite part (approximately of order 300 x 300) of the infinite Hamiltonian matrix, represented with the atomic wave functions at the various lattice sites as a basis, is selected by replacing the infinite lattice by a finite

cluster of atoms. The finite matrix is diagonalised, and then the density of states is found from the distribution of the eigenvalues. In this way a histogram-like approximation for the local density of states is obtained.

Another way for obtaining the local density of states is the continued fraction (or recursion) method (Haydock et al 1972, Haydock et al 1975, Haydock 1980), discussed in section 4.a. In this method, an expansion for the local Green function in the form of an infinite continued fraction is obtained. In practice the continued fraction has to be truncated at some point, and thus a discrete spectrum of weighted delta-functions is obtained.

Several schemes are available in order to obtain a better approximation for the local density of states from these initial results. The most common scheme is the quadratic termination (Haydock et al 1975, Haydock 1980; see also section 4.a). The coefficients in the continued fraction beyond the truncation point are replaced by their limits at infinity, and this results in the replacement of the truncated "tail" of the continued fraction by the square root of a quadratic expression. This form of the continued fraction method came to be widely used. As examples we shall mention calculations of the density of states in the bulk and at the surface of disordered alloys (Desjonquères and Cyrot-Lackmann 1977), calculations of the density of states for crystalline and amorphous silicon (Kelly and Bullett 1976), and caculations of the density of states for the bulk and surface of crystalline silicon (Ortenburger et al 1976).

Other schemes in use are a polynomial fitting (Gaspard and Cyrot-Lackmann 1973; see also section 4.a), and schemes based

upon a more sophisticated analysis of the continued fraction coefficients (Turchi et al 1982, Magnus 1983, Trias et al 1983).

The Green function, which is closely related to the density of states, can sometimes be directly calculated, especially in the simpler cases. This is done by means of numerical integration schemes, often involving elliptic integrals. For example, such calculations have been carried out for the square lattice (Katsura and Inawashiro 1971), for the simple cubic lattice (Katsura et al 1971), for the body centred cubic lattice (Katsura and Horiguchi 1971), and for the face centred cubic lattice (Morita and Horiguchi 1971a).

Various methods for calculating the local density of states from the moments of the Hamiltonian (see section 1.d or 3.a for a definition) have also been suggested (Fisher and camp 1972, Gaspard and Cyrot-Lackmann 1973, Lambin and Gaspard 1982). Some of these methods (Gaspard and Cyrot-Lackmann 1973, Lambin and Gaspard 1982) are closely related to the continued fraction method (see also sections 1.d and 4.b). The method of modified moments (Wheeler and Blumstein 1972, Blumstein and Wheeler 1973, Wheeler 1974, Wheeler et al 1974; see also sections 1.d and 4.c) is another method for calculating the local density of states, which makes use of the moments of the Hamiltonian.

The quadratic Padé method (Mayer et al 1984, Mayer and Tong 1985), discussed in this work, is another method for calculating the local density of states from the moments of the Hamiltonian.

We have seen thus an assortment of methods for calculating the local density of states. In this work we shall discuss in detail

the quadratic Padé method. We shall also use the continued fraction and the modified moments methods in this work, in order to compare their results with those of the quadratic Padé method.

1.d. The moments of the Hamiltonian in density of states calculations

The moments of the Hamiltonian for a lattice site $\vec{r}$ are the matrix elements of the powers of the Hamiltonian (in matrix representation) for that site, i.e. the n^{th} moment is given by

$$\mu_n(\vec{r}) = \langle \vec{r} | H^n | \vec{r} \rangle , \qquad (1.d.1)$$

where $|\vec{r}\rangle$ is the atomic wave function for the site $\vec{r}$.

The moments are related to the local density of states $\rho(\vec{r},E)$ by (Heine 1980)

$$\mu_n(\vec{r}) = \int_{-\infty}^{\infty} \rho(\vec{r},E) E^n dE \; ; \; n=0,1,2,\ldots . \qquad (1.d.2)$$

The moments of a regular lattice are closely related to the random walks on the lattice (Thorpe 1972). In the simple model, where only the nearest neighbour interaction is present in the lattice, the n^{th} moment is equal to the number of different walks on the lattice which return to the starting point in n steps, multiplied by the n^{th} power of the nearest neighbour interaction energy.

A general discussion of moments calculations can be found in section 3.a. Further discussion of the subject, with specific examples, can be found in sections 5.a and 5.e, and in appendix C.

The concept of the moments in this physical context is a special case of the general mathematical concept of moments of a function. The moments of a general function g(x) are defined by

$$\mu_n = \int_{-\infty}^{\infty} g(x) x^n dx \; ; \; n=0,1,2,\ldots . \qquad (1.d.3)$$

The general mathematical problem of obtaining an approximation for a function g(x) out of its moments has been a subject of studies for many years (Shohat and Tamarkin 1963, Akhiezer 1965). In our physical context it becomes the problem of obtaining an approximation for the local density of states from the moments of the Hamiltonian. This specific problem, too, has been the subject of some studies in the past, as we shall see below.

One way to reconstruct the density of states from the moments was based on a Padé approximant analysis (Fisher and Camp 1972). Another way was a calculation of the continued fraction expansion for the Green function (the same expansion, as obtained by the continued fraction method) from the moments (Gaspard and Cyrot-Lackmann 1973, Lambin and Gaspard 1982). The coefficients of the continued fraction expansion are obtained in terms of determinants of matrices, whose elements are the various moments.

These previous studies point out a close relation between the continued fraction method and the moments of the Hamiltonian. Another relation between the two, via the Padé approximant, is discussed in section 4.b of this work. Thus the widely used continued fraction method, even though not explicitly using the moments in the calculation procedure, is very closely related to them as well.

A different way of obtaining the density of states from the moments is by transforming them into modified moments with the aid of a recurrence relation, and then using a power series expansion based on those (Wheeler and Blumstein 1972, Blumstein and Wheeler 1973, Wheeler 1974, Wheeler et al 1974; see also section 4.c). This method has originally been used for phonon

density of states calculations, but it can also be used for electron density of states calculations, as we shall see in this work (in sections 4.c and 5.g).

The quadratic Padé method (Mayer et al 1984, Mayer and Tong 1985), discussed in detail in this work, falls again in this general category of methods of obtaining the local density of states from the moments of the Hamiltonian.

Chapter 2

The quadratic Padé approximant and its calculation

2.a. The generalised Hermite-Padé approximant

The generalised Hermite-Padé approximant of the first kind of degree m (Padé 1894, Burley et al 1981, Nuttall 1984) is defined as follows. Given m power series $F_j(x)$, $j=1,2,\ldots,m$, the approximant of order $n=(n_1,n_2,\ldots,n_m)$ consists of m polynomials $P_j(n,x)$ of degree n_j in x, $j=1,2,\ldots,m$, that satisfy the relation

$$\sum_{j=1}^{m} P_j(n,x)F_j(x)=O(x^N) \quad ; \quad N=\sum_{j=1}^{m} n_j+m-1. \qquad (2.a.1)$$

If we write the power series and the polynomials in explicit form as

$$F_j(x)=\sum_{k=0}^{\infty} f_{j,k}x^k \quad ; \quad P_j(n,x)=\sum_{k=0}^{n_j} p_{j,k}x^k \quad ; \quad j=1,2,\ldots,m, \qquad (2.a.2)$$

then equation (2.a.1) can be rewritten as

$$\sum_{j=1}^{m}\sum_{k=0}^{N_j} p_{j,k}f_{j,l-k}=0 \quad ; \quad l=0,1,2,\ldots,N-1 \quad ; \quad N_j=\min.(n_j,l). \qquad (2.a.3)$$

Only the first N-1 coefficients in each of the power series need to be known in order to find the coefficients of the polynomials, as only they are used in (2.a.3). The overall number of coefficients in the polynomials $P_j(n,x)$, $j=1,2,\ldots,m$, is equal to $\sum_{j=1}^{m}(n_j+1)=\sum_{j=1}^{m}n_j+m=N+1$. From expression (2.a.3) we see that we have N linear homogeneous equations for them. This means that normally the coefficients of the polynomials are uniquely determined this way up to a multiplicative constant.

Some special cases of the generalised Hermite-Padé approximant are of particular interest. If m=2, $F_1(x)=G(x)$, and $F_2(x)=-1$,

then the well known ordinary Padé approximant (Padé 1892, Padé 1894, Baker and Graves-Morris 1981a and b) is obtained. A short discussion of the ordinary Padé approximant can be found in section 4.b. If m=3, $F_1(x)=G^2(x)$, $F_2(x)=G(x)$, and $F_3(x)=1$, then the quadratic Padé approximant (Padé 1892, Gammel 1973, Shafer 1974, Mayer et al 1984, Mayer and Tong 1985) is obtained. If m=3, $F_1(x)=G'(x)$, $F_2(x)=G(x)$, and $F_3(x)=1$, then the differential Padé approximant (Gammel 1973) is obtained.

2.b. The quadratic Padé approximant

The quadratic Padé approximant has already been mentioned in the previous section as a special case of the generalised Hermite-Padé approximant of the first kind. Here we shall define it explicitly.

We assume that $F(x)=\Sigma_{k=0}^{\infty} f_k x^k$ is a power series, and that only the first N+1 coefficients, namely $f_0, f_1, \ldots, f_N$ are known. The quadratic Padé approximant of order (n_1,n_2,n_3) for this power series consists of three polynomials $P_j^{(n_j)}(x)$ of degree n_j in x, j=1,2,3, that satisfy the relation

$$P_1^{(n_1)}(x)F^2(x)+P_2^{(n_2)}(x)F(x)+P_3^{(n_3)}(x)=O(x^{n_1+n_2+n_3+2}). \qquad (2.b.1)$$

If only the first N+1 coefficients are known, then the quadratic Padé approximant can be found as long as the order (n_1,n_2,n_3) satisfies $n_1+n_2+n_3+1\leq N$.

Similarly to what has been explained in the previous section for the general case, equation (2.b.1) yields a set of $n_1+n_2+n_3+2$ linear homogeneous equations for the $n_1+n_2+n_3+3$ coefficients of the three polynomials $P_j^{(n_j)}(x)$, j=1,2,3, and thus these coefficients are uniquely determined up to a multiplicative factor. In other words, if one of the coefficients is arbitrarily chosen, the remaining $n_1+n_2+n_3+2$ are uniquely determined.

The polynomials of the quadratic Padé approximant may thus be found by simply solving the set of linear equations for the coefficients. There is, however, a more efficient method for finding the coefficients, which is based upon the use of a four term recurrence relation. This method is described in detail in

the next section.

When the polynomials $P_j^{(n_j)}(x)$, $j=1,2,3$, are known, the power series $F(x)$ can be approximated by the function $f(x)$ which satisfies

$$P_1^{(n_1)}(x)f^2(x)+P_2^{(n_2)}(x)f(x)+P_3^{(n_3)}(x)=0. \qquad (2.b.2)$$

From the comparison between equations (2.b.1) and (2.b.2) we see that the coefficients in the power series expansion of $f(x)$, up to that of $x^{n_1+n_2+n_3+1}$, are identical to those in the original power series $F(x)$.

The function $f(x)$ can be written explicitly as

$$f(x)=(-P_2^{(n_2)}(x)\pm([P_2^{(n_2)}(x)]^2-4P_1^{(n_1)}(x)P_3^{(n_3)}(x))^{1/2})/2P_1^{(n_1)}(x). \qquad (2.b.3)$$

The only remaining problem is the proper choice of the sign in front of the square root. This can be done as follows. One chooses a small value of x, for which the finite sum $\sum_{k=0}^{N} f_k x^k$, available from the $N+1$ known coefficients of the original power series, can be expected to be close to the true value of $F(x)$. For this value of x, denoted by x_0, the proper choice of the sign in (2.b.3) can now be made, and thus the correct value of $f(x_0)$ (the one closer to the true value of $F(x_0)$) is known. The correct choice of the sign for any other value of x can now be made, by using analytic continuation from x_0.

Analytical work about the generalised Hermite-Padé approximant (Nuttall 1984) indicates that in the case of m power series, the asymptotic behaviour of the polynomials can be described by means of a Riemann surface with m sheets, each one of those being a

copy of the complex plane. In the case of the quadratic Padé approximant the Riemann surface thus consists of three sheets. One choice of the sign in (2.b.3) gives the approximate value of F(x) on the first (physical) Riemann sheet, which is the value of interest, and the other choice of the sign gives the approximate value of F(x) on the second Riemann sheet, which lies beneath the first one, joined to it through branch cuts.

In many cases the function f(x) will be a better approximation for the true value of the power series F(x), than the original finite sum $\Sigma_{k=0}^{N} f_k x^k$, available from the N+1 known coefficients of the original power series. As equation (2.b.3) indicates, f(x) can even approximately reproduce a complex value of the original power series F(x), even if all the coefficients in the latter are real. An example of such a case is given in appendix A.

2.c. The four term recurrence relation for calculating three polynomial Hermite-Padé approximants

We present here a method, that we have developed, for calculating the three polynomial generalised Hermite-Padé approximant of order (n,n,n), which is based upon the use of a four term recurrence relation. Methods using recurrence relations for calculating Hermite-Padé polynomials have been suggested in the past (Padé 1894, Burley et al 1991). The recurrence relation in our method, however, has an especially simple and convenient form. Our method can be used in particular for the calculation of the quadratic Padé approximant of order (n,n,n).

This method is more efficient than the direct solution of the set of linear equations for the polynomial coefficients (section 2.a, equation (2.a.3)). It also has the advantage, that in the process of calculating the order (n,n,n) approximant all the intermediate orders (0,0,0), (1,1,1), etc. are obtained as well, and one often wishes to use 2 or 3 different orders of the approximant and compare the results.

We use a slightly different notation in this section. Instead of using the notation $P_j^{(n_j)}(x)$ for the j^{th} polynomial (of degree n_j in x) in the approximant, we use the notation $P_j(\eta,x)$, where $\eta=(n_1,n_2,n_3)$ denotes the order of the approximant, i.e. the degrees in x of the three polynomials in the approximant.

We define a sequence of triplets $\eta_k=(n_{k,1},n_{k,2},n_{k,3})$:

$$\eta_1=(0,0,0),\ \eta_2=(0,0,1),\ \eta_3=(0,1,1),$$

$$\eta_k=\eta_{k-3}+(1,1,1) \text{ for } k=4,5,\ldots,3n+1. \qquad (2.c.1)$$

These triplets denote the different orders that are calculated in the intermediate steps, until order $\eta_{3n+1}=(n,n,n)$ is reached.

The first three sets of polynomials, those of orders η_1, η_2, and η_3, are calculated directly from the expressions

$$\sum_{j=1}^{3} P_j(\eta_k,x)F_j(x)=O(x^{k+1}) \; ; \; k=1,2,3. \qquad (2.c.2)$$

If the polynomials and power series are given by

$$P_j(\eta_k,x)=\sum_{l=0}^{n_{k,j}} p_{j,k,l}x^l \; , \; F_j(x)=\sum_{k=0}^{\infty} f_{j,k}x^k, \qquad (2.c.3)$$

then the coefficient of x^m in $P_j(\eta_k,x)F_j(x)$ is given by

$$c_{j,k,m}=\sum_{l=0}^{L_j} p_{j,k,l}f_{j,m-l}, \text{ where } L_j=\min.(m,n_{k,j}). \qquad (2.c.4)$$

This means there are here k+1 linear homogeneous equations for the $n_{k,1}+n_{k,2}+n_{k,3}+3=k+2$ coefficients $p_{j,k,l}$. If one of them is arbitrarily chosen, then the remaining ones are normally uniquely determined. For example, $p_{1,k,0}$ (the coefficient of x^0 in $P_1(\eta_k,x)$) can be chosen as 1. In order to find this way the coefficients of $P_j(\eta_k,x)$ for k=1,2,3 one has to solve sets of 2, 3 and 4 linear equations, after $p_{1,k,0}$ has been set to be 1. Now the polynomial sets of orders η_1, η_2, and η_3 are known, and they serve as the initial values for the four term recurrence relation.

The recurrence relation, which relates the polynomial $P_j(\eta_{k+1},x)$ to the polynomials $P_j(\eta_{k-2},x)$, $P_j(\eta_{k-1},x)$, and $P_j(\eta_k,x)$, for j=1,2,3, is given by

$$P_j(\eta_{k+1},x)=x\,P_j(\eta_{k-2},x)+a_kP_j(\eta_{k-1},x)+b_kP_j(\eta_k,x) \; ; \; j=1,2,3. \qquad (2.c.5)$$

As $\eta_{k+1}=\eta_{k-2}+(1,1,1)$, it is immediately obvious that $P_j(\eta_{k+1},x)$ is of the right degree in x for j=1,2,3.

As we have $\Sigma_{j=1}^{3}P_j(\eta_{k-1},x)F_j(x)=O(x^{k+1-1})$ for l=0,1,2, we also have $\Sigma_{j=1}^{3}P_j(\eta_{k+1},x)F_j(x)=O(x^{k})$ no matter what a_k and b_k are. Thus, by choosing them properly, $O(x^{k+2})$, the required order, can be obtained. As only two coefficients are needed, they are the same for j=1,2,3.

In order to find a_k and b_k we substitute the recurrence relation into $\Sigma_{j=1}^{3}P_j(\eta_{k+1},x)F_j(x)=O(x^{k+2})$. This yields the expression

$$\sum_{j=1}^{3}[x\,P_j(\eta_{k-2},x)+a_kP_j(\eta_{k-1},x)+b_kP_j(\eta_k,x)]F_j(x)=O(x^{k+2}). \qquad (2.c.6)$$

Using the expressions (2.c.3) for $P_j(\eta_k,x)$ and $F_j(x)$ we have

$$x\,P_j(\eta_{k-2},x)+a_kP_j(\eta_{k-1},x)+b_kP_j(\eta_k,x)=$$

$$\sum_{l=0}^{n_{k-2,j}}p_{j,k-2,l}x^{l+1}+a_k\sum_{l=0}^{n_{k-1,j}}p_{j,k-1,l}x^{l}+b_k\sum_{l=0}^{n_{k,j}}p_{j,k,l}x^{l}. \qquad (2.c.7)$$

After multiplication by $F_j(x)$ the coefficient of x^m is

$$\sum_{l=0}^{L_{k-2,j}}p_{j,k-2,l}f_{j,m-l-1}+a_k\sum_{l=0}^{L_{k-1,j}}p_{j,k-1,l}f_{j,m-l}+b_k\sum_{l=0}^{L_{k,j}}p_{j,k,l}f_{j,m-l} \qquad (2.c.8)$$

Here $L_{K,j}=\min.(n_{K,j},m)$ for K=k-2,k-1,k, and $f_{j,-1}=0$ by definition.

This means that for m=0,1,2,....,k+1 we have

$$\alpha_m a_k+\beta_m b_k=\gamma_m, \qquad (2.c.9)$$

where

$$\alpha_m=\sum_{j=1}^{3}\sum_{l=0}^{L_{k-1,j}} p_{j,k-1,l} f_{j,m-l} \; ; \; \beta_m=\sum_{j=1}^{3}\sum_{l=0}^{L_{k,j}} p_{j,k,l} f_{j,m-l} \; ;$$

$$\gamma_m=-\sum_{j=1}^{3}\sum_{l=0}^{L_{k-2,j}} p_{j,k-2,l} f_{j,m-l-1} . \qquad (2.c.10)$$

Using (2.c.2) we see, that we have $\Sigma_{j=1}^{3} P_j(\eta_{k-1},x)F_j(x)=O(x^k)$, $\Sigma_{j=1}^{3} P_j(\eta_k,x)F_j(x)=O(x^{k+1})$, and $-x\Sigma_{j=1}^{3} P_j(\eta_{k-2},x)F_j(x)=O(x^k)$. As α_m, β_m, and γ_m are the coefficients of x^m in these expressions respectively, we have $\alpha_m=\beta_m=\gamma_m=0$ for $m=0,1,2,\ldots,k-1$, and also $\beta_k=0$. Therefore we are left only with two equations:

$$\alpha_k a_k=\gamma_k \; ; \; \alpha_{k+1} a_k+\beta_{k+1} b_k=\gamma_{k+1} . \qquad (2.c.11)$$

Thus we have

$$a_k=\gamma_k/\alpha_k \; ; \; b_k=(\alpha_k\gamma_{k+1}-\alpha_{k+1}\gamma_k)/\alpha_k\beta_{k+1} . \qquad (2.c.12)$$

With a_k and b_k known $P_j(\eta_{k+1},x)$ can be found. The coefficient of x^m in $P_j(\eta_{k+1},x)$ is given by

$$p_{j,k+1,m}=p_{j,k-2,m-1}+a_k p_{j,k-1,m}+b_k p_{j,k,m} \; ; \; j=1,2,3. \qquad (2.c.13)$$

$p_{j,k-2,-1}=0$ by definition. Finally the polynomials are normalised by dividing all the coefficients by that of x^0 in $P_1(\eta_{k+1},x)$.

The process is started with $k=3$ and repeated until $k=3n$ is reached. $P_j(\eta_{3n+1},x)$, $j=1,2,3$, are the polynomials of the desired (n,n,n) order Hermite-Padé approximant. Order (n,n,n) is alternatively denoted as order n for short.

The computation of the Hermite-Pade approximant, either by means of this method or by solving the set of linear equations directly, is numerically unstable, and thus requires multiple precision arithmetic. In the case of a CYBER 835 computer triple

precision arithmetic (144 binary digits, i.e. about 43 decimals, per number) is required in order to reach the order 16 approximant. In spite of the need for multiple precision arithmetic the computation time is short (a few seconds) thanks to the efficiency of the method.

Chapter 3

Application of the quadratic Padé approximant to the calculation of the local density of states

3.a. Calculation of the moments of the Hamiltonian

The quadratic Padé approximant method for calculating the local density of states (Mayer et al 1984, Mayer and Tong 1985) makes use of the moments of the Hamiltonian. So do also our version of the continued fraction method (i.e. obtaining the continued fraction expansion from the Padé approximant, as discussed in section 4.a), and the modified moments method. In order to use any of these methods, we have thus first to calculate the moments of the Hamiltonian. Here we shall review the definition of the moments (originally given in section 1.d), and discuss the ways in which they can be calculated.

The Hamiltonian for the lattice is represented in a matrix form, using the atomic wave functions $|\vec{r}\rangle$ at the various lattice sites as a basis (Haydock et al 1975). The matrix elements of the Hamiltonian are thus the interaction energies between these sites. It is also possible to use the atomic bonds instead of the atomic sites based wave functions as a basis for the Hamiltonian (Kelly and Bullett 1976a and b, Ortenburger et al 1976). In all the cases studied in this work only one wave function per site (or per bond) is used, but in the more general cases several wave functions per site may be required (Slater and Koster 1954).

The n^{th} moment of the Hamiltonian for the lattice site $\vec{r}$ is given by the matrix element $\langle\vec{r}|H^n|\vec{r}\rangle$ of the n^{th} power of the Hamiltonian (Gaspard and Cyrot-Lackmann 1973), and is denoted by

$u_n(\vec{r})$.

In the most general case the moments can be calculated directly from the Hamiltonian matrix by raising it to successive powers. In many cases, however, one can make use of the sparseness of the Hamiltonian matrix, i.e. the fact that the interaction energy between a given lattice site and the other sites is non-zero only for a few nearest neighbour sites. This would significantly reduce the amount of computation involved. A more detailed discussion on this kind of calculation can be found in section 5.e, where an example of such a case, a bond based model for the valence band of silicon, is discussed.

In the case of a regular or nearly regular lattice with only the nearest neighbour interaction present, expressions for the moments in closed form can often be obtained. We shall obtain such expressions for the moments in the following cases.

I. The regular lattices - square, simple cubic, body centred cubic (bcc), face centred cubic (fcc), and diamond lattices.

II. A regular binary alloy with two types of atoms at alternating sites of a simple cubic lattice.

III. A semi-infinite simple cubic lattice, at a site located a given number of layers away from the surface

These calculations, and the resulting expressions for the moments can be found in section 5.a and in appendix C.

3.b. The use of the quadratic Padé approximant for obtaining the local density of states from the moments

The calculation of the local density of states is closely related to the local Green function (Economou 1979). The latter is given by the expression

$$G(\vec{r},E)=\langle\vec{r}|(E-H)^{-1}|\vec{r}\rangle, \qquad (3.b.1)$$

where $\vec{r}$ is the site at which the local Green function is evaluated, $|\vec{r}\rangle$ is the wave function at this site, and H is the Hamiltonian.

The local density of states at the site $\vec{r}$ is obtained from the local Green function at the same site by means of the relation (1.b.6), reproduced here:

$$\rho(\vec{r},E)=(2\pi i)^{-1}\lim_{\varepsilon\to 0^+}[G(\vec{r},E+i\varepsilon)-G(\vec{r},E-i\varepsilon)]. \qquad (3.b.2)$$

The density of states itself is obtained by averaging the local density of states over all the lattice sites. Thus it is given by

$$\rho(E)=(1/N)\sum_{\vec{r}}\rho(\vec{r},E), \qquad (3.b.3)$$

where N is the number of sites in the lattice.

In the case of a regular lattice, where all the lattice sites are equivalent, the local density of states $\rho(\vec{r},E)$ and the density of states $\rho(E)$ are identical.

$(E-H)^{-1}$ in expression (3.b.1) can be formally expanded as a power series in 1/E. This way one can express the local Green function $G(\vec{r},E)$ in the form

$$G(\vec{r},E)=(1/E)\langle\vec{r}|(1-H/E)^{-1}|\vec{r}\rangle=(1/E)\sum_{n=0}^{\infty}\langle\vec{r}|H^n|\vec{r}\rangle(1/E)^n. \qquad (3.b.4)$$

We recall now from section 3.a, that the n^{th} moment of the Hamiltonian, $\mu_n(\vec{r})$, is given by

$$\mu_n(\vec{r})=\langle\vec{r}|H^n|\vec{r}\rangle. \qquad (3.b.5)$$

Thus the local Green function can be expressed in terms of the moments as

$$G(\vec{r},E)=\sum_{n=0}^{\infty}\mu_n(\vec{r})(1/E)^{n+1}. \qquad (3.b.6)$$

We define now a new variable $x=1/E$, and in terms of this new variable the local Green function is expressed as

$$G(\vec{r},E)=\sum_{n=1}^{\infty}\mu_{n-1}(\vec{r})x^n. \qquad (3.b.7)$$

If we define now a power series $G(x)=\Sigma_{k=0}^{\infty}g_kx^k$ with

$$g_0=0 \;;\; g_k=\mu_{k-1}(\vec{r}),\ k=1,2,\ldots, \qquad (3.b.8)$$

then we see that we have a power series expansion of the local Green function $G(\vec{r},E)$ in terms of $x=1/E$. The coefficients of the infinite power series, namely the moments, are real, but the sum of the infinite power series itself is generally complex. More precisely, the infinite sum $\Sigma_{k=0}^{\infty}g_k(\lambda+i\varepsilon)^k$ remains complex, even when $\varepsilon\to0$. The example in appendix A further clarifies this point.

In this kind of situation, as we have seen in section 2.b and in appendix A, the use of the quadratic Padé approximant is often very advantageous. We therefore calculate the quadratic Padé approximant of order n for the power series $G(x)=G(\vec{r},E)$, as outlined in sections 2.b and 2.c. The $\vec{r}$-dependence in G(x) has

been omitted here for the sake of convenience. For this purpose we need only the first 3n+1 moments of the Hamiltonian. The actual choice of n is dictated by the number of moments which are available in practice and by the numerical instability limitations of the computation itself (see the last paragraph in section 2.c).

After calculating the quadratic Padé approximant we have the approximant's three polynomials $P_j^{(n)}(x)$, j=1,2,3, of degree n in x, and they satisfy the relation

$$P_1^{(n)}(x)G^2(x)+P_2^{(n)}(x)G(x)+P_3^{(n)}(x)=O(x^{3n+2}). \qquad (3.b.9)$$

As outlined in section 2.b, G(x) is now approximated by the function g(x) which satisfies

$$P_1^{(n)}(x)g^2(x)+P_2^{(n)}(x)g(x)+P_3^{(n)}(x)=0. \qquad (3.b.10)$$

We define now a new set of polynomials $p_j^{(n)}(E)$ by

$$p_j^{(n)}(E)=E^n P_j^{(n)}(1/E) \;;\; j=1,2,3. \qquad (3.b.11)$$

Equation (3.b.10) becomes thus

$$p_1^{(n)}(E)g^2(E)+p_2^{(n)}(E)g(E)+p_3^{(n)}(E)=0. \qquad (3.b.12)$$

g(E) now approximates $G(\vec{r},E)$ at the site $\vec{r}$ for which the moments have been calculated.

For a given value of the energy E, g(E) is thus the solution of a quadratic equation, given by

$$g(E)=(-p_2^{(n)}(E)\pm[R^{(n)}(E)]^{1/2})/2p_1^{(n)}(E), \qquad (3.b.13)$$

where

$$R^{(n)}(E)=[p_2^{(n)}(E)]^2-4p_1^{(n)}(E)p_3^{(n)}(E). \qquad (3.b.14)$$

Using equation (3.b.2) the approximation for the local density of states is given by

$$\rho(\vec{r},E)=\begin{cases} |[-R^{(n)}(E)]^{1/2}/2\pi p_1^{(n)}(E)| & \text{if } R^{(n)}(E)<0 \\ 0 & \text{if } R^{(n)}(E)\geq 0. \end{cases} \qquad (3.b.15)$$

In many cases, as we shall see in section 5.a, only the even numbered moments are non-zero. In such a case we use the change of variable $x=1/E^2$ (rather than $x=1/E$), and thus the coefficients in the power series $G(x)=\Sigma_{k=0}^{\infty}g_k x^k$ are given by

$$g_0=0 \; ; \; g_k=\mu_{2(k-1)}(\vec{r}), \; k=1,2,\ldots . \qquad (3.b.16)$$

The calculation of the quadratic Padé approximant is carried out exactly as before, and the approximation for the local density of states is obtained the same way as before as well. However, as in this case the expansion of the local Green function in terms of the moments is given by

$$G(\vec{r},E)=\sum_{n=0}^{\infty}\mu_{2n}(\vec{r})(1/E)^{2n+1}=E\sum_{n=1}^{\infty}\mu_{2(n-1)}x^n, \qquad (3.b.17)$$

the approximation for the local density of states is given by

$$\rho(\vec{r},E)=\begin{cases} |E[-R^{(n)}(E)]^{1/2}/2\pi p_1^{(n)}(E)| & \text{if } R^{(n)}(E)<0 \\ 0 & \text{if } R^{(n)}(E)\geq 0. \end{cases} \qquad (3.b.18)$$

When obtaining (3.b.15) and (3.b.18), one has to choose the proper sign in front of the square root in (3.b.13). This is done by using analytic continuation from a large value of E (i.e.

small value of x) for which the sum of the given finite part of the power series G(x) comes close enough to the true value of the local Green function at that point. We have verified this way, for various cases, that the approximation for the local density of states always comes out positive. Therefore we use the absolute value in expressions (3.b.15) and (3.b.18) for practical calculations.

Chapter 4

Other methods for obtaining the local density of states

4.a. Review of the continued fraction method

We present here a review of the continued fraction method (Haydock et al 1972, Haydock et al 1975, Haydock 1980) and the ways an approximation for the local density of states can be obtained by using it. We shall use this method in sections 5.c and 5.g in order to calculate the local density of states for the various cases studied and compare the results with those obtained by using the quadratic Pade method

The continued fraction (or recursion) method is based upon the creation of a new basis for the Hamiltonian from the original basis of the atomic wave functions related to the lattice sites. The original basis functions $|r\rangle$ are denoted for this purpose as $|1\rangle$, $|2\rangle$, $|3\rangle$, etc., where $|1\rangle$ refers to the wave function at the lattice site for which the local density of states is to be calculated. The new basis functions, which are linear combinations of the original ones, are denoted by $|1\rangle$, $|2\rangle$, $|3\rangle$, etc. The Hamiltonian is denoted by H.

The new basis functions are generated from the original ones by means of a three term recurrence relation given by

$$b_n|n+1\rangle=(H-a_n)|n\rangle-b_{n-1}|n-1\rangle. \qquad (4.a.1)$$

and the initial conditions are given by

$$b_0=0 \quad |1\rangle=|1\rangle \qquad (4.a.2)$$

The coefficients a_n and b_n are given by

$$a_n=(n|H|n) \qquad b_n=(n+1|H|n). \tag{4.a.3}$$

The new basis |1>, |2>, |3>, etc. is orthonormal, as the above equations indicate.

From equation (4 a.1) we also see that in the new basis the Hamiltonian is represented by a tridiagonal matrix of semi-infinite dimension, given by

$$H=\begin{matrix} a_1 & b_1 & 0 & 0 & \\ b_1 & a_2 & b_2 & 0 & \cdots \\ 0 & b_2 & a_3 & b_3 & \cdots \\ 0 & 0 & b_3 & a_4 & \\ \cdots & \cdots & \cdots & \cdots & \end{matrix} \tag{4.a.4}$$

The local Green function at the site |1>=|1> is given by $G(\vec{r},E)=(1|(E-H)^{-1}|1)$, and it can be expressed as an infinite continued fraction given by (Haydock 1980)

$$G(\vec{r},E) = \cfrac{1}{E-a_1-\cfrac{b_1^2}{E-a_2-\cfrac{b_2^2}{E-a_3-\cdots}}} \tag{4.a.5}$$

In practice only a finite number of the coefficinets a_n, b_n can be calculated. If $a_1, a_2, \ldots, a_N$ and $b_1, b_2, \ldots, b_{N-1}$ are known, then the Hamiltonian is truncated to a N x N tridiagonal matrix, and the continued fraction representing the local Green function $G(\vec{r},e)$ is truncated at a_N. The Hamiltonian is approximated thus by the finite matrix

$$H_N = \begin{pmatrix} a_1, & b_1, & 0, & \ldots, & 0 \\ b_1, & a_2, & b_2, & \ldots, & 0 \\ 0, & b_2, & a_3, & \ldots, & 0 \\ \ldots & \ldots & \ldots & \ldots & \ldots \\ 0, & 0, & 0, & \ldots, & a_N \end{pmatrix}, \qquad (4.a.6)$$

and the local Green function is approximated by the finite continued fraction

$$G_N(\vec{r},E) = \cfrac{1}{E-a_1-\cfrac{b_1^2}{E-a_2-\ldots-\cfrac{b_{N-1}^2}{E-a_N}}}. \qquad (4.a.7)$$

The finite (truncated) continued fraction $G_N(E)$ (the parameter $\vec{r}$ is omitted from now on for more convenience) can be expressed as a rational function $Q_N(E)/P_N(E)$, where $Q_N(E)$ and $P_N(E)$ are polynomials of degrees N-1 and N in E respectively. $P_N(E)$ is the characteristic polynomial of the N x N Hamiltonian H_N. $Q_N(E)$ is that of the (N-1) x (N-1) matrix which is obtained from it when the first row and column are removed. $P_N(E)$ and $Q_N(E)$ can be obtained by means of the recurrence relation (Haydock 1980)

$$P_n(E)=(E-a_n)P_{n-1}(E)-b_{n-1}^2P_{n-2}(E),$$

$$Q_n(E)=(E-a_n)Q_{n-1}(E)-b_{n-1}^2Q_{n-2}(E), \qquad (4.a.8)$$

where the initial values are

$$P_0(E)=1 \; ; \; P_1(E)=E-a_1,$$

$$Q_0(E)=0 \; , \; Q_1(E)=1. \qquad (4.a.9)$$

By using the recurrence relation with n=2,3,...,N in that order

$P_N(E)$ and $Q_N(E)$ are obtained.

The approximation for the local density of states $\rho_N(E)$ can be found now from the local Green function by using the expression (3.b.2). Here this gives $\rho_N(E)$ in terms of a sum of weighted delta-functions: (Haydock 1975, Haydock 1980)

$$\rho_N(E)=\sum_{n=1}^{N} W_n \delta(E-E_n). \qquad (4.a.10)$$

$E_1, E_2, \ldots, E_N$ are the N roots of $P_N(E)$, i.e. the N eigenvalues of the N x N Hamiltonian H_N. As the latter is symmetrical, they are all real numbers. $W_1, W_2, \ldots, W_N$ are the N corresponding weights. They are given by

$$W_n=Q_N(E_n)/P_N'(E_n) \; ; \; n=1,2,\ldots,N. \qquad (4.a.11)$$

The derivative is taken with respect to E. W_n and E_n are related to the first 2N moments by

$$\mu_n=\sum_{m=1}^{N} W_m E_m^{\,n} \; ; \; n=0,1,2,\ldots,2N-1. \qquad (4.a.12)$$

The integrated local density of states is defined by

$$n_N(E)=\int_{-\infty}^{E} \rho_N(z)dz. \qquad (4.a.13)$$

In the case discussed here it is a step function given by

$$n_N(E)=\begin{cases} 0 & \text{if } E<E_1 \\ \sum_{m=1}^{n} W_m & \text{if } E_n<E<E_{n+1} \quad (\text{for } n=1,2,\ldots,N-1) \\ 1 & \text{if } E>E_N \end{cases} \qquad (4.a.14)$$

This step function can be smoothed by having the centres of the "steps" joined by straight lines as shown in Figure 1.

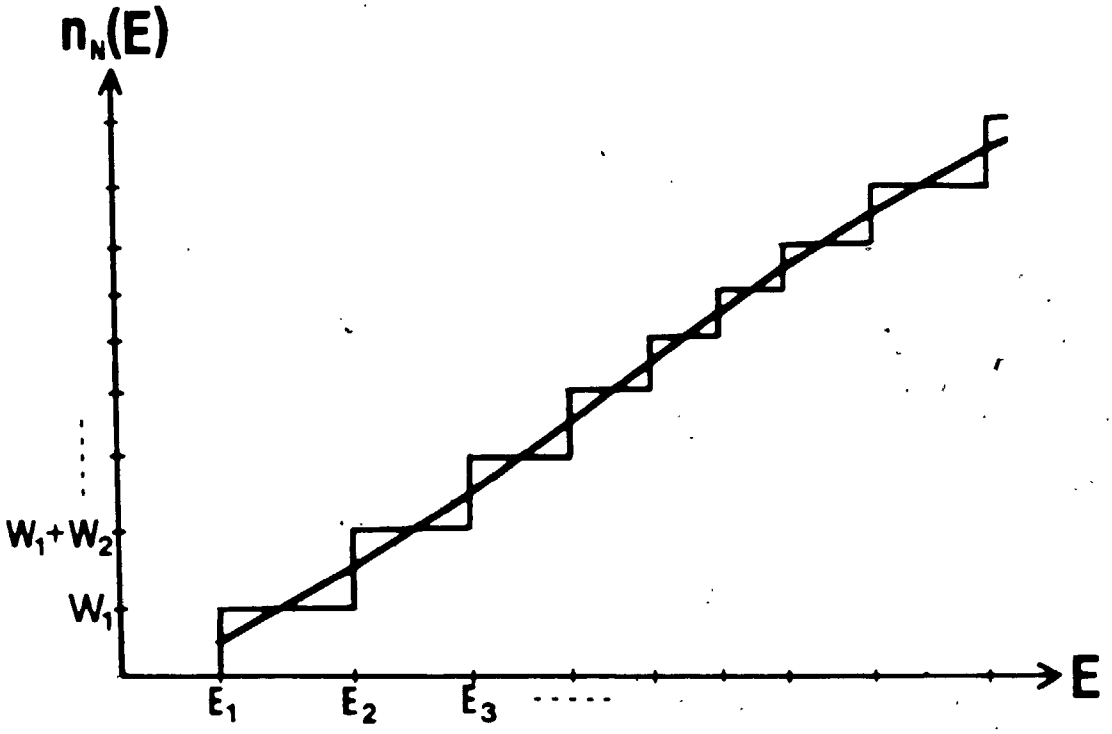

Figure 1

Schematic diagram of the integrated local density of states as obtained from the truncated continued fraction in the form of a step function. $E_1, E_2, \ldots$ are the positions of the delta-functions, and $W_1, W_2, \ldots$ are the corresponding weights in the original approximation for the local density of states in the form of a sum of weighted delta-functions. The lines connecting the centres of the "steps" are used in order to obtain the improved approximation for the local density of states in the form of a histogram.

This way, for $E_n<E\leq E_{n+1}$ $n_N(E)$ is given by

$$n_N(E)=\sum_{m=1}^{n-1} W_m+W_n/2+(W_n+W_{n+1})(E-E_n)/2(E_{n+1}-E_n) \qquad (4.a.15)$$

By differentiating with respect to E we have now a histogram type representation for the local density of states $\rho_N(E)$ itself:

$$\rho_N(E)=\begin{cases} 0 & \text{if } E<E_1 \text{ or } E>E_N \\ (W_n+W_{n+1})/2(E_{n+1}-E_n) & \text{if } E_n<E\leq E_{n+1}. \end{cases} \qquad (4.a.16)$$

This is already a much better approximation for the local density of states than the original sum of weighted delta-functions.

Instead of smoothing the step function (4.a.14) by straight lines one can also use a polynomial fitting (Gaspard and Cyrot-Lackmann 1973). This way a smooth approximation for the local density of states is obtained instead of the histogram described above. We shall not discuss the polynomial fitting here, as an even better method for improving the approximation for the local density of states is available, as discussed below.

If the energy spectrum consists of a single energy band the coefficients a_n and b_n approach certain limits when n goes to infinity (Gaspard and Cyrot-Lackmann 1973, Hodges 1977, Haydock 1980). We shall denote these limits by a and b respectively. Instead of just truncating the continued fraction at a_N, we have it continued from there on with the constants a and b in place of the unknown coefficients a_n and b_n for n=N+1,N+2,... . Thus we have

$$G_N(E) = \cfrac{1}{E-a_1-\cfrac{b_1^2}{E-a_2-\cfrac{b_2^2}{E-a_3-\ldots-\cfrac{b_{N-1}^2}{E-a_N-\cfrac{b^2}{E-a-\cfrac{b^2}{E-a-\ldots}}}}}} \qquad (4.a.17)$$

Now let g(E) denote the "tail" beyond the original truncation point, i.e.

$$g(E) = \cfrac{b^2}{E-a-\cfrac{b^2}{E-a-\ldots}} \qquad (4.a.18)$$

Using the periodic character of the "tail" we have

$$g(E)=b^2/[E-a-g(E)], \qquad (4.a.19)$$

and therefore

$$g(E)=(1/2)((E-a)-[(E-a)^2-4b^2]^{1/2}). \qquad (4.a.20)$$

The approximation for the local Green function becomes now

$$G_N(E) = \cfrac{1}{E-a_1-\cfrac{b_1^2}{E-a_2-\cfrac{b_2^2}{E-a_3-\ldots-\cfrac{b_{N-1}^2}{E-a_N-g(E)}}}} \qquad (4.a.21)$$

g(E) relates the limits a and b to the lower and upper band

edges, denoted by E_l and E_h respectively. g(E) is real for E<a-2b and for E>a+2b. It is imaginary for a-2b<E<a+2b. The band edges are thus given by .

$$E_l=a-2b \; ; \; E_h=a+2b. \qquad (4.a.22)$$

Conversely, the limits a and b are given in terms of the band edges by

$$a=(E_l+E_h)/2 \; , \; b=(E_h-E_l)/4. \qquad (4.a.23)$$

We define now

$$\eta(E)=[4b^2-(E-a)^2]^{1/2} \; ; \; a_0=2a_N-a. \qquad (4.a.24)$$

Thus we have

$$b_{N-1}^2/[E-a_N-g(E)]=2b_{N-1}^2/[E-a_0+i\eta(E)], \qquad (4.a.25)$$

and therefore the expression for $G_N(E)$ becomes

$$G_N(E) = \cfrac{1}{E-a_1-\cfrac{b_1^2}{E-a_2-\cfrac{b_2^2}{E-a_3-\ldots-\cfrac{2b_{N-1}^2}{E-a_0+i\eta(E)}}}} \qquad (4.a.26)$$

We have found, that $G_N(E)$ can be expressed in terms of the polynomials $P_n(E)$ and $Q_n(E)$ as follows

$$G_N(E)=\frac{[(E-a_0)Q_{N-1}(E)-2b_{N-1}^2Q_{N-2}(E)]+iQ_{N-1}(E)\eta(E)}{[(E-a_0)P_{N-1}(E)-2b_{N-1}^2P_{N-2}(E)]+iP_{N-1}(E)\eta(E)} \qquad (4.a.27)$$

A proof of (4.a.27) can be found in appendix B.

The local density of states $\rho_N(E)$ is found from (3.b.2) as before. Outside the band $\eta(E)$ is pure imaginary. Thus $G_N(E)$, as given in expression (4.a.27), is real, and therefore $\rho_N(E)$ is zero there. Inside the band $\eta(E)$ is real. Thus we have there

$$\rho_N(E)=(2/\pi)b_{N-1}^2\frac{P_{N-2}(E)Q_{N-1}(E)-P_{N-1}(E)Q_{N-2}(E)}{[(E-a_0)P_{N-1}(E)-2b_{N-1}^2P_{N-2}(E)]^2+P_{N-1}^2(E)\eta^2(E)}\eta(E). \tag{4.a.28}$$

We recall now the recurrence relation for the polynomials $P_n(E)$ and $Q_n(E)$, given by equations (4.a.8). By multiplying the first expression by $Q_{n-1}(E)$ and the second expression by $P_{n-1}(E)$ and subtracting the first expression from the second we obtain

$$P_{n-1}(E)Q_n(E)-P_n(E)Q_{n-1}(E)=b_{n-1}^2[P_{n-2}(E)Q_{n-1}(E)-P_{n-1}(E)Q_{n-2}(E)]. \tag{4.a.29}$$

By using this relation repeatedly for n-1,n-2,....2,1 in that order we obtain

$$P_{n-1}(E)Q_n(E)-P_n(E)Q_{n-1}(E)=\sum_{i=1}^{n-1}b_i^2, \tag{4.a.30}$$

as $P_0(E)Q_1(E)-P_1(E)Q_0(E)=1$. Thus we have

$$b_{N-1}^2[P_{N-2}(E)Q_{N-1}(E)-P_{N-1}(E)Q_{N-2}(E)]=\sum_{i=1}^{N-1}b_i^2 \tag{4.a.31}$$

We also have

$$(E-a_0)^2+4b^2-E^2=E^2-2a_0E+a_0^2+4b^2-E^2+2aE-a^2=$$

$$2(a-a_0)E+(a_0+a)(a_0-a)+4b^2=$$

$$4(a-a_N)E+4a_N(a_N-a)+4b^2=$$

$$4[(a-a_N)(E-a_N)+b^2]. \qquad (4.a.32)$$

Using these results we have

$$\rho_N(E)=\left(\prod_{i=1}^{N-1} b_i^2\right)n(E)/2\pi\{[(a-a_N)(E-a_N)+b^2]P_{N-1}^2(E)+b_{N-1}^4P_{N-2}^2(E)-$$

$$(E+a-2a_N)b_{N-1}^2P_{N-1}(E)P_{N-2}(E)\}. \qquad (4.a.33)$$

As $a=a_N$, this can be simplified to

$$\rho_N(E)=\left(\prod_{i=1}^{N-1} b_i^2\right)n(E)/2\pi[b^2P_{N-1}^2(E)+b_{N-1}^4P_{N-2}^2(E)-$$

$$(E-a)b_{N-1}^2P_{N-1}(E)P_{N-2}(E)]. \qquad (4.a.34)$$

Following this analysis of the one band case (originally carried out by Haydock and his co-workers), we have carried out a similar analysis for the two band case, which we now present.

If the energy spectrum consists of two energy bands (or a band with a gap in it), the coefficients a_n and b_n of the continued fraction alternatingly converge to two pairs of limits (Gaspard and Cyrot-Lackmann 1973, Turchi et al 1982), and thus we have

$$\lim_{n\to\infty} a_{2n-1}=A_1 \quad \lim_{n\to\infty} a_{2n}=A_2$$

$$\lim_{n\to\infty} b_{2n-1}=B_1 \quad \lim_{n\to\infty} b_{2n}=B_2. \qquad (4.a.35)$$

The quadratic termination of the continued fraction, when truncated at a_N with an odd N, is found from the periodicity of the "tail", as done in the one band case, and is given by

$$g(E) = \cfrac{B_2^2}{E-A_2-\cfrac{B_1^2}{E-A_1-g(E)}} \quad . \tag{4.a.36}$$

The value of g(E) is thus

$$g(E)=(E-A_1)/2-(B_1^2-B_2^2)/2(E-A_2)\pm$$

$$([(E-A_1)(E-A_2)-(B_1^2+B_2^2)]^2+4B_1^2B_2^2)^{1/2}/2(E-A_2). \tag{4.a.37}$$

If the continued fraction is truncated at a_N with an even N, then A_1, B_1 and A_2, B_2 in the expression (4.a.37) for g(E) have to be interchanged.

If we define now:

$$a_0=\begin{cases} 2a_N-A_1-(B_1^2-B_2^2)/(E-A_2) & \text{if N is odd} \\ 2a_N-A_2-(B_2^2-B_1^2)/(E-A_1) & \text{if N is even,} \end{cases} \tag{4.a.38}$$

and

$$\eta(E)=\begin{cases} (4B_1^2B_2^2-[(E-A_1)(E-A_2)-(B_1^2+B_2^2)]^2)^{1/2}/(E-A_2) & \text{if N is odd} \\ (4B_1^2B_2^2-[(E-A_1)(E-A_2)-(B_1^2+B_2^2)]^2)^{1/2}/(E-A_1) & \text{if N is even} \end{cases} \tag{4.a.39}$$

then the previous treatment of the continued fraction is still valid, and we obtain $\rho_N(E)=0$ if $\eta(E)$ is real, and

$$\rho_N(E)=2\left(\prod_{i=1}^{N-1} b_i^2\right)|\eta(E)|/\pi([(E-a_0)P_{N-1}(E)-2b_{N-1}^2P_{N-2}(E)]^2+$$

$$P_{N-1}^2(E)|\eta(E)|^2) \tag{4.a.40}$$

if $\eta(E)$ is imaginary.

The relation between A_1, A_2, B_1, B_2 and the band edge posi-

tions is found from the following arguments. If $n(E)=0$ then we have

$$(E-A_1)(E-A_2)-(B_1^2+B_2^2)=\pm 2B_1B_2, \qquad (4.a.41)$$

and therefore we have

$$(E-A_1)(E-A_2)=(B_1\pm B_2)^2 \qquad (4.a.42)$$

at the band edges. Thus the 4 band edges are given by

$$E_{1,2,3,4}=(1/2)\{(A_1+A_2)\pm[(A_1-A_2)^2+4(B_1\pm B_2)^2]^{1/2}\}. \qquad (4.a.43)$$

We shall use expressions (4.a.16), (4.a.33), and (4.a.40) for the approximate local density of states in order to compare the results obtained from them with the results obtained by using the quadratic Padé approximant.

4.b. The relation between the continued fraction and the ordinary Padé approximant

The ordinary Padé approximant of order (n,m) for a given function G(x), expanded as a power series $\Sigma_{k=0}^{\infty} g_k x^k$, consists of two polynomials, $R_n(x)$ and $S_m(x)$, of degrees n and m in x respectively, that satisfy

$$R_n(x)G(x)-S_m(x)=O(x^{n+m+1}). \qquad (4.b.1)$$

Only the first n+m+1 coefficients in the power series expansion of G(x) are needed in order to find these polynomials.

The original function G(x) is now approximated by the rational function

$$g(x)=S_m(x)/R_n(x). \qquad (4.b.2)$$

The first n+m+1 coefficients in the power series expansion of g(x) are identical to those of G(x). g(x) often is a better approximation for the true value of G(x) than the finite sum $\Sigma_{k=0}^{n+m} g_k x^k$.

The order (n,n) Padé approximant can be found by means of a three term recurrence relation. Orders (0,0) and (1,1) are found directly from the set of linear equations obtained from

$$R_n(x)G(x)-S_n(x)=O(x^{2n+1}) \; ; \; n=0,1. \qquad (4.b.3)$$

Using $G(x)=\Sigma_{k=0}^{\infty} g_k x^k$, we have then:

$$R_0(x)=1 \qquad ; \; S_0(x)=g_0$$

$$R_1(x)=1-(g_2/g_1)x \; ; \; S_1(x)=g_0+[(g_1^2-g_0g_2)/g_1]x \qquad (4.b.4)$$

If $g_1=0$, one has to start with a pair of higher orders (m,m) and (m+1,m+1). The coefficient of x^0 in $R_n(x)$ is chosen to be 1 for the sake of definiteness. Otherwise the coefficients are determined only up to a multiplicative constant.

The three term recurrence relation is

$$R_{n+1}(x)=(x+\alpha_n)R_n(x)+\beta_n x^2 R_{n-1}(x)$$

$$S_{n+1}(x)=(x+\alpha_n)S_n(x)+\beta_n x^2 S_{n-1}(x). \qquad (4.b.5)$$

The recurrence relation is used for the practical calculation by substituting it into the expression (4.b.1) for order (n+1,n+1) and then expanding and gathering terms. Only two equations, those corresponding to the coefficients of x^{2n+1} and x^{2n+2}, have to be solved, in order to obtain α_n and β_n. This is similar to the way the quadratic Pade approximant is calculated (section 2.c).

If we define

$$r_n(E)=E^n R_n(1/E) \; ; \; s_n(E)=E^n S_n(1/E), \qquad (4.b.6)$$

then we have

$$r_{n+1}(E)=(1+\alpha_n E)r_n(E)+\beta_n r_{n-1}(E)$$

$$s_{n+1}(E)=(1+\alpha_n E)s_n(E)+\beta_n s_{n-1}(E). \qquad (4.b.7)$$

This recurrence relation is very similar to the recurrence relation for the polynomials $P_n(E)$ and $Q_n(E)$ of the continued fraction method, especially if we rewrite it in the form

$$p_{n+1}(E)=(E+1/\alpha_n)p_n(E)+(\beta_n/\alpha_{n-1}\alpha_n)p_{n-1}(E) \; ; \; p_k(E)=r_k(E)/\prod_{j=1}^{k-1}\alpha_j$$

$$q_{n+1}(E)=(E+1-\lambda_n)q_n(E)+(\xi_n-\lambda_{n-1}\lambda_n)q_{n-1}(E), \quad q_k(E)=s_k(E)\prod_{j=1}^{k-1}\lambda_j \qquad 4.b.8$$

It really turns out that $p_n(E)$ and $q_n(E)$ are the same polynomials as $P_n(E)$ and $Q_n(E)$ up to a constant factor (Haydok 1980). If we normalise them by choosing the coefficient of E^n in $p_n(E)$ as 1, they become exactly the same. Thus, comparing (4.a.8) and (4.b.8), we find a relation between the coefficients λ_n and ξ_n used here and the coefficients a_n and b_n of the continued fraction method.

$$a_1=-1, \quad a_n=-1-\lambda_{n-1}, \quad b_n^2=-\xi_{n+1}-\lambda_n\lambda_{n+1} \qquad 4.b.9$$

Thus, when calculating the N,N Padé approximant for the local Green function, using the three term recurrence relation all the coefficients of the continued fraction, i.e. $a_1, a_2, \ldots, a_N$ and $b_1, b_2, \ldots, b_{N-1}$ are obtained as well. We shall make use of this result in order to obtain the continued fraction expansion from the moments in sections 5.c and 5.g, so that we can compare the continued fraction method results with the quadratic Padé method results which are obtained from the moments as well.

So far we have seen that the ordinary Padé approximant of order N,N is equivalent to the continued fraction truncated at a_N. Now we shall present a scheme, that we have developed for further improving the convergence of the Padé approximant and see that it is very closely related to the quadratic termination scheme for the truncated continued fraction.

In the transition from 4.b.1 to 4.b.2, we have omitted the

term $O(x^{n+m+1})$. If we leave this term intact and use definition (4.b.6) we get for the order (n,n) Padé approximant the relation

$$p_n(E)G(E)-q_n(E)=O(E^{-(n+1)}). \qquad (4.b.10)$$

The detailed analytical study of Hermite-Padé approximants (Nuttall 1984) shows that the right hand side of (4.b.10) can be expressed in the form

$$O(E^{-(n+1)})=A_n\tau_n(E)\phi^n(E), \qquad (4.b.11)$$

where A_n is a constant, $\phi(E)$ is a function of E, and $\tau_n(E)$ is another function of E which depends only weakly on n.

By normalising the polynomials $p_n(E)$ and $q_n(E)$ through the division of all the coefficients by that of $E^{-(n+1)}$ in $O(E^{-(n+1)})$ A_n is set to 1. The coefficient of $E^{-(n+1)}$ in the infinite sum $O(E^{-(n+1)})=p_n(E)G(E)-q_n(E)$ is equal to $-\sum_{i=1}^{n}b_i$ (for n=0 it is 1), as we show below.

For $n=0$, $p_n(E)G(E)-q_n(E)=G(E)$, and the coefficient of E^{-1} there is $c_0=\langle\hat{r}|H^0|\hat{r}\rangle=\langle\hat{r}|\hat{r}\rangle=1$. For a general n we replace G(E) by the approximation $q_{n+1}(E)/p_{n+1}(E)$. This approximation has the same coefficients in the expansion in E^{-1} as G(E) itself up to the coefficient of $E^{-(n+1)}$. This means that this replacement does not change the coefficient of $E^{-(n+1)}$ in $p_n(E)G(E)-q_n(E)$. In fact it does not change even that of $E^{-(n+2)}$. Using expression (4.a.30) we have

$$p_n(E)\left[q_{n+1}(E)/p_{n+1}(E)\right]-q_n(E)=$$

$$\left[p_n(E)q_{n+1}(E)-p_{n+1}(E)q_n(E)\right]/p_{n+1}(E)=\sum_{i=1}^{n}b_i^2\,p_{n+1}(E) \qquad (4.b.12)$$

As the coefficient of E^{n+1}, the highest power of E, in $p_{n+1}(E)$, is 1, the coefficient of $E^{-(n+1)}$ is $\Pi_{i=1}^{n} b_i^2$.

The normalised polynomials, denoted by $p_n^*(E)$ and $q_n^*(E)$, are then obtained from the original ones by dividing all the coefficients by $\Pi_{i=1}^{n} b_i^2$. This means that the normalised polynomials can be obtained directly by using the recurrence relation

$$p_n^*(E)=[(E-a_n)p_{n-1}^*(E)-p_{n-2}^*(E)]/b_n^2$$

$$q_n^*(E)=[(E-a_n)q_{n-1}^*(E)-q_{n-2}^*(E)]/b_n^2, \qquad (4.b.13)$$

with the initial values

$$p_0^*(E)=1 \; : \; p_1^*(E)=(E-a_1)/b_1^2$$

$$q_0^*(E)=0 \; : \; q_1^*(E)=1/b_1^2. \qquad (4.b.14)$$

Using the normalised polynomials and (4.b.11) we have

$$p_{N-1}^*(E)G(E)-q_{N-1}^*(E)=\zeta_{N-1}(E)\psi^{N-1}(E),$$

$$p_N^*(E)G(E)-q_N^*(E)=\zeta_N(E)\psi^N(E),$$

$$p_{N+1}^*(E)G(E)-q_{N+1}^*(E)=\zeta_{N+1}(E)\psi^{N+1}(E). \qquad (4.b.15)$$

We neglect now the dependence of $\zeta_n(E)$ on n and take ratios. This way we have

$$[p_{N+1}^*(E)G_N(E)-q_{N+1}^*(E)]/[p_N^*(E)G_N(E)-q_N^*(E)]=$$

$$[p_N^*(E)G_N(E)-q_N^*(E)]/[p_{N-1}^*(E)G_N(E)-q_{N-1}^*(E)]=\psi(E). \qquad (4.b.16)$$

$G_N(E)$ is now the approximation for G(E), the local Green function.

This yields a quadratic equation for $G_N(E)$

$$([p_N^*(E)]^2-p_{N-1}^*(E)p_{N+1}^*(E))G_N^2(E)+$$

$$[p_{N-1}^*(E)q_{N+1}^*(E)+p_{N+1}^*(E)q_{N-1}^*(E)-2p_N^*(E)q_N^*(E)]G_N(E)+$$

$$([q_N^*(E)]^2-q_{N-1}^*(E)q_{N+1}^*(E))=0. \qquad (4.b.17)$$

If the two solutions are real, then the imaginary part of $G_N(E)$ is zero in both. If they are complex, then the imaginary parts of $G_N(E)$ in both have the same magnitude, but opposite signs. Thus the approximate local density of states $\rho_N(E)$ is uniquely determined, and given by $\rho_N(E)=(1/\pi)|\mathrm{Im}.[G_N(E)]|$. This way we again obtain an approximation for the local density of states in terms of a smooth function.

By using the recurrence relation (4.b.13) we obtain

$$[p_{N+1}^*(E)G_N(E)-q_{N+1}^*(E)]\,[p_N^*(E)G_N(E)-q_N^*(E)]=$$

$$([E-a_{N+1}-[p_{N-1}^*(E)G_N(E)-q_{N-1}^*(E)]\,[p_N^*(E)G_N(E)-q_N^*(E)])\,b_{N+1}^2. \qquad (4.b.18)$$

Using the relation with $\psi(E)$ in (4.b.16) we have now

$$\psi(E)=[E-a_{N+1}-1/\psi(E)]\,b_{N+1}^2 \qquad (4.b.19)$$

Therefore we can express $\psi(E)$ explicitly as

$$\psi(E)=([E-a_{N+1}-[E-a_{N+1}]^2-4b_{N+1}^2]^{1/2})/2b_{N+1}^2. \qquad (4.b.20)$$

Using (4.b.16 for N-1 instead of N) we have now

$$[p_N^*(E)G_N(E)-q_N^*(E)]\,[p_{N-1}^*(E)G_N(E)-q_{N-1}^*(E)]=$$

$$((E-a_N)-[p_{N-2}^*(E)G_N(E)-q_{N-2}^*(E)]/[p_{N-1}^*(E)G_N(E)-q_{N-1}^*(E)])/b_N^2. \qquad (4.b.21)$$

As the left hand side is equal to $\psi(E)$, we have

$$[p_{N-1}^*(E)G_N(E)-q_{N-1}^*(E)]/[p_{N-2}^*(E)G_N(E)-q_{N-2}^*(E)]=$$

$$1/[E-a_N-b_N^2\psi(E)]. \qquad (4.b.22)$$

By using the same procedure for N-2 we obtain now

$$[p_{N-2}^*(E)G_N(E)-q_{N-2}^*(E)]/[p_{N-3}^*(E)G_N(E)-q_{N-3}^*(E)]=$$

$$\cfrac{1}{E-a_{N-1}-\cfrac{b_{N-1}^2}{E-a_N-b_N^2\psi(E)}}. \qquad (4.b.23)$$

By repeating this procedure for n=N-3, n=N-4, etc., until n=1 is reached, we obtain a continued fraction type expression for $G_N(E)$:

$$[p_1^*(E)G_N(E)-q_1^*(E)]/[p_0^*(E)G_N(E)-q_0^*(E)]=$$

$$\cfrac{1}{E-a_2-\cfrac{b_2^2}{E-a_3-\cfrac{b_3^2}{E-a_4-\ldots-\cfrac{b_{N-1}^2}{E-a_N-b_N^2\psi(E)}}}}. \qquad (4.b.24)$$

However, using (4.b.14), we also have

$$[p_1^*(E)G_N(E)-q_1^*(E)]/[p_0^*(E)G_N(E)-q_0^*(E)]=$$

$$[(E-a_1)-1/G_N(E)]/b_1^2, \qquad (4.b.25)$$

and thus, using (4.b.20), (4.b.24), and (4.b.25), we have

$$G_N(E)=\cfrac{1}{E-a_1-\cfrac{b_1^2}{E-a_2-\cfrac{b_2^2}{E-a_3-\cfrac{b_{N-1}^2}{E-a_N-\Phi(E)}}}} \qquad (4.b.26)$$

where

$$\Phi(E)=(b_N^2\ 2b_{N+1}^2)\cdot\ E-a_{N+1})\pm[(E-a_{N+1})^2-4b_{N+1}^2]^{1/2}). \qquad (4.b\ 27)$$

Now we compare expressions (4.b.26) and (4.b.27) with expressions (4.a.21) and (4.a.20) respectively. For a large n $a_n=a$ and $b_n=b$, and therefore for large values of N $\Phi(E)=g(E)$. Thus the approximation for the local Green function (4.b.26), obtained from the ordinary Padé approximant, for a given E, is very close in value to the approximation (4.a.21), obtained by using the continued fraction with the quadratic termination, when N is large

4.c. The method of modified moments

The method of modified moments (Wheeler and Blumstein 1972, Blumstein and Wheeler 1973, Wheeler 1974, Wheeler et al 1974) is another method for calculating the local density of states from the moments. It has originally been used for calculating phonon density of states. Here we present a brief review of the method in the context of calculating electron density of states. We shall use this method in section 5.g in order to calculate the density of states for the valence band of silicon.

We assume that we have a single energy band, and that the band edge positions are known to us. We denote the position of the lower band edge by E_a, and that of the upper band edge by E_b. We denote the local density of states by $\rho(E)$ (omitting the dependence on the lattice site $\vec{r}$ throughout this section).

We choose a weight function $H(E)$, which is positive inside the energy band and zero outside. We try to make the choice of $H(E)$ so that the band edge singularities are reproduced by it as much as possible.

The orthogonal polynomials $p_n(E)$ related to $H(E)$ are defined by

$$\int_{E_a}^{E_b} H(E)p_m(E)p_n(E)dE=\delta_{n,m}/N_n^2. \qquad (4.c.1)$$

N_n is a normalisation factor defined by this equation. The polynomials satisfy the three term recurrence relation

$$p_{n+1}(E)=(E-a_n)p_n(E)-b_n p_{n-1}(E) \qquad (4.c.2)$$

with the initial conditions

$$p_{-1}(E)=0 \quad ; \quad p_0(E)=1. \qquad (4.c.3)$$

The regular moments μ_n are related to the local density of states by (cf. expression (1.d.3))

$$\mu_n = \int_{E_a}^{E_b} \rho(E) E^n dE. \qquad (4.c.4)$$

The modified moments ν_n are related to the local density of states by

$$\nu_n = \int_{E_a}^{E_b} \rho(E) p_n(E) dE. \qquad (4.c.5)$$

Using these expressions a method for calculating the modified moments from the regular ones can be obtained. This method works as follows. We define a set of matrix elements $Y_{k,l}$ recursively

$$Y_{k+1,l}=Y_{k,l+1}-a_k Y_{k,l}-b_k Y_{k-1,l} \qquad Y_{0,l}=\mu_l \qquad Y_{-1,l}=0 \qquad (4.c.6)$$

For each k we have then $Y_{k,0}=\nu_k$

The local density of states is now approximated by

$$\rho(E) \approx H(E) \sum_{n=0}^{N} \nu_n^* p_n^*(E). \qquad (4.c.7)$$

ν_n^* are the normalised modified moments and $p_n^*(E)$ are the normalised orthogonal polynomials They are given by

$$\nu_n^*=N_n \nu_n \qquad p_n^*(E)=N_n p_n(E). \qquad (4.c.8)$$

The convergence of the power series in the expression (4.c.7) for $\rho(E)$ can be enhanced by using a Padé approximant. If the Padé approximant of order (n,n) for $\sum_{k=0}^{\infty} \nu_k^* z^k$ is given by $Q_n(z)/R_n(z)$, where $Q_n(z)=\sum_{k=0}^{n} q_k z^k$ and $R_n(z)=\sum_{k=0}^{n} r_k z^k$, then we have

$$\rho(E)=H(E)[\sum_{k=0}^{n} s_k p_k^*(E)]/[\sum_{k=0}^{n} t_k p_k^*(E)], \qquad (4.c.9)$$

where

$$s_k=\sum_{l=k}^{n}(q_l r_{l-k}-\bar{q}_{l-k} r_{l+2}),$$

$$t_k=\sum_{l=k}^{n} r_{l-k}(r_l-r_{l+2}). \qquad (4.c.10)$$

$r_{n+1}=r_{n+2}=0$ by definition.

In three dimensions one usually has square root type singularities at the band edges. Therefore the shifted Chebyshev polynomials of the second kind are used. With the band edges located at E_a and E_b, the weight function is given by

$$H(E) = \frac{4}{\pi(E_b - E_a)} \left(1 - \left[\frac{2E - (E_a+E_b)}{(E_b - E_a)} \right]^2 \right)^{1/2}. \qquad (4.c.11)$$

The recurrence coefficients for the polynomials are

$$a_n=(E_a+E_b)/2 \; ; \; b_n=(E_b-E_a)^2/16 \quad \text{for all } n. \qquad (4.c.12)$$

The normalisation factors are $N_n=[-4/(E_b-E_a)]^n$ for all n.

We shall use this method in section 5.g in order to calculate the local density of states for the valence band of Si. The results will be compared with those obtained from the quadratic Padé and continued fraction methods.

Chapter 5

Results of local density of states calculations

5.a. Calculation of the moments for some regular and nearly regular lattices

In the case of a regular or nearly regular lattice with a simple model for the interaction between the lattice sites, expressions in closed form for the moments can often be obtained, as we shall see in this section. We use here the tight binding model (Callaway 1964) with the nearest neighbour interaction of the s bond being the only interaction present.

We shall present here a systematic derivation of the expressions for the regular lattices (some of which are found in previous work, e.g. Thorpe 1972), and obtain expressions for the cases of the regular binary alloy and the semi-infinite simple cubic lattice.

First we consider the regular lattices. In such a case the local density of states $n(\vec{r},E)$ is identical to the density of states $n(E)$, and thus the parameter $\vec{r}$ will be omitted as well as the term "local".

The energy is first expressed in terms of the wave vector $\vec{k}$. The Green function can then be expressed in the form (Lukes 1969)

$$G(E)=(1/\Omega_0)\int(E-E(\vec{k}))^{-1}d^3\vec{k} \qquad (5.a.1)$$

Ω_0 denotes the volume of a unit cell in $\vec{k}$-space. The integration is carried out over this unit cell.

Expression (5.a.1) for the Green function is now expanded as a power series in $1/E$ and thus we obtain

$$G(E)=(1/\Omega_0 E)\sum_{n=0}^{\infty}(1/E^n)\int_{\Omega_0} E^n(\vec{k})d^3\vec{k}. \qquad (5.a.2)$$

We recall now the relation between the Green function and the moments (expression (3.b.6)):

$$G(E)=\sum_{n=0}^{\infty}\mu_n/E^{n+1}. \qquad (5.a.3)$$

The comparison between expressions (5.a.2) and (5.a.3) shows that the moments can be expressed as

$$\mu_n=(1/\Omega_0)\int_{\Omega_0} E^n(\vec{k})d^3\vec{k}\ ;\ n=0,1,2,\ldots . \qquad (5.a.4)$$

Expression (5.a.4) serves as the basis for the calculation of the moments. The expression for $E(\vec{k})$ for the regular lattice in question is first obtained, and then the integration of its various powers over the unit cell is carried out. We present here the calculations, carried out this way, for the square lattice and for the diamond lattice. The calculations for the simple cubic, bcc, and fcc lattices can be found in appendix C.

In the case of the square lattice $E(\vec{k})$ is given by

$$E(\vec{k})=2V[\cos(k_x a)+\cos(k_y a)]. \qquad (5.a.5)$$

V is the nearest neighbour interaction energy and a is the lattice constant. The unit cell in $\vec{k}$-space is given by $-\pi/a\leq k_x\leq\pi/a$, $-\pi/a\leq k_y\leq\pi/a$, and thus, for this lattice, $\Omega_0=(2\pi/a)^2$. Therefore we have

$$\mu_n=(a/2\pi)^2(2V)^n\int_{-\frac{\pi}{a}}^{\frac{\pi}{a}}\int_{-\frac{\pi}{a}}^{\frac{\pi}{a}}[\cos(k_x a)+\cos(k_y a)]^n dk_x dk_y. \qquad (5.a.6)$$

By changing variables to $\theta_x=k_x a$ and $\theta_y=k_y a$ we obtain

$$\mu_n=(a/2\pi)^2(2V)^n(1/a^2)\int_{-\pi}^{\pi}\int_{-\pi}^{\pi}(\cos\theta_x+\cos\theta_y)^n d\theta_x d\theta_y=$$

$$(1/4\pi^2)(2V)^n\sum_{m=0}^{n}\binom{n}{m}\int_{-\pi}^{\pi}\int_{-\pi}^{\pi}\cos^m\theta_x\cos^{n-m}\theta_y d\theta_x d\theta_y. \qquad (5.a.7)$$

As we have

$$\int_{-\pi}^{\pi}\cos^n\theta d\theta=\left[\sin\theta\cos^{n-1}\theta\right]_{-\pi}^{\pi}+(n-1)\int_{-\pi}^{\pi}\sin^2\theta\cos^{n-2}\theta d\theta=$$

$$(n-1)\left(\int_{-\pi}^{\pi}\cos^{n-2}\theta d\theta-\int_{-\pi}^{\pi}\cos^n\theta d\theta\right), \qquad (5.a.8)$$

we obtain the recurrence relation

$$\int_{-\pi}^{\pi}\cos^n\theta d\theta=[(n-1)/n]\int_{-\pi}^{\pi}\cos^{n-2}\theta d\theta. \qquad (5.a.9)$$

As $\int_{-\pi}^{\pi}d\theta=2\pi$ and $\int_{-\pi}^{\pi}\cos\theta d\theta=0$, this recurrence relation yields

$$\int_{-\pi}^{\pi}\cos^n\theta d\theta=\begin{cases}0 & \text{for odd } n\\ (1/2^n)\binom{n}{n/2}2\pi & \text{for even } n.\end{cases} \qquad (5.a.10)$$

Thus

$$\int_{-\pi}^{\pi}\cos^{2n}\theta d\theta=(1/4^n)\binom{2n}{n}2\pi \qquad (5.a.11)$$

and

$$\int_{-\pi}^{\pi}\cos^{2n+1}\theta d\theta=0. \qquad (5.a.12)$$

Substitution of (5.a.11) into (5.a.7) yields now

$$\mu_{2n}=(1/4\pi^2)(2V)^{2n}\sum_{m=0}^{n}\binom{2n}{2m}\left[(1/4^m)\binom{2m}{m}2\pi\right]\left[(1/4^{n-m})\binom{2(n-m)}{n-m}2\pi\right]=$$

$$V^{2n}\sum_{m=0}^{n}\binom{2n}{2m}\binom{2m}{m}\binom{2(n-m)}{n-m}=V^{2n}\sum_{m=0}^{n}\left((2n)!/(m!)^2[(n-m)!]^2\right)=$$

$$V^{2n}\binom{2n}{n}\sum_{m=0}^{n}\binom{n}{m}^2=V^{2n}\binom{2n}{n}^2. \qquad (5.a.13)$$

Substitution of (5.a.12) into (5.a.7) obviously yields $\mu_{2n+1}=0$.

If we express the energy in units of V we have thus

$$\mu_{2n}=\binom{2n}{n}^2 \quad ; \quad \mu_{2n+1}=0. \qquad (5.a.14)$$

In the case of the diamond lattice $E(\vec{k})$ is a 2 x 2 matrix, as there are two types of sites (regarding the positions of the nearest neighbours). The first type has the neighbours at (a/4)(1,1,1), (a/4)(1,-1,-1), (a/4)(-1,1,-1), and (a/4)(-1,-1,1). The second type has them at (a/4)(-1,-1,-1), (a/4)(-1,1,1), (a/4)(1,-1,1), and (a/4)(1,1,-1). a is the size of the cubic unit cell, and the site in question is located at (0,0,0). See also Figure 2. The nearest neighbour interaction energy is denoted by V as before.

For the first case we have

$$\begin{aligned}\varepsilon(\vec{k})&=V(\exp[i(k_x+k_y+k_z)a/4]+\exp[i(k_x-k_y-k_z)a/4]+\\
&\exp[i(-k_x+k_y-k_z)a/4]+\exp[i(-k_x-k_y+k_z)a/4])=\\
&2V(\exp(ik_xa/4)\cos[(k_y+k_z)a/4]+2\exp(-ik_xa/4)\cos[(k_y-k_z)a/4])=\\
&2V(\exp(ik_xa/4)[\cos(k_ya/4)\cos(k_za/4)-\sin(k_ya/4)\sin(k_za/4)]+\\
&\exp(-ik_xa/4)[\cos(k_ya/4)\cos(k_za/4)+\sin(k_ya/4)\sin(k_za/4)])=\\
&4V[\cos(k_xa/4)\cos(k_ya/4)\cos(k_za/4)-\\
&i\sin(k_xa/4)\sin(k_ya/4)\sin(k_za/4)]. \qquad (5.a.15)\end{aligned}$$

For the second case it is easily seen that $\varepsilon^*(\vec{k})$ is obtained. Therefore we have

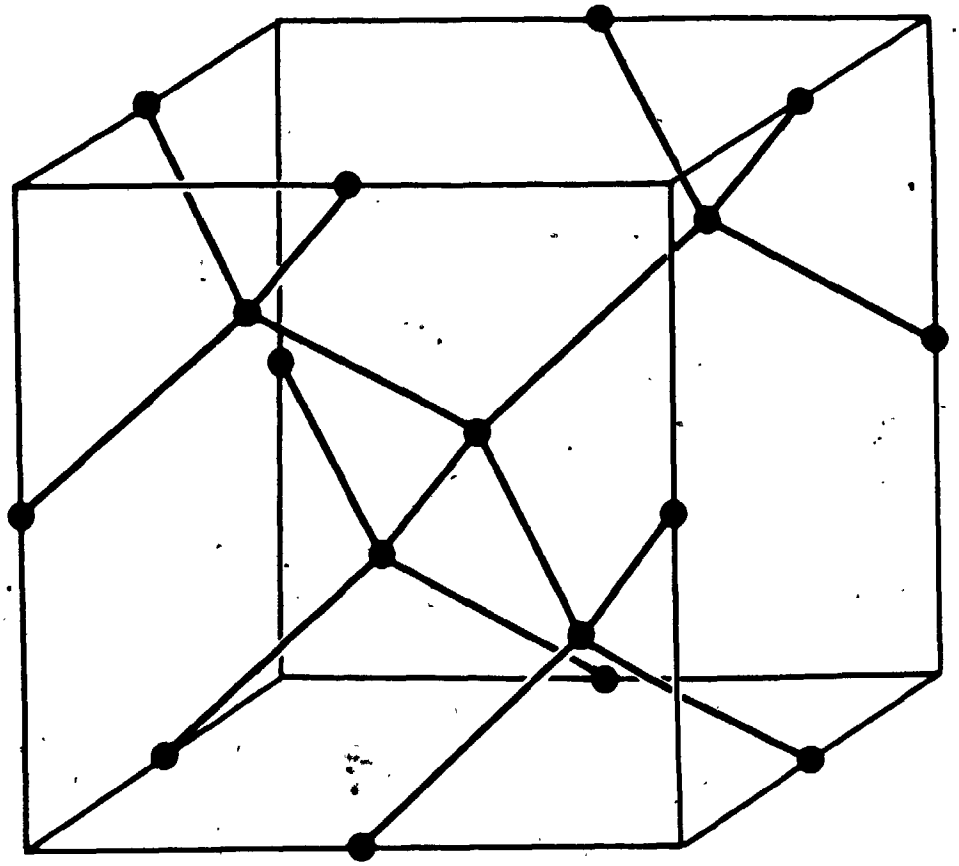

Figure 2

The cubic unit cell used in the treatment of the diamond lattice. It contains 8 lattice sites (depicted by circles) and 16 bonds (depicted by lines connecting the nearest neighbour sites).

$$E(\vec{k}) = \begin{pmatrix} 0 & \varepsilon(\vec{k}) \\ \varepsilon^*(\vec{k}) & 0 \end{pmatrix}. \qquad (5.a.16)$$

The trace of $E^n(\vec{k})$, divided by 2, is $|\varepsilon(\vec{k})|^n$ for even n and 0 for odd n, and we have here

$$|\varepsilon(\vec{k})|^{2n} = (4V)^{2n}[\cos^2(k_x a/4)\cos^2(k_y a/4)\cos^2(k_z a/4) + \sin^2(k_x a/4)\sin^2(k_y a/4)\sin^2(k_z a/4)]^n. \qquad (5.a.17)$$

Using $\theta_x = k_x a/4$, $\theta_y = k_y a/4$, and $\theta_z = k_z a/4$, we obtain

$$\mu_{2n} = (a/2\pi)^3 (4V)^{2n} \int_{-\pi/a}^{\pi/a}\int\int |\varepsilon(\vec{k})|^{2n} dk_x dk_y dk_z = (8/\pi^3)(4V)^{2n} \int_{-\pi/4}^{\pi/4}\int\int (\cos^2\theta_x\cos^2\theta_y\cos^2\theta_z + \sin^2\theta_x\sin^2\theta_y\sin^2\theta_z)^n d\theta_x d\theta_y d\theta_z. \qquad (5.a.18)$$

Using the fact that $\sin\theta = \cos(\pi/2 - \theta)$ and the cosine's periodicity we can rewrite (5.a.18) as

$$\mu_{2n} = (1/8\pi^3)(4V)^{2n} \int_{-\pi}^{\pi}\int_{-\pi}^{\pi}\int_{-\pi}^{\pi} (\cos^2\theta_x\cos^2\theta_y\cos^2\theta_z + \sin^2\theta_x\sin^2\theta_x\sin^2\theta_z)^n d\theta_x d\theta_y d\theta_z. \qquad (5.a.19)$$

Expansion of this expression yields now

$$\mu_{2n} = (1/8\pi^3)(4V)^{2n} \sum_{m=0}^{n} \binom{n}{m} \int_{-\pi}^{\pi}\int_{-\pi}^{\pi}\int_{-\pi}^{\pi} \cos^{2(n-m)}\theta_x \cos^{2(n-m)}\theta_y \cos^{2(n-m)}\theta_z \times \sin^{2m}\theta_x \sin^{2m}\theta_y \sin^{2m}\theta_z d\theta_x d\theta_y d\theta_z. \qquad (5.a.20)$$

Now we can make use of the following:

$$\int_{-\pi}^{\pi} \cos^{2n}\theta \sin^{2m}\theta d\theta = -[1/(2n+1)]\left[\cos^{2n+1}\theta \sin^{2m-1}\theta\right]_{-\pi}^{\pi} + [(2m-1)/(2n+1)] \int_{-\pi}^{\pi} \cos^{2n+2}\theta \sin^{2m-2}\theta d\theta =$$

$$[(2m-1)/(2n+1)]\int_{-\pi}^{\pi}\cos^{2n+2}\theta\sin^{2m-2}\theta d\theta=$$

$$[(2m-1)(2m-3)/(2n+1)(2n+3)]\int_{-\pi}^{\pi}\cos^{2n+4}\theta\sin^{2m-4}\theta d\theta=\ldots=$$

$$[(2m-1)(2m-3)x\ldots x3x1/(2n+1)(2n+3)x\ldots x(2n+2m-1)]\int_{-\pi}^{\pi}\cos^{2n+2m}\theta d\theta=$$

$$([1x3x\ldots x(2m-3)(2m-1)][1x3x\ldots x(2n-3)(2n-1)]/[1x3x\ldots x$$

$$(2n+2m-3)(2n+2m-1)])\int_{-\pi}^{\pi}\cos^{2(n+m)}\theta d\theta=$$

$$((2m)!(2n)!(n+m)!2^{n+m}/m!2^{m}n!2^{n}[2(n+m)]!)\int_{-\pi}^{\pi}\cos^{2(n+m)}\theta d\theta=$$

$$((2m)!(2n)!(n+m)!/m!n![2(n+m)]!)\int_{-\pi}^{\pi}\cos^{2(n+m)}\theta d\theta. \qquad (5.a.21)$$

Using (5.a.11) we have

$$\int_{-\pi}^{\pi}\cos^{2(n+m)}\theta d\theta=(1/4^{n+m})\binom{2(n+m)}{n+m}2\pi=$$

$$([2(n+m)]!/4^{n+m}[(n+m)!]^{2})2\pi, \qquad (5.a.22)$$

and thus we have

$$\int_{-\pi}^{\pi}\cos^{2n}\theta\sin^{2m}\theta d\theta=[(2m)!(2n)!/4^{n+m}m!n!(n+m)!]2\pi. \qquad (5.a.23)$$

Therefore we also have

$$\int_{-\pi}^{\pi}\cos^{2(n-m)}\theta\sin^{2m}\theta d\theta=((2m)![2(n-m)]!/4^{n}m!n!(n-m)!)2\pi. \qquad (5.a.24)$$

Using (5.a.24), the expression (5.a.20) for μ_{2n} becomes

$$\mu_{2n}=(1/8\pi^{3})(4V)^{2n}\sum_{m=0}^{n}\binom{n}{m}(((2m)![2(n-m)]!/4^{n}m!n!(n-m)!)2\pi)^{3}=$$

$$V^{2n}\sum_{m=0}^{n}([(2m)!]^{3}([2(n-m)]!)^{3}/4^{n}(m!)^{4}(n!)^{2}[(n-m)!]^{4})=$$

$$V^{2n}\sum_{m=0}^{n}([(2n)!]^{2}/4^{n}(n!)^{4})((n!)^{2}/(m!)^{2}[(n-m)!]^{2})[(2m)!/(m!)^{2}]x$$

$$([2(n-m)]!/[(n-m)!]^2)([(2m)!]^2([2(n-m)]!)^2/[(2n)!]^2)=$$

$$V^{2n}(1/4^n)\binom{2n}{n}^2\sum_{m=0}^{n}[\binom{n}{m}^2\binom{2m}{m}\binom{2(n-m)}{n-m}/\binom{2n}{2m}^2]. \qquad (5.a.25)$$

It turns out that this can be also written in a simpler form:

$$\mu_{2n}=V^{2n}\sum_{m=0}^{n}\binom{n}{m}^2\binom{2m}{m}\binom{2(n-m)}{n-m}. \qquad (5.a.26)$$

With the energy expressed in units of V we have thus

$$\mu_{2n}=\sum_{m=0}^{n}\binom{n}{m}^2\binom{2m}{m}\binom{2(n-m)}{n-m} \; ; \; \mu_{2n+1}=0. \qquad (5.a.27)$$

Expressing the energy in units of V, we obtain in a similar manner the following formulae:

The moments for the simple cubic lattice:

$$\mu_{2n}=\binom{2n}{n}\sum_{m=0}^{n}\binom{2m}{m}\binom{n}{m}^2 \; ; \; \mu_{2n+1}=0. \qquad (5.a.28)$$

The moments for the body centred cubic (bcc) lattice:

$$\mu_{2n}=\binom{2n}{n}^3 \; ; \; \mu_{2n+1}=0. \qquad (5.a.29)$$

The moments for the face centred cubic (fcc) lattice:

$$\mu_{2n}=\sum_{m=0}^{n}\sum_{l=0}^{m}\binom{2(n-m+1)}{n-m+1}\binom{2m}{m}\binom{2(n-1)}{n-1}\binom{2n}{2m}\binom{2m}{2l} \; ;$$

$$\mu_{2n+1}=\sum_{m=1}^{n}\sum_{l=1}^{m}\binom{2(n-m+1)}{n-m+1}\binom{2m}{m}\binom{2(n-l+1)}{n-l+1}\binom{2n+1}{2m}\binom{2m}{2l-1}. \qquad (5.a.30)$$

The derivation of these formulae can be found in appendix C.

The expressions we have obtained for the moments are with the self-energies of the lattice sites set at zero. If we set the self-energies at E_0 instead, i.e. change the reference point for measuring the energy, then the moments change as well. The new moments are, however, easily obtained from the original ones.

Let the original moments are denoted by (cf. (3.b.5))

$$\eta_n=\langle\vec{r}|H^n|\vec{r}\rangle \; ; \; n=0,1,2,\ldots \; . \qquad (5.a.31)$$

If we change the self-energies from 0 to E_0, this means that we change the Hamiltonian from H to $H+E_0$. The new moments are thus

$$\mu_n=\langle\vec{r}|(H+E_0)^n|\vec{r}\rangle=\langle\vec{r}|\sum_{m=0}^{n}\binom{n}{m}H^m E_0^{n-m}|\vec{r}\rangle=\sum_{m=0}^{n}\binom{n}{m}E_0^{n-m}\langle\vec{r}|H^m|\vec{r}\rangle=$$

$$\sum_{m=0}^{n}\binom{n}{m}E_0^{n-m}\eta_m . \qquad (5.a.32)$$

This is true for any set of moments, and not only for the cases of the regular lattices given above.

We look now at the case of a regular binary alloy on a regular lattice. In such a binary alloy there are two types of atoms with self-energies E_1 and E_2. All the nearest neighbours of each atom are of the opposite type. Such a binary alloy can exist on a regular lattice, if and only if each closed path, going out from any lattice site and returning to the same site, has an even number of "steps". Thus such a regular binary alloy can exist on any of the above mentioned regular lattices except for the face centred cubic lattice.

The Hamiltonian of the regular binary alloy can be written as H=D+W, where W is the Hamiltonian of the corresponding regular lattice, and D (in matrix representation) is a diagonal matrix. $D_{j,j}$ is equal to E_1 or E_2 according to the type of the corresponding site j. Let $|V_n\rangle$ denote $H^n|\vec{r}\rangle$ and $|W_n\rangle$ denote $W^n|\vec{r}\rangle$, where $\vec{r}$ is the site for which the moments are to be calculated.

$|V_n\rangle$ can be expressed as a linear combination of $|W_j\rangle$, j=0,1,2,...,n:

$$|V_n\rangle = E_1^{\,n}|W_0\rangle + \sum_{m=1}^{\text{int.}(n/2)} \Big[\sum_{l=0}^{n-2m} \binom{n-m-1}{m}\binom{m+l-1}{m-1} E_1^{\,n-2m-l} E_2^{\,l} \Big] |W_{2m}\rangle + \sum_{m=1}^{\text{int.}((n+1)/2)} \Big[\sum_{l=0}^{n+1-2m} \binom{n-m-1}{m-1}\binom{m+l-1}{m-1} E_1^{\,n+1-2m-l} E_2^{\,l} \Big] |W_{2m-1}\rangle . \tag{5.a.33}$$

This formula will be proven by induction.

For n=0 we have $|V_0\rangle = |W_0\rangle = |\vec{r}\rangle$, and thus expression (5.a.33) is valid. Now we assume, that the expression (5.a.33) is valid for j=0,1,2,...,n. Its validity for j=n+1 is to be proven.

We have the relation

$$|V_{n+1}\rangle = H|V_n\rangle = (D+W)|V_n\rangle . \tag{5.a.34}$$

As mentioned above, a regular binary alloy can exist only on a lattice on which a path going from site to site (random walk) can return to its starting site only in an even number of "steps". For such a lattice only the even numbered regular moments are non-zero. $|W_{2n}\rangle = W^{2n}|\vec{r}\rangle$ will be then a linear combination of sites separated from $\vec{r}$ by an even number (2n) of "steps" (of any possible path combining them with $\vec{r}$), and thus of the same type as $\vec{r}$ on the binary alloy. $|W_{2n+1}\rangle$ will be a linear combination of sites of the opposite type only.

$\vec{r}$ is assumed to be of type E_1. Thus D acting on $|W_{2n}\rangle$ will simply multiply it by E_1. D acting on $|W_{2n+1}\rangle$ will multiply it by E_2. Using this information we have

$$|V_{n+1}\rangle = (D+W)|V_n\rangle = (D+W)\Big(E_1^{\,n}W_0 + \sum_{m=1}^{\text{int.}(n/2)} \Big[\sum_{l=0}^{n-2m} \binom{n-m-1}{m}\binom{m+l-1}{m-1} E_1^{\,n-2m-l} E_2^{\,l} \Big] |W_{2m}\rangle +$$

$$\sum_{m=1}^{\text{int.}((n+1)/2)}\Big[\sum_{l=0}^{n+1-2m}\binom{n-m-1}{m-1}\binom{m+l-1}{m-1}E_1^{\,n+1-2m-l}E_2^{\,l}\Big]|W_{2m-1}\rangle=$$

$$(E_1+W)(E_1^{\,n}|W_0\rangle+\sum_{m=1}^{\text{int.}(n/2)}\Big[\sum_{l=0}^{n-2m}\binom{n-m-1}{m}\binom{m+l-1}{m-1}E_1^{\,n-2m-l}E_2^{\,l}\Big]|W_{2m}\rangle)+$$

$$(E_2+W)(\sum_{m=1}^{\text{int.}((n+1)/2)}\Big[\sum_{l=0}^{n+1-2m}\binom{n-m-1}{m-1}\binom{m+l-1}{m-1}E_1^{\,n+1-2m-l}E_2^{\,l}\Big]|W_{2m-1}\rangle)=$$

$$E_1^{\,n}|W_1\rangle+E_1^{\,n+1}|W_0\rangle+$$

$$\sum_{m=1}^{\text{int.}(n/2)}\Big[\sum_{l=0}^{n-2m}\binom{n-m-1}{m}\binom{m+l-1}{m-1}E_1^{\,n-2m-l}E_2^{\,l}\Big]|W_{2m+1}\rangle+$$

$$\sum_{m=1}^{\text{int.}(n/2)}\Big[\sum_{l=0}^{n-2m}\binom{n-m-1}{m}\binom{m+l-1}{m-1}E_1^{\,n+1-2m-l}E_2^{\,l}\Big]|W_{2m}\rangle+$$

$$\sum_{m=1}^{\text{int.}((n+1)/2)}\Big[\sum_{l=0}^{n+1-2m}\binom{n-m-1}{m-1}\binom{m+l-1}{m-1}E_1^{\,n+1-2m-l}E_2^{\,l}\Big]|W_{2m}\rangle+$$

$$\sum_{m=1}^{\text{int.}((n+1)/2)}\Big[\sum_{l=0}^{n+1-2m}\binom{n-m-1}{m-1}\binom{m+l-1}{m-1}E_1^{\,n+1-2m-l}E_2^{\,l+1}\Big]|W_{2m-1}\rangle. \tag{5.a.35}$$

We can further simplify now:

$$E_1^{\,n+1}|W_0\rangle+\sum_{m=1}^{\text{int.}(n/2)}\Big[\sum_{l=0}^{n-2m}\binom{n-m-1}{m}\binom{m+l-1}{m-1}E_1^{\,n+1-2m-l}E_2^{\,l}\Big]|W_{2m}\rangle+$$

$$\sum_{m=1}^{\text{int.}((n+1)/2)}\Big[\sum_{l=0}^{n+1-2m}\binom{n-m-1}{m-1}\binom{m+l-1}{m-1}E_1^{\,n+1-2m-l}E_2^{\,l}\Big]|W_{2m}\rangle=$$

$$E_1^{\,n+1}|W_0\rangle+\sum_{m=1}^{\text{int.}(n/2)}\Big(\sum_{l=0}^{n+1-2m}\Big[\binom{n-m-1}{m}+\binom{n-m-1}{m-1}\Big]x$$

$$\binom{m+l-1}{m-1}E_1^{\,n+1-2m-l}E_2^{\,l}\Big)|W_{2m}\rangle+|\varepsilon\rangle=$$

$$E_1^{\,n+1}|W_0\rangle+\sum_{m=1}^{\text{int.}(n/2)}\Big[\sum_{l=0}^{n+1-2m}\binom{n+1-m-1}{m}x$$

$$\binom{m+l-1}{m-1}E_1^{\,n+1-2m-l}E_2^{\,l}\Big]|W_{2m}\rangle+|\varepsilon\rangle=$$

$$E_1^{\,n+1}|W_0\rangle+\sum_{m=1}^{\text{int.}((n+1)/2)}\Big[\sum_{l=0}^{n+1-2m}\binom{n+1-m-1}{m}x$$

$$\binom{m+l-1}{m-1}E_1^{\,n+1-2m-l}E_2^{\,l}\Big]|W_{2m}\rangle. \tag{5.a.36}$$

Explanation: $|\varepsilon\rangle$ is defined to be 0 if n is even and $|W_{n+1}\rangle$ if n

is odd. For $l=n+1-2m$ we have $\binom{n-m-1}{m}=\binom{m-1}{m}=0$, and thus no problem arises from this additional term. If n is even, then we have int.(n/2)=int.((n+1)/2), and thus no problem arises from the change in the upper limit of the first summation. If n is odd, then for m=int.((n+1)/2) n+1-2m=0, and the extra term in the sum is $|W_{n+1}>$. This is also the extra term in the new sum, where int.(n/2) is replaced by int.((n+1)/2). Besides, the theorem $\binom{n}{m-1}+\binom{n}{m}=\binom{n+1}{m}$ has been used here.

We can also simplify:

$$
\begin{aligned}
&E_1^n|W_1>+\sum_{m=1}^{\text{int.}(n/2)}\Big[\sum_{l=0}^{n-2m}\binom{n-m-1}{m}\binom{m+l-1}{m-1}E_1^{n-2m-l}E_2^{l}\Big]|W_{2m+1}>+\\
&\sum_{m=1}^{\text{int.}((n+1)/2)}\Big[\sum_{l=0}^{n+1-2m}\binom{n-m-1}{m-1}\binom{m+l-1}{m-1}E_1^{n+1-2m-l}E_2^{l+1}\Big]|W_{2m-1}>=\\
&E_1^n|W_1>+\sum_{m=2}^{\text{int.}((n+2)/2)}\Big[\sum_{l=0}^{n+2-2m}\binom{n+1-m-1}{m-1}\times\\
&\binom{m+l-2}{m-2}E_1^{n+2-2m-l}E_2^{l}\Big]|W_{2m-1}>+\\
&\sum_{m=1}^{\text{int.}((n+1)/2)}\Big[\sum_{l=0}^{n+2-2m}\binom{n+1-m-1}{m-1}\binom{m+l-2}{m-1}E_1^{n+2-2m-l}E_2^{l}\Big]|W_{2m-1}>=\\
&\sum_{m=1}^{\text{int.}((n+2)/2)}\Big[\sum_{l=0}^{n+2-2m}\binom{n+1-m-1}{m-1}\binom{m+l-2}{m-2}E_1^{n+2-2m-l}E_2^{l}\Big]|W_{2m-1}>+\\
&\sum_{m=1}^{\text{int.}((n+2)/2)}\Big[\sum_{l=0}^{n+2-2m}\binom{n+1-m-1}{m-1}\binom{m+l-2}{m-1}E_1^{n+2-2m-l}E_2^{l}\Big]|W_{2m-1}>=\\
&\sum_{m=1}^{\text{int.}((n+2)/2)}\Big(\sum_{l=0}^{n+2-2m}\binom{n+1-m-1}{m-1}\Big[\binom{m+l-2}{m-2}+\binom{m+l-2}{m-1}\Big]\times\\
&E_1^{n+2-2m-l}E_2^{l}\Big)|W_{2m-1}>=\\
&\sum_{m=1}^{\text{int.}((n+2)/2)}\Big[\sum_{l=0}^{n+2-2m}\binom{n+1-m-1}{m-1}\binom{m+l-1}{m-1}E_1^{n+2-2m-l}E_2^{l}\Big]|W_{2m-1}>.
\end{aligned}
\tag{5.a.37}
$$

Explanation: In the first sum m is replaced by m-1. In the second sum l is replaced by l-1. The extra terms of l=0 cause no prob-

lem, as $\binom{m-2}{m-1}=0$ for all m. In the first sum, when m=1, we have $\binom{m+l-2}{m-2}=0$ for all l≠0. For l=0 $\binom{m+l-2}{m-2}=\binom{-1}{-1}=1$. Thus for m=1 the whole sum (over l) becomes $E_1^n|W_1>$. In the other sum, when int.((n+1)/2) is replaced by int.((n+2)/2), no change occurs, because even for an even n, when m=int.((n+2)/2), then only l=0 appears in the second summation, and $\binom{m-2}{m-1}=0$. Finally the theorem $\binom{n}{m-1}+\binom{n}{m}=\binom{n+1}{m}$ is used.

Using these results we have

$$|V_{n+1}>=E_1^{n+1}|W_0>+\sum_{m=1}^{\text{int.}((n+1)/2)}\left[\sum_{l=0}^{n+1-2m}\binom{n+1-m-1}{m}x\right.$$
$$\left.\binom{m+l-1}{m-1}E_1^{n+1-2m-l}E_2^{l}\right]|W_{2m}>+$$
$$\sum_{m=1}^{\text{int.}((n+2)/2)}\left[\sum_{l=0}^{n+2-2m}\binom{n+1-m-1}{m-1}\binom{m+l-1}{m-1}E_1^{n+2-2m-l}E_2^{l}\right]|W_{2m-1}>. \qquad (5.a.38)$$

This completes the proof by induction.

If the moments of the regular lattice are denoted by η_n, and those of the binary alloy by μ_n, then we have

$$\eta_n=<\vec{r}|W^n|\vec{r}>=<\vec{r}|W_n> \; ; \; \mu_n=<\vec{r}|H^n|\vec{r}>=<\vec{r}|V_n>. \qquad (5.a.39)$$

$\eta_n=0$ for odd n, and therefore the expression (5.a.33) for $|V_n>$ yields

$$\mu_n=E_1^n\eta_0+\sum_{m=1}^{\text{int.}(n/2)}\left[\sum_{l=0}^{n-2m}\binom{n-m-1}{m}\binom{m+l-1}{m-1}E_1^{n-2m-l}E_2^{l}\right]\eta_{2m}. \qquad (5.a.40)$$

If $\vec{r}$ is of type E_2, the same expression still holds, but with E_1 and E_2 interchanged.

Now we turn our attention to the case of the semi-infinite simple cubic lattice. The nearest neighbour interaction is denoted by V.

Here the full periodicity is not present any more. Therefore the method used for the bulk regular lattice can not be used here. A different method is used instead. The lattice sites are placed on a three dimensional infinite grid. The site at (0,0,0) is used as $\vec{r}$ for calculating $H^n|\vec{r}>$ for n=0,1,2,... . For a given n, if the site at (i,j,k) is denoted by |i,j,k>, then we have

$$H^n|0,0,0>=V\sum_i\sum_j\sum_k a^n_{i,j,k}|i,j,k>\ ;$$

$$a^n_{i,j,k}=\sum_{m=0}^{n}\sum_{l=0}^{m}\binom{n}{m}\binom{m}{l}\binom{l}{(l+i)/2}\binom{m-l}{(m-l+j)/2}\binom{n-m}{(n-m+k)/2}. \qquad (5.a.41)$$

$\binom{n}{m}=0$ by definition for m<0, m>n, and non-integer m.

This will be proven by induction. For n=0 it is trivial. As

$$H|i,j,k>=V(|i-1,j,k>+|i+1,j,k>+|i,j-1,k>+|i,j+1,k>+$$
$$|i,j,k-1>+|i,j,k+1>), \qquad (5.a.42)$$

we also have

$$a^{n+1}_{i,j,k}=a^n_{i-1,j,k}+a^n_{i+1,j,k}+a^n_{i,j-1,k}+a^n_{i,j+1,k}+a^n_{i,j,k-1}+a^n_{i,j,k+1} \qquad (5.a.43)$$

By using the theorem $\binom{n}{m-1}+\binom{n}{m}=\binom{n+1}{m}$ we obtain

$$\binom{l}{(l+i-1)/2}+\binom{l}{(l+i+1)/2}=\binom{l+1}{(l+1+i)/2}\ ;$$

$$\binom{m-l}{(m-l+j-1)/2}+\binom{m-l}{(m-l+j+1)/2}=\binom{m+1-l}{(m+1-l+j)/2}\ ;$$

$$\binom{n-m}{(n-m+k-1)/2}+\binom{n-m}{(n-m+k+1)/2}=\binom{n+1-m}{(n+1-m+k)/2}. \qquad (5.a.44)$$

Therefore we have

$$a^n_{i-1,j,k}+a^n_{i+1,j,k}=$$

$$\sum_{m=0}^{n}\sum_{l=0}^{m}\binom{n}{m}\binom{m}{l}\binom{l+1}{(l+i+1)/2}\binom{m-l}{(m-l+j)/2}\binom{n-m}{(n-m+k)/2}=$$

$$\sum_{m=0}^{n}\sum_{l=0}^{m+1}\binom{n}{m}\binom{m}{l-1}\binom{l}{(l+i)/2}\binom{m+1-l}{(m+1-l+j)/2}\binom{n-m}{(n-m+k)/2}=$$

$$\sum_{m=0}^{n+1}\sum_{l=0}^{m}\binom{n}{m-1}\binom{m-1}{l-1}\binom{l}{(l+i)/2}\binom{m-l}{(m-l+j)/2}\binom{n+1-m}{(n+1-m+k)/2}. \qquad (5.a.45)$$

Explanation: In the first step l is replaced by l-1. As $\binom{m}{-1}=0$, the extra l=0 terms cause no change. In the second step m is replaced by m-1. As $\binom{n}{-1}=0$, the extra m=0 term causes no change either.

We also have

$$a^n_{i,j-1,k}+a^n_{i,j+1,k}=$$

$$\sum_{m=0}^{n}\sum_{l=0}^{m}\binom{n}{m}\binom{m}{l}\binom{l}{(l+i)/2}\binom{m+1-l}{(m+1-l+j)/2}\binom{n-m}{(n-m+k)/2}=$$

$$\sum_{m=0}^{n+1}\sum_{l=0}^{m}\binom{n}{m-1}\binom{m-1}{l}\binom{l}{(l+i)/2}\binom{m-l}{(m-l+j)/2}\binom{n+1-m}{(n+1-m+k)/2}. \qquad (5.a.46)$$

Explanation: m is replaced by m-1. The l=m extra terms cause no change, as $\binom{m-1}{m}=0$. The m=0 extra term causes no change as $\binom{n}{-1}=0$.

We also have

$$a^n_{i,j,k-1}+a^n_{i,j,k+1}=$$

$$\sum_{m=0}^{n}\sum_{l=0}^{m}\binom{n}{m}\binom{m}{l}\binom{l}{(l+i)/2}\binom{m-l}{(m-l+j)/2}\binom{n+1-m}{(n+1-m+k)/2}=$$

$$\sum_{m=0}^{n+1}\sum_{l=0}^{m}\binom{n}{m}\binom{m}{l}\binom{l}{(l+i)/2}\binom{m-l}{(m-l+j)/2}\binom{n+1-m}{(n+1-m+k)/2}. \qquad (5.a.47)$$

Explanation: The m=n+1 extra term causes no change, as $\binom{n}{n+1}=0$.

Now we have

$$\binom{n}{m-1}\binom{m-1}{l-1}+\binom{n}{m-1}\binom{m-1}{l}+\binom{n}{m}\binom{m}{l}=\binom{n}{m-1}\binom{m}{l}+\binom{n}{m}\binom{m}{l}=\binom{n+1}{m}\binom{m}{l}. \quad (5.a.48)$$

Using this result and adding the previous three expressions we obtain

$$a^{n+1}_{i,j,k}=\sum_{m=0}^{n+1}\sum_{l=0}^{m}\binom{n+1}{m}\binom{m}{l}\binom{l}{(l+i)/2}\binom{m-l}{(m-l+j)/2}\binom{n+1-m}{(n+1-m+k)/2}. \quad (5.a.49)$$

This completes the proof by induction.

If the surface is at k=0, then for the N^{th} layer (the surface being the first layer, i.e. N=1) we have

$$H^n|0,0,N-1\rangle=V^n\sum_i\sum_j\sum_k b^{n,N}_{i,j,k}|i,j,k\rangle \ ;$$

$$b^{n,N}_{i,j,k}=a^n_{i,j,k+1-N}-a^n_{i,j,k+1+N}. \quad (5.a.50)$$

This can be proven as follows. For n=0 this is trivial. For k>0 the recurrence relation for the $b^{n,N}_{i,j,k}$ is the same as for the $a^n_{i,j,k}$, so that there is no problem. For k=0 we have

$$b^{n,N}_{i,j,k-1}=b^{n,N}_{i,j,-1}=a^n_{i,j,-N}-a^n_{i,j,N}=0. \quad (5.a.51)$$

Thus the original recurrence relation still can be used, and the proof by induction is valid as before.

The n^{th} moment for a site in the N^{th} layer is

$$\mu_{n,N}=\langle 0,0,N-1|H^n|0,0,N-1\rangle=b^{n,N}_{0,0,N-1}V^n=(a^n_{0,0,0}-a^n_{0,0,2N})V^n. \quad (5.a.52)$$

However, we have

$$a^n_{0,0,0}=\sum_{m=0}^{n}\sum_{l=0}^{m}\binom{n}{m}\binom{m}{l}\binom{l}{l/2}\binom{m-l}{(m-l)/2}\binom{n-m}{(n-m)/2}. \quad (5.a.53)$$

As l has to be even to have $a^n_{0,0,0}\neq 0$, so has m, and thus so has also n. Thus we have

$$a^{2n}_{0,0,0} = \sum_{m=0}^{n} \sum_{l=0}^{m} \binom{2n}{2m}\binom{2m}{2l}\binom{2l}{l}\binom{2(m-1)}{m-1}\binom{2(n-m)}{n-m} \; ; \; a^{2n+1}_{0,0,0}=0. \qquad (5.a.54)$$

However, we have

$$\binom{2m}{2l}\binom{2l}{l}\binom{2(m-1)}{m-1} =$$

$$(2m)!(2l)![2(m-1)]!/(2l)![2(m-1)]!(l!)^2[(m-1)!]^2 =$$

$$(2m)!(m!)^2/(m!)^2(l!)^2[(m-1)!]^2 = \binom{2m}{m}\binom{m}{l}^2 \qquad (5.a.55)$$

and

$$\sum_{l=0}^{m} \binom{m}{l}^2 = \binom{2m}{m}. \qquad (5.a.56)$$

Thus we have

$$a^{2n}_{0,0,0} = \sum_{m=0}^{n} \binom{2n}{2m}\binom{2m}{m}^2\binom{2(n-m)}{n-m} =$$

$$\sum_{m=0}^{n} ((2n)![(2m)!]^2[2(n-m)]!/(2m)![2(n-m)]!(m!)^4[(n-m)!]^2) =$$

$$\sum_{m=0}^{n} ((2n)!(2m)!(n!)^2/(n!)^2(m!)^2(m!)^2[(n-m)!]^2) =$$

$$\binom{2n}{n}\sum_{m=0}^{n}\binom{2m}{m}\binom{n}{m}^2. \qquad (5.a.57)$$

This is the familiar expression for u_{2n} (for the ordinary simple cubic lattice), when E is expressed in units of V, as expected.

We also have

$$a^{n}_{0,0,2N} = \sum_{m=0}^{n} \sum_{l=0}^{m} \binom{n}{m}\binom{m}{l}\binom{l}{l/2}\binom{m-1}{(m-1)/2}\binom{n-m}{(n-m+2N)/2}. \qquad (5.a.58)$$

$a^{n}_{0,0,0} \neq 0$ for even n only for the same reasons as before. Using the previous results we have thus

$$a^{2n}_{0,0,2N} = \sum_{m=0}^{n} \binom{2n}{2m}\binom{2m}{m}^2\binom{2(n-m)}{n-m+N}. \qquad (5.a.59)$$

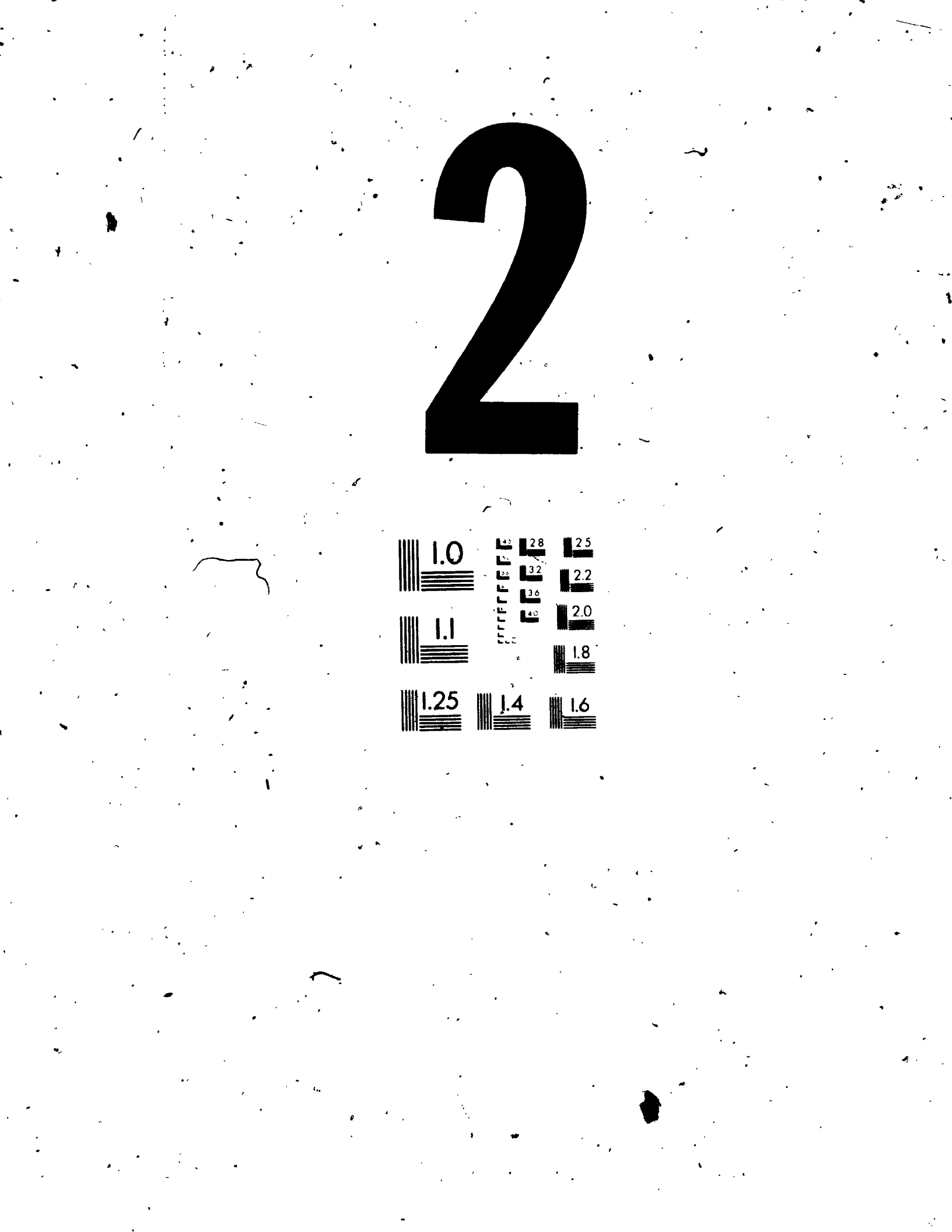
2
1.0
1.1
1.25
1.4
1.6
2.0
1.8
2.2
2.5
2.8
3.2
3.6
4.0

However, we have

$$\binom{2(n-m)}{n-m+N}=\binom{2(n-m)}{n-m}\Big[\prod_{i=1}^{N}(n-m+1-i)\Big/\prod_{i=1}^{N}(n-m+i)\Big]. \qquad (5.a.60)$$

Using this we obtain

$$\mu_{2n,N}=a^{2n}_{0,0,0}-a^{2n}_{0,0,2N}=\sum_{m=0}^{n}\binom{2n}{2m}\binom{2m}{m}^2\binom{2(n-m)}{n-m}\times$$
$$\Big(1-\Big[\prod_{i=1}^{N}(n-m+1-i)\Big/\prod_{i=1}^{N}(n-m+i)\Big]\Big)=$$
$$\binom{2n}{n}^2\sum_{m=0}^{n}\binom{2m}{m}\binom{n}{m}^2\Big(1-\Big[\prod_{i=1}^{N}(n-m+1-i)\Big/\prod_{i=1}^{N}(n-m+i)\Big]\Big)\ ;$$

$$\mu_{2n+1,N}=a^{2n+1}_{0,0,0}-a^{2n+1}_{0,0,2N}=0, \qquad (5.a.61)$$

when E is expressed in units of V.

This completes our discussion of the analytical calculation of moments. We shall use the results obtained here in the next two sections in order to calculate the local density of states from the moments for the lattices discussed in this section.

5.b. The local density of states for the lattices discussed in section 5.a. as obtained by using the quadratic Padé approximant

We present here the results obtained for the local density of states for the various cases discussed in the previous section by using the quadratic Padé approximant method. In each case the moments have been first calculated by using the relevant analytical expression from section 5.a. Then the quadratic Padé approximant of some order N has been calculated, as outlined in section 2.c, and finally the local density of states has been found from the quadartic Padé polynomials, as outlined in section 3.b. The value of N (the order of the quadratic Padé approximant) was usually between 14 and 16.

In the cases of the square, simple cubic, body centred cubic, and diamond lattices, only the even numbered moments are non-zero. therefore expression (3.b.18) has been used for calculating the local density of states. The energy is expressed in each case in terms of the nearest neighbour interaction energy V. As expression (3.b.18) is not accurate near E=0, the values of the density of states for $|E|<\varepsilon$ have been approximated by the value for $E=\varepsilon$, where ε is typically equal to 0.1 or less (in units of V).

The results for the square lattice, simple cubic lattice, body centred cubic lattice, and diamond lattice, can be seen in Figures 3, 4, 5, and 6 respectively. All the results shown are for order N=16. The exact results are represented by dashed lines. They have been obtained as explained in section 5.d.

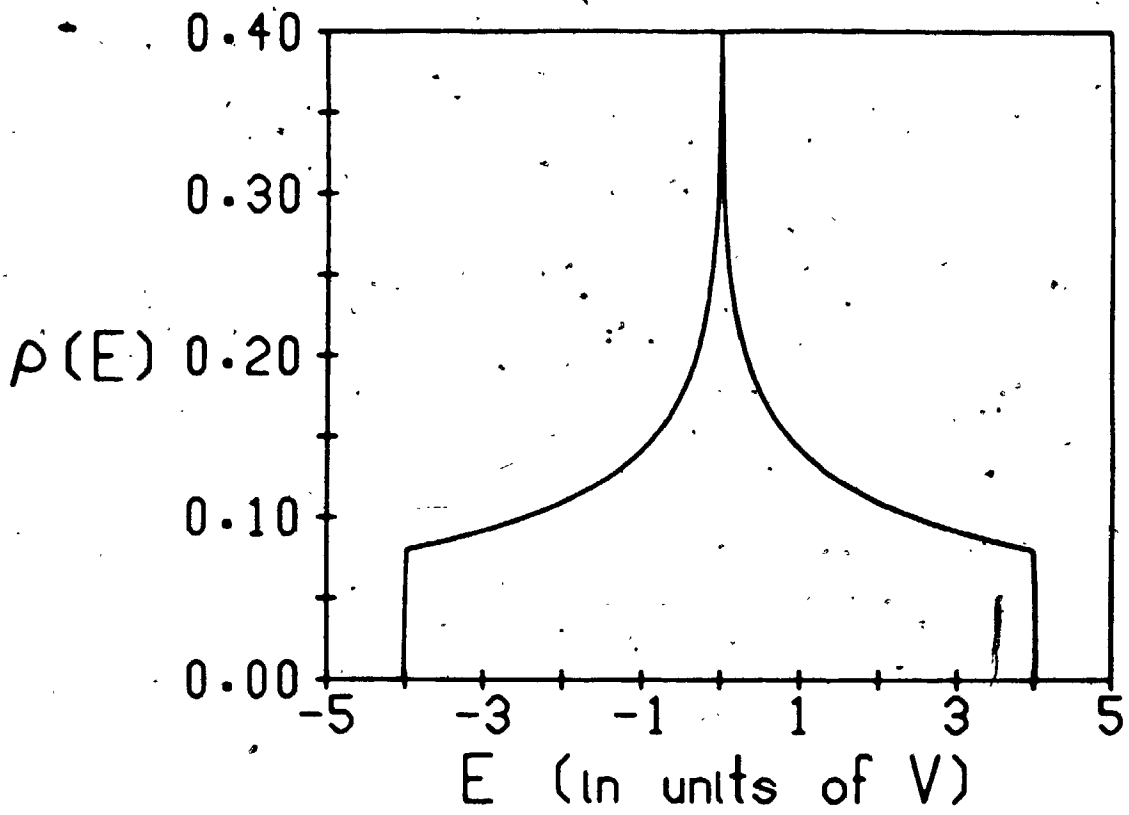

Figure 3

The density of states for the square lattice, as obtained from the order N=16 quadratic Pade approximant. V is the nearest neighbour interaction energy.

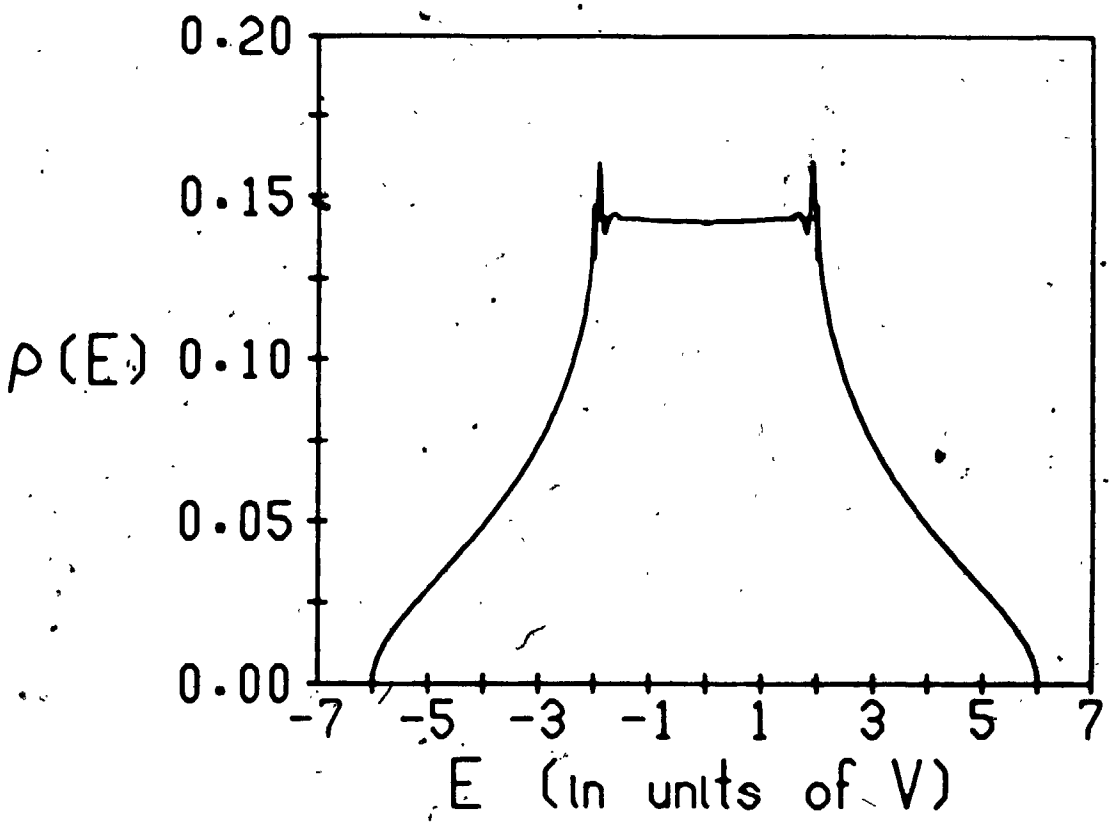

Figure 4

The density of states for the simple cubic lattice, as obtained from the order N=16 quadratic Padé approximant. The exact results are represented by dashed lines. V is the nearest neighbour interaction energy.

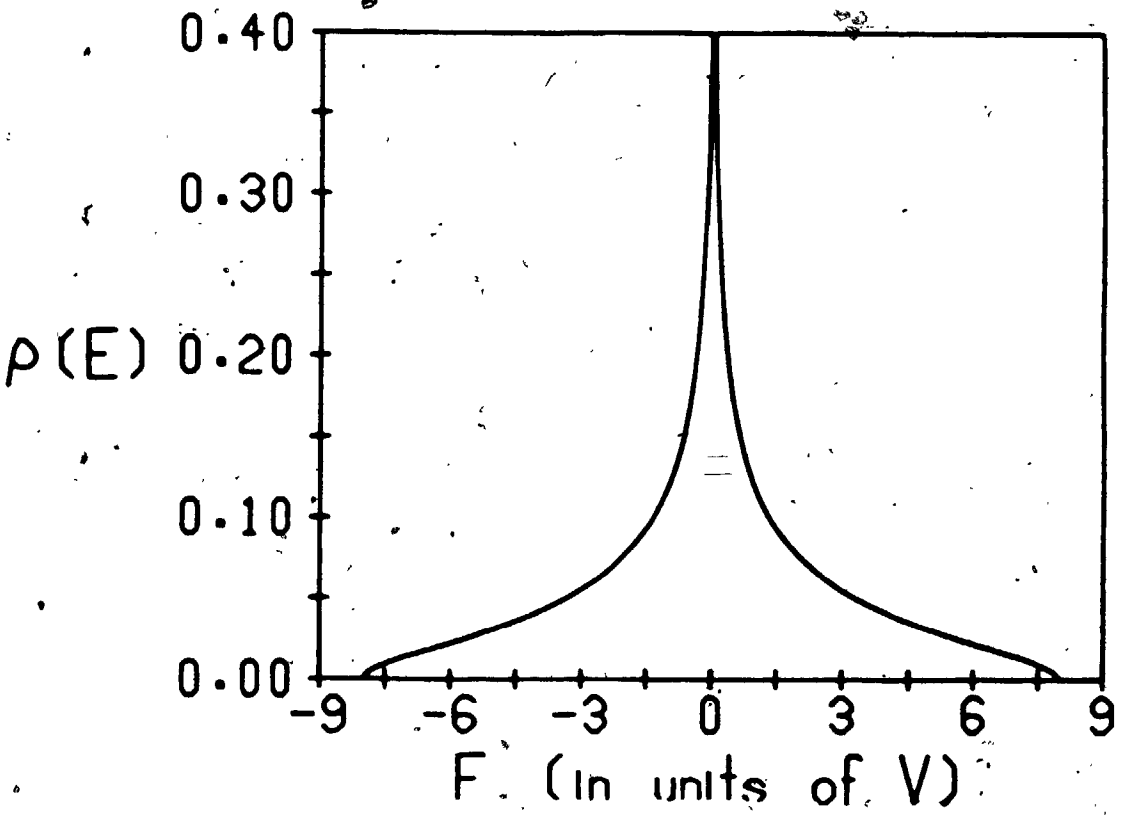

Figure 5

The density of states for the body centred cubic lattice, as obtained from the order N=16 quadratic Padé approximant. V is the nearest neighbour interaction energy.

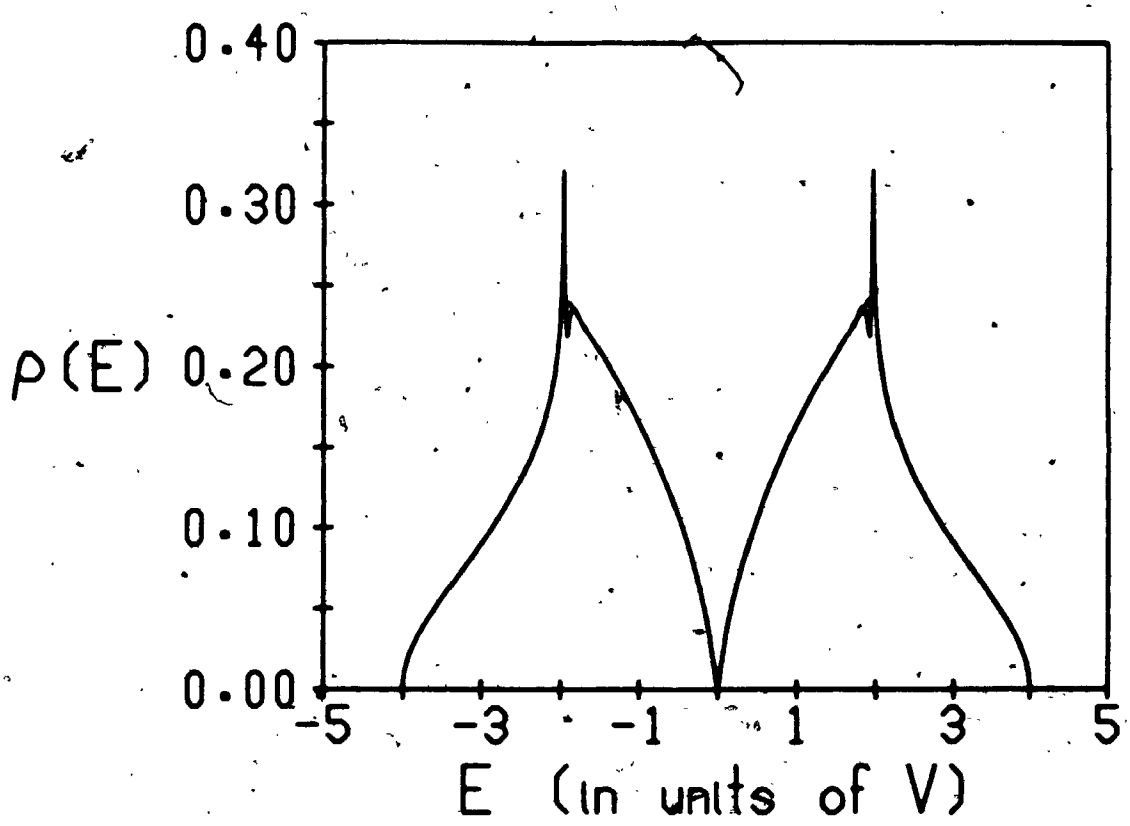

Figure 6

The density of states for the diamond lattice, as obtained from the order N=16 quadratic Padé approximant. The exact results are represented by dashed lines. V is the nearest neighbour interaction energy.

In the case of the face centred cubic lattice all the moments except for the second moment (μ_1) are non-zero. Because μ_1 is zero, the quadratic Padé approximant of order (0,0,1) can not be calculated. In order to overcome this problem we change the self-energy of the lattice sites from 0 to 4V. Using expression (5.a.32) we obtain the new moments. These are all non-zero, and therefore the calculation of the local density of states can be carried out now without further difficulties.

The results for the face centred cubic lattice can be seen in Figure 7. These results are for order N=16. The exact results are represented by dashed lines. They have been obtained as explained in section 5.d.

We now consider the case of the regular binary alloy. We have calculated the local density of states, $\rho_1(E)$, at a site with energy E_1 in the case of the regular binary alloy on the simple cubic lattice. The values of E_1 and E_2 were -V and V respectively, where V is the nearest neighbour interaction energy.

The results for this case can be seen in Figure 8. These results are for order N=16. The exact results are represented by dashed lines. They have been obtained as explained in section 5.d. In the case of a site with energy E_2 the local density of states, $\rho_2(E)$, is just the mirror image of $\rho_1(E)$, related to it by

$$\rho_2(E)=\rho_1((E_1+E_2)/2-E). \qquad (5.b.1)$$

The density of states, $\rho(E)$, given by

$$\rho(E)=[\rho_1(E)+\rho_2(E)]/2, \qquad (5.b.2)$$

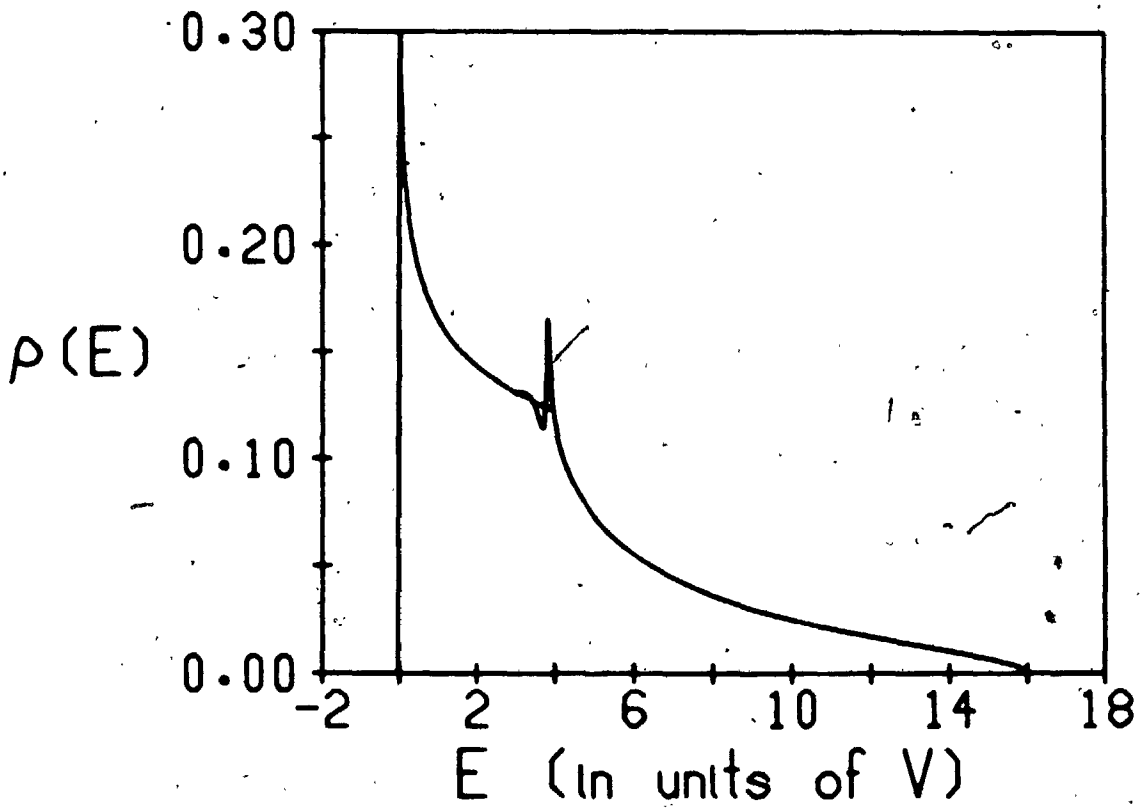

Figure 7

The density of states for the face centred cubic lattice, with the self-energy of the lattice sites set at 4V, as obtained from the order N=16 quadratic Padé approximant. The exact results are represented by dashed lines. V is the nearest neighbour interaction energy.

can be seen in figure 9. We see that the band gap has been well reproduced by the quadratic Padé approximant method. A further discussion of this point can be found in section 5.d.

Finally we consider the case of the semi-infinite simple cubic lattice. We have calculated the local density of states at the surface, as well as one, two, and three layers away from the surface. As here again only the even numbered moments are non-zero, expression (3.b.18) has been used in the calculation, and the same treatment as before for the values near E=0 has been applied.

The results for the local density of states at a site at the surface can be seen in Figure 10. The results for a site one, two, and three layers away from the surface, can be seen in Figures 11, 12, and 13 respectively. All the results shown are for order N=16 of the quadratic Padé approximant. We see that as we move farther away from the surface, the results resemble more and more those for the ordinary (bulk) simple cubic lattice (Figure 4).

In order to obtain a first estimate for the accuracy of the results obtained in this section we have compared them with the results obtained for exactly the same cases by using a quadratic Padé approximant of a different order, e.g. order N=14 or N=15. This comparison indicates that all our results are fairly accurate, with the only exception being the vicinity of the Van Hove singularities inside the band(s) in the cases of the simple cubic, face centred cubic, and diamond lattices, and in the case of the regular binary alloy on the simple cubic lattice. Non-

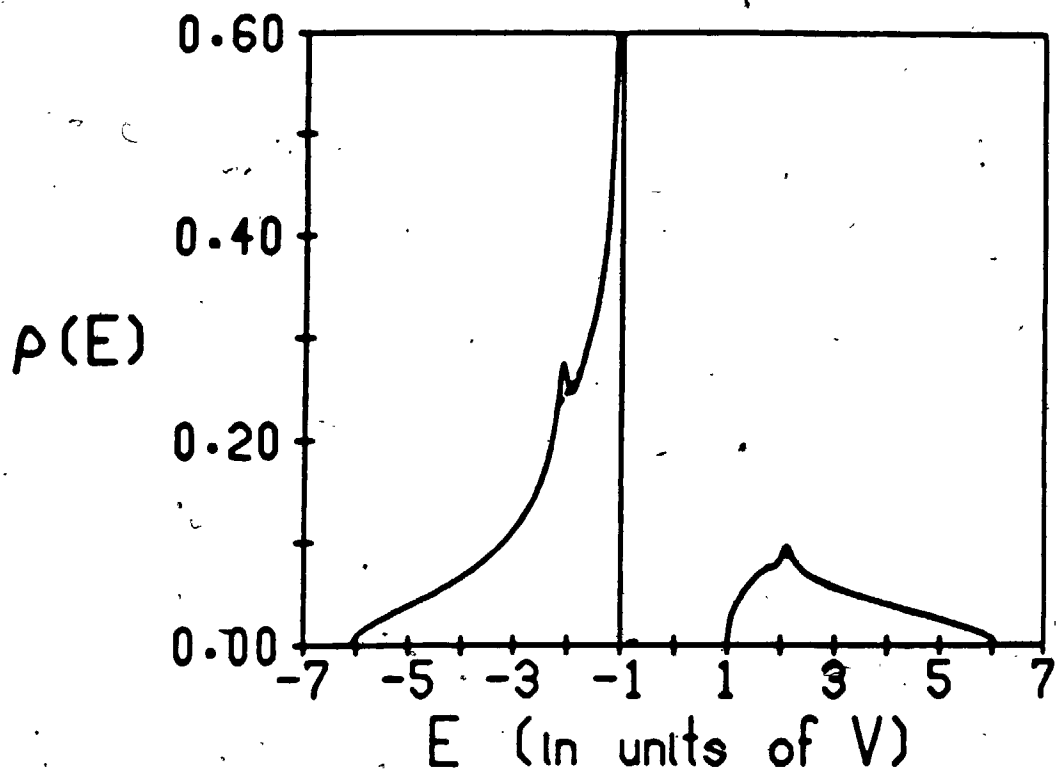

Figure 8

The local density of states for the regular binary alloy on the simple cubic lattice, with site energies $E_1=-V$ and $E_2=V$, for a site with self-energy E_1, as obtained from the order N=16 quadratic Padé approximant. The exact results are represented by dashed lines. V is the nearest neighbour interaction energy.

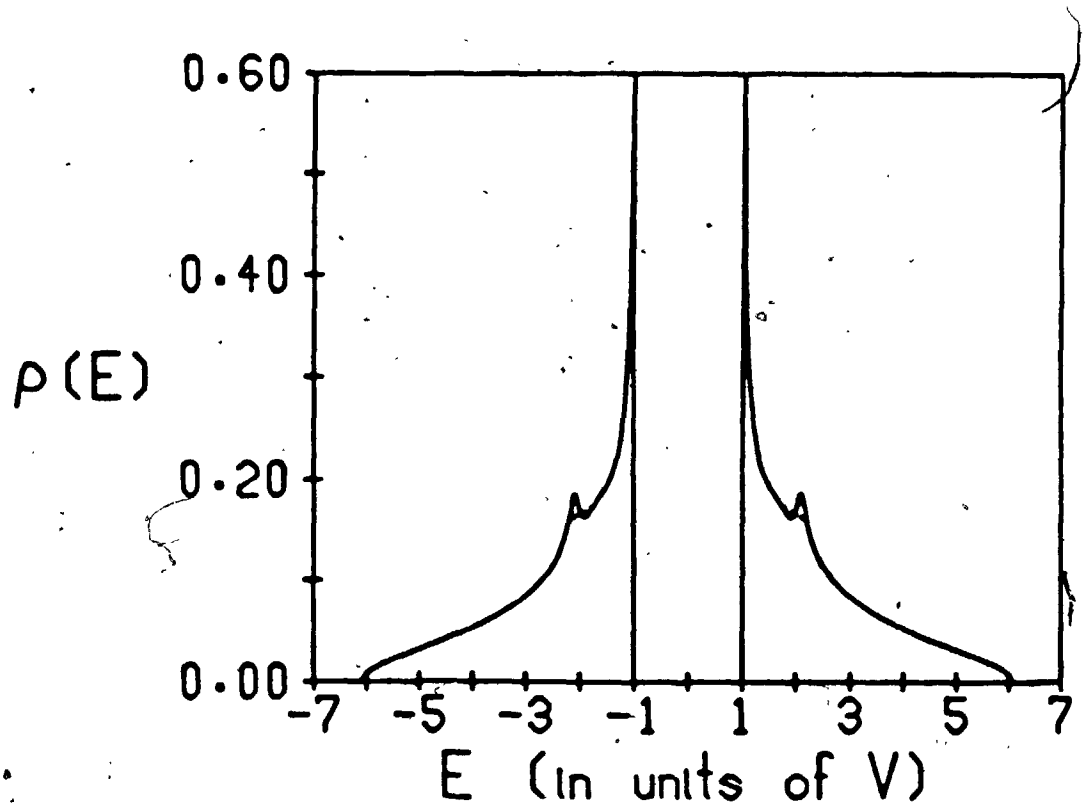

Figure 9

The density of states for the regular binary alloy on the simple cubic lattice, with site energies $E_1=-V$ and $E_2=V$, as obtained from the order N=16 quadratic Padé approximant. The exact results are represented by dashed lines. V is the nearest neighbour interaction energy.

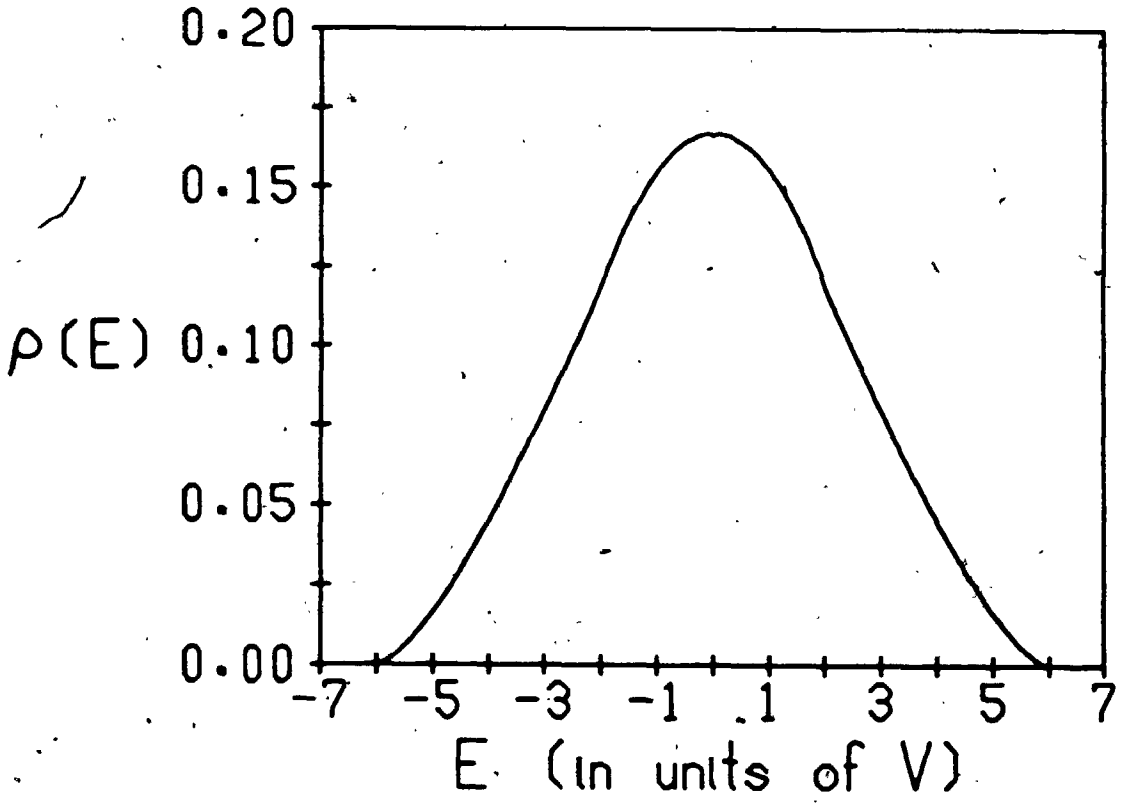

Figure 10

The local density of states for a site located at the surface of the semi-infinite simple cubic lattice, as obtained from the order N=16 quadratic Padé approximant. V is the nearest neighbour interaction energy.

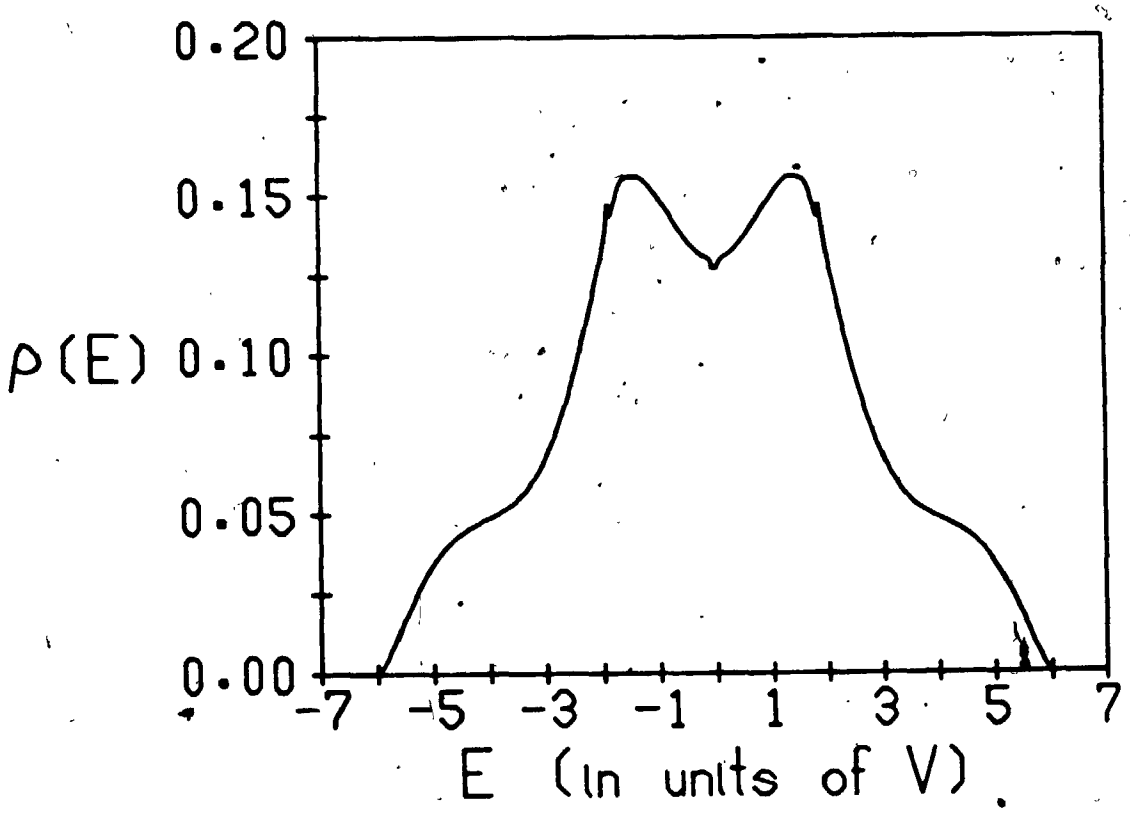

Figure 11

The local density of states for a site located one layer away from the surface of the semi-infinite simple cubic lattice, as obtained from the order N=16 quadratic Padé approximant. V is the nearest neighbour interaction energy.

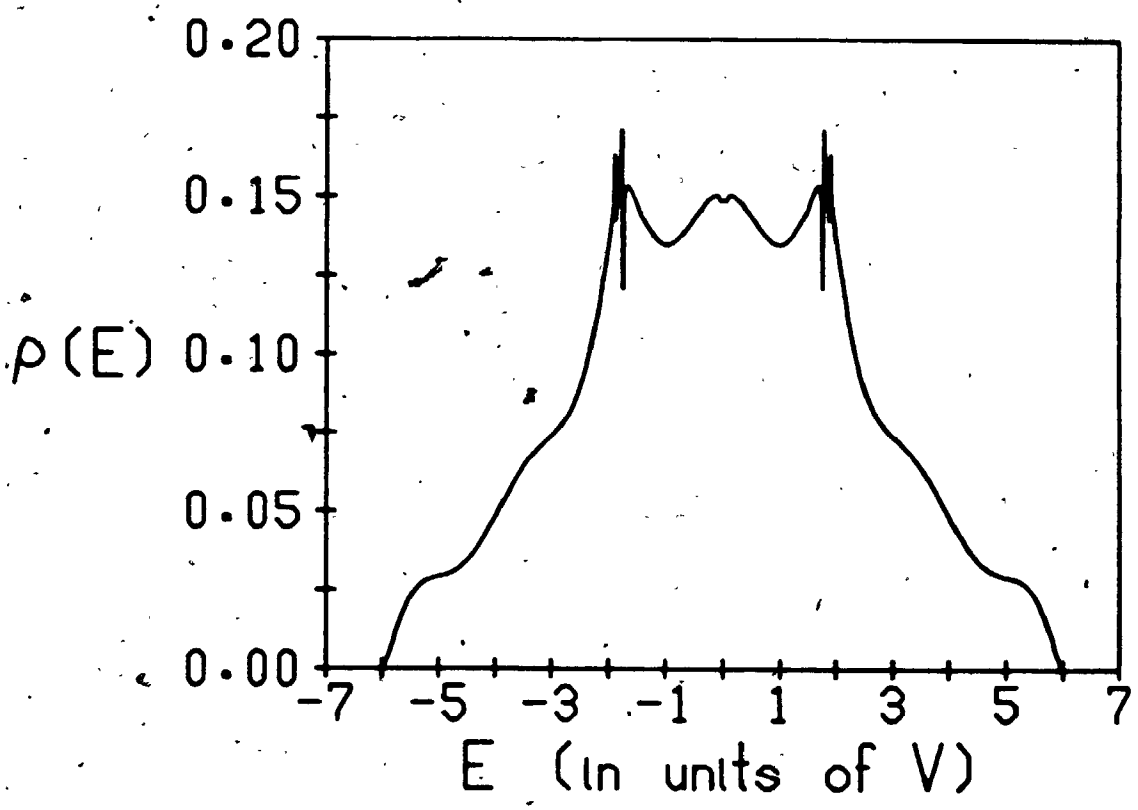

Figure 12

The local density of states for a site located two layers away from the surface of the semi-infinite simple cubic lattice, as obtained from the order N=16 quadratic Padé approximant. V is the nearest neighbour interaction energy.

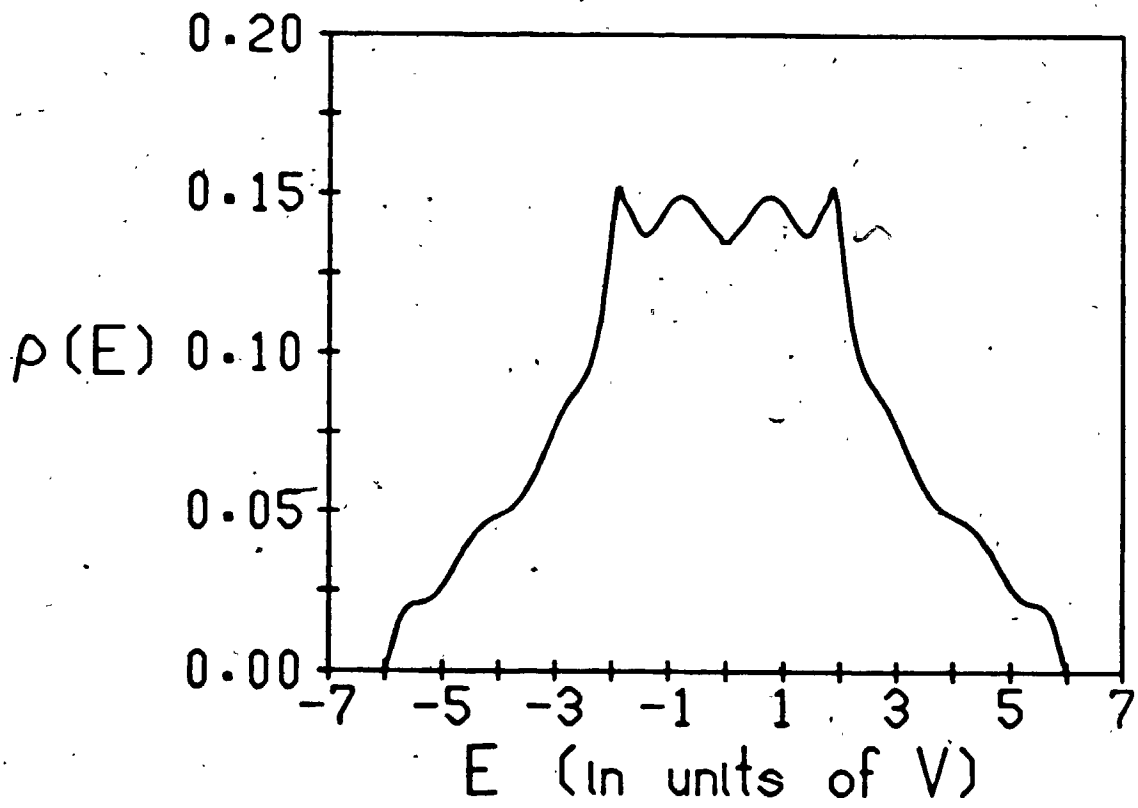

Figure 13

The local density of states for a site located three layers away from the surface of the semi-infinite simple cubic lattice, as obtained from the order N=16 quadratic Padé approximant. V is the nearest neighbour interaction energy.

physical oscillations show up in the vicinity of these singularities in the above mentioned cases. Some non-physical oscillations can be seen in the case of the semi-infinite simple cubic lattice as well, especially for the deeper lying layers (i.e. farther away from the surface). A detailed discussion of this subject can be found in sections 6.a and 6.b.

5.c. Comparison of the quadratic Padé results for the lattices discussed in section 5.a with the the results for the same lattices, as obtained by using the continued fraction method

We present here the results obtained for the local density of states, for the various cases discussed in section 5.a, by using the continued fraction method. In each case we have first calculated the ordinary Padé approximant of some order N, normally around N=25, by using the recurrence relation (4.b.5). From the recurrence coefficients, found through this calculation, we have obtained the coefficients $a_1, a_2, \ldots, a_N$ and $b_1, b_2, \ldots b_{N-1}$ of the continued fraction, according to expression (4.b.9).

The direct result from the truncated continued fraction, as discussed in section 4.a, is an approximation for the local density of states in the form of a sum of weighted delta-functions (expression (4.a.10)). This basic approximation for the local density of states for the square lattice can be seen in Figure 14. This kind of approximation for the case of the diamond lattice can be seen in Figure 15. Both are for the order N=25 Pade approximant. The eigenvalues of the truncated Hamiltonian H_N (expression (4.a.6)), which are the positions of the delta-functions, have been found by means of the Laguerre method (Wilkinson 1965), and the corresponding weights for the delta-functions have been found then from expression (4.a.11).

The improved approximation for the local density of states in histogram form (expression (4.a.16)) for the square lattice and the diamond lattice can be seen in Figures 16 and 17 respectively. These approximations are again for the order N=25 Padé

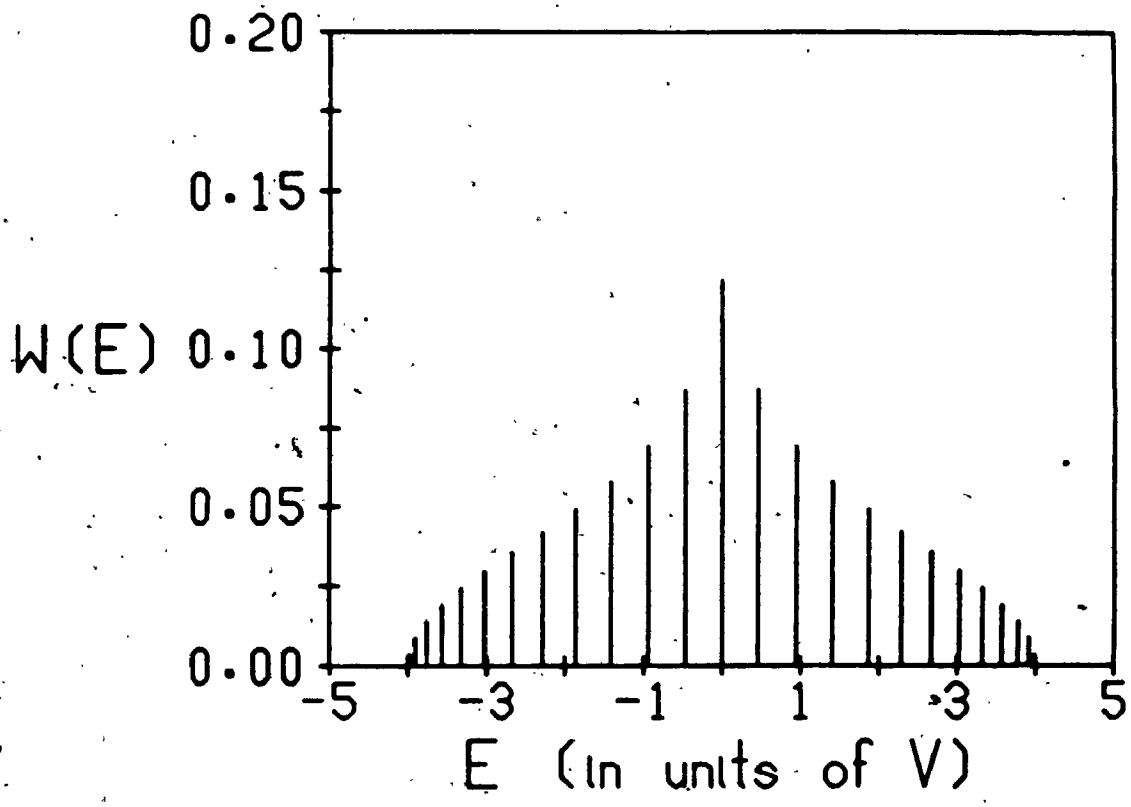

Figure 14

The weighted delta-functions for the square lattice, as obtained from the order N=25 Padé approximant (equivalent to the continued fraction truncated at N=25). The position of each line on the energy axis indicates the position of a delta-function, and the length indicates the corresponding weight. V is the nearest neighbour interaction energy.

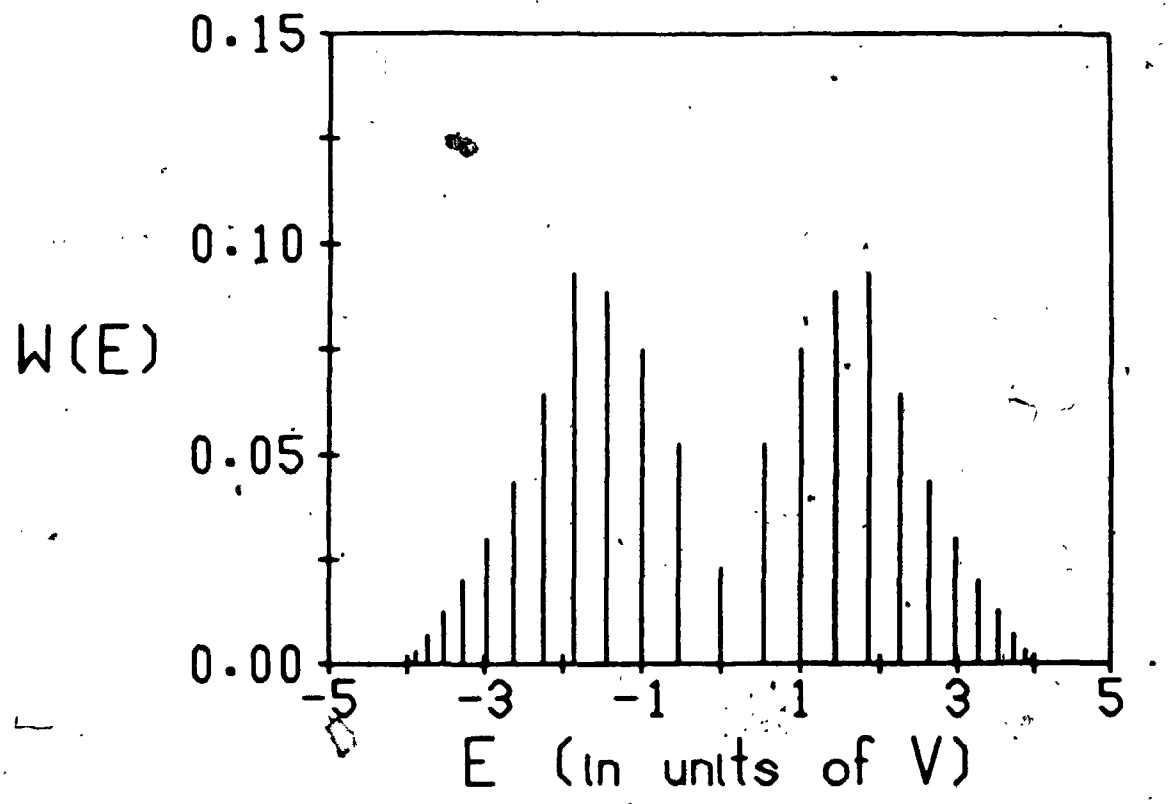

Figure 15

The weighted delta-functions for the diamond lattice, as obtained from the order N=25 Padé approximant (equivalent to the continued fraction truncated at N=25). The position of each line on the energy axis indicates the position of a delta-function, and the length indicates the corresponding weight. V is the nearest neighbour interaction energy.

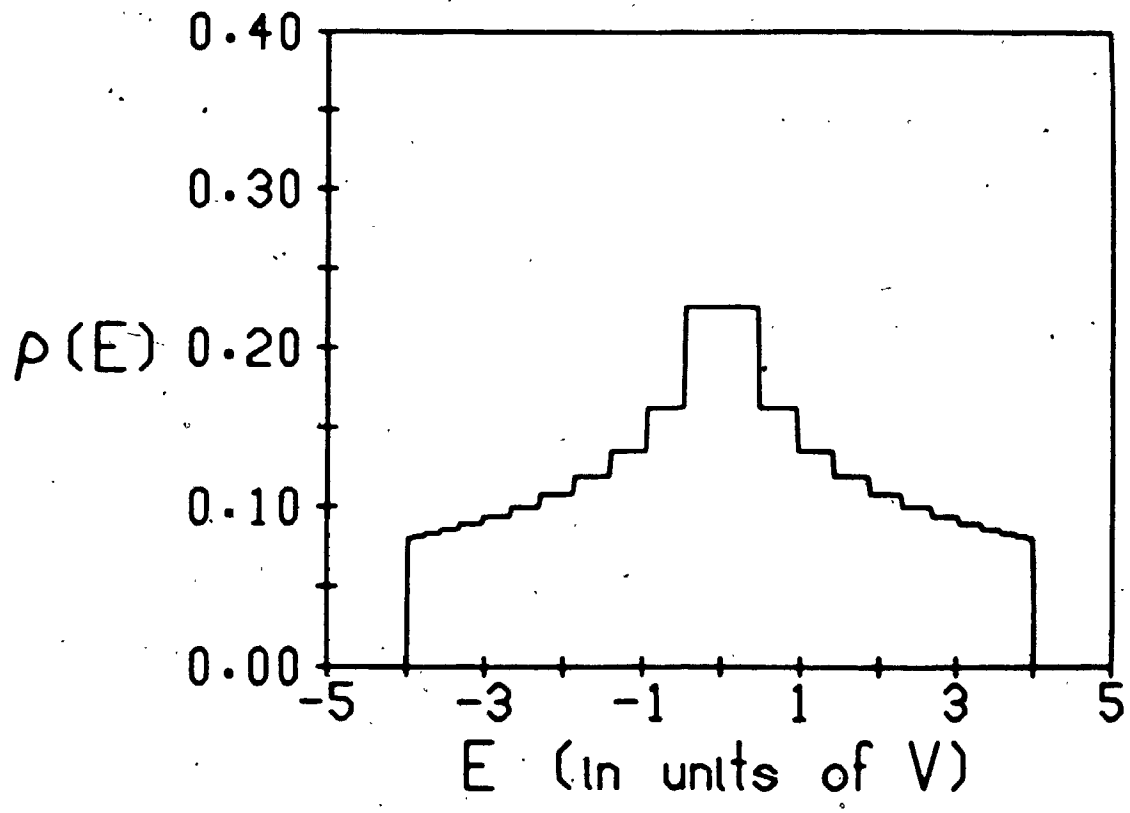

Figure 16

The density of states for the square lattice in histogram representation, as obtained from the order N=25 Padé approximant (equivalent to the continued fraction truncated at N=25). V is the nearest neighbour interaction energy.

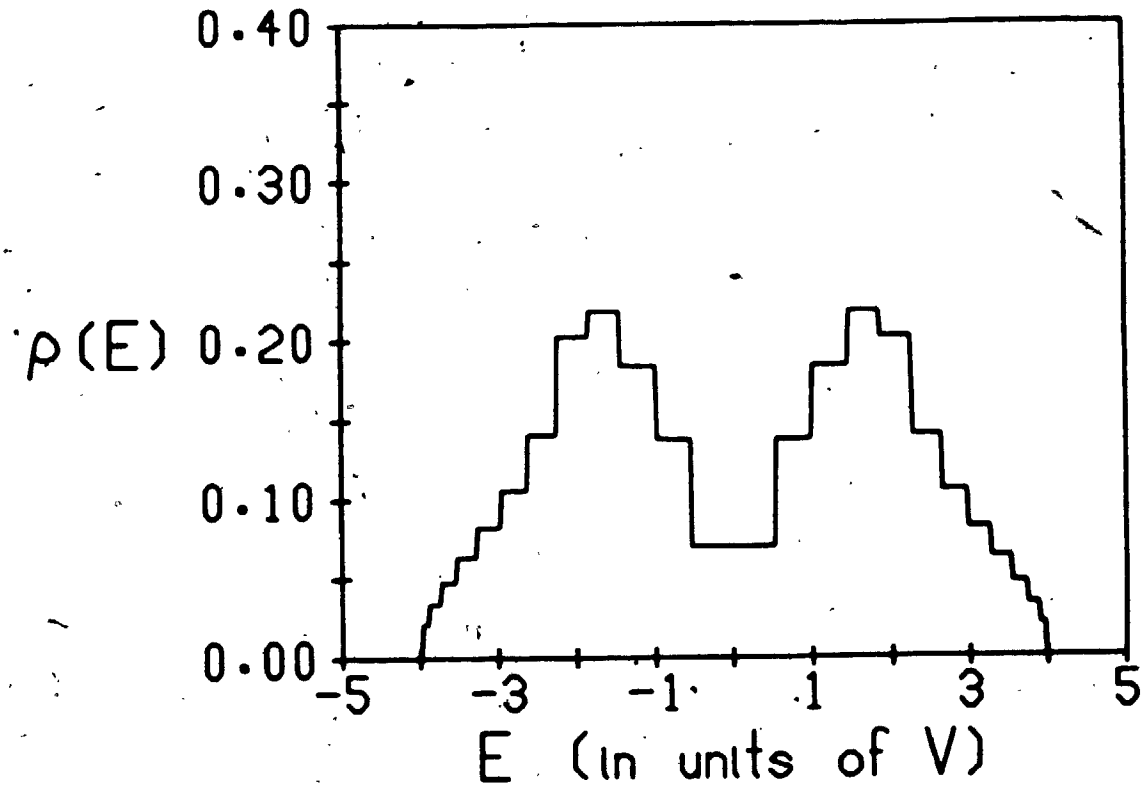

Figure 17

The density of states for the diamond lattice in histogram representation, as obtained from the order N=25 Padé approximant (equivalent to the continued fraction truncated at N=25). V is the nearest neighbour interaction energy.

approximant.

As we have seen in section 4.a, a further improvement of the continued fraction method results is possible by using the quadratic termination. The approximation for the local density of states in the case of a single energy band is then given by expression (4.a.33). The approximation in the case of two energy bands is given by expression (4.a.40). In order to use these expressions, however, one has to know in advance the positions of the band edges.

In the case of a regular lattice the band edge positions can be found from expression (5.a.1). The Green function is known to be complex inside the energy band(s) and real outside (Economou 1979). Thus, for energy values outside the band, we expect $E-E(\vec{k})$ in expression (5.a.1) to be positive for all $\vec{k}\epsilon\Omega_0$. From the expression for $E(\vec{k})$ for a given lattice we can thus deduce where the band edges should be located. The results for the regular lattices, obtained this way, are summarised in Table 1.

As an example we discuss in detail the case of the face centred cubic lattice. The expression for $E(\vec{k})$ is (cf. (C.13))

$$E(\vec{k})=4V[\cos(k_x a/2)\cos(k_y a/2)+\cos(k_x a/2)\cos(k_z a/2)+ \cos(k_y a/2)\cos(k_z a/2)]. \qquad (5.c.1)$$

The unit cell in $\vec{k}$-space is given by $-2\pi/a\leq k_i\leq 2\pi/a$, $i=x,y,z$. Thus, if $\theta_i=k_i a/2$, $i=x,y,z$, we have

$$E(\vec{\theta})=4V(\cos\theta_x\cos\theta_y+\cos\theta_x\cos\theta_z+\cos\theta_y\cos\theta_z)\ ; \quad -\pi\leq\theta_x,\theta_y,\theta_z\leq\pi. \qquad (5.c.2)$$

Table 1

The band edge positions for the regular lattices, as obtained from the study of expression (5.a.1). The band edge positions are given in units of the nearest neighbour interaction energy.

Lattice	Expression for E(k)	Lower band edge	Upper band edge
Square	(5.a.5)	-4	4
Simple cubic	(C.1)	-6	6
BCC	(C.8)	-8	8
FCC	(C.13)	-4	12
Diamond	(5.a.15)	-4	4

Note: In the case of the fcc lattice, the values given in the table are with the self-energy of the sites set at E_0=0. If it is set at E_0=4V, then the band edges become 0 and 16 in units of V.

$E(\vec{\theta})$ has a minimum value of -4V (for example, when $\theta_x=0$, $\theta_y=\pi$, and $\theta_z=\pi$), and a maximum value of 12V (when $\theta_x=0$, $\theta_y=0$, and $\theta_z=0$). Thus the band edge positions are -4 and 12 in units of V. If the self-energies of the lattice sites are changed from 0 to 4V, then the band edge positions are changed to 0 and 16 in units of V.

Using the coefficients of the continued fraction and the information about the band edge positions, we have obtained the approximate local density of states for the regular lattices from expression (4.a.33). The results for the square, simple cubic, body centred cubic, face centred cubic, and diamond lattices, can be seen in Figures 18, 19, 20, 21, and 22 respectively. All the results are derived from the order N=25 Padé approximant.

The continued fraction method results in the form of a sum of weighted delta-functions and in the form of a histogram have been presented for illustration purposes only. The results obtained by using the quadratic termination, on the other hand, are of main interest to us, and they will be compared with the quadratic Padé method results.

In the case of the square lattice we see that the logarithmic singularity at $E=0$ (Katsura and Inawashiro 1971) is reproduced in a more accurate manner when the quadratic Padé approximant is used. The non-physical oscillations seen in the continued fraction results, especially near the band edges, are virtually non-existent in the quadratic Padé results.

In the case of the simple cubic lattice we see that the singularities at $E=\pm 2V$ (Joyce 1973) are smoothed out by the continued

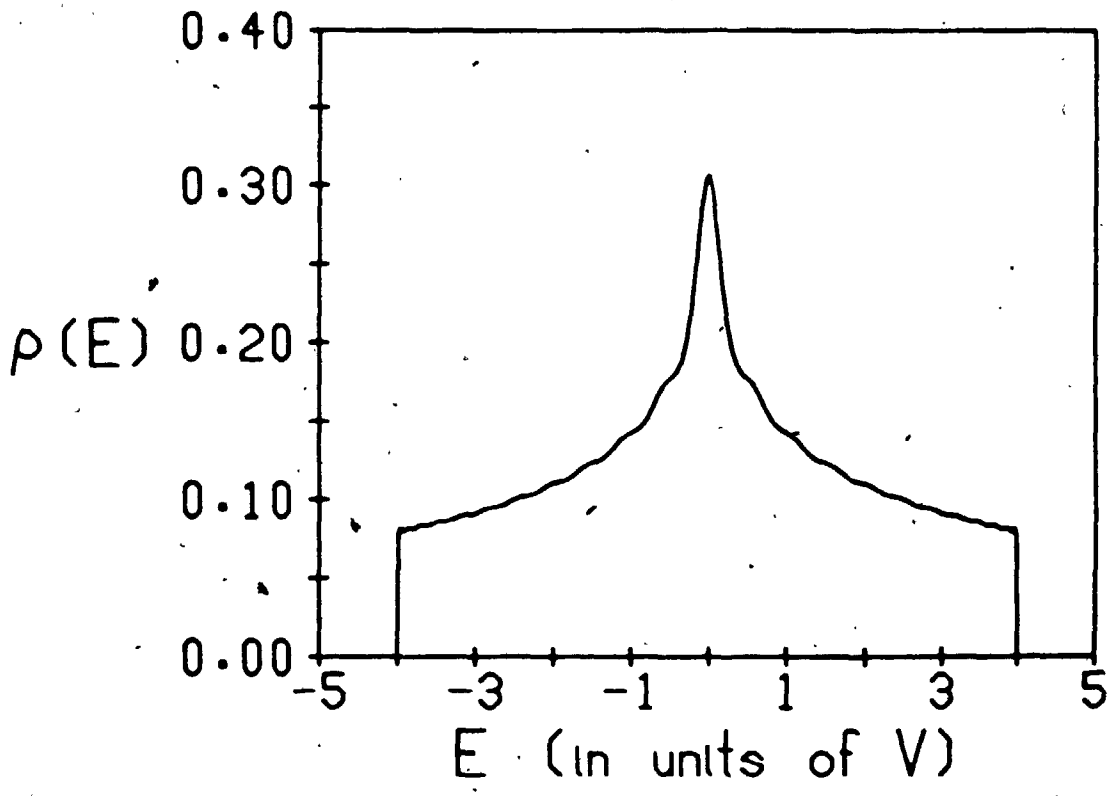

Figure 18

The density of states for the square lattice, as obtained from the continued fraction truncated at N=25, when the quadratic termination scheme is used. V is the nearest neighbour interaction energy.

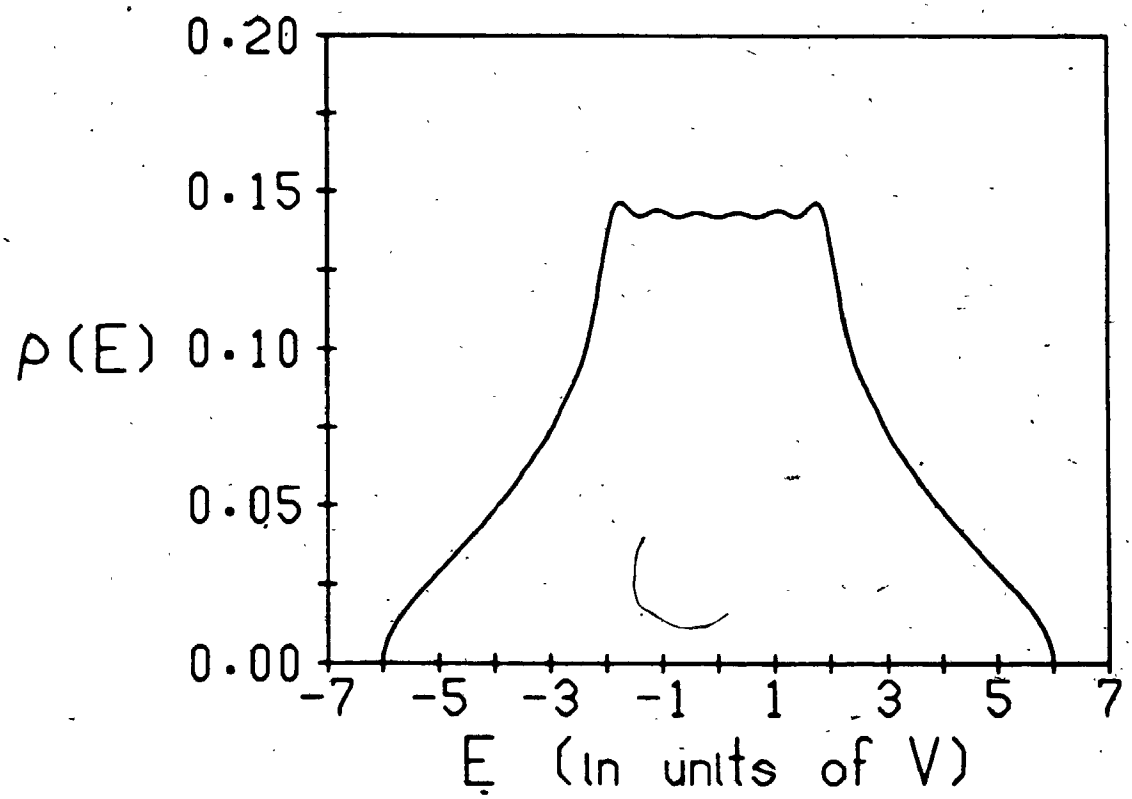

Figure 19

The density of states for the simple cubic lattice, as obtained from the continued fraction truncated at N=25, when the quadratic termination scheme is used. V is the nearest neighbour interaction energy.

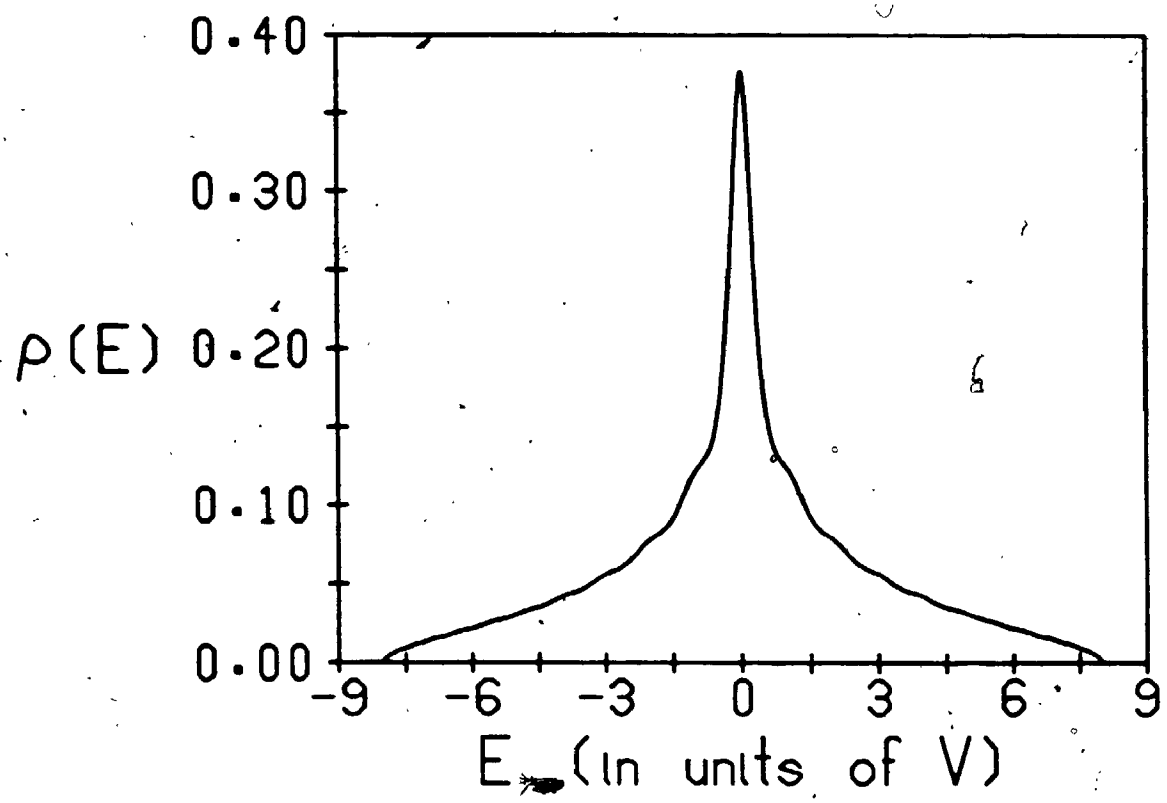

Figure 20

The density of states for the body centred cubic lattice, as obtained from the continued fraction truncated at N=25, when the quadratic termination scheme is used. V is the nearest neighbour interaction energy.

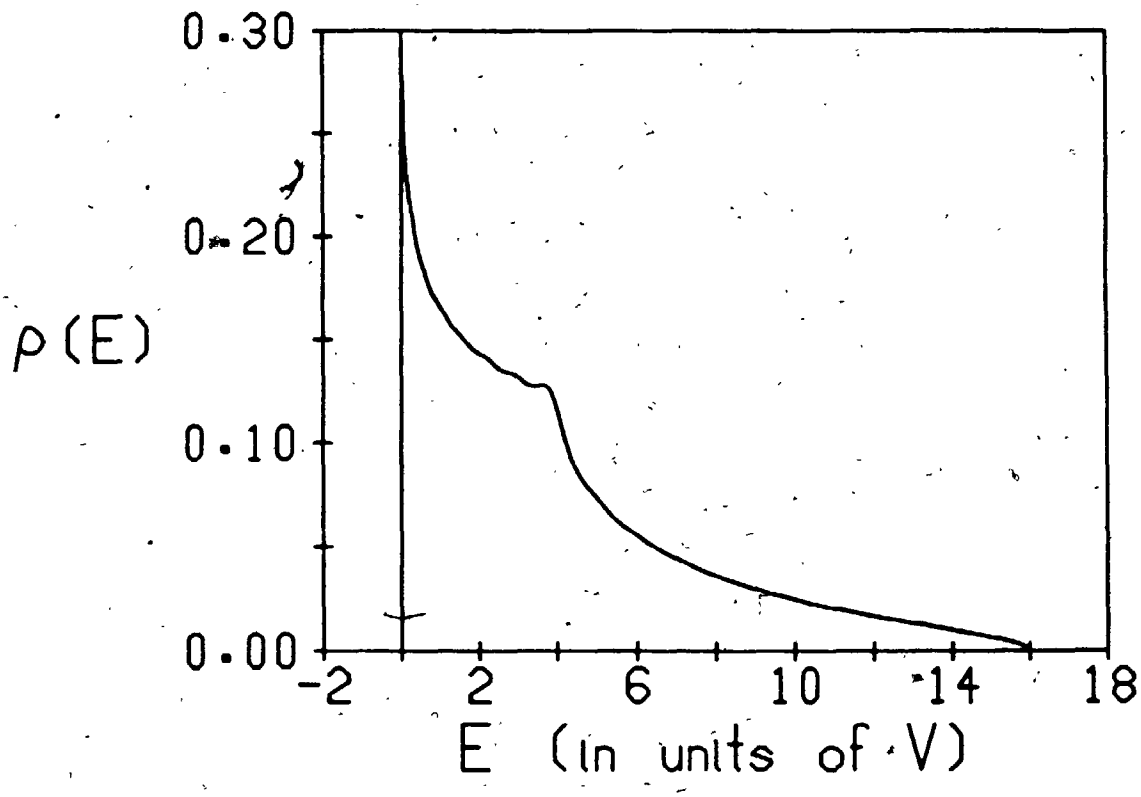

Figure 21

The density of states for the face centred cubic lattice, with the self-energies of the lattice sites set at 4V, as obtained from the continued fraction truncated at N=25, when the quadratic termination scheme is used. V is the nearest neighbour interaction energy.

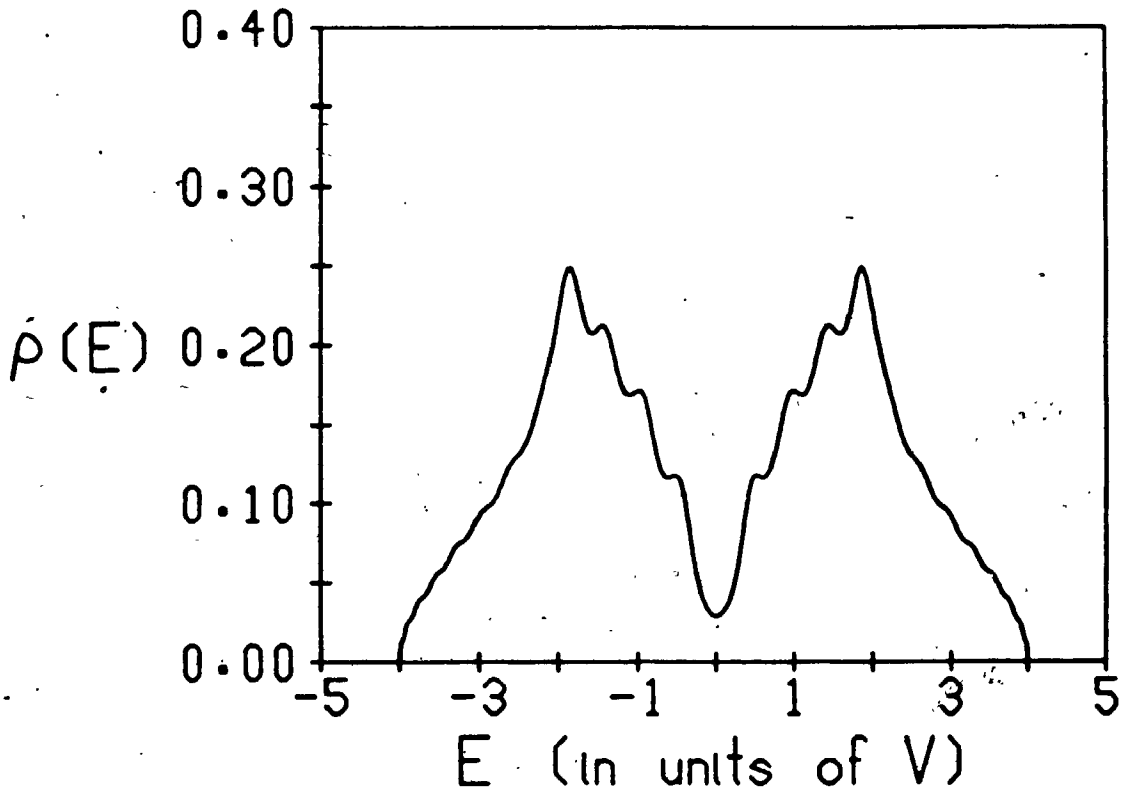

Figure 22

The density of states for the diamond lattice, as obtained from the continued fraction truncated at N=25, when the quadratic termination scheme is used. V is the nearest neighbour interaction energy.

fraction method. In the case of the quadratic Pade method, on the other hand, non-physical oscillations show up near these singularities. Thus both methods do not accurately reproduce these singularities. Otherwise, especially within the region $-2V<E<2V$, the continued fraction results show some small non-physical oscillations, which are virtually non-existent when the quadratic Padé method is used (except for the oscillations near the singularity points $E=\pm 2V$ themselves).

In the case of the body centred cubic lattice we again have a logarithmic singularity at $E=0$ (Katsura and Horiguchi 1971, Morita and Horiguchi 1971a). The quadratic Pade results reproduce this singularity much better than the continued fraction results. Besides, here again the continued fraction results show some small non-physical oscillations, which are absent in the quadratic Padé results.

In the case of the face centred cubic lattice we have a logarithmic singularity at $E=0$ (with the self-energy of the lattice sites set at $4V$) and a singularity inside the band at $E=4V$ (Morita and Horiguchi 1971a). Both methods rather similarly reproduce the logarithmic singularity at $E=0$. The singularity at $E=4V$ is poorly reproduced by either method. In the continued fraction results it is smoothed out, and in the quadratic Padé results non-physical oscillations show up there. Otherwise, slight non-physical oscillations are seen in the continued fraction results, especially within the range $0<E<4V$, while the quadratic Pade results are free from them (except for those near the singularity point $E=4V$ itself).

In the case of the diamond lattice the singularities (besides

those at the band edges) are located at E=±2V and at E=0. These positions of the singularities can be deduced from the positions of the singularities in the face centred cubic lattice, by making use of the relation between the densities of states of the two lattices, which is discussed in section 5.d. In the quadratic Padé results non-physical oscillations show up at the singularities located at E=±2V, but otherwise the results are accurate. In the continued fraction results, on the other hand, significant non-physical oscillations show up between E=-2V and E=2V, and the singularities themselves are smoothed out; especially the one at E=0.

Thus we see, so far, that the quadratic Padé results are, on the average, more accurate than the continued fraction results. The band edge singularities and logarithmic singularities inside the band are usually reasonably well reproduced by the quadratic Padé results. Only near other types of singularities inside the band non-physical oscillations show up. In the continued fraction results, on the other hand, the singularities are often smoothed out. Away from the singularities the quadratic Padé results are generally highly accurate (as we shall see quantitatively and in more detail in the next section), while some small non-physical oscillations often show up in the continued fraction results. Besides, no prior knowledge of the band edge positions is required when the quadratic Pade mathod is used, as it is required for the continued fraction method, when the quadratic termination is applied.

Now we look at the case of the regular binary alloy on the

simple cubic lattice. As before, we choose the self-energies of the two types of sites as $E_1=-V$ and $E_2=V$, where V is the nearest neighbour interaction energy. We wish to calculate the local density of states for a site with energy E_1 by means of the continued fraction method.

Using the usual procedure, as outlined in the beginning of this section, we have obtained the coefficients $a_1, a_2, \ldots, a_N$ and $b_1, b_2, \ldots, b_{N-1}$ of the continued fraction. Using these we have obtained the positions and weights of the delta-functions, and hence the histogram type approximation for the local density of states (expression (4.a.16)), which is shown in Figure 23. The results shown in the figure have been obtained from the order N=25 Pade approximant. The band gap is obscure in these results, and the approximation itself is rather poor, as can be expected due to its nature.

We prefer, therefore, to use the quadratic termination instead of the histogram approximation. In order to do so we need to know the positions of the band edges, or, conversely, the limiting values of the continued fraction coefficients, which are related to them. As we have two energy bands in this case, expression (4.a.40) for the local density of states has to be used. The continued fraction coefficients themselves alternatingly converge to two sets of limits (expression (4.a.35)).

In appendix D we show, that in the case of a regular binary alloy on a regular lattice, the continued fraction coefficients $a_1, a_2, \ldots, a_N$ for a site with energy E_1 are given by (cf. expression (D.2))

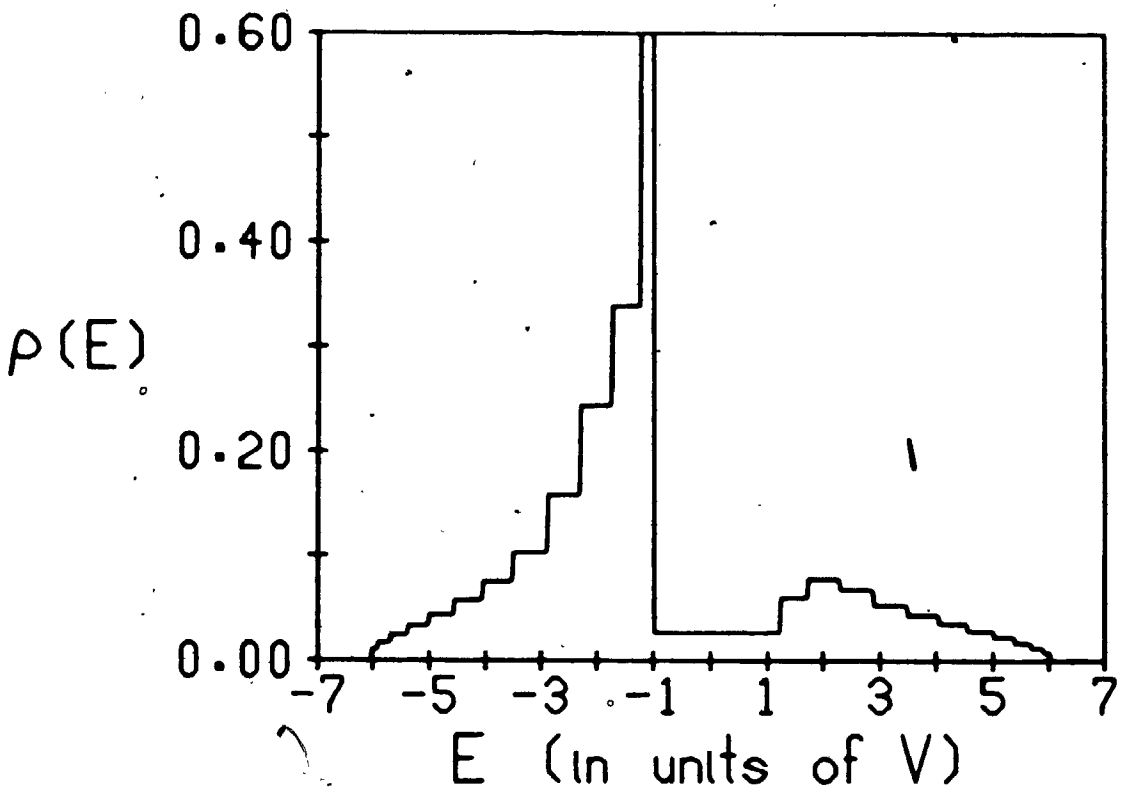

Figure 23

The local density of states for the regular binary alloy on the simple cubic lattice, with site energies E_1=-V and E_2=V, for a site with self-energy E_1, in histogram representation, as obtained from the order N=25 Padé approximant (equivalent to the continued fraction truncated at N=25), V is the nearest neighbour interaction energy.

$$a_{2n-1}=E_1 \; ; \; a_{2n}=E_2 \; ; \; n=1,2,\ldots , \qquad (5.c.3)$$

whereas the coefficients $b_1, b_2, \ldots, b_{N-1}$ are the same as for the regular lattice itself. For a site with energy E_2 the same is true, but with E_1 and E_2 interchanged.

Thus, in our case we have

$$A_1=\lim_{n\to\infty} a_{2n-1}=-1 \; ; \; A_2=\lim_{n\to\infty} a_{2n}=1,$$

$$B_1=\lim_{n\to\infty} b_{2n-1}=b \; ; \; B_2=\lim_{n\to\infty} b_{2n}=b, \qquad (5.c.4)$$

where b is equal to 3 (the limit of the b_n in the case of the simple cubic lattice). All these values are in units of V.

Making use of these results, we obtain the approximate local density of states from expression (4.a.40). The results are shown in Figure 24. They have been obtained from order N=25 of the Padé approximant. We also see, by using expression (4.a.43), that the band edges are located at $E=\pm\sqrt{37}$ V and at $E=\pm V$.

Comparison with the quadratic Padé results (Figure 8) reveals that both methods do not reproduce very well the singularities inside the energy bands (located at $E=\pm\sqrt{5}$ V in this case, as we shall see in the next section). In the quadratic Padé results non-physical oscillations show up near these singularities, while in the continued fraction results they are smoothed out. Otherwise both results seem to be of comparable quality. However, we should note, that the quadratic Padé method does not require any prior knowledge of the positions of the four band edges in this case, or even knowledge of the fact that two bands are present here rather than one, whereas for the continued fraction method with the quadratic termination such prior knowledge is essential.

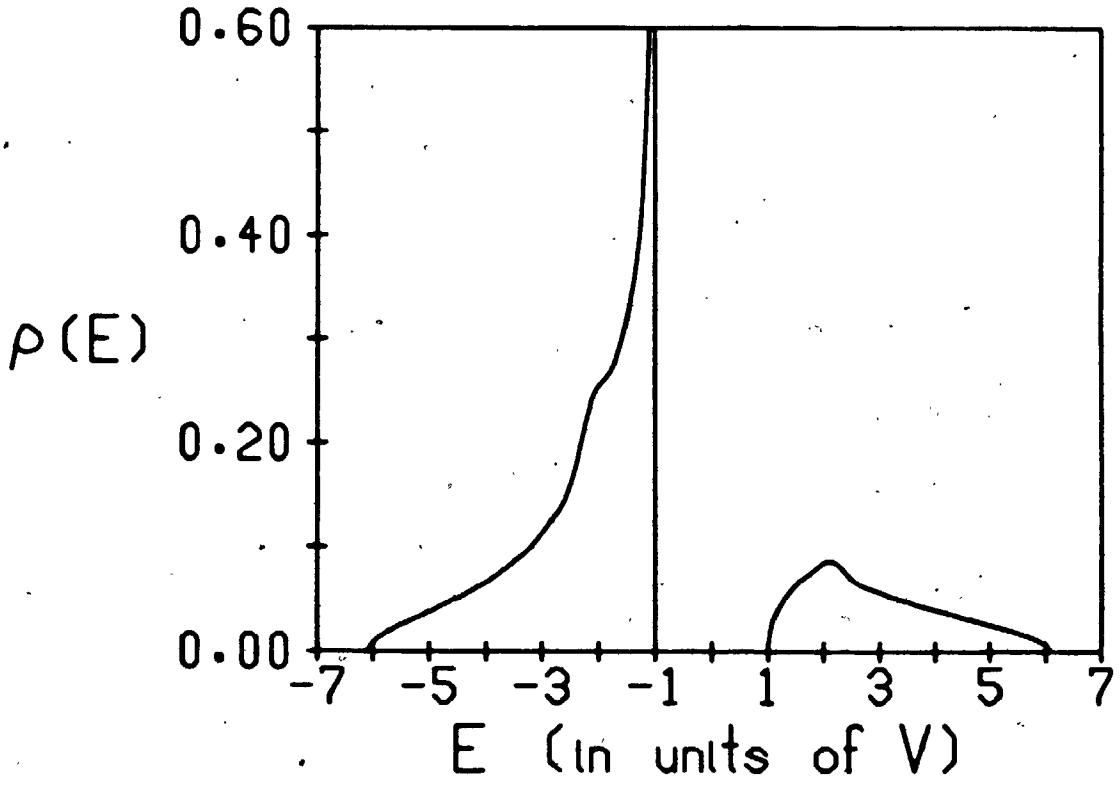

Figure 24

The local density of states for the regular binary alloy on the simple cubic lattice, with site energies E_1=-V and E_2=V, for a site with self-energy E_1, as obtained from the continued fraction truncated at N=25, when the quadratic termination scheme is used. V is the nearest neighbour interaction energy.

Finally we look at the case of the semi-infinite simple cubic lattice. The band edge positions are at E=±6V as in the bulk (Haydock 1975). Using the same procedure as before, we have obtained the approximate local density of states for sites located at the surface, as well as one, two, and three layers away from the surface. The results were obtained by using the continued fraction with the quadratic termination, and they were derived from the order N=25 Padé approximant.

The results for sites located at the surface, one, two, and three layers away from the surface, can be seen in Figures 25, 26, 27, and 28 respectively.

Comparison with the quadratic Pade results (Figures 10, 11, 12, and 13) shows that both methods produce results of comparable quality in this case. The quadratic Pade results, however, have the certain disadvantage, that some non-physical oscillations occasionally show up (around E=±2V, where the singularities are located in the case of the regular (bulk) simple cubic lattice). On the other hand, they have the usual advantage, that no prior knowledge of the band edge positions is required in order to obtain them.

We conclude this section with a brief review of the results of our comparison between the quadratic Padé and continued fraction results for the cases discussed so far. The continued fraction method with the quadratic termination has the disadvantage, that a prior knowledge of the band edge positions is required in order to use it. Besides, it tends to smooth out the singularities inside the energy band(s), and sometimes it produces some non-

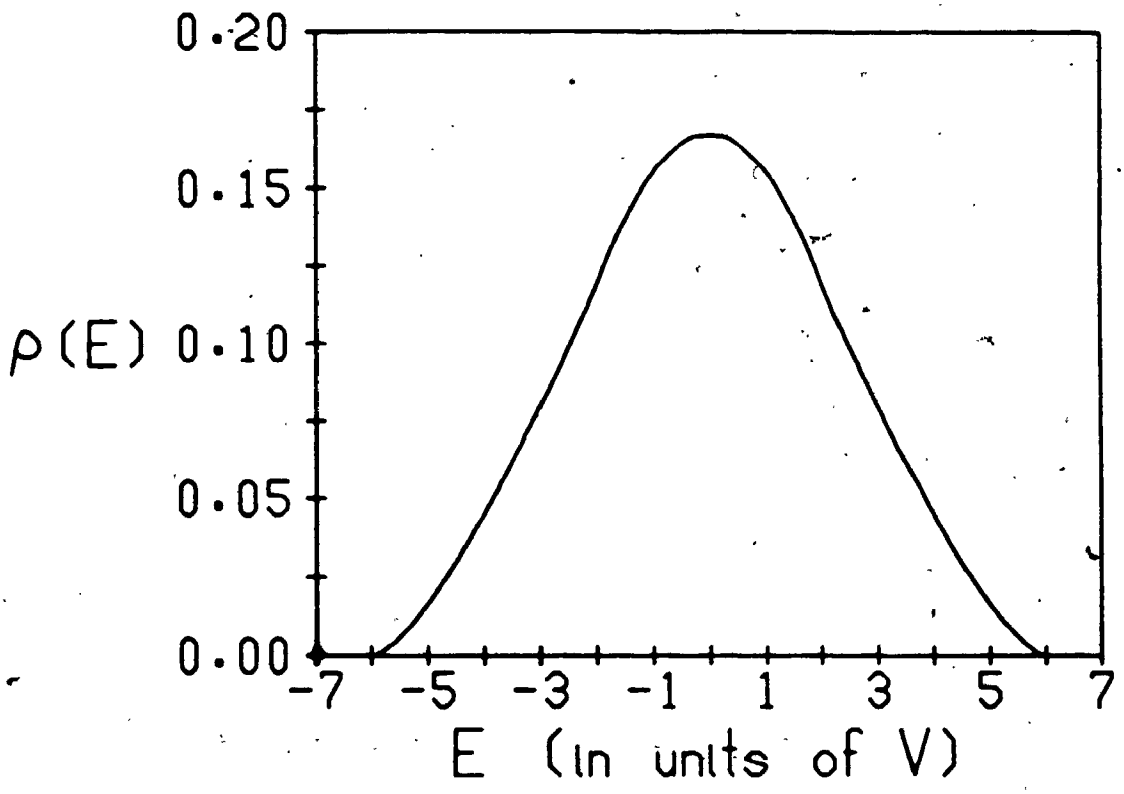

Figure 25

The local density of states for a site located at the surface of the semi-infinite simple cubic lattice, as obtained from the continued fraction truncated at N=25, when the quadratic termination scheme is used. V is the nearest neighbour interaction energy.

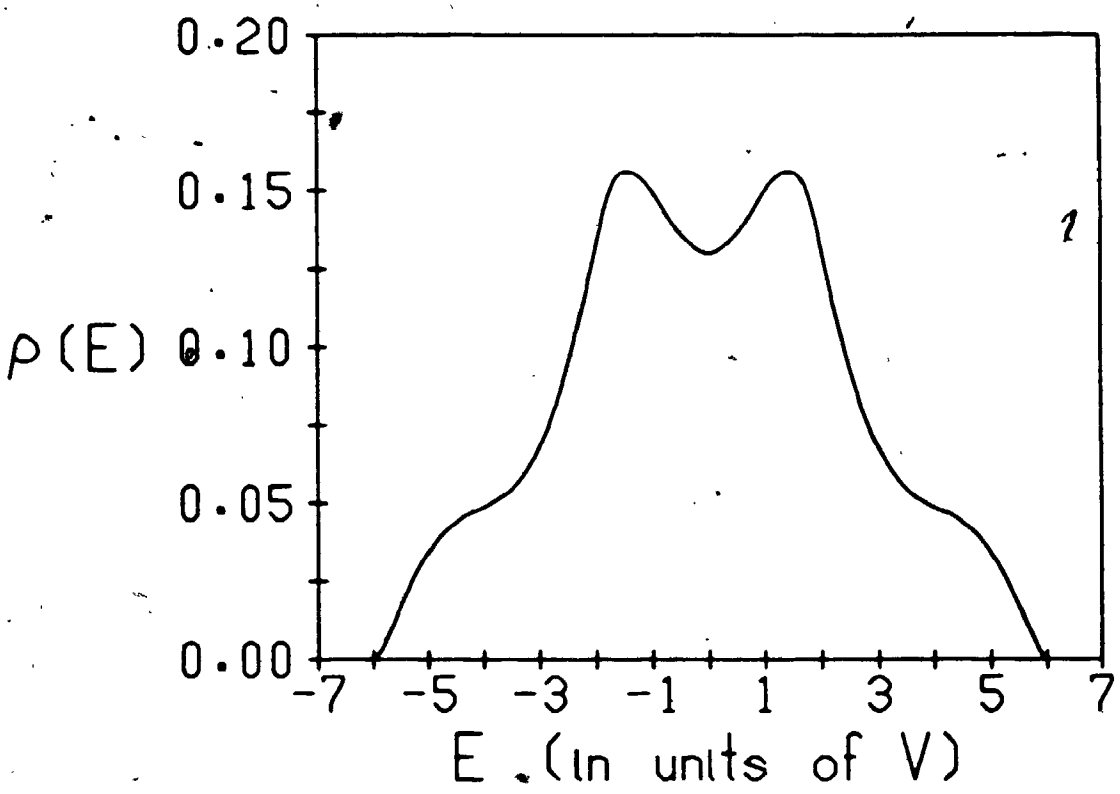

Figure 26

The local density of states for a site located one layer away from the surface of the semi-infinite simple cubic lattice, as obtained from the continued fraction truncated at N=25, when the quadratic termination scheme is used. V is the nearest neighbour interaction energy.

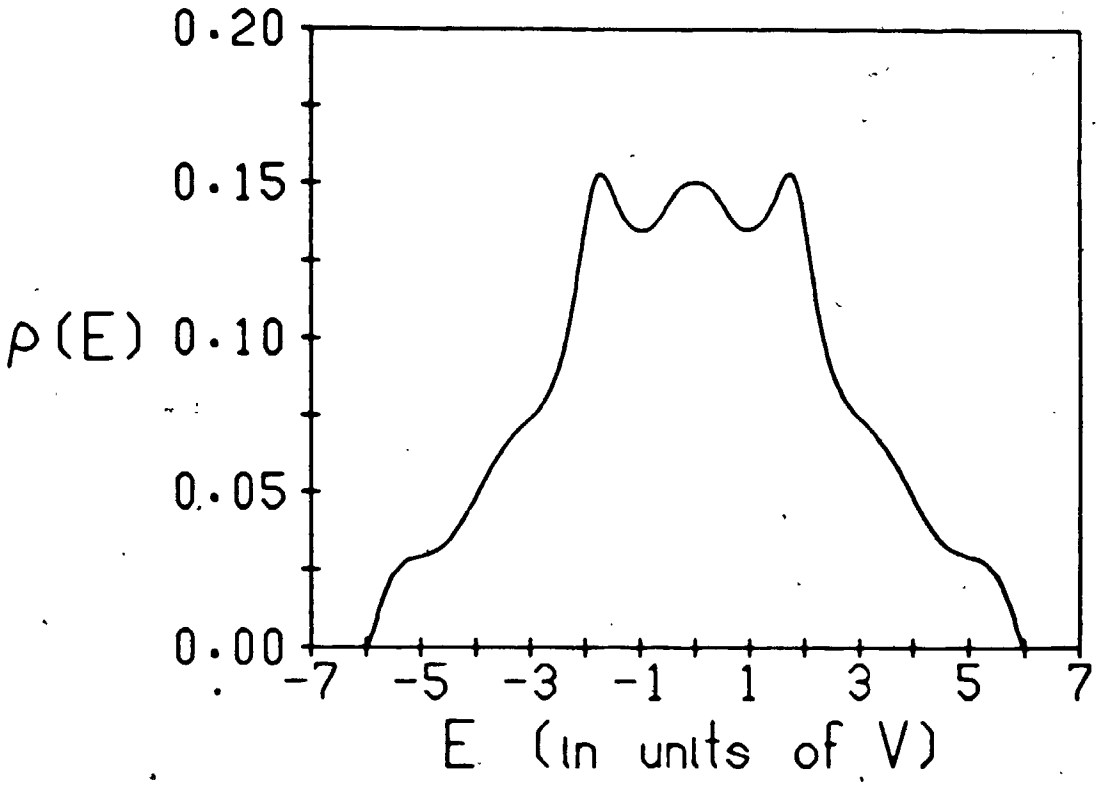

Figure 27

The local density of states for a site located two layers away from the surface of the semi-infinite simple cubic lattice, as obtained from the continued fraction truncated at N=25, when the quadratic termination scheme is used. V is the nearest neighbour interaction energy.

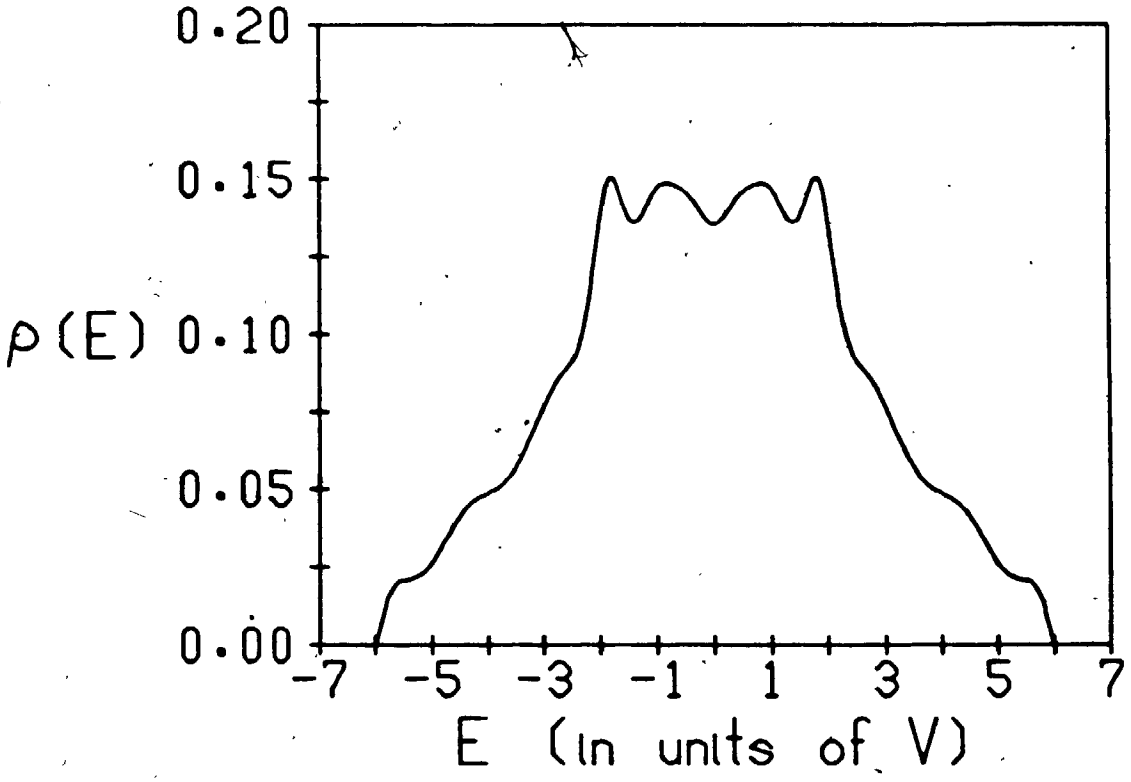

Figure 28

The local density of states for a site located three layers away from the surface of the semi-infinite simple cubic lattice, as obtained from the continued fraction truncated at N=25, when the quadratic termination scheme is used. V is the nearest neighbour interaction energy.

physical oscillations or "wiggles" in certain parts of the energy band. The quadratic Padé method does not require any prior knowledge about the positions of the band edges, band gaps, etc.. It has, however, a disadvantage - the presence of non-physical oscillations in the vicinity of singularities in the energy band(s).

5.d. Comparison of the quadratic Padé results for the regular lattices and the regular binary alloy with the exact values for the density of states

In this section we compare the results obtained by means of the quadratic Padé approximant method with the exact values of the density of states, wherever these are available. This way a more quantitative study of the accuracy of the quadratic Padé results is possible.

The density of states of the square lattice can be expressed in terms of a hypergeometric function (Katsura and Inawashiro 1971):

$$\rho(E)=(1/4\pi)\,{}_2F_1(1/2,1/2;1;x)\ ;\ x=1-E^2/16V^2. \tag{5.d.1}$$

The hypergeometric function ${}_2F_1(a,b;c;x)$ is defined by (Abramowitz and Stegun 1972)

$${}_2F_1(a,b;c;x)=\sum_{n=0}^{\infty}(1/n!)\Big\{\prod_{m=0}^{n-1}[(a+m)(b+m)/(c+m)]\Big\}x^n. \tag{5.d.2}$$

The density of states for this case can also be expressed in terms of an elliptic integral (Economou 1979):

$$\rho(E)=-(2/\pi^2E)\,\mathrm{Im}.[K(k)]\ ;\ k=4V/E. \tag{5.d.3}$$

$K(k)$ is the complete elliptic integral of the first kind, defined by (Abramowitz and Stegun 1972)

$$K(k)=\int_0^{\pi/2}[1-k^2\sin^2\theta]^{-1/2}d\theta. \tag{5.d.4}$$

As a rapidly converging iterative method for calculating $K(k)$ is available (Morita and Horiguchi 1971b), this expression for $\rho(E)$

is much better suited for the practical calculation.

The Green functions for the simple cubic, body centred cubic (bcc), and face centred cubic (fcc) lattices have been calculated by means of elliptic integrals and tabulated (Morita and Horiguchi 1971b) with 10 significant figures. The density of states is immediately obtained from there by dividing the imaginary part of the Green function by π. This way the accuracy of the quadratic Pade results for these lattices can readily be tested.

As the units used in the tables is different from ours, we should note here the conversion factors. In the case of the simple cubic lattice the energy values in the table have to be multiplied by 2 in order to obtain the corresponding values in our units. The values of the Green function have to be divided by 2. In the case of the bcc lattice the conversion factor (defined in the same way) is 8, and in the case of the fcc lattice it is 4.

The moments of the diamond lattice and those of the face centred cubic lattice are related by (Thorpe 1972)

$$\mu_{2n}=\sum_{m=0}^{n}\binom{n}{m}4^{n-m}V^{2n-m}\eta_m. \qquad (5.d.5)$$

μ_{2n} denote the moments of the diamond lattice, and η_m denote those of the face centred cubic lattice. V is the nearest neighbour interaction energy. By comparing this expression with (5.a.32) we see that we have

$$\rho_0(E)=(E/V)\rho_F(E^2/V-4V). \qquad (5.d.6)$$

$\rho_0(E)$ is the density of states of the diamond lattice, and $\rho_F(E)$ is that of the face centred cubic lattice (with the self-energy

of the lattice sites set at 0).

As the local density of states for the face centred cubic lattice is available to us, so is now that of the diamond lattice. We also see this way, that the diamond lattice has singularities inside the energy band at E=±2V and at E=0, as the face centred cubic lattice has them at E=-4V and at E=0 (when the self-energy of the lattice sites is 0).

In the case of the regular binary alloy the local density of states at either type of site can be related to that of the corresponding regular lattice (Morita and Horiguchi 1972). We present here a summary of their results.

Let $\rho_j(E)$ denote the local density of states for the sites with self-energy E_j, $j=1,2$. Let $\rho_0(E)$ denote that of the corresponding regular lattice. The relation is:

$$\rho_1(E)=[(E-E_2)/(E-E_1)]^{1/2}\rho_0(Z) \;;$$

$$\rho_2(E)=[(E-E_1)/(E-E_2)]^{1/2}\rho_0(Z) \;.$$

$$Z=[(E-E_1)(E-E_2)]^{1/2}. \qquad (5.d.7)$$

This holds for the range $E<\min.(E_1,E_2)$ and $E>\max.(E_1,E_2)$, where Z is real. In the range $\min.(E_1,E_2)<E<\max.(E_1,E_2)$ $\rho_1(E)=\rho_2(E)=0$.

This can be proven as follows. The Hamiltonian for the binary alloy is given by H=D+W. W is the Hamiltonian of the corresponding regular lattice, and D is a diagonal matrix. $D_{j,j}$ is E_1 or E_2 according to the type of the corresponding site j. With nearest neighbour interaction being the only one present, only sites of opposite types interact. Therefore for $i\neq j$ $H_{i,j}\neq 0$ only if i

and j are sites of opposite types.

We define two diagonal matrices, R and S, as follows:

$$R_{j,j}=\begin{cases} g_2 & \text{if } H_{j,j}=E_1 \\ g_1 & \text{if } H_{j,j}=E_2 \end{cases}; \qquad (5.d.8)$$

$$S_{j,j}=\begin{cases} 1/g_1 & \text{if } H_{j,j}=E_1 \\ 1/g_2 & \text{if } H_{j,j}=E_2. \end{cases} \qquad (5.d.9)$$

g_1 and g_2 are constants yet to be determined.

Now we look at the matrix $F=R(E-H)S$. For $i\neq j$ we have the relation $F_{i,j}=(E-H)_{i,j}$. Thus the off-diagonal elements of the matrices F and E-H are the same. For the diagonal elements, however, we have

$$F_{j,j}=\begin{cases} (g_2/g_1)(E-E_1) & \text{if } H_{j,j}=E_1 \\ (g_1/g_2)(E-E_2) & \text{if } H_{j,j}=E_2. \end{cases} \qquad (5.d.10)$$

By choosing g_1/g_2 to be equal to $[(E-E_1)/(E-E_2)]^{1/2}$ all the diagonal elements of F become equal to $Z=[(E-E_1)(E-E_2)]^{1/2}$, no matter of what type the corresponding site j is.

Now, as we have $F=Z-W$, we also have

$$E-H=R^{-1}F\,S^{-1}=R^{-1}(Z-W)S^{-1}, \qquad (5.d.11)$$

and therefore

$$(E-H)^{-1}=S(Z-W)^{-1}R. \qquad (5.d.12)$$

If $G(\vec{r},E)$ denotes the local Green function of the binary alloy (for the site $\vec{r}$), and $G_0(E)$ that of the regular lattice, then we have

$$G(\vec{r},E)=\langle\vec{r}|(E-H)^{-1}|\vec{r}\rangle=\langle\vec{r}|S(Z-W)^{-1}R|\vec{r}\rangle=$$

$$\sum_{\vec{s}}\sum_{\vec{t}}\langle\vec{r}|S|\vec{s}\rangle\langle\vec{s}|(Z-W)^{-1}|\vec{t}\rangle\langle\vec{t}|R|\vec{r}\rangle=$$

$$\langle\vec{r}|S|\vec{r}\rangle G_0(Z)\langle\vec{r}|R|\vec{r}\rangle. \qquad (5.d.13)$$

Therefore, for a site with energy E_1 we have

$$G(\vec{r},E)=(g_2/g_1)G_0(Z)=[(E-E_2)/(E-E_1)]^{1/2}G_0(Z), \qquad (5.d.14)$$

and for a site with energy E_2 we have

$$G(\vec{r},E)=(g_1/g_2)G_0(Z)=[(E-E_1)/(E-E_2)]^{1/2}G_0(Z). \qquad (5.d.15)$$

By taking the imaginary parts of the above expressions the relation (5.d.7) between the densities of states is obtained. In the range $\min.(E_1,E_2)<E<\max.(E_1,E_2)$ Z is pure imaginary, and the Green function of the regular lattice, $G_0(Z)$, is pure imaginary as well. Thus $[(E-E_2)/(E-E_1)]^{1/2}G_0(Z)$ and $[(E-E_1)/(E-E_2]^{1/2}G_0(Z)$ are real, and hence $\rho_1(E)=\rho_2(E)=0$. Outside this range (5.d.7) is directly obtained.

As the densities of states of the regular lattices are known, as we have seen above, those of the regular binary alloys on them can be calculated from the relation (5.d.7).

With the aid of (5.d.7) we can also relate the band edge positions for the density of states of the regular binary alloy to those for the corresponding regular lattice. If the band edges of the regular lattice are located at $E=\pm E_0$ (as the band is symmetric sround E=0), then the outer band edges of the binary alloy are located at the values of E that satisfy

$$E_0=[(E-E_1)(E-E_2)]^{1/2}. \qquad (5.d.16)$$

Thus the outer band edges are located at

$$E=(1/2)\{(E_1+E_2)\pm[(E_1-E_2)^2+4E_0^2]^{1/2}\}. \qquad (5.d.17)$$

The inner band edges (band gap edges) are located at $\min.(E_1,E_2)$ and at $\max.(E_1,E_2)$, as seen before.

We have seen thus how the exact values of the local densities of states for the regular lattices and the regular binary alloys on them can be obtained. Now we shall make use of these exact values in order to study the accuracy of our results, obtained from the quadratic Pade approximant method. The results discussed here have been obtained by using the order N=16 quadratic Pade approximant.

In the case of the square lattice we find that our results are accurate to 6 figures or more in most of the energy band. The accuracy drops only very close to the singularities at the band edges (E=±4V) and near the logarithmic singularity at the centre of the band (E=0). However, even very close to the singularities the accuracy is still considerable. For example, for E=±3.99V (near the band edges) it is better than 0.01%, and for E=±0.1V (near the band centre) it is better than 0.5%.

In the case of the simple cubic lattice we find that in the ranges -6V<E<-2.2V and 2.2V<E<6V our results are accurate to 6 figures or more. This is true even at the band edges themselves. When approaching the singularities at E=±2V (from these sides) the accuracy drops, but even at E=±2.02V it is still better than 0.5%. In the ranges -1.7V<E<-0.1V and 0.1V<E<1.7V our results are

accurate to 4 figures. In the range $-0.1V<E<0.1V$ the accuracy of our results drops, but it is still 1% or better. Only in the ranges $-2V<E<-1.7V$ and $1.7V<E<2V$, i.e. near the Van Hove singularities, the non-physical oscillations occur, and thus our accuracy is lost.

In the case of the body centred cubic lattice the accuracy of our results is 6 figures or more in most of the band, including the band edges themselves. Only near the logarithmic singularity at $E=0$ our accuracy drops. However, even at $E=\pm 0.15V$ it is still better than 0.5%.

In the case of the face centred cubic lattice (with the self-energy of the sites set at 4V) the accuracy of our results is 6 figures or more in the range $4.2V<E<16V$, including the band edge itself. However, even as close to the singularity at $E=4V$ (from this side), as $E=4.04V$, the accuracy is still better than 1%. In the range $0.1V<E<3.2V$ our results are accurate to 3 or 4 figures. For $0<E<0.1V$ our accuracy drops, as we approach the logarithmic singularity at $E=0$. For $3.2V<E<4V$ our accuracy drops again, as we approach the Van Hove singularity at $E=4V$. At $E=3.5V$ it is only about 2.5%, and further close to 4V the non-physical oscillations set in, and our accuracy is lost.

In the case of the diamond lattice we have an accuracy of 6 figures or more in the ranges $-4V<E<-2.1V$ and $2.1V<E<4V$, and even as close to the singularities at $E=\pm 2V$ (from these sides), as $E=\pm 2.01V$, the accuracy is still better than 1%. In the ranges $-1.7V<E<-0.1V$ and $0.1V<E<1.7V$ the accuracy is between 3 and 5 figures. In the range $-0.1V<E<0.1V$ the accuracy drops as we approach the singularity at $E=0$, but the general shape is still

correct (no non-physical oscillations present). In the ranges $-2V<E<-1.7V$ and $1.7V<E<2V$ the accuracy drops, as we approach the Van Hove singularities at $E=\pm 2V$, and non-physical oscillations set in.

In the case of the regular binary alloy on the simple cubic lattice (with $E_1=-V$ and $E_2=V$) we make use of expressions (5.d.7) and (5.d.17) and find that the outer band edges are located at $E=\pm\sqrt{37}$ V, the inner band edges (band gap edges) are located at $E=\pm V$, and the Van Hove singularities inside the energy bands are located at $E=\pm\sqrt{5}$ V.

In the ranges $-\sqrt{37}$ V$<E<-2.4$V and $2.4V<E<\sqrt{37}$ V the accuracy is 6 figures or better. Closer to $E=\pm\sqrt{5}$ V (from the direction of the outer band edges) it drops, but even as close to the singularity points as $E=\pm 2.26V$ it is still better than 2%. In the ranges $-1.7V<E<-1.02V$ and $1.02V<E<1.7V$ our accuracy is about 3 figures. Closer to $\pm V$ it is expected to drop. In the ranges $-\sqrt{5}$ V$<E<-1.7$V and $1.7V<E<\sqrt{5}$ V the accuracy drops, as we approach the Van Hove singularities, and non-physical oscillations set in.

Thus we have seen in this section, that our results are fairly accurate except for the vicinity of some singularities. This agrees with our more qualitative discussion of these results in the previous two sections. A further discussion of these comparison results can be found in section 6.a.

We can also express our conclusions in the following form. When the order of the quadratic Padé approximant is increased, the results become more accurate, as they converge to the true values of the density of states. Near most singularity points,

however, the convergence rate is very slow, and thus accurate results can not be obtained there in a practical computation.

5.e. The density of states for the valence band of Si, using a realistic model, as obtained by using the quadratic Padé approximant method

As the basis for the calculation of the density of states for the valence band of silicon we use a model which is based on the interaction between the bonds, rather than between the lattice sites themselves (Ortenburger et al 1976).

The lattice of silicon is the diamond lattice. The bonds are located between each pair of nearest neighbour sites. The cubic unit cell contains 16 bonds, and it can be seen in Figure 2. The model used here assumes that only the nearest neighbour and second nearest neighbour bonds interact. The interaction energies themselves have been semi-empirically obtained (Ciraci and Batra 1975).

Each bond has 6 nearest neighbours and 18 second nearest neighbours. Out of the 18 second nearest neighbours 12 are oriented at an angle of 60 degrees to the original bond, and the remaining 12 - at an angle of 180 degrees. The interaction energies are -1.34eV for the nearest neighbours, -0.06eV for the second nearest neighbours at 60°, and 0.28eV for the second nearest neighbours at 180° (Ortenburger et al 1976). The spacial configuration of the bonds can also be seen in Figure 29.

We see thus that each bond interacts only with 24 other bonds, and thus the Hamiltonian in matrix representation (with the bond wave functions as the basis) is a sparse matrix. Therefore we can use a map in order to obtain the moments, rather than take powers of the Hamiltonian in full.

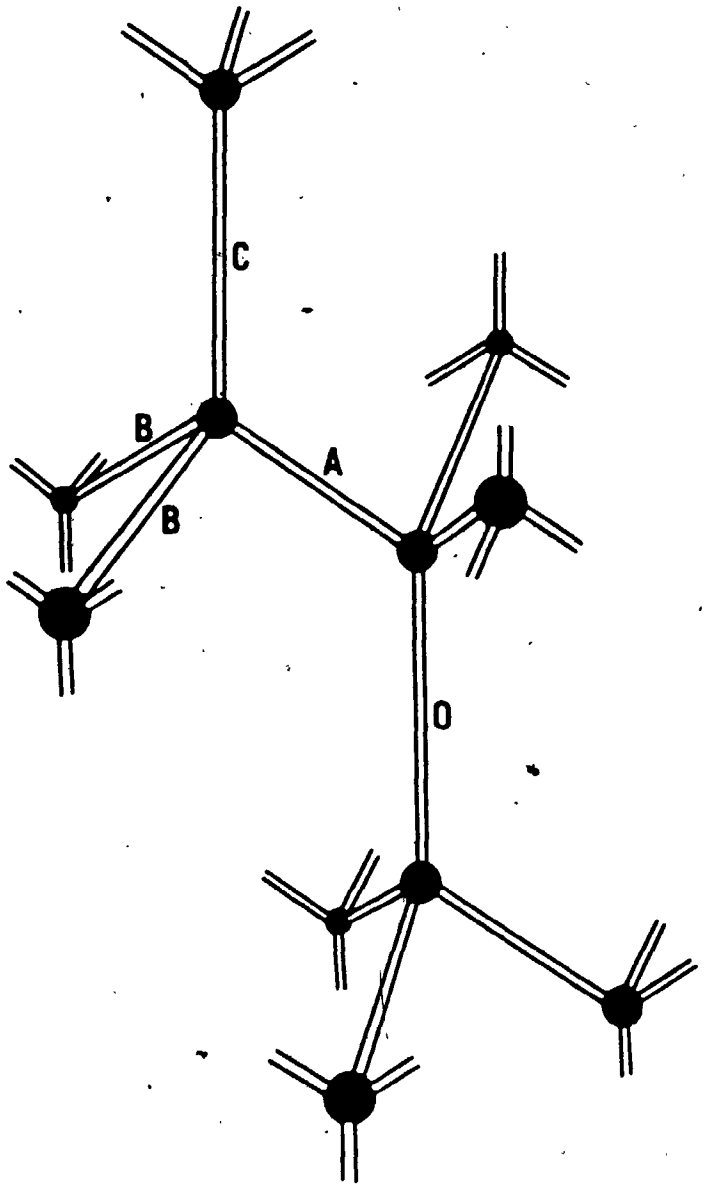

Figure 29

A section of the diamond lattice, used as the basis for the bonds model for silicon. O denotes the bond of origin, used as reference. A denotes a nearest neighbour bond. B denotes a second nearest neighbour bond oriented at 60° to the bond of origin. C denotes a second nearest neighbour bond oriented at 180° to the bond of origin.

The calculation is carried out as follows. First we create a three-dimensional grid and assign each bond a position on the grid. Each bond is thus denoted by a triplet of integers, which indicate where it is located. The map tells us then how to locate the nearest and second nearest neighbours of a bond according to the triplet of integers assigned to it.

Initially the bond at which the density of states is to be calculated (any bond will do, as all are identical) is assigned the value 1, and all the other bonds are assigned the value 0. The Hamiltonian is now applied to the grid again and again. Each bond is given an initial value of 0 as its value after the application of the Hamiltonian. Then the bonds are scanned one by one. If a bond has a value ϵ before the application of the Hamiltonian, then ϵ multiplied by the appropriate interaction energy is added to the value of each of the 24 neighbours with which it interacts. These are located by means of the previously mentioned map.

After the n^{th} application of the Hamiltonian the value assigned to the bond of origin (originally assigned the value 1) is the n^{th} moment. This way the moments can be calculated one after the other, as far as the size of the grid used permits it.

Using this method we have obtained the first 38 moments for this model. As the self-energy of the bonds is -9.6eV in this case, we have then used expression (5.a.32) in order to obtain the moments for this self-energy from the original ones.

From the moments we have calculated the approximate density of states by means of the quadratic Padé approximant method, following the procedure outlined in the beginning of section 5.a. The

results obtained by using the quadratic Pade approximants of orders 11 and 12 can be seen in Figures 30 and 31 respectively.

By comparing the results for these two different orders, we see that except for the vicinity of the lower and upper band edges (roughly the ranges -17eV<E<-14eV and -7eV<E<-5eV) our results are inadequate. As we have seen in the previous section, that the quadratic Padé method fails near singularities, and that its accuracy decreases in regions located between singularities (see alao section 6.a), we can attribute the failure of the method in this case to the large number of singularities present in the energy band.

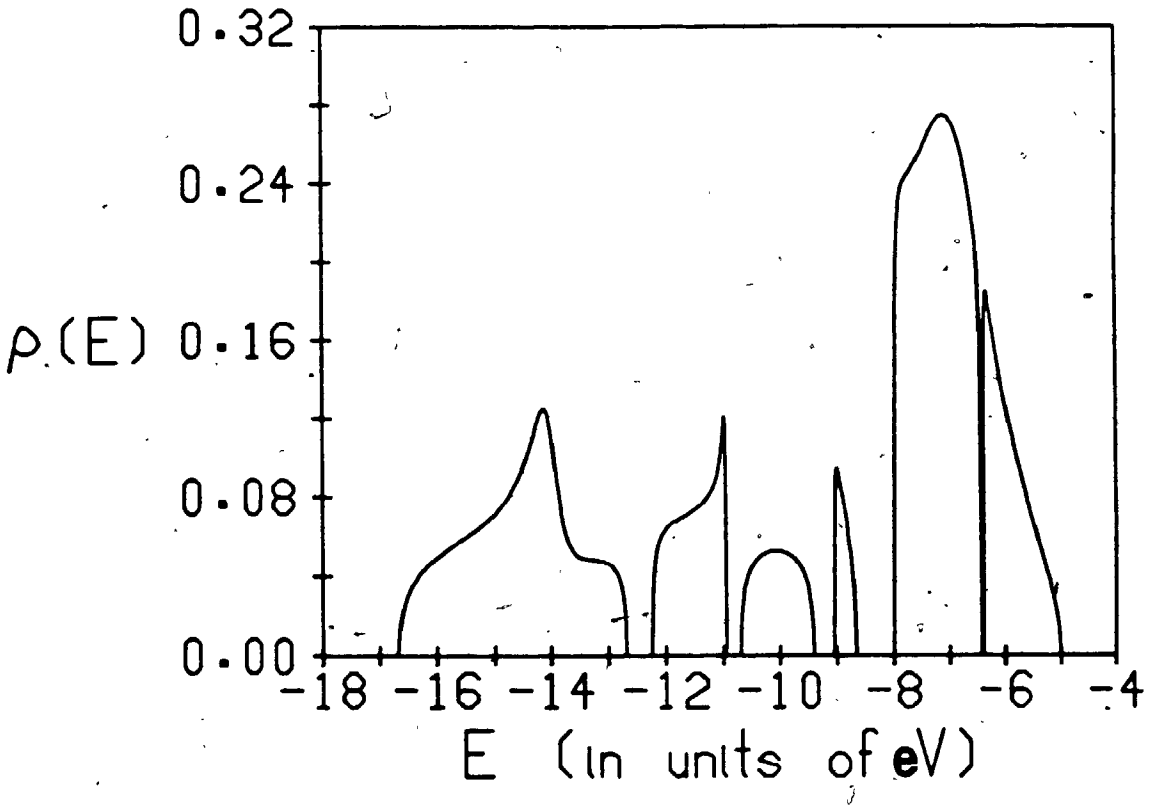

Figure 30

The density of states for the valence band of silicon, as obtained from the order N=11 quadratic Padé approximant.

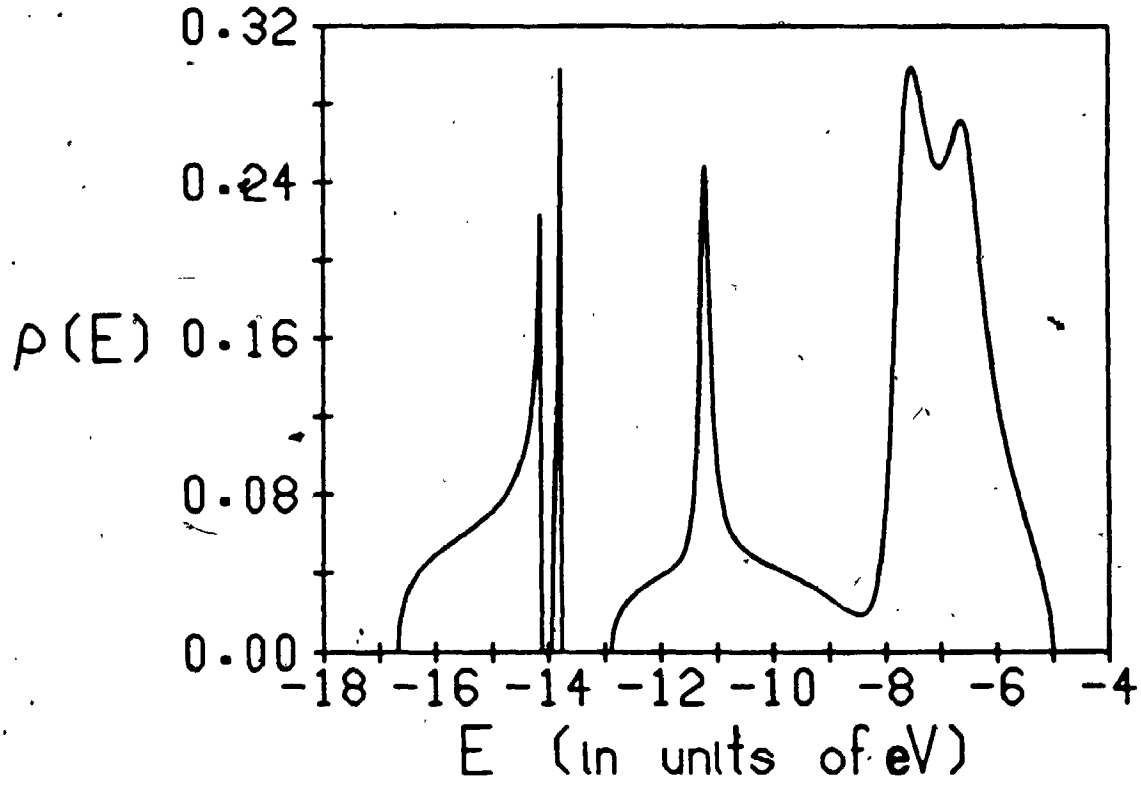

Figure 31

The density of states for the valence band of silicon, as obtained from the order N=12 quadratic Padé approximant.

5.f. Enhancing the convergence of the quadratic Padé approximant

As we have seen in the previous section, the quadratic Padé method turns out to be inadequate when a realistic case with a relatively large number of singularities is concerned. In such a case much higher orders of the quadratic Padé approximant may be needed in order to obtain reasonable results. As this is usually not practical due to the insufficient number of moments available and due to the numerical instability of the method itself, a different approach is required.

In section 4.b. we have seen a method for enhancing the convergence of the ordinary Padé approximant. We follow now the same lines in order to obtain a method for enhancing the convergence of the quadratic Padé approximant. The lattice site index $\vec{r}$ and the term "local" are omitted throughout this section.

If $O(x^{3n+2})$ is not replaced by 0 in expression (3.b.9), then expression (3.b.12) becomes

$$p_1^{(n)}(E)G^2(E)+p_2^{(n)}(E)G(E)+p_3^{(n)}(E)=O(E^{-(2n+2)}). \qquad (5.f.1)$$

The right hand side term, $O(E^{-(2n+2)})$, can be expressed as (Nuttall 1984)

$$O(E^{-(2n+2)})=A_n\zeta_n(E)\exp(n\phi(E))=A_n\zeta_n(E)\psi^n(E), \qquad (5.f.2)$$

where $\psi(E)=\exp(\phi(E))$. A_n is a constant. $\zeta_n(E)$ is a function of E that depends only weakly on n. Thus we have

$$p_1^{(n)}(E)G^2(E)+p_2^{(n)}G(E)+p_3^{(n)}(E)=A_n\zeta_n(E)\psi^n(E). \qquad (5.f.3)$$

By dividing all the polynomials' coefficients by the coefficient

of $E^{-(2n+2)}$ in $O(E^{-(2n+2)})$ A_n is set to be 1. This coefficient is found by carrying out the polynomial algebra on the left hand side of (5.f.3) for $E^{-(2n+2)}$.

If the n-dependence of $\zeta_n(E)$ is neglected now, then we have for three adjacent orders of the quadratic Padé approximant:

$$p_1^{(k)}(E)g^2(E)+p_2^{(k)}(E)g(E)+p_3^{(k)}(E)=\zeta(E)\,\phi^k(E)\,;\quad k=n-1,n,n+1, \qquad (5.f.4)$$

where $g(E)$ approximates the Green function $G(E)$. The previously mentioned normalisation is assumed to have been carried out here.

By taking ratios of these expressions we obtain now

$$[p_1^{(n+1)}(E)g^2(E)+p_2^{(n+1)}(E)g(E)+p_3^{(n+1)}(E)]\times$$
$$[p_1^{(n)}(E)g^2(E)+p_2^{(n)}(E)g(E)+p_3^{(n)}(E)]^{-1}=$$
$$[p_1^{(n)}(E)g^2(E)+p_2^{(n)}(E)g(E)+p_3^{(n)}(E)]\times$$
$$[p_1^{(n-1)}(E)g^2(E)+p_2^{(n-1)}(E)g(E)+p_3^{(n-1)}(E)]^{-1}. \qquad (5.f.5)$$

This yields a quartic equation for $g(E)$

$$([p_1^{(n)}(E)]^2-p_1^{(n-1)}(E)p_1^{(n+1)}(E))g^4(E)+$$
$$[2p_1^{(n)}(E)p_2^{(n)}(E)-p_1^{(n-1)}(E)p_2^{(n+1)}(E)-p_1^{(n+1)}(E)p_2^{(n-1)}(E)]g^3(E)+$$
$$(2p_1^{(n)}(E)p_3^{(n)}(E)+[p_2^{(n)}(E)]^2-p_1^{(n-1)}(E)p_3^{(n+1)}(E)-$$
$$p_1^{(n+1)}(E)p_3^{(n-1)}(E)-p_2^{(n-1)}(E)p_2^{(n+1)}(E))g^2(E)+$$
$$[2p_2^{(n)}(E)p_3^{(n)}(E)-p_2^{(n-1)}(E)p_3^{(n+1)}(E)-p_2^{(n+1)}(E)p_3^{(n-1)}(E)]g(E)+$$
$$([p_3^{(n)}(E)]^2-p_3^{(n-1)}(E)p_3^{(n+1)}(E))=0. \qquad (5.f.6)$$

Equation (5.f.6) has 0, 1, or 2 pairs of complex conjugate

solutions. Therefore one has only two possible values for $|Im.[g(E)]|$: both zero, one zero and one non-zero, or both non-zero, respectively. $\rho(E)$ is approximated by $(1/\pi)|Im.[g(E)]|$. By calculating $\rho(E)$ this way for a series of values of E along the real axis (in E-space) a set of pairs of values for $\rho(E)$ is obtained. They can be sorted now to form two smooth functions; one of which will be the approximation for the density of states.

Due to numerical reasons the Jenkins-Traub algorithm (Jenkins and Traub 1970), rather than the analytical formula, has to be used in order to solve the quartic equation for g(E).

We have seen thus a method which can be used in order to enhance the convergence of the quadratic Padé results, and hence might be useful in cases where the usual quadratic Padé method turns out to be inadequate.

5.g. The density of states for the valence band of Si, as obtained by using the enhanced version of the quadratic Padé method, and comparison with the results obtained from the continued fraction and modified moments methods

We return now to the bonds model for the valence band of silicon, discussed in section 5.e. Using the moments for this case, we have recalculated the density of states by means of the enhanced version of the quadratic Padé method, as discussed in the previous section.

The results can be seen in Figures 32 and 33. The results in Figure 32 have been obtained by using orders 9, 10, and 11 of the quadratic Pade approximant. The results in Figure 33 have been obtained by using orders 10, 11, and 12.

Comparison between the results for the two different sets of orders indicates, that the general shape of the density of states has now been obtained, even though not with the high accuracy which has been reached in the simpler cases. The accuracy is the highest near the band edges, and it drops as one moves past the singularities towards the central portion of the band. The "dip" seen near E=-6.5eV in Figure 32 obviously is non-physical, as is the "spike" near E=-11eV in Figure 33.

In order to study our results more carefully, we have calculated the density of states by using the continued fraction and modified moments methods as well. In order to use these methods we need to know in advance the positions of the band edges. We have obtained them from the zeroes of the polynomial $R^{(n)}(E)$, obtained from the quadratic Padé polynomials (expression 3.b.14),

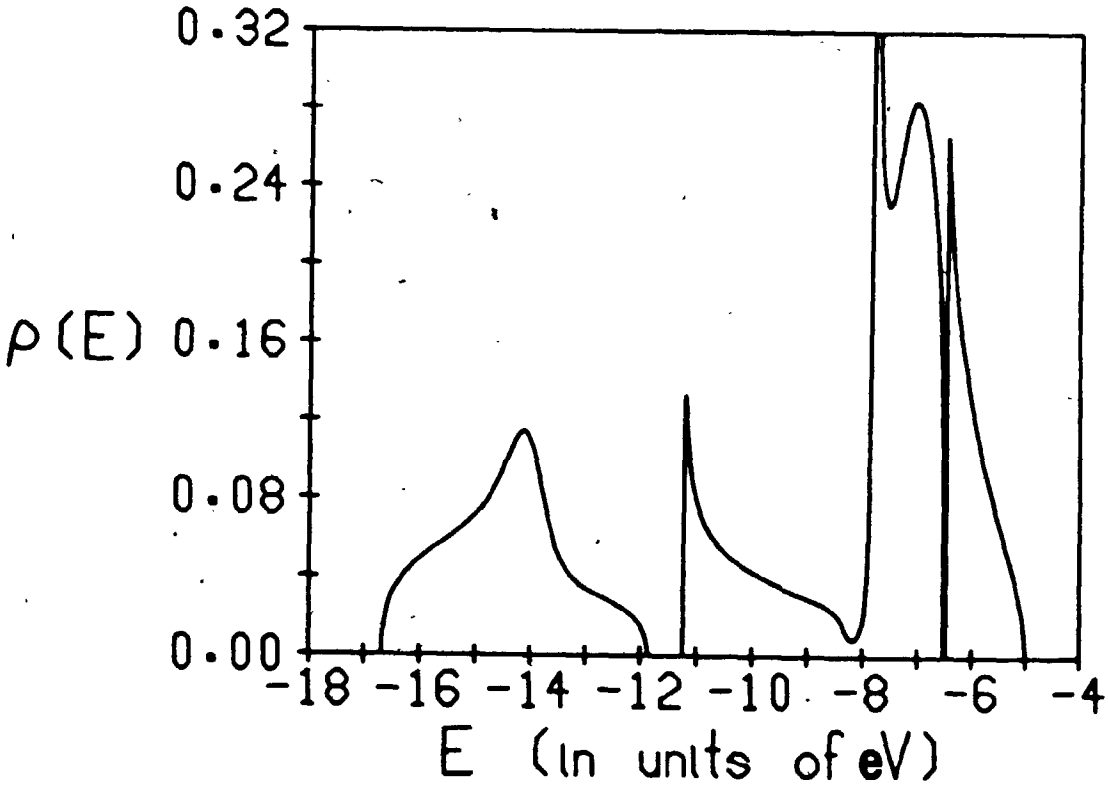

Figure 32

The density of states for the valence band of silicon, as obtained from the enhanced version of the quadratic Padé method, using orders 9, 10, and 11 of the quadratic Padé approximant.

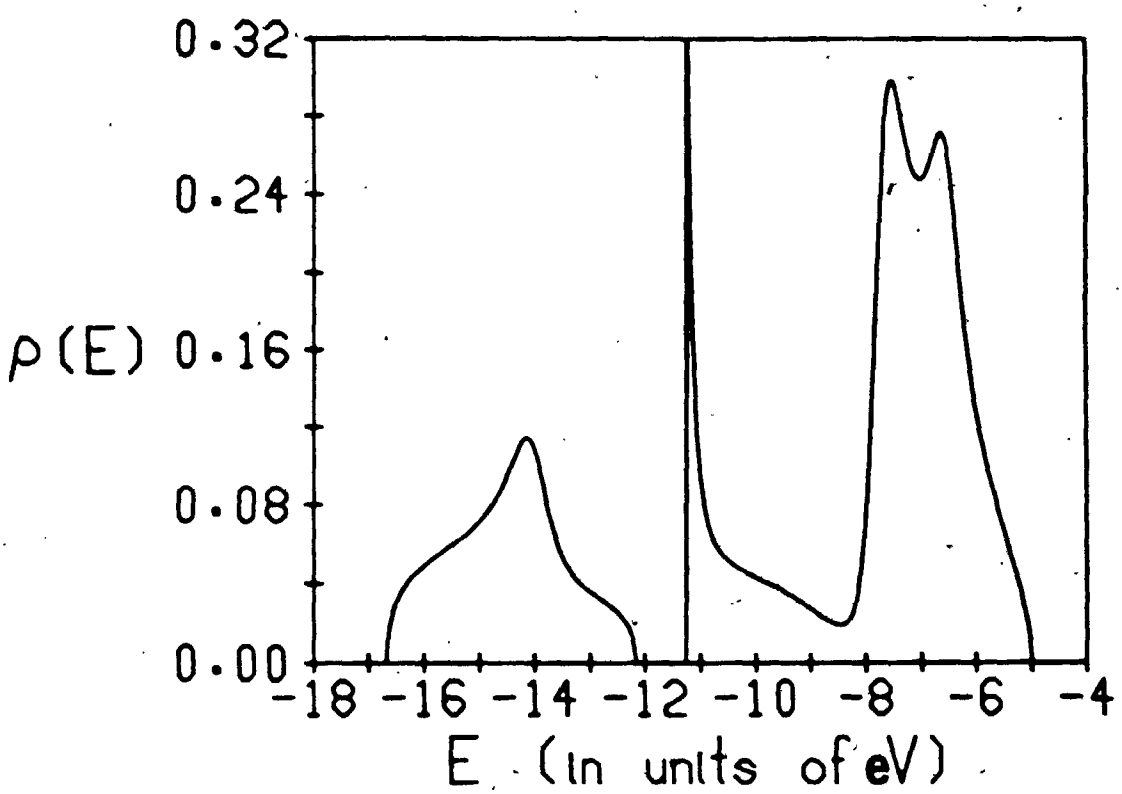

Figure 33

The density of states for the valence band of silicon, as obtained from the enhanced version of the quadratic Padé method, using orders 10, 11, and 12 of the quadratic Padé approximant.

as explained in section 6.b. The band edges are found to be located at E=-16.68eV and at E=-5.00eV.

The results obtained from the continued fraction method in the histogram form (expression (4.a.16)) can be seen in Figure 34. The results obtained by using the quadratic termination (expression (4.a.33)) can be seen in Figure 35. These results have been obtained from the order N=19 Padé approximant.

The calculation of the density of states with the modified moments method has been carried out as outlined in section 4.c. The results obtained from the original sum (expression (4.c.7)) can be seen in Figure 36. The results obtained from the sum enhanced by a Padé approximant (expression (4.c.9)) can be seen in Figure 37. These results have been obtained by using all the 38 available moments.

Comparison between the enhanced quadratic Padé results, the continued fraction results (with the quadratic termination), and the modified moments method results (enhanced by the Padé approximant), shows, that they are all of comparable quality, especially if we bear in mind that the latter two methods tend to smooth out the singularities, whereas the quadratic Padé method tends to produce non-physical oscillations in their vicinity.

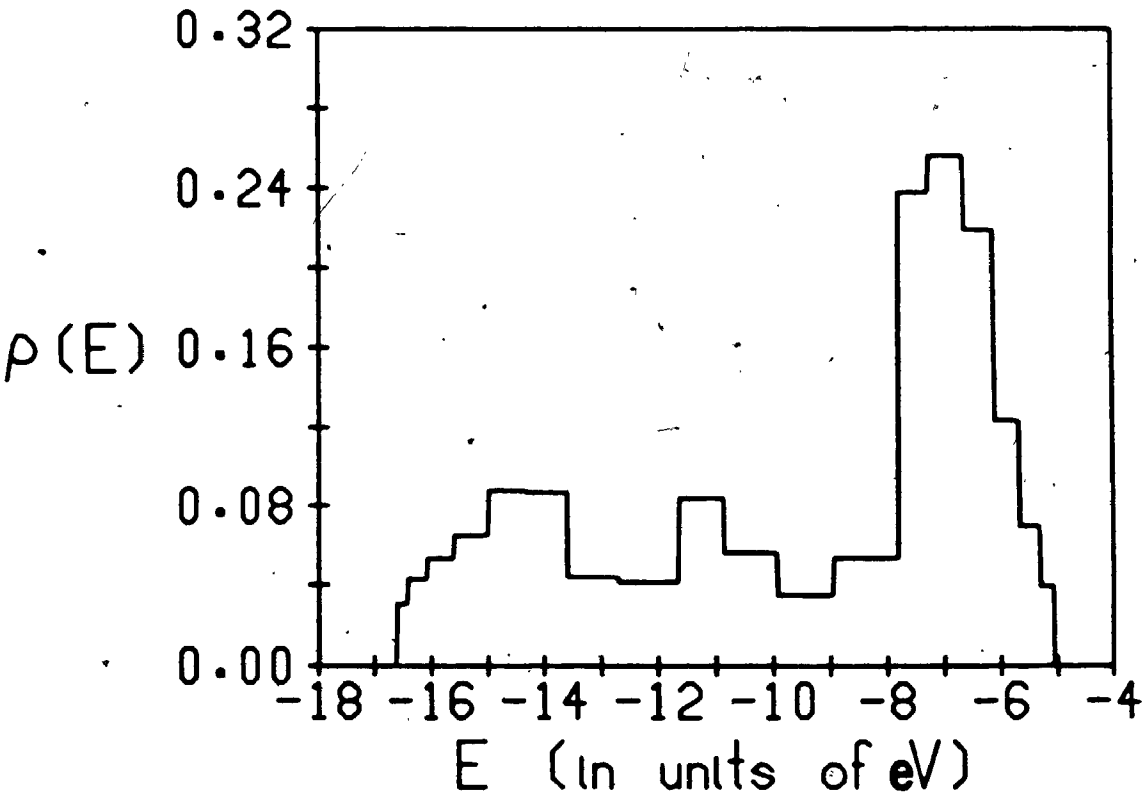

Figure 34

The density of states for the valence band of silicon, in histogram representation, as obtained from the order N=19 Padé approximant (equivalent to the continued fraction truncated at N=19).

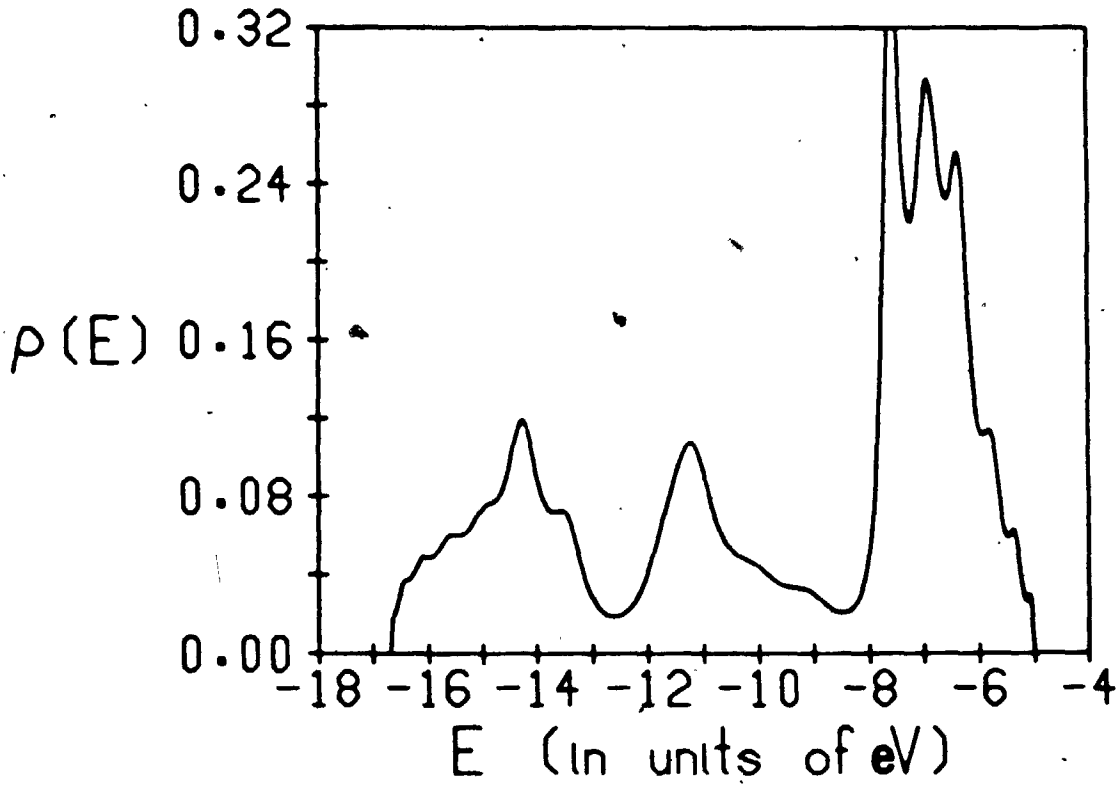

Figure 35

The density of states for the valence band of silicon, as obtained from the continued fraction truncated at N=19, when the quadratic termination scheme is used.

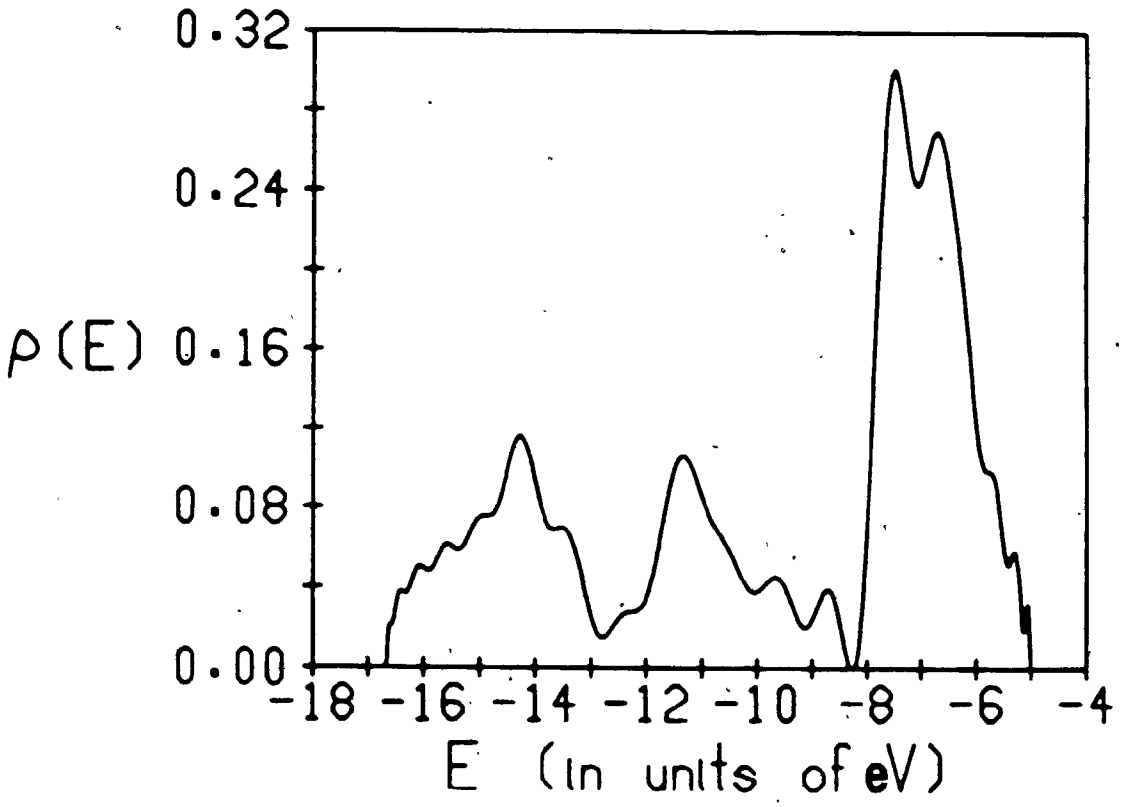

Figure 36

The density of states for the valence band of silicon, as obtained from the modified moments method, when the first 38 moments of the Hamiltonian are used.

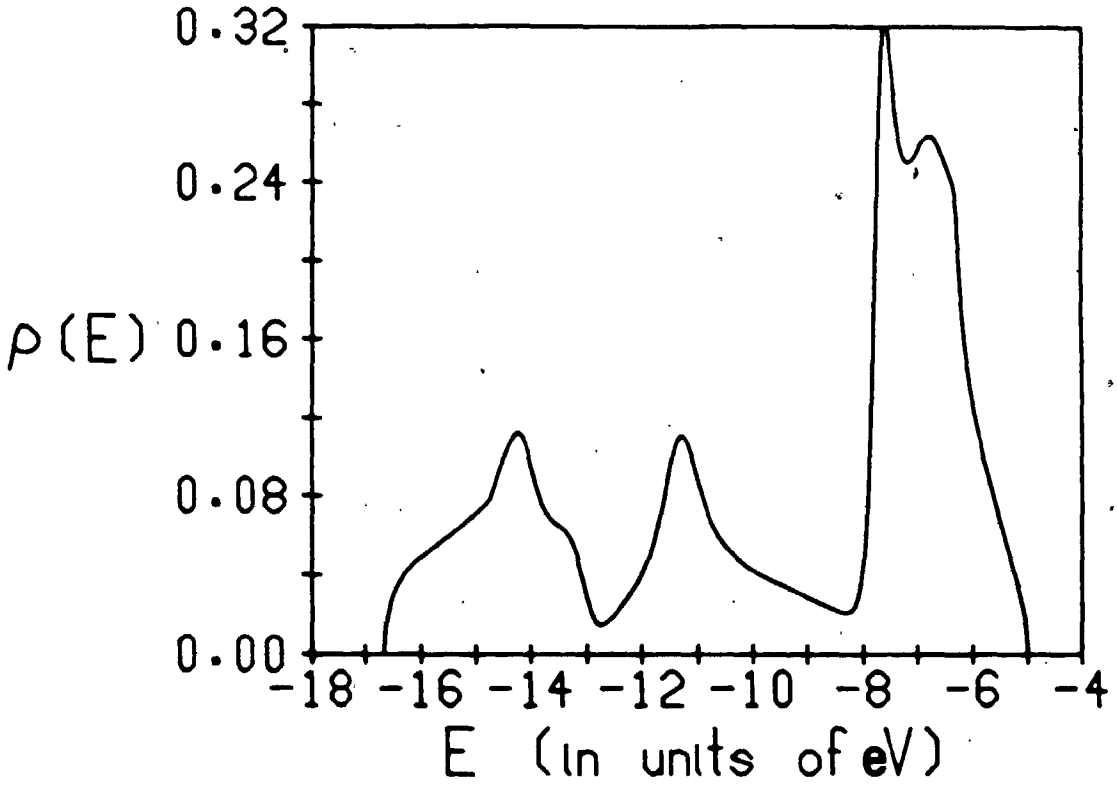

Figure 37

The density of states for the valence band of silicon, as obtained from the modified moments method, with the convergence enhanced by means of a Padé approximant, when the first 38 moments of the Hamiltonian are used.

Chapter 6

Discussion of the quadratic Padé method

6.a. The behaviour of the quadratic Padé results near and between singularities

As we have seen in sections 5.b through 5.e and 5.g, the main limitation of the quadratic Padé method is its failure in the vicinity of singularity points. Therefore the subject of the influence the singularity points have upon the quadratic Padé results deserves further investigation.

The quantitative study of the quadratic Padé results for the cubic lattices and the diamond lattice in section 5.d indicates, that the band edge singularities of the square root type, i.e. singularities where the density of states behaves like $\rho(E) \propto (E-E_0)^{1/2}$, are very accurately reproduced. This fact is not too surprising, if we look at expressions (3.b.15) and (3.b.18), which are used in order to calculate the local density of states from the quadratic Padé approximant polynomials.

The quantitative study of the quadratic Padé results for the square, body centred cubic, face centred cubic, and diamond lattices indicates, that singularities of a logarithmic character are fairly accurately reproduced. Even though the accuracy drops when they are approached, no non-physical oscillations show up near them. A similar type of behaviour occurs at band edge singularities of the type $\rho(E) \propto (E-E_0)^{-1/2}$, as the study of the quadratic Padé results for the regular binary alloy on the simple cubic lattice indicates.

Near singularities inside the energy band(s), which are not of

logarithmic character, however, significant non-physical oscillations occur. These oscillations tend to occur on one side of the singularity point, whereas on the other side the results remain fairly accurate even quite close to the singularity point itself.

The accuracy of the quadratic Padé results in the regions between singularities shows distinct behavioural patterns as well. The accuracy is the highest in the region between a band edge singularity of the square root type and the first internal singularity encountered thereafter. It is lower in the region between a band edge singularity of a type other than the square root type, and the first internal singularity encountered afterwards. It is even lower in the region between two internal singularities. When several internal singularities are present, as in the case of the bonds model for the valence band of silicon, the accuracy drops to nil when moving towards the centre of the energy band, i.e. past a large number of singularity points.

We also note that the non-physical oscillations, observed near the internal singularity points, tend to show up on the side of the singularity point, where the overall accuracy is lower.

6.b. The zeroes of the quadratic Padé polynomials and their relation to the singularity points of the local density of states

The non-physical oscillations observed near the singularities (of the true local density of states) in the quadratic Padé results turn out to be caused by zeroes of the polynomials $p_1^{(n)}(E)$ and $R^{(n)}(E)$ of the quadratic Padé approximant (see section 3.b for the definition of these polynomials) showing up in their vicinity. Therefore we have studied the zeroes of the polynomials $p_j^{(n)}(E)$, $j=1,2,3$, and $R^{(n)}(E)$, for the cases for which the local density of states has been calculated in sections 5.b and 5.e. We have calculated the zeroes by means of the Jenkins-Traub algorithm (Jenkins and Traub 1970).

The results for the square lattice can be seen in Figure 38. They have been obtained from the order N=16 quadratic Padé approximant. We see that the zeroes all fall along the imaginary axis (in the complex energy plane), and along the real axis in the regions $E<-4$ and $E>4$ (with the nearest neighbour interaction energy set to 1). We see especially large concentrations of zeroes around $E=0$ and $E=\pm 4$, i.e. near the singularity points.

The results for the simple cubic lattice can be seen in Figure 39. They have been obtained from the order N=16 quadratic Padé approximant. We see that the zeroes fall along the complex axis, and along distinct curves, which reach the real axis with an increased concentration of zeroes near $E=\pm 2$, i.e. near the Van Hove singularities inside the energy band. We also see a pair of zeroes of $R^{(n)}(E)$ extremely close to the band edge positions at

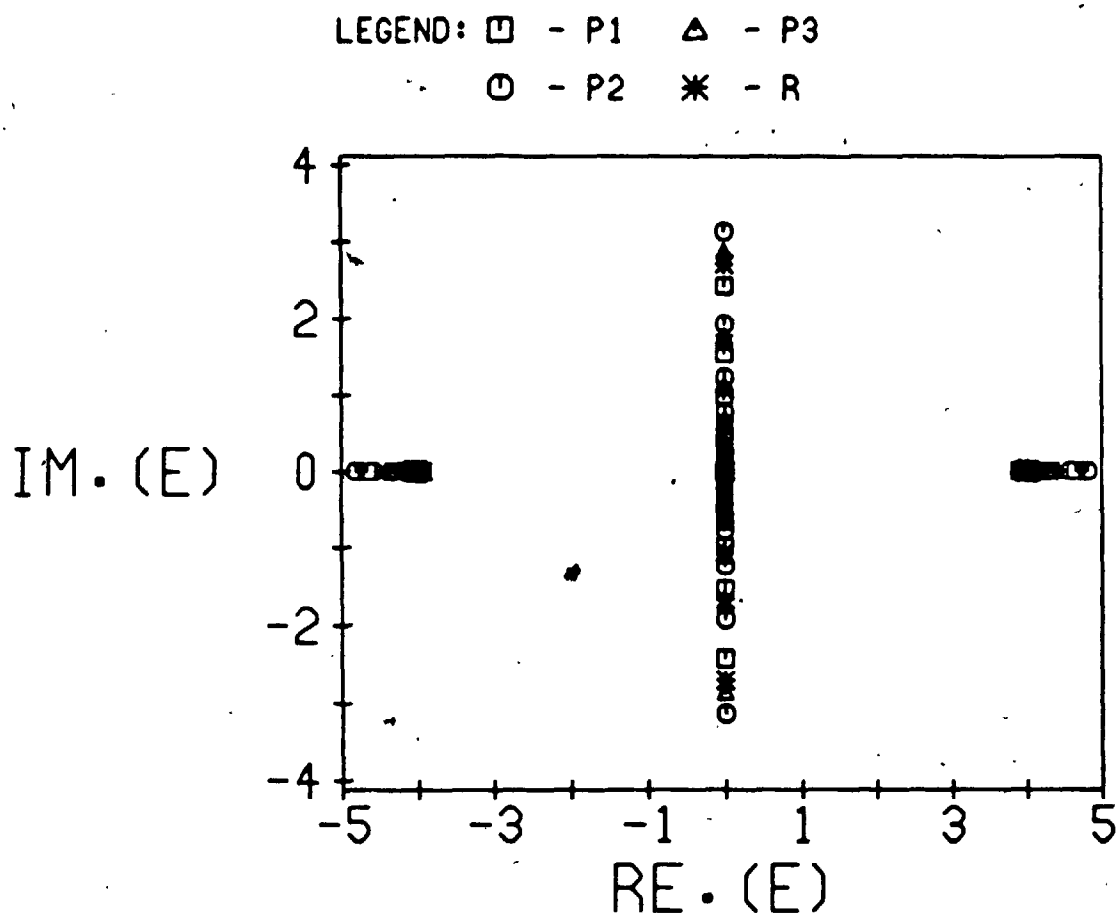

Figure 38

The zeroes of the polynomials $p_j^{(n)}(E)$, $j=1,2,3$, and $R^{(n)}(E)$, for the order N=16 quadratic Pade approximant, in the case of the square lattice. The nearest neighbour interaction energy is equal to 1.

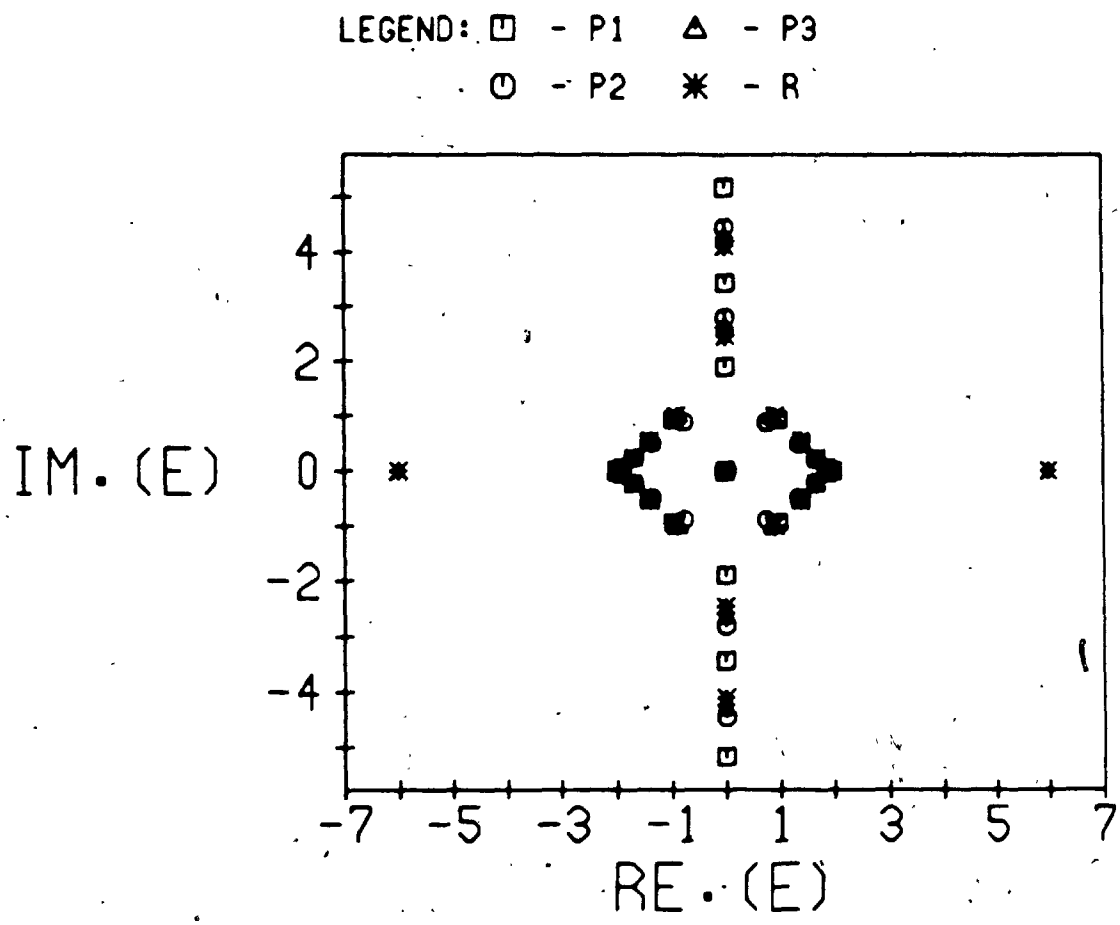

Figure 39

The zeroes of the polynomials $p_j^{(n)}(E)$, j=1,2,3, and $R^{(n)}(E)$, for the order N=16 quadratic Pade approximant, in the case of the simple cubic lattice. The nearest neighbour interaction energy is equal to 1.

E=±6.

The results for the body centred cubic lattice can be seen in Figure 40. They have been obtained from the order N=16 quadratic Padé approximant. We see that the zeroes fall along the imaginary axis, and their concentration increases near E=0. We also see a pair of zeroes of $R^{(n)}(E)$ extremely close to the band edge positions at E=±8.

The results for the face centred cubic lattice can be seen in Figure 41 The self-energy of the lattice sites has been set to 4. and order N=16 of the quadratic Pade approximant has been used. We see that the zeroes fall along distinct curves, and tend to concentrate near the singularities at E=0 and E=4. We also see a very dense cluster of zeroes around E=12.5, i.e. inside the energy band, and a zero of $R^{(n)}(E)$ extremely close to the band edge position at E=16

The results for the diamond lattice can be seen in Figure 42. They are again for the order N=16 quadratic Padé approximant. We see that the zeroes mostly fall along the imaginary axis with a concentration near the singularity at E=0, and along curves which reach the real axis near the singularities at E=-2, again with an increased concentration of zeroes over there. We see very dense clusters of zeroes around E=±3.6 inside the energy band, and a pair of zeroes of $R^{(n)}(E)$ extremely close to the band edge positions at E=-4

The results for the regular binary alloy on the simple cubic lattice can be seen in Figure 43 The self-energies of the lattice sites are E_1=-1 and E_2=1 These results are for a site with energy E_1, and they have been obtained from the order N=16 quad-

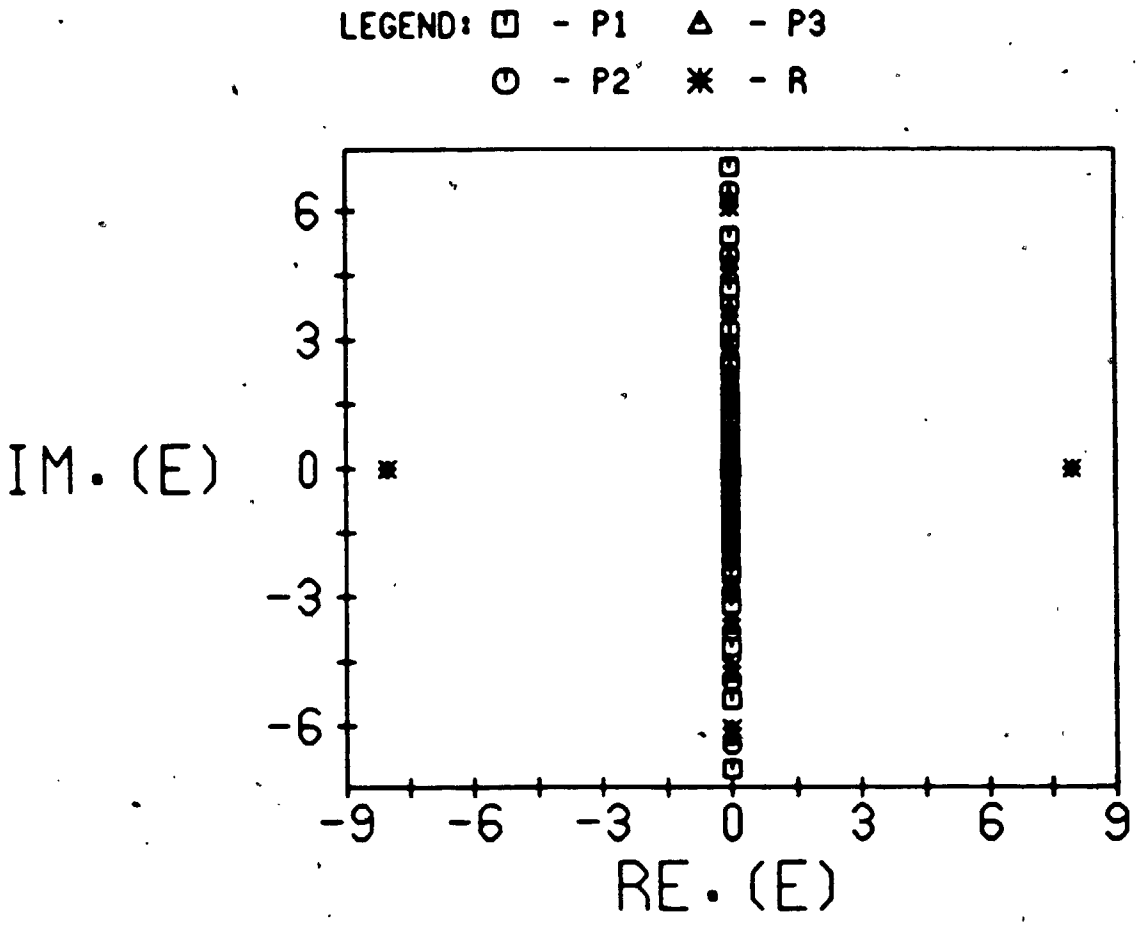

Figure 40

The zeroes of the polynomials $p_j^{(n)}(E)$, $j=1,2,3$, and $R^{(n)}(E)$, for the order N=16 quadratic Padé approximant, in the case of the body centred cubic lattice. The nearest neighbour interaction energy is equal to 1.

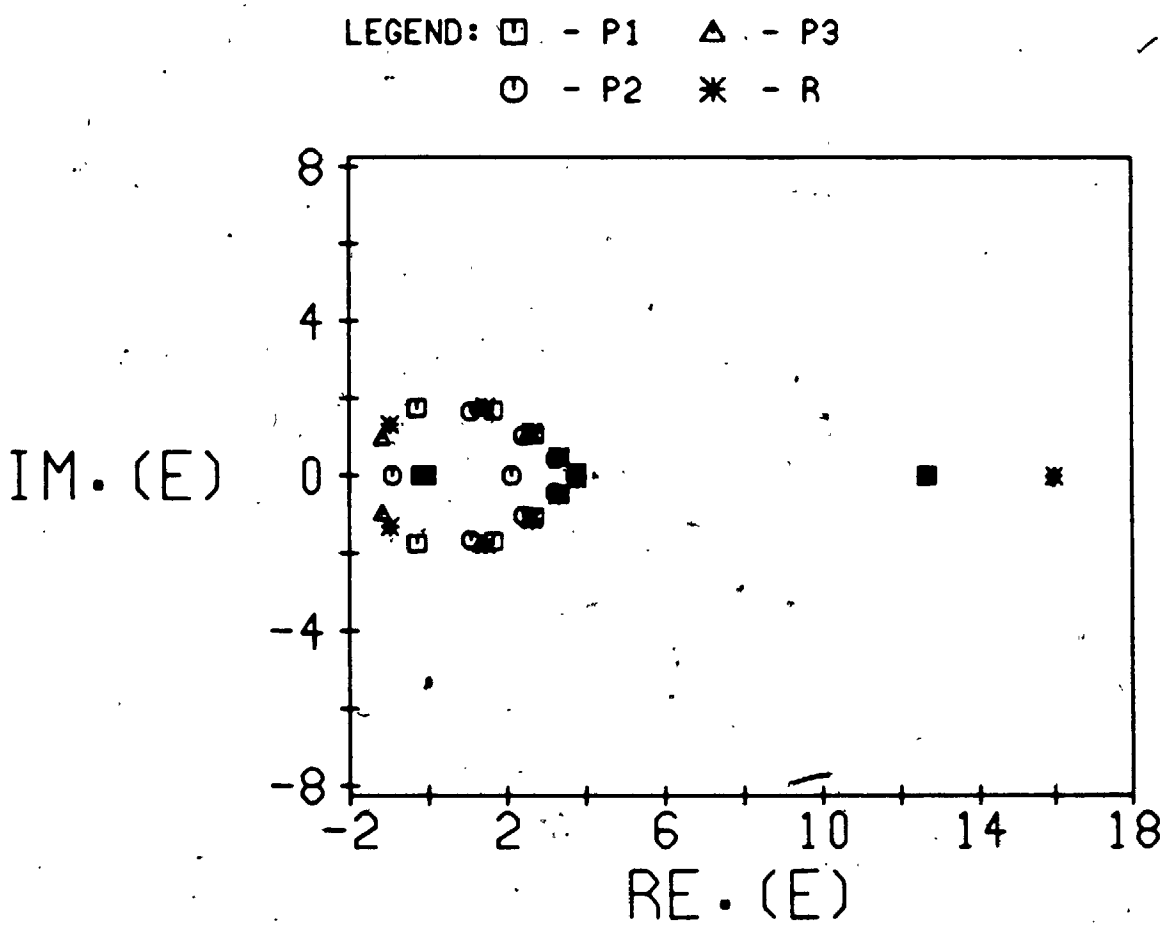

Figure 41

The zeroes of the polynomials $p_j^{(n)}(E)$, j=1,2,3, and $R^{(n)}(E)$, for the order N=16 quadratic Pade approximant, in the case of the face centred cubic lattice. The nearest neighbour interaction energy is equal to 1, and the self-energy of the lattice sites is equal to 4.

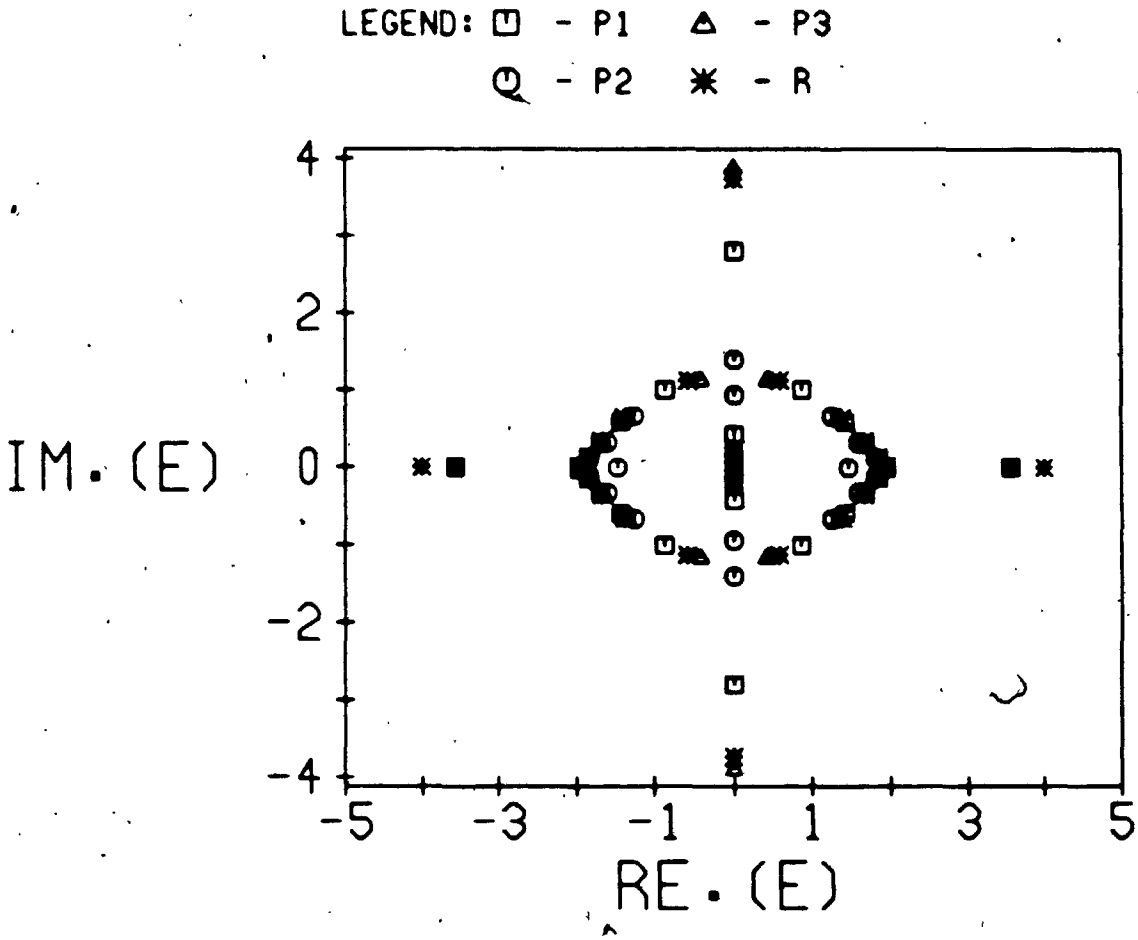

Figure 42

The zeroes of the polynomials $p_j^{(n)}(E)$, j=1,2,3, and $R^{(n)}(E)$, for the order N=16 quadratic Pade approximant, in the case of the diamond lattice. The nearest neighbour interaction energy is equal to 1.

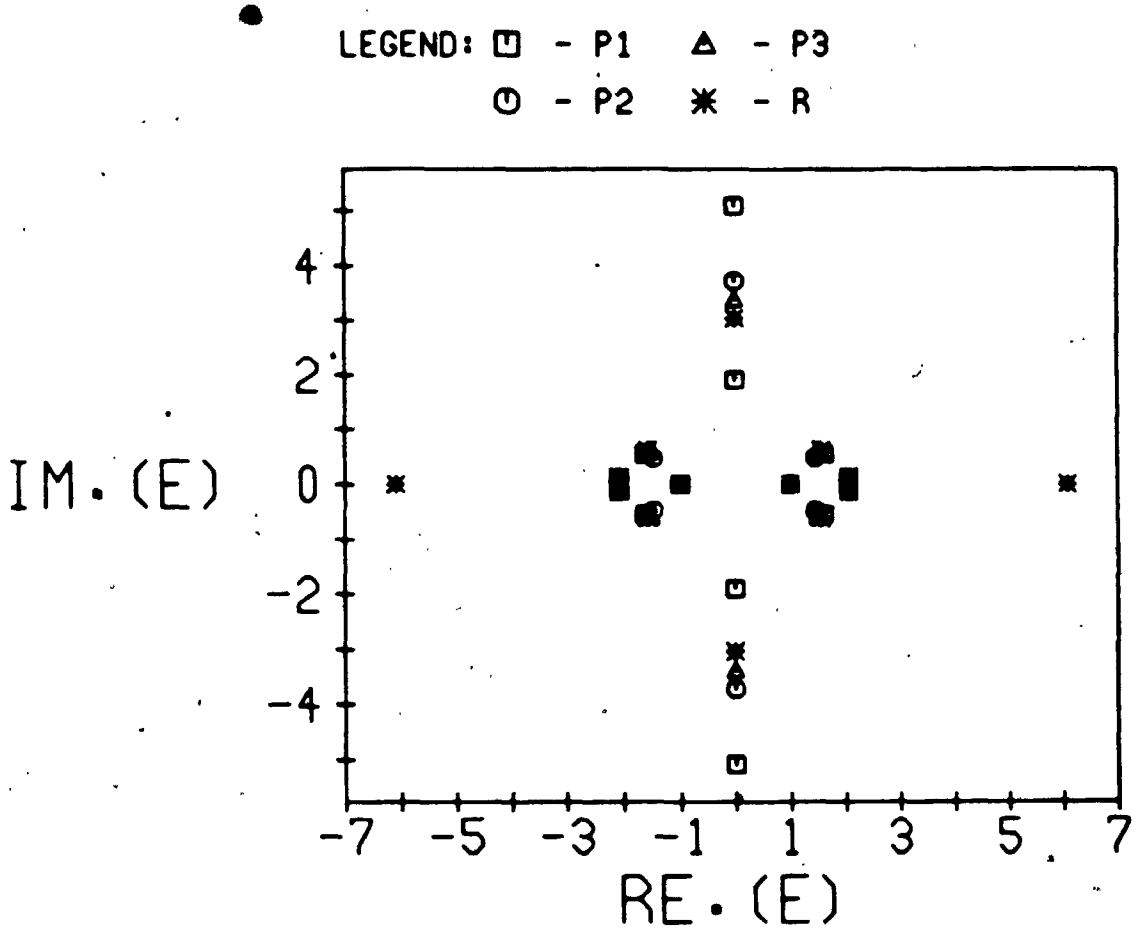

Figure 43

The zeroes of the polynomials $p_j^{(n)}(E)$, $j=1,2,3$, and $R^{(n)}(E)$, for the order $N=16$ quadratic Padé approximant, in the case of the regular binary alloy on the simple cubic lattice. The nearest neighbour interaction energy is equal to 1. The site energies are $E_1=-1$ and $E_2=1$, and these results are for a site with self-energy E_1.

ratic Padé approximant. We see that the zeroes fall along the imaginary axis, and along curves which approach the real axis near the singularities at $E=\pm 1$ and at $E=\pm\sqrt{5}$. We also see a pair of zeroes of $R^{(n)}(E)$ extremely close to the band edge positions at $E=\pm\sqrt{37}$.

The results for the semi-infinite simple cubic lattice for a site at the surface can be seen in Figure 44. The results for sites located 1, 2, and 3 layers away from the surface can be seen in Figures 45, 46, and 47 respectively. The results for the site at the surface are very similar to those for the regular simple cubic lattice. The results for the sites located away from the surface still bear the similarity to those for the regular simple cubic lattice, but now some zeroes also fall along additional curves, which reach the real axis near the band edge positions at $E=\pm 6$.

The results for the valence band of silicon (using the bonds model) can be seen in Figures 48 and 49, which are respectively for orders N=11 and N=12 of the quadratic Padé approximant. We see in each case a large number of zeroes concentrated on the real axis inside the energy band, or very close to it. The orders used here, however, are not high enough in order to observe any distinct patterns or curves in the complex energy plane, which the zeroes tend to follow. A pair of zeroes of $R^{(n)}(E)$ fall in each case very close to the band edge positions, located at $E=-16.68$eV and $E=-5.00$eV.

A more quantitative study of these results reveals a few more details. The zeroes of $R^{(n)}(E)$ near the band edges are located

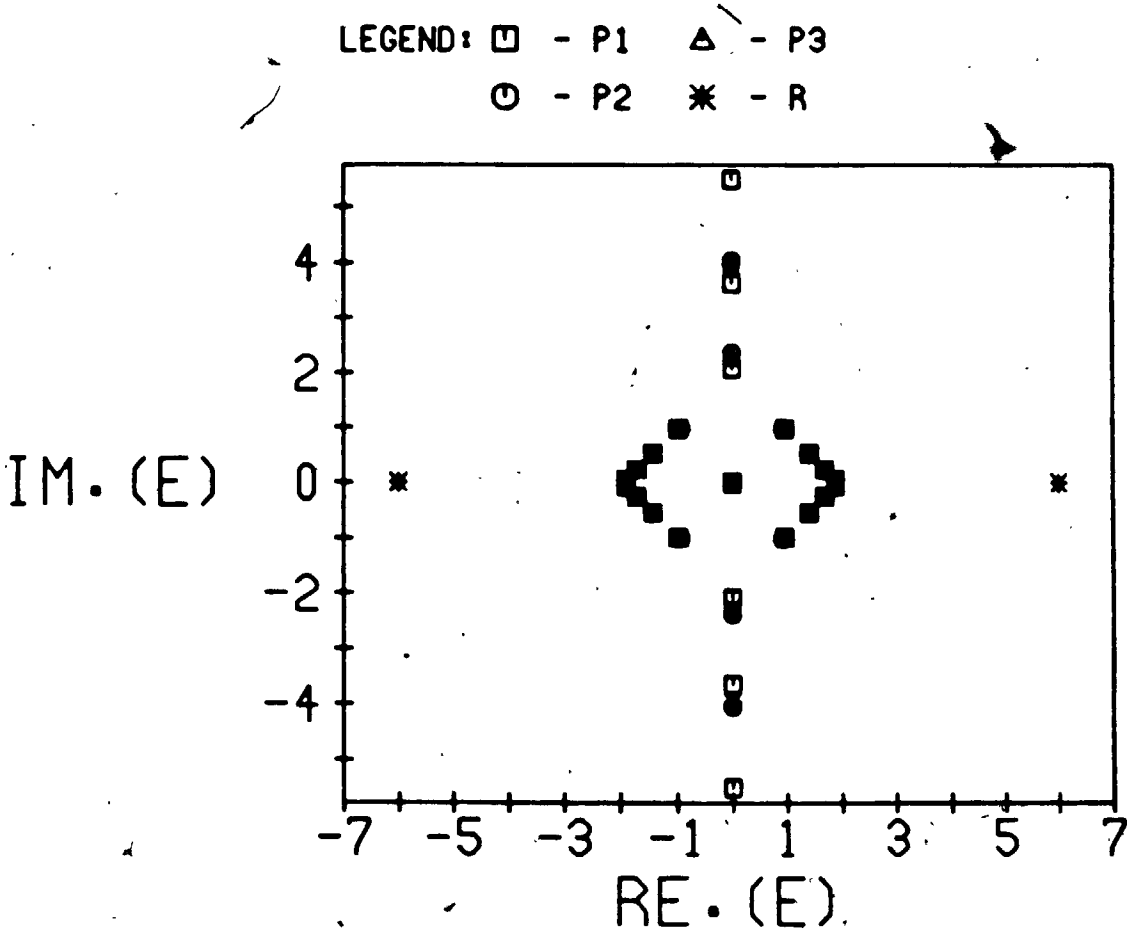

Figure 44

The zeroes of the polynomials $p_j^{(n)}(E)$, j=1,2,3, and $R^{(n)}(E)$, for the order N=16 quadratic Pade approximant, in the case of the semi-infinite simple cubic lattice. The nearest neighbour interaction energy is equal to 1, and these results are for a site located at the surface.

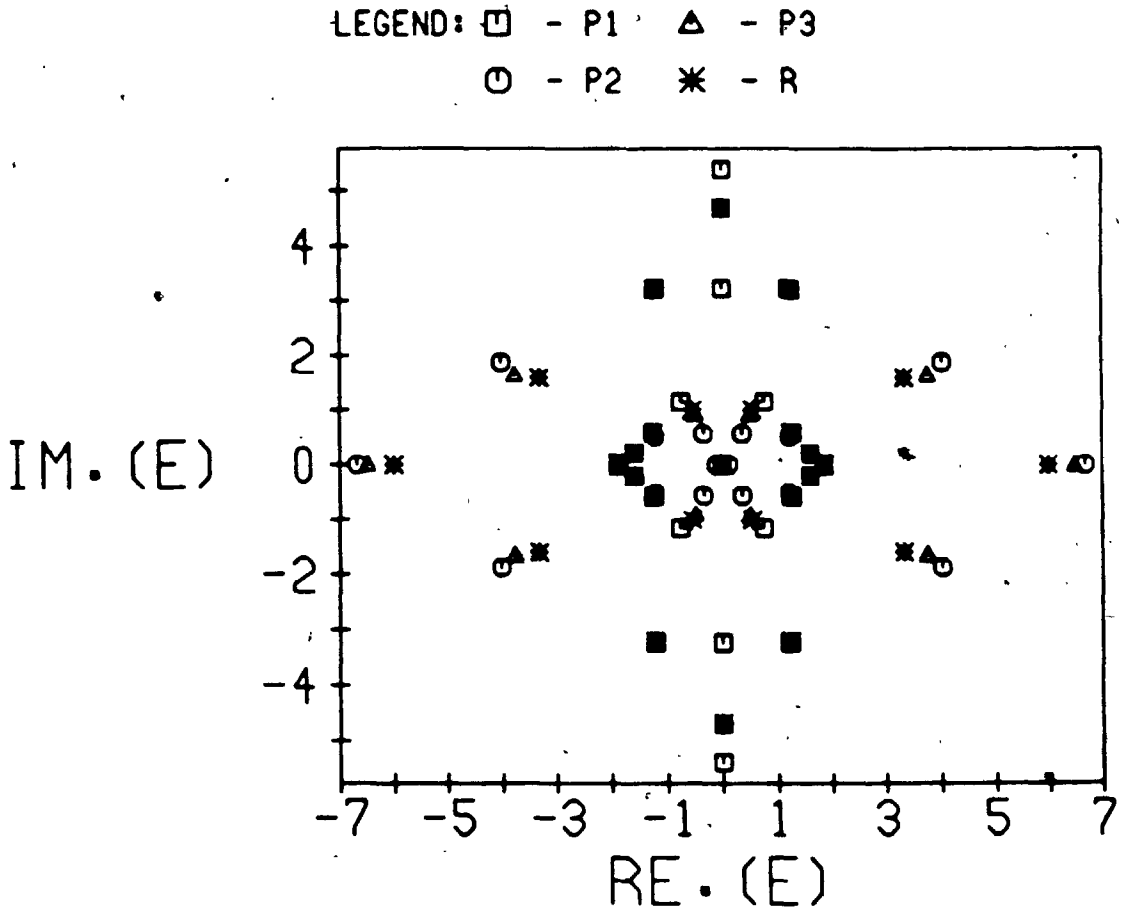

Figure 45

The zeroes of the polynomials $p_j^{(n)}(E)$, j=1,2,3, and $R^{(n)}(E)$, for the order N=16 quadratic Pade approximant, in the case of the semi-infinite simple cubic lattice. The nearest neighbour interaction energy is equal to 1, and these results are for a site located one layer away from the surface.

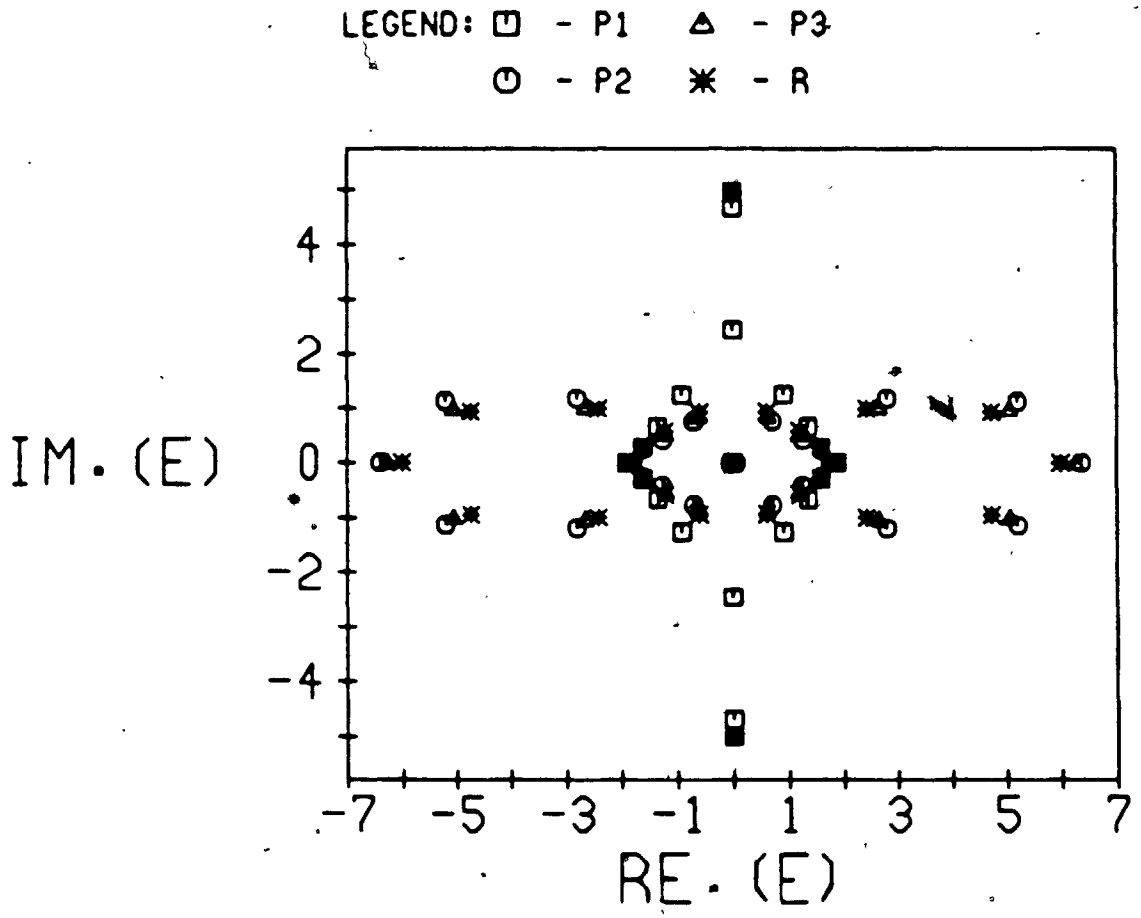

Figure 46

The zeroes of the polynomials $p_j^{(n)}(E)$, j=1,2,3, and $R^{(n)}(E)$, for the order N=16 quadratic Padé approximant, in the case of the semi-infinite simple cubic lattice. The nearest neighbour interaction energy is equal to 1, and these results are for a site located two layers away from the surface.

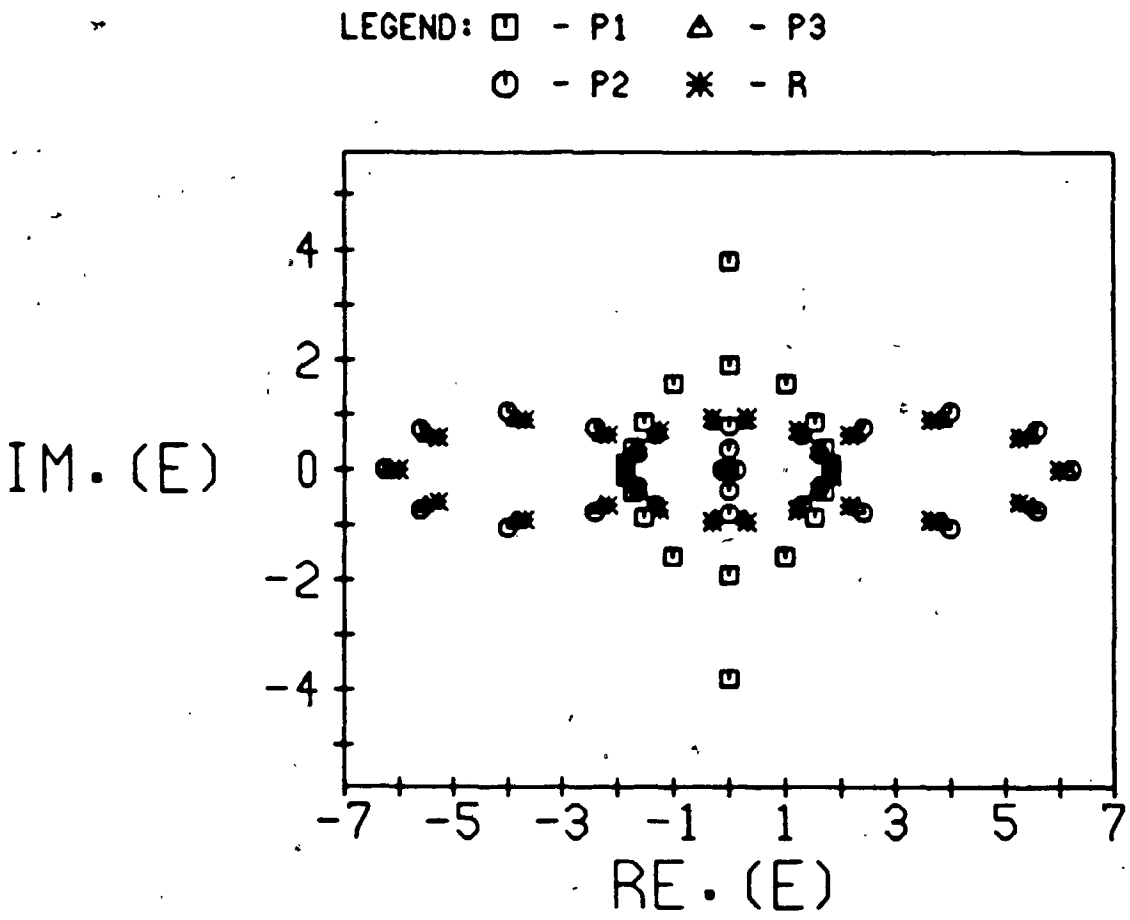

Figure 47

The zeroes of the polynomials $p_j^{(n)}(E)$, j=1,2,3, and $R^{(n)}(E)$, for the order N=16 quadratic Pade approximant, in the case of the semi-infinite simple cubic lattice. The nearest neighbour interaction energy is equal to 1, and these results are for a site located three layers away from the surface.

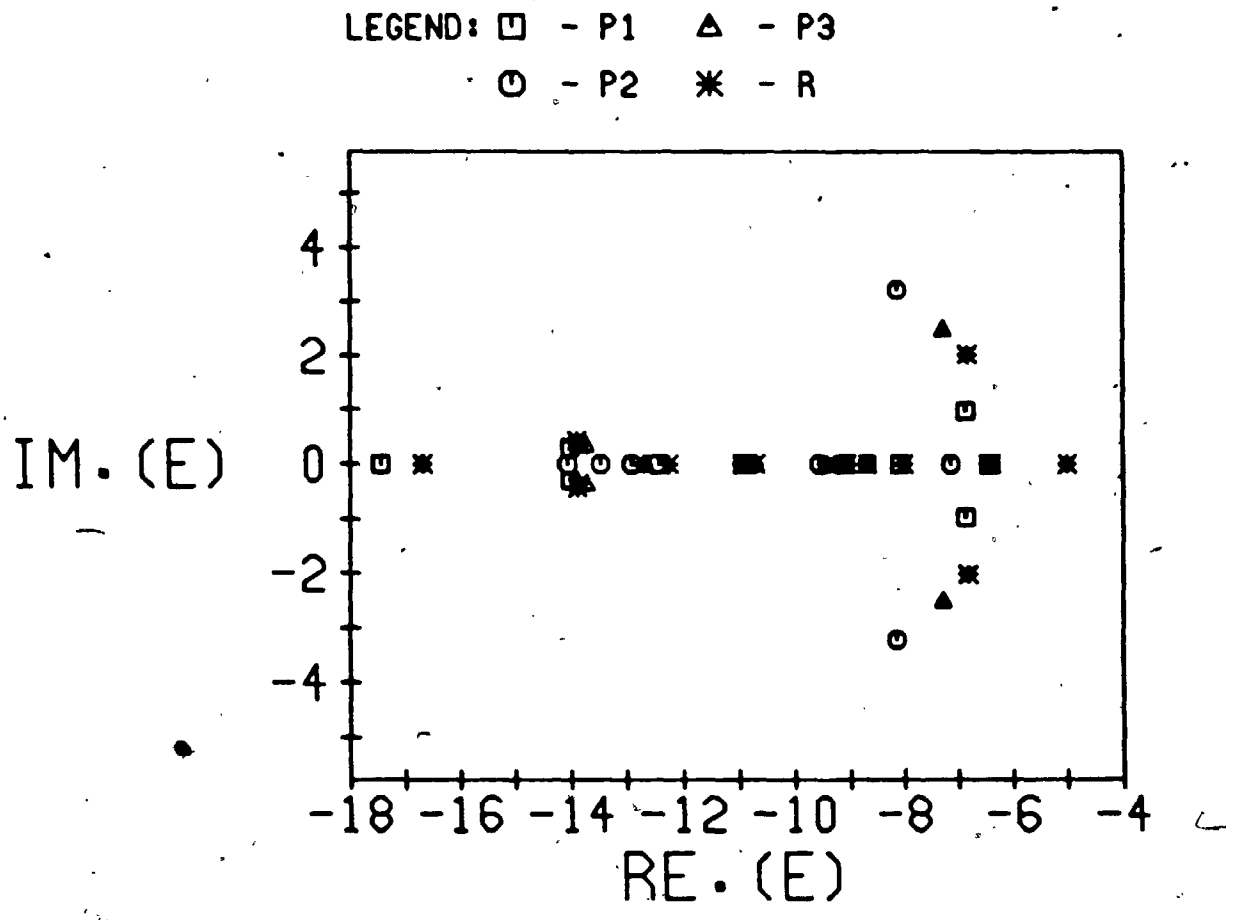

Figure 48

The zeroes of the polynomials $p_j^{(n)}(E)$, j=1,2,3, and $R^{(n)}(E)$, for the order N=11 quadratic Padé approximant, in the case of the bonds model for the valence band of silicon. The energy is given in units of eV.

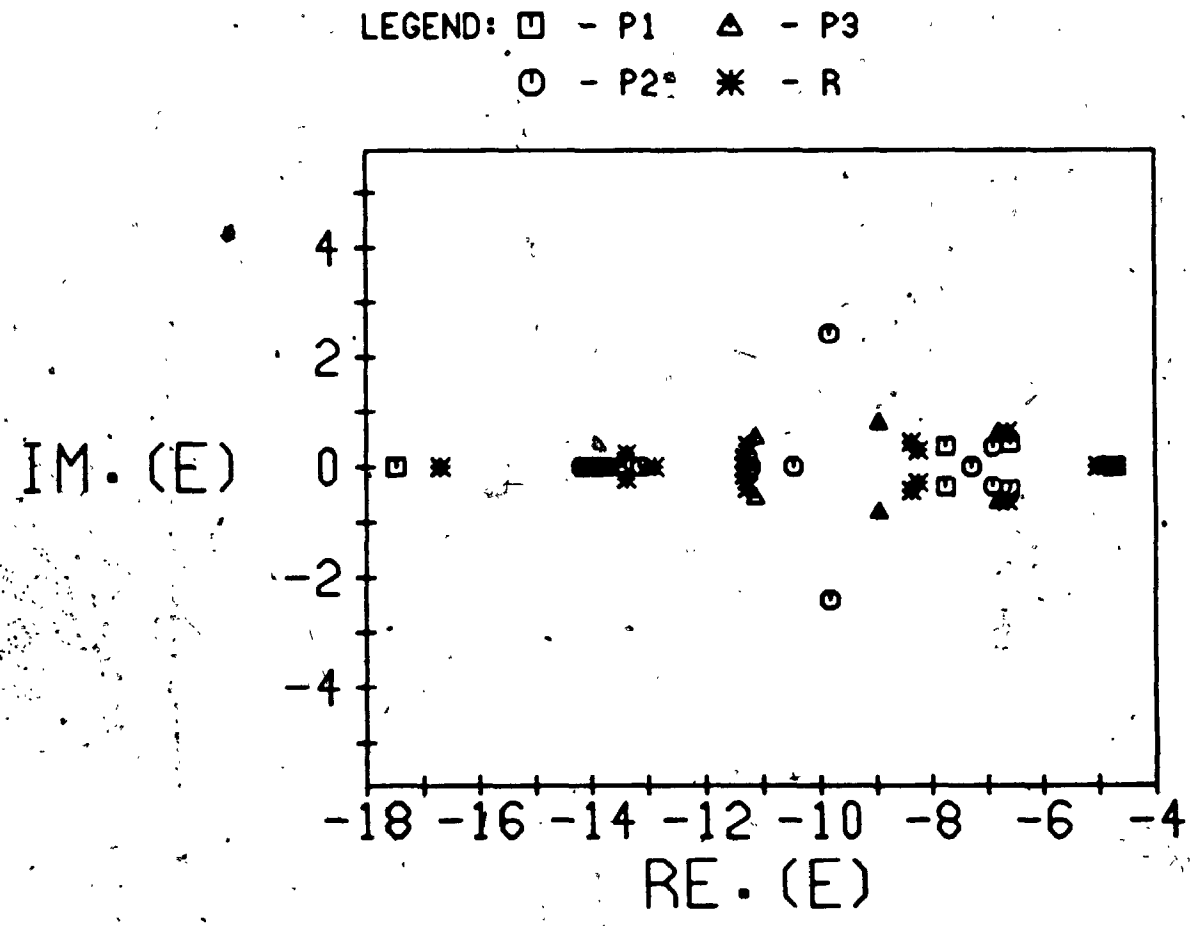

Figure 49

The zeroes of the polynomials $p_j^{(n)}(E)$, j=1,2,3, and $R^{(n)}(E)$, for the order N=12 quadratic Padé approximant, in the case of the bonds model for the valence band of silicon. The energy is given in units of eV.

extremely close to the true band edge positions. If the band edge singularities are of the square root type, the zeroes are extremely close to the true band edge positions - as close as 10^{-10}. Even with other types of band edge singularities they are still very close - as close as 10^{-4} or 10^{-5}. We also see that most of the other zeroes of $R^{(n)}(E)$ occur in pairs, with the members of each pair separated by a very small amount.

We also find that the dense zero clusters within the energy bands in the cases of the face centred cubic and diamond lattices (located around E=12.5 and E=±3.6 respectively) consist of a zero of $p_1^{(n)}(E)$ between two zeroes of $R^{(n)}(E)$, all as close to each other as 10^{-6}. No non-physical oscillations have been observed near these zeroes, as the range over which they occur is much narrower than the separation between the sample points used in the practical calculation of the density of states.

We can summarise the results of our study of the zeroes as follows. The zeroes of $p_j^{(n)}(E)$, j=1,2,3, fall along distinct curves in the complex energy plane, and tend to concentrate near the singularities (of the true density of states), except for the band edge singularities of the square root type. The zeroes of $R^{(n)}(E)$ show a rather similar behaviour. Except for a few zeroes (2N for N bands, assuming that the order of the approximant is high enough) that appear at the band edges, extremely close to the true positions, as can be expected from expression (3.b.15) (or (3.b.18)), all other zeroes of $R^{(n)}(E)$ (or at least most of them) fall along the same curves as those of $p_j^{(n)}(E)$, j=1,2,3, and they usually occur in pairs, the members of each pair being separated by a very small amount.

This way the zeroes of $R^{(n)}(E)$ at the band edges act as branch points that define the branch cuts along the real energy axis, where the energy bands are. The cuts in the approximation are extremely close to the correct positions. The remaining zeroes of $R^{(n)}(E)$, which occur in very close pairs, form short branch cuts in other parts of the complex energy plane. If $\rho(\vec{r},E)$ denotes the approximation for the local density of states, obtained by means of the quadratic Padé approximant, then $\int_{-\infty}^{\infty}\rho(\vec{r},E)dE$ will be slightly less than 1 due to the presence of the other branch cuts outside the real axis. However, as these other branch cuts are extremely short in length, this error is expected to be quite small.

The rest of the zeroes form boundaries on the second (non-physical) Riemann sheet below. The Green function's analytic continuation can be carried into this sheet as far as the boundary, but not further. These boundaries intersect the branch cuts on the real axis (energy bands) or approach them very closely at the singularities of the bands, thus causing the non-physical oscillations observed in the quadratic Padé results in these regions.

6.c. The applicability and limitations of the quadratic Padé method

We have seen that the quadratic Padé method has certain advantages and disadvantages, when compared to other methods for calculating the local density of states, which are of similar generality and complexity, namely the continued fraction method and the modified moments method.

The quadratic Padé method has several advantages over the other methods. The first noteworthy advantage is, that the quadratic Pade method directly approximates the local density of states by a smooth function. The continued fraction method, on the other hand, directly produces an approximation by a smooth function only when the continued fraction expansion is infinite, and thus in any practical calculation, where the continued fraction has to be truncated at some point, only a sum of weighted delta-functions is obtained (see sections 1.d and 4.a). An approximation for the local density of states in the form of a smooth function can be obtained in various ways, but this involves the knowledge of the band edge positions, as in the quadratic termination (Haydock 1975, Haydock 1980; see also section 4.a), or some kind of analysis of the available continued fraction coefficients (Turchi et al 1982, Magnus 1983, Trias et al 1983; see also sections 1.d and 4.a).

The second important advantage of the quadratic Padé method is the fact, that it does not require a prior knowledge of the positions of the band edges. The band edges are directly reproduced with high accuracy, as we have seen in sections 5.d, 6.a, and

6.b. The continued fraction method, on the other hand, usually requires a prior knowledge of the band edge positions, in order to obtain a good approximation for the local density of states from the truncated continued fraction (usually by means of the quadratic termination). The modified moments method also requires a prior knowledge of the band edge positions, as we can see from its review in section 4.c.

A closely related advantage of the quadratic Padé method is its ability to reproduce multi-band spectra without prior knowledge of the band edge and band gap positions, as we have seen in the case of the regular binary alloy. The continued fraction method, on the other hand, can not directly distinguish between a band gap and a region where the local density of states is just lower, without additional information about the location of the band gap. The modified moments method is suitable for one band problems only, at least in the form available to us (see section 4.c).

The main drawback of the quadratic Padé method is its tendency to produce non-physical oscillations in the vicinity of singularity points in the enrgy band(s). This may become a serious problem in realistic cases, where the number of singularities is usually large. We have also seen, in section 5.f, that this problem can be somewhat overcome by using a convergence enhancement scheme.

Another drawback is the numerical instability of the method, which makes it necessary to use multiple precision arithmetic for the actual computation (see the last paragraph of section 2.c). This is, however, not a serious drawback, as the computational

method used (section 2.c) is fairly efficient, and the computation time (of the density of states from the given moments via the quadra[redacted] Padé polynomials) is quite small - a few seconds (even though[redacted]iple precision arithmetic is used).

We see thus that the quadratic Padé method, if necessary, in its enhanced version, can be used for density of states calculations in cases, where the number of singularity points inside the energy band(s) is not too large. In other cases it is still useful, as the band edge positions can be found with considerable accuracy from the zeroes of the polynomial $R^{(n)}(E)$ (see sections 3.b and 6.b), and then used for the density of states calculation by means of the continued fraction method (with the quadratic termination) or the modified moments method.

In cases where we are mainly interested in the density of states near the band edges, the quadratic Padé method can be generally expected to yield rather accurate results, as we have seen that the accuracy of the method is the highest near the band edges, and it drops only when moving, past the singularity points, into the central portion of the band.

Appendix A

Convergence enhancement of a power series by means of the quadratic Padé approximant

As an example for the use of the quadratic Padé approximant for convergence enhancement of power series we choose the function $F(x)=(1-x)^{1/3}$. The power series expansion of F(x) is given by

$$F(x)=1-\sum_{n=1}^{\infty}\left[\prod_{m=1}^{n-1}(3m-1)/3^n n!\right]x^n. \qquad (A.1)$$

We see that F(x) is complex for $x>1$, even though all the coefficients in the power series itself are real. The power series converges to the true value of F(x), namely $(1-x)^{1/3}$, only for $-1\leq x<1$.

We assume now that only the first 8 coefficients in F(x) are known, i.e. F(x) is originally approximated by the finite sum

$$F(x)\simeq 1-\frac{1}{3}x-\frac{1}{9}x^2-\frac{5}{81}x^3-\frac{10}{243}x^4-\frac{22}{729}x^5-\frac{154}{6561}x^6-\frac{374}{19683}x^7. \qquad (A.2)$$

The quadratic Padé approximant of order (2,2,2) is calculated now by using (2.b.1). If the coefficient of x^0 in $P_1^{(2)}(x)$ is arbitrarily chosen as 1, one is left with a set of 8 linear equations with 8 variables for the remaining coefficients. The polynomials of the quadratic Padé approximant are thus found to be given by

$$P_1^{(2)}(x)=1-2x-\frac{1}{27}x^2,$$

$$P_2^{(2)}(x)=-2+2x+\frac{8}{27}x^2,$$

$$P_3^{(2)}(x)=1-\frac{28}{27}x^2. \qquad (A.3)$$

The function f(x), which is an approximation for the true value of F(x), is found now by using (2.b.3). The result is

$$f(x)=[(2-2x-\frac{8}{27}x^2)\pm\frac{8}{3}x(1-x-\frac{1}{108}x^2)^{1/2}]/2(1-2x-\frac{1}{27}x^2). \qquad (A.4)$$

Table 2 shows a comparison between the values for F(x), as obtained by using the finite series expansion (A.2) and the quadratic Pade approximant based expression (A.4), and the exact value $(1-x)^{1/3}$, for selected values of x.

A look at the table reveals that the use of the quadratic Pade approximant greatly enhances the convergence of the power series to the true value of F(x). This is true even for X>1, where even the ordinary Pade approximant (Baker and Graves-Morris 1981a and b), often used for enhancing the convergence of power series, is not useful.

Table 2

Comparison between the exact values of $F(x)=(1-x)^{1/3}$, the values obtained by using the first 8 terms in the power series expansion, and the values obtained by using the quadratic Padé approximant of order (2,2,2), for selected values of x.

x	power series	quadratic Padé approximant	exact value of $(1-x)^{1/3}$
-100	1.876943×10^{12}	5.868054	4.657010
-50	1.448709×10^{10}	3.861117	3.708430
-20	2.290973×10^{7}	2.774250	2.758924
-10	1.692009×10^{5}	2.226185	2.223980
-5	1.193908×10^{3}	1.817350	1.817121
-2	2.953259	1.442255	1.442250
-1	1.268506	1.259921	1.259921
-0.5	1.144758	1.144714	1.144714
-0.2	1.062659	1.062659	1.062659
0	1.000000	1.000000	1.000000
0.2	0.928318	0.928318	0.928318
0.5	0.793809	0.793700	0.793701
1	0.380023	0.142857+0.123718i	0.000000
2	-6.163441	0.505882+0.862602i	0.500000+0.866025i
5	-1.982405×10^{3}	0.776119+1.381605i	0.793701+1.374730i
10	-2.169882×10^{5}	1.048940+1.850238i	1.040042+1.801405i
20	-2.592740×10^{7}	1.454253+2.361105i	1.334201+2.310904i
50	-1.522111×10^{10}	2.188865+2.955579i	1.829653+3.169052i
100	-1.923895×10^{12}	2.775841+3.241405i	2.313033+4.006290i

Appendix B

A proof for the rational expression for the approximate local Green function for the truncated continued fraction with a quadratic termination.

We are going to show here, by induction, that the approximation for the local density of states, using the continued fraction expansion, truncated at a_N, with the quadratic termination (expression (4.a.26)), is equivalent to the rational expression for the approximate local density of states (expression (4.a.27)).

Using the recurrence relation for the polynomials $P_n(E)$ and $Q_n(E)$ (expressions (4.a.8) and (4.a.9)) we have for N=2:

$$P_{N-1}(E)=E-a_1 \quad ; \quad P_{N-2}(E)=1,$$

$$Q_{N-1}(E)=1 \quad ; \quad Q_{N-2}(E)=0. \qquad (B.1)$$

Thus expression (4.a.27) for this case becomes

$$G_N(E) = \frac{(E-a_0)+i\eta(E)}{[(E-a_0)(E-a_1)-2b_1^2]+i(E-a_1)\eta(E)} = \frac{1}{E-a_1-\dfrac{2b_1^2}{E-a_0+i\eta(E)}} \qquad (B.2)$$

Thus the expression (4.a.27) is equivalent to the expression (4.a.26) for N=2.

Now we assume that the two expressions are equivalent for N. We have the relation

$$E-a_{N-1}-\cfrac{b_{N-1}^2}{E-a_N-\cfrac{2b_N^2}{E-a_0+i\eta(E)}} =$$

$$E-a_{N-1}-\frac{b_{N-1}^2(E-a_0)+ib_{N-1}^2\eta(E)}{[(E-a_0)(E-a_N)-2b_N^2]+i(E-a_N)\eta(E)} \qquad (B.3)$$

When we use it for the continued fraction expression (4.a.26) for $G_{N+1}(E)$, then we get an expression similar to that for $G_N(E)$, but with thw following differences:

$2b_{N-1}^2$ is replaced by $b_{N-1}^2(E-a_0)+ib_{N-1}^2\eta(E)$,

$E-a_0$ is replaced by $(E-a_0)(E-a_N)-2b_N^2$,

$\eta(E)$ is replaced by $(E-a_N)\eta(E)$.

By using the equivalence for $G_N(E)$, which has been assumed to be valid, we obtain:

$$G_{N+1}(E) = \frac{C_1Q_{N-1}(E)-C_2Q_{N-2}(E)+iQ_{N-1}(E)(E-a_N)\eta(E)}{C_1P_{N-1}(E)-C_2P_{N-2}(E)+iP_{N-1}(E)(E-a_N)\eta(E)} , \qquad (B.4)$$

where

$$C_1=(E-a_0)(E-a_N)-2b_N^2 \; ; \; C_2=b_{N-1}^2(E-a_0)+ib_{N-1}^2\eta(E) . \qquad (B.5)$$

By using the recurrence relation (4.a.8) for the polynomials $Q_n(E)$ we have

$$[(E-a_0)(E-a_N)-2b_N^2]Q_{N-1}(E)-[b_{N-1}^2(E-a_0)+ib_{N-1}^2\eta(E)]Q_{N-2}(E)+$$

$$iQ_{N-1}(E)(E-a_N)\eta(E)=$$

$$(E-a_0)[(E-a_N)Q_{N-1}(E)-b_{N-1}^2Q_{N-2}(E)]-2b_N^2Q_{N-1}(E)+$$

$$i[(E-a_N)Q_{N-1}(E)-b_{N-1}^2Q_{N-2}(E)]\eta(E)=$$

$$[(E-a_0)Q_N(E)-2b_N^2Q_{N-1}(E)]+iQ_N(E)\eta(E). \qquad (B.6)$$

We use a similar treatment for the denominator, as the polynomials $P_n(E)$ follow the same recurrence relation, and thus we obtain

$$G_{N+1}(E) = \frac{[(E-a_0)Q_N(E)-2b_N^2Q_{N-1}(E)]+iQ_N(E)\eta(E)}{[(E-a_0)P_N(E)-2b_N^2P_{N-1}(E)]+iP_N(E)\eta(E)} . \qquad (B.7)$$

This completes the proof by induction.

Appendix C

The calculation of the moments for the simple cubic, body centred cubic, and face centred cubic lattices

In this appendix we derive the expressions for the moments of the simple cubic lattice (expression (5.a.28)), the body centred cubic lattice (expression (5.a.29)), and the face centred cubic lattice (expression (5.a.30)). In each case V denotes the nearest neighbour interaction energy, and a denotes the lattice constant (size of the cubic unit cell).

In the case of the simple cubic lattice we have

$$E(\vec{k})=2V[\cos(k_x a)+\cos(k_y a)+\cos(k_z a)]. \qquad (C.1)$$

The unit cell in $\vec{k}$-space is given by $-\pi/a<k_i<\pi/a$, $i=x,y,z$, and thus $\Omega_0=(2\pi/a)^3$. Therefore we have

$$\mu_n=(a/2\pi)^3(2V)^n\int_{-\pi/a}^{\pi/a}\int\int[\cos(k_x a)+\cos(k_y a)+\cos(k_z a)]^n dk_x dk_y dk_z. \qquad (C.2)$$

By using new variables - $\theta_x=k_x a$, $\theta_y=k_y a$, and $\theta_z=k_z a$ - this becomes

$$\mu_n=(a/2\pi)^3(2V)^n(1/a^3)\int_{-\pi}^{\pi}\int\int(\cos\theta_x+\cos\theta_y+\cos\theta_z)^n d\theta_x d\theta_y d\theta_z=$$

$$(1/8\pi^3)(2V)^n\sum_{m=0}^{n}\binom{n}{m}\int_{-\pi}^{\pi}\int\int(\cos\theta_x+\cos\theta_y)^m\cos^{n-m}\theta_z\, d\theta_x d\theta_y d\theta_z. \qquad (C.3)$$

Making use of (5.a.7), (5.a.11), and (5.a.13), we have

$$\int_{-\pi}^{\pi}\int(\cos\theta_x+\cos\theta_y)^{2m}d\theta_x d\theta_y=(1/4^m)\binom{2m}{m}4\pi^2 \qquad (C.4)$$

and

$$\int_{-\pi}^{\pi} \cos^{2(n-m)}\theta_z d\theta_z = (1/4^{n-m})\binom{2(n-m)}{n-m} 2\pi. \qquad (C.5)$$

Substituting these results into (C.3) we have now

$$\mu_{2n} = (1/8\pi^3)(2V)^{2n} \sum_{m=0}^{n} \binom{2n}{2m}[(1/4^m)\binom{2m}{m}^2 4\pi^2][(1/4^{n-m})\binom{2(n-m)}{n-m}2\pi] =$$

$$V^{2n} \sum_{m=0}^{n} \binom{2n}{2m}\binom{2m}{m}^2 \binom{2(n-m)}{n-m} = V^{2n} \sum_{m=0}^{n} \{(2n)!(2m)!/(m!)^4[(n-m)!]^2\} =$$

$$V^{2n}\binom{2n}{n} \sum_{m=0}^{n} \binom{2m}{m}\binom{n}{m}^2. \qquad (C.6)$$

Obviously $\mu_{2n+1}=0$ as before.

With the energy in units of V we have thus

$$\mu_{2n} = \binom{2n}{n} \sum_{m=0}^{n} \binom{2m}{m}\binom{n}{m}^2 \; ; \; \mu_{2n+1}=0. \qquad (C.7)$$

This is exactly expression (5.a.28).

In the case of the body centred cubic lattice we have

$$E(\vec{k}) = 2V[\cos(k_x a/2 + k_y a/2 + k_z a/2) + \cos(k_x a/2 + k_y a/2 - k_z a/2) +$$

$$\cos(k_x a/2 - k_y a/2 + k_z a/2) + \cos(-k_x a/2 + k_y a/2 + k_z a/2)] =$$

$$8V\cos(k_x a/2)\cos(k_y a/2)\cos(k_z a/2). \qquad (C.8)$$

The unit cell and Ω_0 are given in this case by $-2\pi/a \leq k_i \leq 2\pi/a$, $i=x,y,z$, and by $(4\pi/a)^3$ respectively, and thus we have

$$\mu_n = (a/4\pi)^3 (8V)^n \int_{-2\pi/a}^{2\pi/a}\int\int [\cos^n(k_x a/2)\cos^n(k_y a/2)\cos^n(k_z a/2)]x$$

$$dk_x dk_y dk_z. \qquad (C.9)$$

By changing the variables to $\theta_x = k_x a/2$, $\theta_y = k_y a/2$, and $\theta_z = k_z a/2$, we obtain

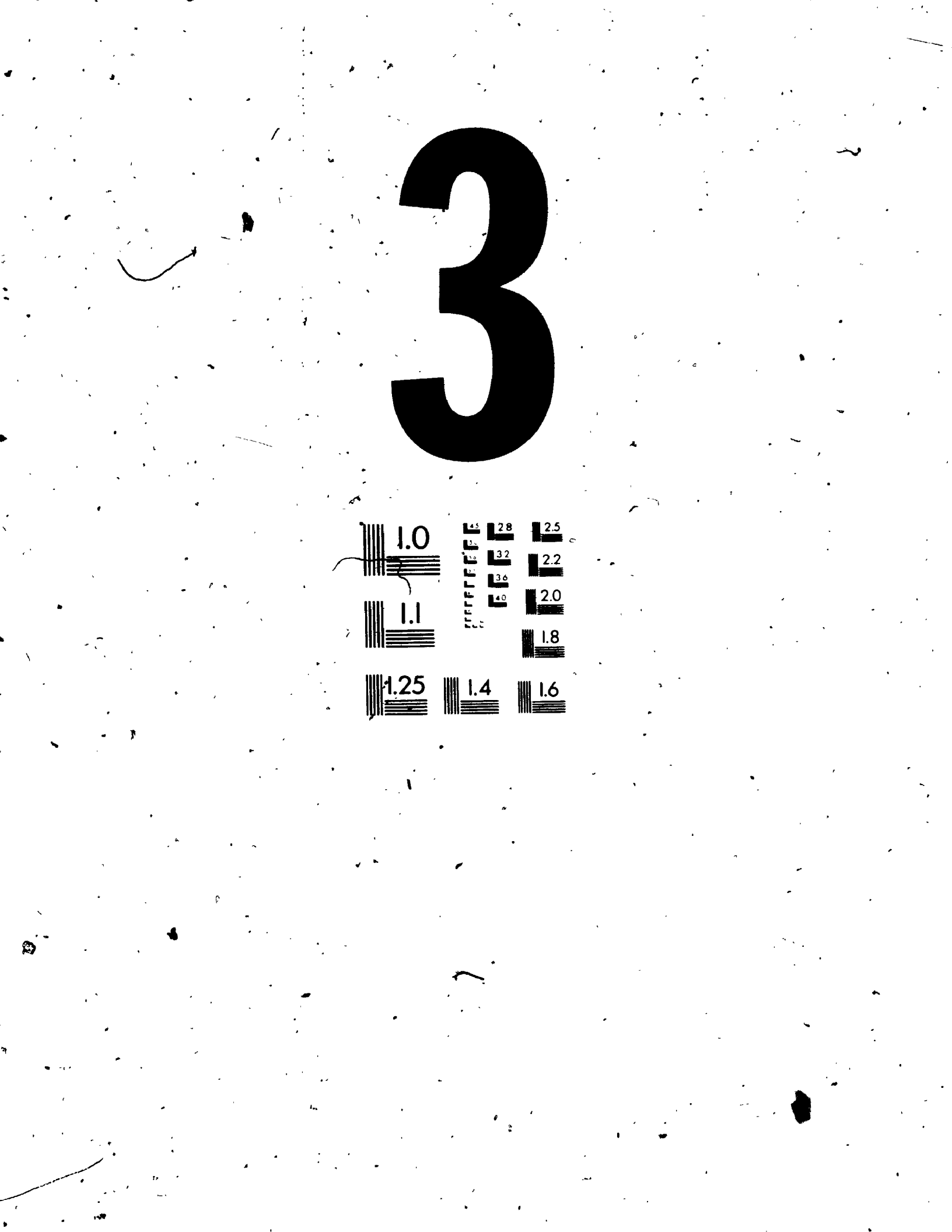
3
1.0
1.1
1.25
1.4
1.6
1.8
2.0
2.2
2.5
28
32
36
40

$$\mu_n=(1/8\pi^3)(8V)^n\int_{-\pi}^{\pi}\int_{-\pi}^{\pi}\int_{-\pi}^{\pi}\cos^n\theta_x\cos^n\theta_y\cos^n\theta_z d\theta_x d\theta_y d\theta_z. \qquad (C.10)$$

By using (5.a.11) we immediately have

$$\mu_{2n}=(1/8\pi^3)(8V)^{2n}[(1/4^n)\binom{2n}{n}2\pi]^3=V^{2n}\binom{2n}{n}^3. \qquad (C.11)$$

$\mu_{2n+1}=0$ for all n as before.

With the energy in units of V we have thus

$$\mu_{2n}=\binom{2n}{n}^3 \; ; \; \mu_{2n+1}=0. \qquad (C.12)$$

This is exactly expression (5.a.29).

In the case of the face centred cubic lattice we have

$$E(\vec{k})=2V[\cos(k_xa/2+k_ya/2)+\cos(k_xa/2-k_ya/2)+\cos(k_xa/2+k_za/2)+$$
$$\cos(k_xa/2-k_za/2)+\cos(k_ya/2+k_za/2)+\cos(k_ya/2-k_za/2)]=$$
$$4V[\cos(k_xa/2)\cos(k_ya/2)+\cos(k_xa/2)\cos(k_za/2)+$$
$$\cos(k_ya/2)\cos(k_za/2)]. \qquad (C.13)$$

With the unit cell and Ω_0 the same as before we have

$$\mu_n=(a/4\pi)^3(4V)^n\int_{-2\pi/a}^{2\pi/a}\int\int[\cos(k_xa/2)\cos(k_ya/2)+\cos(k_xa/2)\cos(k_za/2)+$$
$$\cos(k_ya/2)\cos(k_za/2)]^n dk_x dk_y dk_z. \qquad (C.14)$$

By changing the variables as before we obtain

$$\mu_n=(1/8\pi^3)(4V)^n\int_{-\pi}^{\pi}\int_{-\pi}^{\pi}\int_{-\pi}^{\pi}(\cos\theta_x\cos\theta_y+\cos\theta_x\cos\theta_z+\cos\theta_y\cos\theta_z)^n x$$
$$d\theta_x d\theta_y d\theta_z=$$
$$(1/8\pi^3)(4V)^n\sum_{m=0}^{n}\sum_{l=0}^{m}\binom{n}{m}\binom{m}{l}\int_{-\pi}^{\pi}\int_{-\pi}^{\pi}\int_{-\pi}^{\pi}(\cos\theta_x\cos\theta_y)^l(\cos\theta_y\cos\theta_z)^{m-l}x$$

$$(\cos\theta_x\cos\theta_z)^{n-m}d\theta_x d\theta_y d\theta_z$$

$$(1/8\pi^3)(4V)^n \sum_{m=0}^{n}\sum_{l=0}^{m}\binom{n}{m}\binom{m}{l}\int_{-\pi}^{\pi}\int_{-\pi}^{\pi}\int_{-\pi}^{\pi}\cos^{n-m+1}\theta_x\cos^{m}\theta_y\cos^{n-l}\theta_z x$$

$$d\theta_x d\theta_y d\theta_z. \qquad (C.15)$$

By using (5.a.10) we have thus

$$\mu_n=(1/8\pi^3)(4V)^n \sum_{m=0}^{n}\sum_{l=0}^{m}\binom{n}{m}\binom{m}{l}[(1/4^{n-m+1})\binom{n-m+1}{(n-m+1)/2}2\pi]x$$

$$[(1/4^{m})\binom{m}{m/2}2\pi][(1/4^{n-l})\binom{n-l}{(n-l)/2}2\pi]=$$

$$(4V)^n(1/4^n)\sum_{m=0}^{n}\sum_{l=0}^{m}\binom{n}{m}\binom{m}{l}\binom{n-m+1}{(n-m+1)/2}\binom{m}{m/2}\binom{n-l}{(n-l)/2}=$$

$$V^n\sum_{m=0}^{n}\sum_{l=0}^{m}\binom{n-m+1}{(n-m+1)/2}\binom{m}{m/2}\binom{n-l}{(n-l)/2}\binom{n}{m}\binom{m}{l}. \qquad (C.16)$$

The convention $\binom{n}{n/2}=0$ for an odd n is used here.

With E expressed in units of V this can be rewritten as

$$\mu_{2n}=\sum_{m=0}^{n}\sum_{l=0}^{m}\binom{2(n-m+1)}{n-m+1}\binom{2m}{m}\binom{2(n-l)}{n-l}\binom{2n}{2m}\binom{2m}{2l}$$

$$\mu_{2n+1}=\sum_{m=1}^{n}\sum_{l=1}^{m}\binom{2(n-m+1)}{n-m+1}\binom{2m}{m}\binom{2(n-l+1)}{n-l+1}\binom{2n+1}{2m}\binom{2m}{2l-1}. \qquad (C.17)$$

This is exactly expression (5.a.30).

Appendix D

The continued fraction coefficients for a regular binary alloy on a regular lattice.

We show here, that in the case of a regular binary alloy on a regular lattice, the coefficients of the continued fraction expansion for a site with energy E_1, denoted by $A_1, A_2, \ldots$ and $B_1, B_2, \ldots$, are related to the coefficients of the continued fraction expansion for the regular lattice itself, denoted by $a_1, a_2, \ldots$ and $b_1, b_2, \ldots$, by

$$A_{2n-1}=a_{2n-1}+E_1 \; ; \; A_{2n}=a_{2n}+E_2 \; ; \; n=1,2,\ldots$$

$$B_n=b_n \; ; \; n=1,2,\ldots . \qquad (D.1)$$

The same holds for a site with energy E_2, but with E_1 and E_2 interchanged.

We recall first, that a regular binary alloy can occur only on a lattice for which only the even numbered moments are non-zero (when the self-energy of the lattice sites is set to 0; see section 5.a). This means that the density of states $\rho(E)$ for such a lattice is symmetrical around E=0. From a study of the continued fraction expansion (expression (4.a.5)) we see that $a_n=0$ for all n in such a case. Thus expression (D.1) becomes

$$A_{2n-1}=E_1 \; ; \; A_{2n}=E_2 \; ; \; n=1,2,\ldots$$

$$B_n=b_n \; ; \; n=1,2,\ldots . \qquad (D.2)$$

Let H denote the Hamiltonian for the regular binary alloy, and let W denote the Hamiltonian for the corresponding regular lat-

tice. They are related to each other by

$$H=D+W, \tag{D.3}$$

where D is (in matrix representation) a diagonal matrix with $D_{j,j}=E_1$ if the site denoted by j has energy E_1, and $D_{j,j}=E_2$ if the site has energy E_2.

We recall now the recurrence relation used for obtaining the continued fraction expansion (expressions (4.a.1) through (4.a.3)). For the regular lattice the recurrence relation becomes here

$$b_n|n+1)=W|n)-b_{n-1}|n-1), \tag{D.4}$$

whereas for the regular binary alloy it becomes

$$B_n|n+1)=(H-A_n)|n)-B_{n-1}|n-1)=(W+D-A_n)|n)-B_{n-1}|n-1). \tag{D.5}$$

$|1), |2), \ldots$ denote the new orthonormal basis for the regular lattice, and $|1), |2), \ldots$ denote the new orthonormal basis for the regular binary alloy.

First we show that $|n)$ is a linear combination only of wave functions of sites which have energy E_1 (E_2) in the binary alloy if n is odd (even). For n=1 we have $|1)=|1\rangle$, and the site of origin has energy E_1. Now we assume that the above statement is true for $n=1,2,\ldots,N$. We note that W acting on a site with energy E_1 (E_2) in the binary alloy yields a linear combination of sites with energy E_2 (E_1), when only the nearest neighbour interaction is present. Using this fact for expression (D.4) we immediately see, that the above statement is then true for n=N+1 as well.

Now we prove the main theorem itself by induction. We obvious-

ly have $|1)=|1)=|1\rangle$ and $B_0=b_0=0$ (see expression (4.a.2)). We also note that D acting on the wave function of a site with energy E_j simply multiplies it by E_j, $j=1,2$. Thus we have (cf. expression (4.a.3))

$$A_1=(1|H|1)=(1|W+D|1)=(1|W+D|1)=(1|W|1)+(1|D|1)=a_1+E_1=E_1 \qquad (D.6)$$

as $a_1=0$.

Now we assume that $|n)=|n)$, $A_n=E_m$ and $B_{n-1}=b_{n-1}$ for $n=1,2,\ldots,N$. m is equal to 1 (2) if n is odd (even). As $|N)=|N)$ is a linear combination of sites with energy E_M (M is 1 (2) if N is odd (even)), we have $D|N)=E_M|N)$, and thus $(D-A_N)|N)=0$, as $A_N=E_M$ as well. Therefore expression (D.5) becomes

$$B_N|N+1)=W|N)-B_{N-1}|N-1)=W|N)-b_{N-1}|N-1). \qquad (D.7)$$

Comparison with expression (D.4) shows us now, that this means that we must have $B_N=b_N$ and $|N+1)=|N+1)$. Thus we also have

$$A_{N+1}=(N+1|H|N+1)=(N+1|W+D|N+1)=(N+1|W+D|N+1)=$$

$$(N+1|W|N+1)+(N+1|D|N+1)=a_{N+1}+E_{N+1}=E_{N+1} \qquad (D.8)$$

as $a_{N+1}=0$. This completes the proof by induction.

We see thus that expression (4.a.35) for the regular binary alloy becomes

$$\lim_{n\to\infty} A_{2n-1}=E_1 \; ; \; \lim_{n\to\infty} A_{2n}=E_2,$$

$$\lim_{n\to\infty} B_{2n-1}=b \; ; \; \lim_{n\to\infty} B_{2n}=b, \qquad (D.9)$$

where $b=\lim_{n\to\infty} b_n$.

By using expression (4.a.43) we can obtain explicit expressions for the positions of the band edges. The band edges are located at

$$E=(1/2)((E_1+E_2)\pm[(E_1-E_2)^2+4(b\pm b)^2]^{1/2}). \qquad (D.10)$$

This means that the lower energy band has its edges at

$$E_l=(1/2)((E_1+E_2)-[(E_1-E_2)^2+16b^2]^{1/2}) \; ; \; E_h=\min.(E_1,E_2), \qquad (D.11)$$

and the upper energy band has its edges at

$$E_l=\max.(E_1,E_2) \; , \; E_h=(1/2)((E_1+E_2)+[(E_1-E_2)^2+16b^2]^{1/2}). \qquad (D.12)$$

An alternative method for obtaining these expressions for the band edge positions can be found in section 5.d.

References

Abramowitz M and Stegun I A (1972) "Handbook of Mathematical Functions", Dover, New York.

Akhiezer N I (1965) "The Classical Moment Problem", Oliver & Boyd, London.

Baker G A and Graves-Morris P (1981) "Encyclopedia of Mathematics and its Applications", Rota G C editor, Vol. 13, Addison-Wesley, London.

Baker G A and Graves-Morris P (1981) "Encyclopedia of Mathematics and its Applications", Rota G C editor, Vol. 14, Addison-Wesley, London.

Blumstein C and Wheeler J C (1973) Phys. Rev. B 8 1764.

Burley S K, John S O and Nuttall J (1981) SIAM J. Numer. Anal. 18 919.

Callaway J (1964) "Energy Band Theory", Academic Press, New York.

Choo F C, Tong B Y and Swenson J R (1974) Phys. Lett. 50A 255.

Ciraci S and Batra I P (1975) Solid St. Commun. 16 1375.

Desjonquères M C and Cyrot-Lackmann F (1977) J. Phys. F: Metal. Phys. 7 61.

Economou E N (1979) "Green's Functions in Quantum Physics", Springer-Verlag, Berlin.

Fisher M E and Camp W J (1972) Phys. Rev. B 5 3730.

Gammel J L (1973) in "Padé Approximants and their Application", Graves-Morris P R editor, Academic Press, New York, pp. 3-9.

Gaspard J P and Cyrot-Lackmann F (1973) J. Phys. C: Solid State Phys. 6 3077.

Haydock R, Heine V and Kelly M J (1972) J. Phys. C: Solid State Phys. 5 2845.

Haydock R, Heine V and Kelly M J (1975) J. Phys. C: Solid State Phys. 8 2591.

Haydock R (1980) in "Solid State Physics - Advances in Research and Application", Ehrenreich H, Seitz F and Turnbull D editors, Vol. 35, Academic Press, New York, pp. 215-294.

Heine V (1980) in "Solid State Physics - Advances in Research and Application", Ehrenreich H, Seitz F and Turnbull D editors, Vol. 35, Academic Press, New York, pp. 1-127.

Hodges C H (1977) J. Phys. Lett. 38 L187.

Jenkins M A and Traub J F (1970) SIAM J. Numer. Anal. 7 545.

Joyce G S (1973) Proc. Roy. Soc. 273 583.

Katsura S and Horiguchi T (1971) J. Math. Phys. 12 230.

Katsura S, Inawashiro S and Abe Y (1971) J. Math. Phys. 12 895.

Katsura S and Inawashiro S (1971) J. Math. Phys. 12 1622.

Kelly M J and Bullett D W (1976) J. Non-Cryst. Solids 21 155.

Kelly M J and Bullett D W (1976) Solid St. Commun. 18 593.

Lambin Ph and Gaspard J P (1982) Phys. Rev. B 26 4356.

Lukes T (1969) in "Solid State Theory - Methods and Applications", Landsberg P T editor, Wiley, New York, pp. 493-499.

Magnus A (1983) " Riccati Acceleration of Jacobi Continued Fractions and Laguerre-Hahn Orthogonal Polynomials", Rapport No. 26, Institute de Mathematique Pure et Appliquee, Universite Catholique de Louvain.

Mayer I L, Nuttall J and Tong B Y (1984) Phys. Rev. B 29 7102.

Mayer I L and Tong B Y (1985) J. Phys. C: Solid State Phys. 18 3297.

Morita T and Horiguchi T (1971) J. Math. Phys. 12 986.

Morita T and Horiguchi T (1971) "Table of the Lattice Green Function for the Cubic Lattices", Tohoku University, Sendai, Japan.

Morita T and Horiguchi T (1972) J. Math. Phys. 13 1243.

Morse M (1938) "Functional Topology and Abstract Variational Theory, Memorial Sciences Mathematique", Fasc. 92, Gauthier-Villars, Paris.

Nuttall J (1984) J. Approx. Th. 42 299.

Ortenburger I B, Ciraci S and Batra I P (1976) J. Phys. C: Solid State Phys. 9 4185.

Padé H (1892) Ann. Sci. Ec. Norm. Super., Suppl. 9 1.

Padé H (1894) J. Math., Ser. 4 10 291.

Shafer R E (1974) SIAM J. Numer. Anal. 11 447.

Shohat J A and Tamarkin J D (1963) "The Problem of Moments, Mathematical Surveys I", American Mathematical Society, Providence, Rhode Island.

Slater J C and Koster G F (1954) Phys. Rev. 94 1498.

Thorpe M F (1972) J. Math. Phys. 13 294.

Tong B Y, Swenson J R and Choo F C (1974) Phys. Rev. B 10 3338.

Tong B Y and Choo F C 1976 Solid ST. Commun. 20 957.

Trias A, Kiwi M and Weissmann M (1983) Phys. Rev. B 28 1859.

Turchi P, Ducastelle F and Tréglia G (1982) J. Phys. C: Solid State Phys. 15 2891.

Van Hove L (1953) Phys. Rev. 89 1189.

Wheeler J C and Blumstein C (1972) Phys. Rev. B 6 4380.

Wheeler J C (1974) Phys. Rev. A 9 825.

Wheeler J C, Prais M G and Blumstein C (1974) Phys. Rev. B 10 2429.

Wilkinson J H (1965) "The Algebraic Eigenvalue Problem", Clarendon Press, Oxford, pp. 443-445.

PART II

Classical stochasticity and ionisation in a square potential well driven by an oscillating laser field

Chapter 7

General review of the physical system

7.a. General introduction

We consider in this work the behaviour of particles inside a square potential well in the presence of an oscillating electric field of a laser. This model is useful for studying tunable quantum well laser systems. Similar models (with other types of potential wells) have been useful in the past for studying a variety of phenomena, such as the ionisation of an atom in a microwave electric field and the dissociation of a molecule in a resonant laser field.

If the number of energy levels in the potential well is large, and they are close together, this kind of physical system can be studied with reasonable accuracy by means of classical dynamics. As we shall see in section 7.d, the classical treatment often yields results, which compare well with experimental data.

In this classical model, when no oscillating field is present, the Hamiltonian is separable (see section 8.a), and therefore the motion of the particle is regular. When the field is applied, and its strength is increased from zero, the motion of the particle gradually loses its regular character, and becomes random-like, even though the system is still perfectly regular in nature. This kind of phenomenon is known as stochasticity.

If the field strength is further increased, the motion of the particle becomes more and more random-like, until it eventually may escape from the potential well. If it does, we say that it becomes ionised. By using an ensemble of particles initially

positioned at random inside the potential well, the rate of ionisation can be studied, and its dependence on the strength and frequency of the field can be found.

In this part of the thesis we carry out this kind of study for particles inside a one dimensional square well potential in an oscillating laser field. We look at the onset of stochasticity and ionisation, and suggest an experimental study of the same system, with which our results may then be compared.

In the following sections of this chapter we discuss the general physical background. First we see that an effectively one dimensional square well potential can actually be fabricated in semiconductors, and that its application to tunable lasers presents us with the situation of such a potential placed in an oscillating laser field. Finally we present our model for studying this system.

In chapter 8 we present a general review of classical dynamics. We discuss the subject of classical and quantum stochasticity, and the way in which they can be studied. Finally we present a survey of previous work carried out on this subject.

In chapter 9 we carry out the study of classical stochasticity in our system. We present the analytical prediction for the onset of stochasticity, and compare it with the numerical results.

In chapter 10 we carry out the study of ionisation in our system. We see how our numerically obtained ionisation rate depends on the intensity and frequency of the laser field. Finally we present a possible explanation of the results that we have observed.

In chapter 11 we look at the prospects for further study of this problem. We discuss the reasons for carrying out a classical study of our system and the difficulties in carrying out a quantum mechanical study of the same system. We then suggest a possible experimental study of the system, with the results of which our classical theoretical results may be compared.

7.b. The fabrication of potential well structures in semiconductors

The possibility of fabricating a potential well of desired shape and dimensions, including the square well potential, which is studied in this work, is a result of the advances in crystal growth techniques in recent years. In this section we shall give a brief review of this subject.

A film of a crystalline semiconductor can be grown in a process known as epitaxy. In this process one has a substrate upon which the film is grown. The crystallinity and orientation of the grown layer are determined by the substrate. If several films of dissimilar semiconductors are grown one on top of the other, thus forming a layered structure, the process is known as heteroepitaxy. This is usually done with semiconducting materials with similar lattice structures.

There are several methods for growing such films. One method used is liquid-phase epitaxy, in which each layer is grown by cooling a heated metallic solution saturated with the components required for that layer, with the solution in contact with the substrate. Another method is chemical-vapour deposition, in which a stream of gaseous components required for the growing layer is directed towards the substrate and reacts with it. The most advanced method, however, is molecular beam epitaxy. In this method one or more thermal beams of atoms or molecules required for the growing layer are directed towards the substrate, which is held at the proper temperature in ultra-high vacuum.

By using these methods, and especially the last one, one can

also deposit two or more different layers one on top of the other - the above mentioned heteroepitaxy process (Esaki and Tsu 1969). By using computer controlled shutters for the molecular beams the depth of the layers can be carefully controlled (Narayanamurti 1984), and thus the desired layer structure can be accurately obtained.

Such a semiconductor crystal, containing layers of two or more different materials (with similar lattice structure) is known as a heterostructure. The interface between two layers is known as a heterojunction. Each material has its band gap at a different position (on the energy scale), and thus the band gap edges show discontinuities at each heterojunction. By choosing the proper materials and depositing layers of these materials with appropriate depths, the desired potential profile (potential well) can be obtained. The variation in the potential is only in the crystal growth direction (perpendicular to the plane of the substrate), and thus the potential well is in effect one dimensional. This way square well structures (Dingle et al 1978, Kasemset et al 1982), and even harmonic oscillator potentials (Narayanamurti 1984) can be obtained.

One of the most common combinations of materials used is GaAs and $Al_xGa_{1-x}As$. The concentration x of the Al can be varied over a considerable range, and this way the positions of the band gap edges in $Al_xGa_{1-x}As$ can be varied. Thus, by depositing layers of GaAs and layers of $Al_xGa_{1-x}As$ (with the appropriate value for x), the desired potential well structure can be obtained. In fact, the above mentioned structures have all been obtained with these materials.

This way, in particular, a single square potential well can be fabricated with the desired width and depth, within certain limits. The width can usually vary between 100 and 1000 Å, and the depth between 0.2 and 0.5 eV. As we shall see in the next section, this potential structure can be used for the manufacture of a tunable laser. In this work we shall study the behaviour of electrons in such a well in the presence of an oscillating laser field. A further discussion of this experimentally fabricated square well potential is presented in section 11.c, where we suggest an experimental test of our theoretical results.

7.c. The application of the potential well structures to tunable lasers

A semiconductor heterostructure with one or more square wells, manufactured as explained in the previous section, can be used as the basis for a laser system (Holonyak et al 1980, Kasemset et al 1982). By irradiating this system with a low-energy laser beam it can be turned into a tunable laser system (Gerck and Miranda 1984). We shall give here a brief discussion of the operation of such a laser. Then we shall discuss its relation to our study of the square well potential.

The structure and operation of such a laser are shown schematically in Figure 50. The square well potential shows up twice, once at the bottom of the conduction band, for electrons, and once at the top of the valence band, for holes. The dominant square well, however, is the one for the electrons. The ground level in the square well at the bottom of the conduction band is populated with electrons from the valence band by some method, such as photo-pumping or injection. This is indicated by the arrow "A" in the diagram.

The system is now irradiated by a laser beam, referred to from now on as the driving laser. It has an intensity I and a frequency ω, as indicated in the diagram. The driving laser causes the energy bands in the square well to shift. The amount of shifting depends on the intensity and frequency of the driving laser. The levels in the lower square well, at the top of the valence band, are shifted as well, but this shift is much smaller, as the effective mass of the holes is much larger in magnitude than that

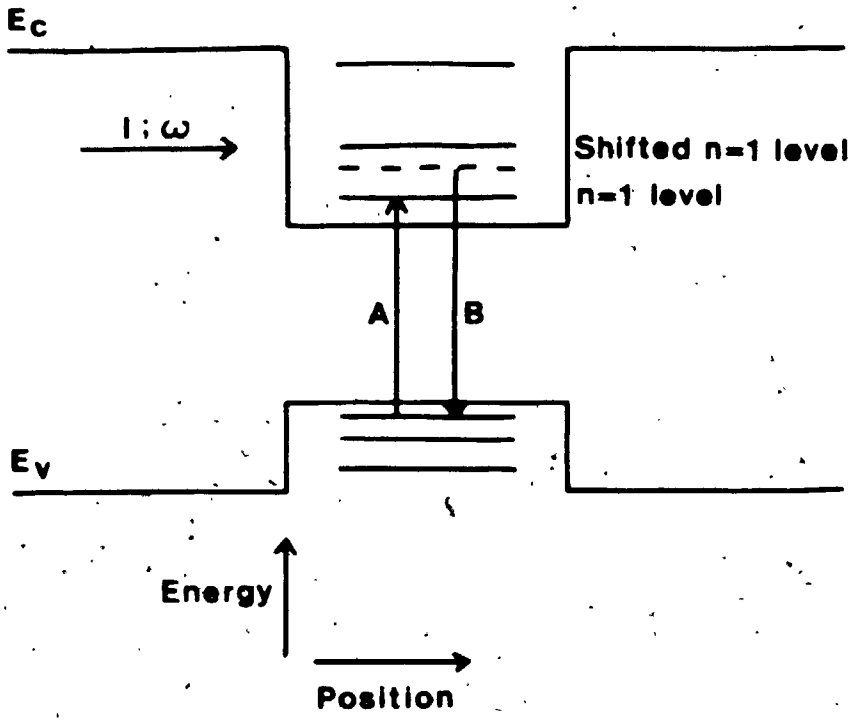

Figure 50

Schematic diagram of a tunable laser with a square well potential in a semiconductor. The ground level in the square well is populated with electrons from the valence band (the arrow "A"). The driving laser (with intensity I and frequency ω) causes this ground level to shift. The recombination process (the arrow "B") occurs from there back to the valence band, and produces the tunable laser beam. It is tunable, because the amount of shifting (of the ground level) depends on the intensity of the driving laser, and thus the wavelength of the tunable laser beam depends on it as well.

of the electrons, and therefore not shown in the diagram.

The electrons in the shifted ground level of the square well (dashed line in the diagram) now recombine with holes in the lower well at the top of the valence band, thus producing the tunable laser beam itself. This process is indicated by the arrow "B" in the diagram. As the wavelength of the tunable laser beam depends on the amount of shifting of the ground level in the square well, it can be varied over a certain range by controlling the intensity of the driving laser beam. This way the laser beam produced by this mechanism is made tunable.

The range over which this laser can be tuned is limited, however, because if the intensity of the driving laser beam is too high, the electrons will escape from the square well into the conduction band through a mechanism like multiphoton absorption or tunnelling. Thus it is of interest to find the range over which the driving laser intensity can be varied, for a given frequency, before the electrons start to escape from the square well.

The situation of a square well potential in an oscillating laser field is thus present in this tunable laser, and thus our theoretical study is closely linked to it. On one hand, the results of our classical study of stochasticity and ionisation in this square well potential can show to what extent the driving laser intensity can be varied before ionisation sets in, in the classical limit, i.e. when the number of quantum levels in the well is large (section 11.a). On the other hand, the tunable laser system can be used in an experimental study, with which our theoretical results can be compared (section 11.b).

7.d. The model of a square well potential in a laser field

The square well potential has a width d and a depth V_0. An electron in it has a mass M, which is the effective mass for an electron for the type of semiconductor, in which the square well is located. This system is acted upon by a laser field of a frequency ω. Because of the small dimensions of the well (a width of less than 1000Å), the amplitude of the laser field can be assumed to be constant over the entire well. The laser field is thus represented by a classical plane wave, given by $E_L\cos(\omega t)$, where E_L is the amplitude of the laser field. This is known as the dipole approximation. The Hamiltonian is thus given by

$$H(p,x,t)=p^2/2M+V(x)+eE_L x\cos(\omega t), \qquad (7.d.1)$$

where V(x) is the square well potential, given by

$$V(x)=\begin{cases}0 & \text{if } 0<x<d\\ V_0 & \text{if } x<0 \text{ or } x>d.\end{cases} \qquad (7.d.2)$$

In the absence of the laser field, the Schrödinger equation can be analytically solved. The solution can be found in many elementary textbooks of quantum mechanics (for example - McGervey 1971). Here we shall give a brief review of the calculation of the bound energy levels, as they are needed for later calculations and discussions.

In order to make the problem symmetrical, and thus simpler, we shift the reference point for the position, so that the well is located between x=-d/2 and x=d/2. From the Schrödinger equation

$$-(\hbar^2/2M)(d^2\psi/dx^2)+V(x)\psi=E\psi \qquad (7.d.3)$$

we see, that the wave functions, which are symmetrical around x=0, are given by

$$\psi(x)=\begin{cases} C\cos(kx) & \text{if } |x|\leq d/2 \\ \exp(-K|x|) & \text{if } |x|\geq d/2, \end{cases} \qquad (7.d.4)$$

and the wave functions, which are antisymmetrical around x=0, are given by

$$\psi(x)=\begin{cases} C\sin(kx) & \text{if } |x|\leq d/2 \\ \mathrm{sgn}(x)\exp(-K|x|) & \text{if } |x|\geq d/2, \end{cases} \qquad (7.d.5)$$

where

$$K=[2M(V_0-E)]^{1/2}/\hbar \qquad (7.d.6)$$

and

$$k=(2ME)^{1/2}/\hbar. \qquad (7.d.7)$$

From the requirement that $\psi(x)$ and $\psi'(x)$ should be continuous at $x=\pm d/2$, we obtain for the even wave function the condition

$$k\,\mathrm{tg}(kd/2)=K=(2MV_0/\hbar^2-k^2)^{1/2}, \qquad (7.d.8)$$

and for the odd wave functions the condition

$$k\,\mathrm{cotg}(kd/2)=-K=-(2MV_0/\hbar^2-k^2)^{1/2}. \qquad (7.d.9)$$

We now introduce the dimensionless parameters N and A, defined by

$$N=(d/\pi\hbar)(2MV_0)^{1/2} \qquad (7.d.10)$$

and

$$A=kd. \qquad (7.d.11)$$

In terms of these expression (7.d.8) becomes

$$A\ tg(A/2)=(N^2\pi^2-A^2)^{1/2}, \qquad (7.d.12)$$

and expression (7.d.9) becomes

$$A\ cotg(A/2)=-(N^2\pi^2-A^2)^{1/2}. \qquad (7.d.13)$$

These equations have together N solutions, if N is an integer, and int.(N)+1 solutions otherwise. We shall always choose values of V_0, so that N is an integer. The N energy levels are thus given by

$$E_n=\hbar^2A_n^2/2Md^2 \ ; \ n=1,2,\ldots,N, \qquad (7.d.14)$$

where A_n is the $((n+1)/2)^{th}$ solution of (7.d.12), if n is odd, and the $(n/2)^{th}$ solution of (7.d.13), if n is even.

In the presence of the laser field, the time-dependent term $eE_Lx\cos(\omega t)$ has to be added to the Hamiltonian. The Schrödinger equation thus becomes time-dependent. It can not be solved analytically any more, and, as we shall see in section 11.a, great difficulties are encountered, when trying to solve it by numerical or approximation methods. The classical treatment of the time-dependent Hamiltonian, on the other hand, can be carried out quite easily.

In the present work we carry out a study of this model by means of classical dynamics in the range where such a treatment is reasonable, and suggest a comparative experimental study of

the same system.

Chapter 8

General review of classical dynamics and stochasticity

8.a. Classical dynamical systems

We consider here a classical dynamical system with N degrees of freedom, which in our case means that the momentum and position are represented by N-dimensional vectors, $\vec{p}=(p_1,p_2,\ldots,p_N)$ and $\vec{x}=(x_1,x_2,\ldots,x_N)$ respectively. The 2N-dimensional space spanned by $\vec{p}$ and $\vec{x}$ is known as momentum-position space or phase space. The system is described by a Hamiltonian $H_0(\vec{p},\vec{x})$, which is a function of the momentum and position vectors.

The equations of motion for the system are obtained from the Hamiltonian, and are given by

$$dx_i/dt=\partial H_0/\partial p_i \; ; \; dp_i/dt=-\partial H_0/\partial x_i \; ; \; i=1,2,\ldots,N. \qquad (8.a.1)$$

Motion in phase space is described by phase curves, which are the solutions of these equations of motion for given initial values of $\vec{p}$ and $\vec{x}$. In other words, motion is described by the time evolution of $\vec{p}$ and $\vec{x}$, i.e. by $p_i(t)$ and $x_i(t)$, $i=1,2,\ldots,N$.

We say that our system is integrable (Richards 1982), if we can find N independent integrals $F_i(\vec{p},\vec{x})$, $i=1,2,\ldots,N$, which satisfy the Poisson bracket relations

$$(H_0,F_i)=\sum_{j=1}^{N}[(\partial H_0/\partial x_j)(\partial F_i/\partial p_j)-(\partial H_0/\partial p_j)(\partial F_i/\partial x_j)]=0 \; ;$$

$$i=1,2,\ldots,N \qquad (8.a.2)$$

and

$$(F_i,F_j)=\sum_{k=1}^{N}[(\partial F_i/\partial x_k)(\partial F_j/\partial p_k)-(\partial F_i/\partial p_k)(\partial F_j/\partial x_k)]=0 \ ;$$

$$i,j=1,2,\ldots,N. \qquad (8.a.3)$$

Hamiltonians which are separable, i.e. can be separated in some coordinate system into a sum of independent Hamiltonians with one degree of freedom each, and hence Hamiltonians of one dimensional systems, in particular, are integrable (Richards 1982).

Each phase curve (path of motion) of an integrable system with N degrees of freedom is confined in phase space to an N-dimensional surface. If the motion is bounded, then the surface is an N-dimensional torus (Arnold 1978). In such a case a new set of variables, action and angle, given by $\vec{I}=(I_1,I_2,\ldots,I_N)$ and $\vec{\theta}=(\theta_1,\theta_2,\ldots,\theta_N)$, can be chosen, so that each torus (describing a possible motion in the system) is uniquely labelled by $\vec{I}$, and the positions within it are uniquely labelled by $\vec{\theta}$. The Hamiltonian H_0, expressed in terms of these new variables, is a function of $\vec{I}$ only.

If we express the position vector $\vec{x}$ in terms of $\vec{I}$ and $\vec{\theta}$, then we have

$$\vec{x}(\vec{I},\vec{\theta}+2\pi\vec{n})=\vec{x}(\vec{I},\vec{\theta}), \qquad (8.a.4)$$

where $\vec{n}$ is any N-dimensional vector of integers. Thus we say that $\vec{\theta}$ is a multi-periodic function.

The equations of motion in action-angle space are given by

$$d\theta_i/dt=\partial H_0/\partial I_i \ ; \ dI_i/dt=-\partial H_0/\partial\theta_i \ ; \ i=1,2,\ldots,N. \qquad (8.a.5)$$

As H_0, when expressed in terms of these variables, does not

depend on $\vec{I}$, these equations of motion reduce to

$$d\theta_i/dt=\partial H_0/\partial I_i \; ; \; dI_i/dt=0, \; i=1,2,\ldots,N, \qquad (8.a.6)$$

and thus the solution is given by

$$\theta_i(t)=\omega_i t+\theta_{0i} \; ; \; I_i(t)=I_{0i} \; ; \; i=1,2,\ldots,N, \qquad (8.a.7)$$

where $\omega_i=\partial H_0/\partial I_i$, and $\vec{\theta}_0$ and $\vec{I}_0$ are the initial values of $\vec{\theta}$ and $\vec{I}$ respectively.

If we add a time-dependent term to the Hamiltonian, or a coupling term (if the system has more than one degree of freedom), then in most cases the system will not be integrable any more. The Hamiltonian is now expressed as $H=H_0+V$, where H_0 is the Hamiltonian of the original integrable system, and V is the perturbing term. If the transition to action and angle variables is carried out in this case, the Hamiltonian H will depend both on $\vec{I}$ and on $\vec{\theta}$. The equations of motion (8.a.1) and (8.a.5) are still valid (with H_0 now replaced by H), but they can not be solved analytically any more, and motion is not confined to an N-dimensional surface in phase space.

As in this work we shall concern ourselves with one-dimensional systems, we note here the following. A one-dimensional system with a time-independent Hamiltonian is always integrable, as we have already seen. When a time-dependent term is added to the Hamiltonian, however, the system will not be integrable any more (in most cases). Bounded motion in momentum-position space, in the case of the unperturbed system, is along closed curves. When viewed in action-angle space, it is along straight lines parallel to the θ-axis.

The equations of motion in momentum-position space (expression (8.a.1)) reduce to

$$dx/dt=\partial H/\partial p \ ; \ dp/dt=-\partial H/\partial x, \qquad (8.a.8)$$

and the equations of motion in action-angle space (expression (8.a.5)) reduce to

$$d\theta/dt=\partial H/\partial I \ ; \ dI/dt=-\partial H/\partial \theta. \qquad (8.a.9)$$

8.b. Stochasticity in dynamical systems

We now consider a one-dimensional classical dynamical system, with a time-dependent perturbing potential present. Such a system is described by a Hamiltonian

$$H(p,x,t)=H_0(p,x)+\varepsilon V(p,x,t), \qquad (8.b.1)$$

where ε is a dimensionless parameter used for controlling the strength of the perturbation. We are interested in the motion in this system in the presence of the perturbing potential.

The equations of motion of the perturbed system can not be solved analytically (in most cases), and thus have to be solved numerically. Numerical studies of such systems have shown, that if the perturbation is sufficiently strong, the motion of particles in the system assumes a random-like character, even though the system is driven only by perfectly regular forces. This kind of motion is called stochastic motion, and the phenomenon itself is known as (classical) stochasticity (Chirikov 1979).

Besides its random-like character, stochastic motion is also characterised by what is called local instability. By this term it is meant, that trajectories of particles, which are initially arbitrarily close to each other, become separated by a distance which increases exponentially with time (Chirikov 1979, Zaslavsky 1981).

The study of stochasticity is most conveniently carried out in action-angle space, especially in the one-dimensional case, where the unperturbed motion is along straight lines parallel to the θ-axis (see section 8.a). As $\theta=0$ is identified with $\theta=2\pi$ (expres-

sion (8.a.4)), these straight lines actually close and form tori.

When the perturbing term is introduced, i.e. ε is increased from zero, the motion along these tori is affected by it. First the torus is distorted from its straight line into a curve, and then it is totally destroyed, and the motion becomes stochastic. We shall now have a more detailed look at this process.

When the perturbation parameter ε is sufficiently small, most tori are only slightly distorted. Certain tori, however, are significantly distorted for arbitrarily small values of ε. They are known as the resonant tori (or resonances), as they correspond to the resonances of the perturbative solution of the equations of motion derived from the Hamiltonian (expression (8.b.1)). This is known as the Kolmogorov-Arnold-Moser (KAM) theorem (Arnold 1978).

We now look at the section of action-angle space between two adjacent resonant tori, and see what happens when ε is gradually increased from the above mentioned initial small value. For this small value of ε only the resonant tori are significantly distorted (they spread out and look like chains of islands), whereas in the region between them the distortion of the tori is very slight. When ε increases, the resonant tori become more distorted (the "islands" become wider) and spread out into the region in between. When ε reaches some critical value, the regular character of the motion in the entire region is totally gone, and we say thus that motion in this part of action-angle space has become stochastic.

This critical value of ε is different for each section of action-angle space (between two resonant tori). Therefore, if we

look at the action-angle space as a whole, as ε increases, we see that in certain sections motion becomes stochastic first, then it becomes stochastic in other sections as well, until, finally, for a sufficiently large ε, motion in the entire action-angle space becomes stochastic. The same behaviour is, of course, observed in the original momentum-position (or phase) space, with the only difference being, that the unperturbed motion is along curves instead of straight lines.

The gradual transition from regular to stochastic motion is illustrated in Figure 51. The figure shows some tori in action-angle space, with a small perturbation present. Motion at the bottom torus has already become stochastic, as the scattered points indicate. There are, however, some traces of an "island chain" due to the presence of a resonance nearby. Above that we see two distinct "island chains" due to resonances, and almost undistorted tori (straight rows of points) in between. If the perturbation were larger, motion in the region between the "island chains" would have become stochastic as well, and then also in the region around and above the uppermost "island chain". This figure was obtained for the square well potential in the oscillating laser field, using the procedure outlined in section 9.c.

The value of the parameter ε, for which motion near a given resonance becomes stochastic, can be predicted. The criterion for the onset of stochasticity is based upon the distortion of the resonant tori into "island chains", and is known as the Chirikov criterion (Chirikov 1979, Richards 1982). It will be explained in detail in section 9.c.

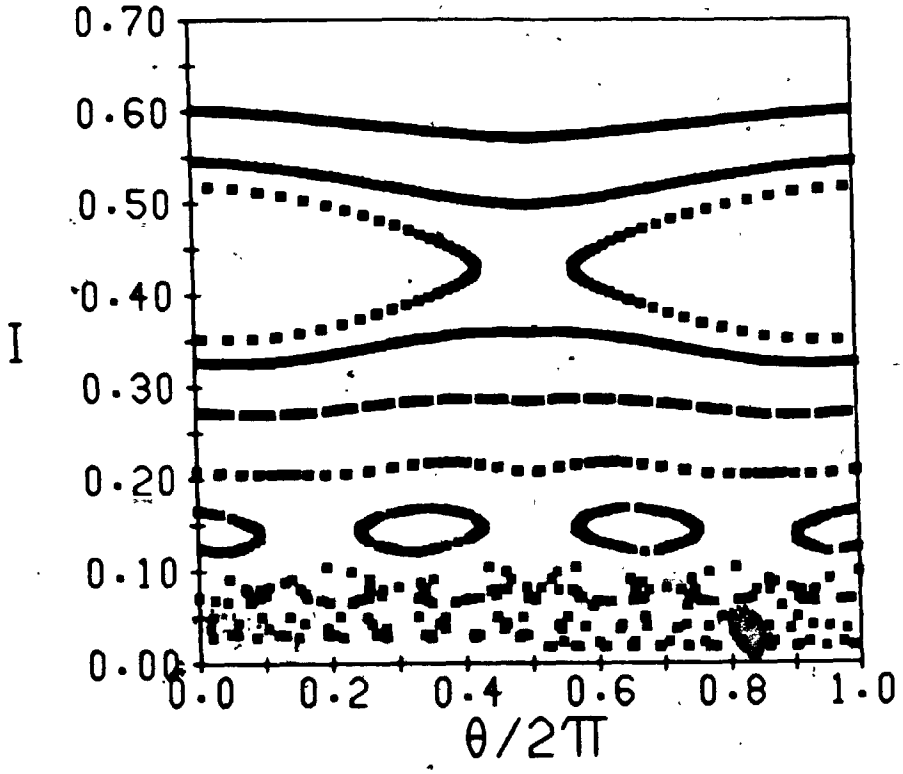

Figure 51

A section of action-angle space with several tori in the case of the square well potential with 4 energy levels (N=4), with the laser frequency parameter η=1.0 and the field strength parameter λ=0.0050 (these parameters are defined in section 9.c). With no laser field (no perturbation) present, all the tori would have been horizontal straight lines. Because of the perturbation the tori are distorted. The one at the bottom has been destroyed, as motion in this region has already become stochastic. The torus above it and the third torus from the top are resonant, and therefore they are significantly distorted (forming "island chains"), whereas the remaining tori, which are not resonant, are only slightly distorted.

So far we have discussed the phenomenon of stochasticity only in the context of classical dynamical systems. The question of its counterpart in quantum mechanical systems is of interest as well. The study of this subject has commenced only recently, and no general clear-cut definition of quantum stochasticity is available yet. As motion along trajectories does not exist in quantum mechanics (one can only talk about the probability of finding the particle at a certain place at a given time), the term "stochasticity" has do be defined otherwise. Several possible definitions can be used, according to the physical system in question. We shall give here some examples.

First we consider systems which are perturbed by a potential which varies periodically with time. At each moment we have a certain probability of finding the particle in each of the energy levels. For each level this probability varies with time. A possible definition of quantum stochasticity in this case is, that these probabilities vary in a random-like manner with time (Hogg and Huberman 1982).

In systems, where the perturbation is time-independent, other definitions need to be used. The perturbation causes the energy levels to split and shift. If the perturbation is strong enough, the order of the levels may change (as the levels cross each other), or, in other words, the levels may become mixed. Quantum stochasticity may thus be defined to occur, when this mixing of energy levels takes place. This has been used for systems where the perturbation takes the form of an applied pressure (Ley-Koo and Cruz 1981) or an applied magnetic field (Zimmermann et al 1982).

We shall restrict ourselves from now on to systems, where the perturbation is in the form of a time-periodic potential.

The question, whether quantum stochasticity is present in systems which display classical stochasticity, i.e. to what extent there is a correspondence between the two, is of much current interest. One way of studying it was by having the perturbation in the form of a sum of equally spaced delta-functions in time, and studying the effect each "kick" (delta-function in time) has on some initial distribution of positions and momenta, both classically and quantum mechanically (Zaslavsky 1981, Korsch and Berry 1981, Berry 1983). Results in this case show a good agreement between the classical and quantum results, thus indicating that if the classical dynamics are stochastic in this case, then the quantum dynamics are stochastic as well. A study of always-bound systems (like a harmonic oscillator) with a time-periodic perturbation (like an oscillating electric field), on the other hand, shows that no quantum stochasticity is present (Hogg and Huberman 1982).

In order to get a better answer to this question of correspondence between classical and quantum stochasticity, an experimental approach has been suggested (Jensen 1982, Jensen 1984). Jensen has studied the physical system of electrons bound to the surface of liquid helium in the presence of microwave radiation. This is an effectively one-dimensional system. He studied the onset of classical stochasticity in the system, and estimated the ionisation rate (the rate at which the electrons will escape from the potential well, formed in this case by their image charges)

from his results. He then suggested an experimental study of the ionisation rate in the same system, the results of which will include any relevant quantum mechanical effects. The comparison with his results will thus show how well the quantum stochasticity (in the experimental system) compares with its classical counterpart.

Our classical study of the square well potential in the oscillating laser field can serve the same purpose, especially if we bear in mind, that the square well potential we have studied is more easily accessible from an experimental point of view (see section 7.b), than the above mentioned liquid helium system.

8.c. Survey of previous studies of classical stochasticity in physical systems

The interest, in recent years, in systems which exhibit chaotic (stochastic) behaviour, on one hand, and in the response of atoms and molecules to intense time-dependent electromagnetic fields, on the other hand, have prompted the study of such physical systems by means of classical dynamics. We present here a brief survey of work done in this field in recent years.

Some of the work done was a general study of non-linear quantum oscillators affected by a periodic perturbation (Shuryak 1976), which was then applied to polyatomic molecules in oscillating electromagnetic fields. This subject of polyatomic molecules in time-dependent electromagnetic fields has been studied by several workers. This includes a discussion of the reasons and advantages for using classical dynamics for the study of such molecules (Lamb 1977), a study of excitation of molecules in a laser field through a stochasticity mechanism (Belobrov et al 1979), a study of the dissociation of the SF_6 molecule in an oscillating laser field (Jones and Percival 1983), and an improved study of the same molecule (Galvão et al 1984). The classical results for the laser intensity, required for the onset of stochasticity in the case of an SF_6 molecule driven by a CO_2 laser, as obtained by Galvão and his co-workers, is in a remarkably good agreement with the experimental results (Ambartsumyan et al 1976).

Another subject studied was the ionisation of highly excited atoms under the action of electromagnetic radiation. Work done in

this area includes a general study of stochasticity as a mechanism for ionisation (Meerson et al 1979), and a study of stochasticity and ionisation of highly excited hydrogen atoms in the oscillating electric field of microwave radiation (Leopold and Percival 1979, Richards 1982). The results of their classical study are in excellent agreement with the experimental results (Bayfield and Koch 1974).

A similar kind of study has been carried out for electrons, which are weakly bound to the surface of liquid helium by their image charges (Grimes et al 1976), in the presence of microwave radiation (Jensen 1982, Jensen 1984). This work has already been mentioned in section 8.b. Classical results have been obtained for the onset of stochasticity, as a mechanism for ionisation, with the suggestion of carrying out the experimental study of the same system, in order to compare the classical theoretical results with the experimental ones, which are quantum mechanical in nature.

Our study of the square well potential structure in a semiconductor in the presence of an oscillating laser field, is again a classical study of stochasticity and ionisation, with the suggestion of comparing these results with those of an experimental study of the same system, in order to see how well the experimental quantum mechanical results compare with the classical predictions. It is also of interest with regard to the tunable laser system, as explained in section 7.c.

Chapter 9

The square well potential in an oscillating laser field - the study of stochasticity

9.a. The transition to action and angle variables .

We assume that we have a particle with mass M inside a potential well V(x) in the presence of a periodically oscillating potential. The Hamiltonian of such a system is given by

$$H(p,x,t)=H_0(p,x)+\varepsilon W(x)\cos(\omega t), \qquad (9.a.1)$$

where $H_0(p,x)$ is the unperturbed Hamiltonian given by

$$H_0(p,x)=p^2/2M+V(x), \qquad (9.a.2)$$

and $\varepsilon W(x)\cos(\omega t)$ is the oscillating potential, considered as a perturbation, with ε being a parameter for controlling the perturbation strength.

In our case $\varepsilon W(x)=eE_L x$, where E_L, the amplitude of the laser electric field, serves as this parameter, and V(x) is given by expression (7.d.2).

We wish to change our variables from momentum p and position x to action I and angle θ, and thus to switch from momentum-position space to action-angle space. In terms of the new variables the motion in the unperturbed system is described by straight lines in action-angle space (see section 8.a), and this makes the study of stochasticity more convenient.

In order to do so we look first at the unperturbed Hamiltonian (expression (9.a.2)). The action for a particle with energy E inside a potential well V(x) in such a case is given by the

expression (Percival and Richards 1982)

$$I(E)=(1/\pi)\int_{x_1(E)}^{x_2(E)}(2M[E-V(x)])^{1/2}dx, \qquad (9.a.3)$$

where $x_1(E)$ and $x_2(E)$ are the turning points, i.e. the values of the position x where $V(x)=E$.

The unperturbed Hamiltonian can now be expressed in terms of the action by inverting the function $I(E)$, as obtained from expression (9.a.3), and identifying $E(I)$ with $H_0(I)$.

The libration frequency Ω_0 is the frequency at which the particle completes a full cycle of its motion, i.e. moves from a given point of origin to one of the turning points, back to the point of origin and on to the second turning point, and then back to the point of origin. The libration frequency is obtained from the Hamiltonian $H_0(I)$ by using the relation

$$\Omega_0(I)=dH_0(I)/dI. \qquad (9.a.4)$$

The angle can now be obtained from the relation

$$\theta(I,x)=M\Omega_0(I)\int_{x_0}^{x}(2M[E(I)-V(y)])^{-1/2}dy, \qquad (9.a.5)$$

where x_0 is the value of x for which $\theta=0$. The angle is periodic with a period of 2π, i.e. $\theta+2n\pi$ is equivalent to θ for any integer n. Thus only the range $[0,2\pi]$ needs to be used for θ.

By inverting the function $\theta(I,x)$ we obtain x as a function of I and θ, and thus we can express the full Hamiltonian (expression (9.a.1)) in terms of our new variables as

$$H(I,\theta,t)=H_0(I)+\varepsilon W(I,\theta)\cos(\omega t). \qquad (9.a.6)$$

In our case, for a particle inside the square well, i.e. with energy $E<V_0$, the turning points are 0 and d, and thus the action is given by

$$I(E)=(1/\pi)\int_0^d (2ME)^{1/2}dx=(d/\pi)(2ME)^{1/2}. \qquad (9.a.7)$$

By inverting this function we obtain the unperturbed Hamiltonian in terms of the action. It is given by

$$H_0(I)=\pi^2 I^2/2Md^2. \qquad (9.a.8)$$

The libration frequency is thus given by

$$\Omega_0(I)=\pi^2 I/Md^2. \qquad (9.a.9)$$

The angle variable in our case is given by

$$\theta(I,x)=M\Omega_0(I)\int_{x_0}^{x}[2ME(I)]^{-1/2}dy=$$
$$\pm(\pi^2 I/d^2)(d/\pi I)(x-x_0)=\pm(\pi/d)(x-x_0). \qquad (9.a.10)$$

We see that θ does not depend on I in our case, and thus it can be denoted as $\theta(x)$. In order to define $\theta(x)$ in a unique manner we look at the physical picture. In the unperturbed case the momentum of the particle is constant (up to the sign), and the particle bounces back and forth between the turning points. We arbitrarily choose $x_0=0$. The particle moves from x=0 to the right, and thus we have to choose the plus sign. When x=d is reached, the particle bounces back, and starts moving to the left. In order to keep $\theta(x)$ single valued and continuous, we have to choose for this part of the motion the minus sign and $x_0=2d$. Thus $\theta(x)$ is given by

$$\theta(x)=\begin{cases}\pi x/d & \text{if } p>0\\ \pi(2-x/d) & \text{if } p<0.\end{cases} \qquad (9.a.11)$$

In physical terms $\theta(x)$ is the distance the particle has travelled since it had last visited the turning point at $x=0$, multiplied by the constant factor π/d.

The position x in terms of the angle θ is found to be given by

$$x(\theta)=\begin{cases}(d/\pi)\theta & \text{if } 0\leq\theta\leq\pi\\ (d/\pi)(2\pi-\theta) & \text{if } \pi\leq\theta\leq2\pi.\end{cases} \qquad (9.a.12)$$

This is easily obtained from expression (9.a.11) for $\theta(x)$, if we note that when $p>0$, the particle moves to the right (from $x=0$ to $x=d$), and thus $0\leq\theta\leq\pi$, and when $p<0$, the particle moves to the left (from $x=d$ back to $x=0$), and thus $\pi\leq\theta\leq2\pi$.

The Hamiltonian in terms of I and θ is thus given by

$$H(I,\theta,t)=H_0(I)+(eE_L d/\pi)F(\theta)\cos(\omega t), \qquad (9.a.13)$$

where $H_0(I)$ is given by expression (9.a.8), and $F(\theta)$ is defined by

$$F(\theta)=\begin{cases}\theta & \text{if } 0\leq\theta\leq\pi\\ 2\pi-\theta & \text{if } \pi\leq\theta\leq2\pi.\end{cases} \qquad (9.a.14)$$

In order to carry out an analysis of the perturbed Hamiltonian in action-angle space later on we make use of the periodicity of the angle θ, and expand the perturbing term as a Fourier series in this variable.

In order to do so, we rewrite the Hamiltonian (expression (9.a.6)) in the form

$$H(I,\theta,t)=H_0(I)+(1/2)\varepsilon W(I,\theta)[\exp(i\omega t)+\exp(-i\omega t)], \qquad (9.a.15)$$

and expand $W(I,\theta)$ as a Fourier series in θ:

$$W(I,\theta)=\sum_{n=-\infty}^{\infty} W_n(I)\exp(in\theta), \qquad (9.a.16)$$

where

$$W_n(I)=(1/2\pi)\int_0^{2\pi} W(I,\theta)\exp(-in\theta)d\theta. \qquad (9.a.17)$$

Using this expansion the Hamiltonian becomes

$$H(I,\theta,t)=H_0(I)+(1/2)\varepsilon\sum_{n=-\infty}^{\infty} W_n(I)\{\exp[i(n\theta+\omega t)]+\exp[i(n\theta-\omega t)]\}. \qquad (9.a.18)$$

In our case the only θ-dependence occurs in $F(\theta)$ (expression (9.a.14)), and thus we only need to expand this function as a Fourier series. For $n\neq 0$ we have

$$\int_0^{2\pi} F(\theta)\exp(-in\theta)d\theta=\int_0^{\pi}\theta\exp(-in\theta)d\theta+\int_{\pi}^{2\pi}(2\pi-\theta)\exp(-in\theta)d\theta=$$

$$\left[(i\theta/n+1/n^2)\exp(-in\theta)\right]_0^{\pi}+\left[(2\pi i/n-i\theta/n-1/n^2)\exp(-in\theta)\right]_{\pi}^{2\pi}=$$

$$-(2/n^2)[1-(-1)^n]. \qquad (9.a.19)$$

The case $n=0$ has to be treated separately. Here we have

$$\int_0^{2\pi} F(\theta)d\theta=\int_0^{\pi}\theta d\theta+\int_{\pi}^{2\pi}(2\pi-\theta)d\theta=\left[\theta^2/2\right]_0^{\pi}-\left[(2\pi-\theta)^2/2\right]_{\pi}^{2\pi}=\pi^2. \qquad (9.a.20)$$

Thus the Fourier series expansion of $F(\theta)$ is given by

$$F(\theta)=\sum_{n=-\infty}^{\infty} F_n\exp(in\theta), \qquad (9.a.21)$$

where

$$F_n = \begin{cases} -2/\pi n^2 & \text{if } n \text{ is odd} \\ 0 & \text{if } n \text{ is even and non-zero} \\ \pi/2 & \text{if } n \text{ is zero.} \end{cases} \qquad (9.a.22)$$

Thus the Hamiltonian $H(I,\theta,t)$ in our case is given by

$$H(I,\theta,t)=H_0(I)+(eE_L d/2\pi)\sum_{n=-\infty}^{\infty} F_n\{\exp[i(n\theta+\omega t)]+\exp[i(n\theta-\omega t)]\}. \qquad (9.a.23)$$

We note that $F_n=F_{-n}$, and therefore we can rewrite this as

$$H(I,\theta,t)=H_0(I)+(eE_L d/2)\cos(\omega t)- (2eE_L d/\pi^2)\sum_{n=1}^{\infty}{}'[\cos(n\theta+\omega t)+\cos(n\theta-\omega t)]/n^2, \qquad (9.a.24)$$

where Σ' indicates that the summation should be carried out only over the odd values of n.

9.b. Resonances and the Chirikov criterion for the onset of stochasticity

We wish now to carry out a quantitative analysis of the transition of our perturbed system from regular to stochastic motion. In order to do so we have to analyse the equations of motion.

The equations of motion in action-angle space are found from the Hamiltonian with the perturbing term expanded as a Fourier series (expression (9.a.18)) by using expression (8.a.9). They are given by

$$d\theta/dt=\Omega_0(I)+(1/2)\varepsilon\sum_{n=-\infty}^{\infty}[dW_n(I)/dI]\{\exp[i(n\theta+\omega t)]+\exp[i(n\theta-\omega t)]\}\ ;$$

$$dI/dt=-(1/2)i\varepsilon\sum_{n=-\infty}^{\infty}nW_n(I)\{\exp[i(n\theta+\omega t)]+\exp[i(n\theta-\omega t)]\}. \qquad (9.b.1)$$

If the perturbation parameter ε is sufficiently small, the approximate solution is given by

$$\theta(t)=\Omega_0(I_0)t+\theta_0-(1/2)i\varepsilon\sum_{n=-\infty}^{\infty}[dW_n(I)/dI]\Big|_{I=I_0}x$$

$$\{\exp(i\{[n\Omega_0(I_0)+\omega]t+n\theta_0\})/[n\Omega_0(I_0)+\omega]+$$

$$\exp(i\{[n\Omega_0(I_0)-\omega]t+n\theta_0\})/[n\Omega_0(I_0)-\omega]\}$$

$$I(t)=I_0-(1/2)\varepsilon\sum_{n=-\infty}^{\infty}nW_n(I_0)x$$

$$\{\exp(i\{[n\Omega_0(I_0)+\omega]t+n\theta_0\})/[n\Omega_0(I_0)+\omega]+$$

$$\exp(i\{[n\Omega_0(I_0)-\omega]t+n\theta_0\})/[n\Omega_0(I_0)-\omega]\}. \qquad (9.b.2)$$

θ_0 and I_0 are the values of θ and I respectively at $t=0$.

This approximation is valid as long as the denominators are not too small, i.e. ω is not too close to $n\Omega_0(I_0)$ for any integer

n. If $\omega=n\Omega_0(I_0)$, then the perturbative solution is not valid any more, and we say that we have a resonance. In terms of the discussion in sections 8.a and 8.b we say, that the torus labelled by I_0 is resonant. We see that for a given value of ω the n^{th} resonance occurs for a value of the action, denoted by I_n, which satisfies

$$\omega=n\Omega_0(I_n). \qquad (9.b.3)$$

In the vicinity of the resonances expression (9.b.2) is not valid. However, it is clear, that the influence of the perturbation is stronger there, than for other values of the action.

If the value of the initial action is close to the n^{th} resonance, and the remaining resonances are sufficienly far away (on the action scale), then all the terms in the Fourier series expansion, except for those which contribute to the resonant terms in (9.b.2), can be neglected. Thus the Hamiltonian (9.a.18) near the n^{th} resonance is approximated by

$$H(I,\theta,t)=H_0(I)+\varepsilon W_n(I)\cos(n\theta-\omega t). \qquad (9.b.4)$$

Now we use the canonical (area preserving) transformation

$$J=I \ ; \ \phi=\theta-\omega t/n, \qquad (9.b.5)$$

which is obtained from the generating function (Percival and Richards 1982)

$$F(J,\theta)=J(\theta-\omega t/n). \qquad (9.b.6)$$

The Hamiltonian in terms of the new variables J and ϕ is obtained from the original one by replacing I by J and θ by $\phi+\omega t/n$,

and then adding the term $\partial F/\partial t=-J\omega/n$. Thus it is given by

$$H(J,\phi)=H_0(J)-J\omega/n+\varepsilon W_n(J)\cos(n\phi). \qquad (9.b.7)$$

The value of J is close to I_n, the value of I (or J) at the n^{th} resonance. Therefore we define a perturbation parameter P by

$$P=J-I_n, \qquad (9.b.8)$$

and then expand $H(J,\phi)$ around I_n in terms of P.

We have

$$H_0(J)=H_0(I_n+P)=H_0(I_n)+P\Omega_0(I_n)+(1/2)P^2\Omega_0'(I_n)+O(P^3), \qquad (9.b.9)$$

and (using (9.b.3))

$$J\omega/n=(P+I_n)\Omega_0(I_n), \qquad (9.b.10)$$

and thus the expansion for $H(J,\phi)$, denoted now as $H(P,\phi)$, becomes

$$H(P,\phi)=H_0(I_n)-I_n\Omega_0(I_n)+(1/2)\Omega_0'(I_n)P^2+\varepsilon W_n(I_n)\cos(n\phi)+O(P^3)+\varepsilon O(P). \qquad (9.b.11)$$

We can remove the additive constant $H_0(I_n)-I_n\Omega_0(I_n)$ by a proper choice of the reference energy level, and neglect the higher order terms in the last expansion. Thus we are left with

$$H(P,\phi)=(1/2)\Omega_0'(I_n)P^2+\varepsilon W_n(I_n)\cos(n\phi), \qquad (9.b.12)$$

which is similar to the Hamiltonian of a simple pendulum. If we have only oscillatory motion of this "pendulum", then P is restricted to the range $|P|<2[\varepsilon|W_n(I_n)/\Omega_0'(I_n)|]^{1/2}$.

This means that near the n^{th} resonance the value of the action

I will oscillate around the value I_n with a maximum amplitude (or half-width) $(\Delta I)_n$, given by

$$(\Delta I)_n=2[\varepsilon|W_n(I_n)/\Omega_0'(I_n)|]^{1/2}. \qquad (9.b.13)$$

The value of the perturbation parameter ε for which the motion near the n^{th} resonance becomes stochastic can be estimated by means of the Chirikov criterion (Chirikov 1979, Richards 1982). The Chirikov criterion states, that the motion near the n^{th} resonance becomes stochastic, when the sum of the half-widths of the n^{th} and the $(n+1)^{th}$ resonances exceeds the distance between the values of I_n and I_{n+1} on the action scale, i.e. when

$$(\Delta I)_n+(\Delta I)_{n+1}\geq|I_n-I_{n+1}|. \qquad (9.b.14)$$

By using this expression, the value of ε for which the n^{th} resonance becomes stochastic, denoted by ε_n, can be found. It is given by

$$\varepsilon_n=(1/4)(I_n-I_{n+1})^2/[|W_n(I_n)/\Omega_0'(I_n)|^{1/2}+ |W_{n+1}(I_{n+1})/\Omega_0'(I_{n+1})|^{1/2}]^2. \qquad (9.b.15)$$

The largest among these ε_n, usually ε_1, is the value of the perturbation parameter ε, for which the motion becomes totally stochastic.

Now we wish to apply the Chirikov criterion to our specific case. From expression (9.a.24) we see, that only the odd numbered resonances are present in our case. If we compare this expression with expression (9.b.4) we see, that W_n (for odd n) in our case is given by

$$W_n=-2ed/\pi^2n^2, \qquad (9.b.16)$$

and thus does not depend on I.

The libration frequency Ω_0 in our case is given by expression (9.a.9). Using expression (9.b.3) for the n^{th} resonance we obtain thus

$$I_n=Md^2\omega/\pi^2n. \qquad (9.b.17)$$

We also see that

$$d\Omega_0/dI=\pi^2/Md^2, \qquad (9.b.18)$$

and thus it does not depend on the action as well.

Now we can make use of expression (9.b.15) in order to obtain $E_L^{(n)}$ (the equivalent of ε_n), the value of the laser electric field strength for which the n^{th} resonance becomes stochastic. We note, that as only odd numbered resonances are present here, n+1 is replaced by n+2 in the original expression for ε_n, when it is used for our case. Therefore we have

$$(1/4)(I_n-I_{n+2})^2=M^2d^4\omega^2/\pi^4n^2(n+2)^2, \qquad (9.b.19)$$

and

$$|W_k/\Omega_0'|^{1/2}=d(2eMd)^{1/2}/\pi^2k \quad , \quad k=n,n+2. \qquad (9.b.20)$$

Thus we finally obtain (for odd n)

$$E_L^{(n)}\cong Md\omega^2/8e(n+1)^2. \qquad (9.b.21)$$

We see that the resonances become stochastic, when E_L is gradually increased, in descending order of their ordinal numbers

n. The motion in the quantum well becomes fully stochastic, when the first (n=1) resonance becomes stochastic, i.e. when the laser field strength reaches the value $E_L = Md\omega^2/32e$.

In order to really have all the resonances present, a certain restriction has to be imposed on V_0, the depth of the square well. From expression (9.a.7) and the demand that $E<V_0$ we obtain

$$I<I_{max}=(d/\pi)(2MV_0)^{1/2}. \qquad (9.b.22)$$

In order to have all the resonances present, we need to have $I_1<I_{max}$, and thus, using expression (9.b.17) for n=1, we obtain

$$V_0>Md^2\omega^2/2\pi^2 \qquad (9.b.23)$$

as the restriction on V_0.

The above values of E_L for the onset of stochasticity are only approximate, as they are based upon the use of perturbation theory and upon the assumption that each resonance is totally unaffected by the others. More accurate values can be obtained from the numerical solution of the equations of motion, which will be discussed in the next section.

9.c. The numerical solution of the equations of motion

The equations of motion, in terms of action and angle, are obtained from the Hamiltonian $H(I,\theta,t)$ (expression (9.a.13)) by using expression (8.a.9). The result is

$$d\theta/dt=\pi^2 I/Md^2 ;$$

$$dI/dt=-(eE_L d/\pi)S(\theta)\cos(\omega t), \qquad (9.c.1)$$

where the function $S(\theta)$ is defined by

$$S(\theta)=\begin{cases} 1 \text{ if } 0<\theta<\pi \\ -1 \text{ if } \pi<\theta<2\pi. \end{cases} \qquad (9.c.2)$$

In order to make things more convenient, we now introduce a series of dimensionless parameters. We express the energy in units of $\hbar^2/2Md^2$, as we have done in section 7.d, and assume that N (expression 7.d.10) is an integer, and thus we have exactly N quantum energy levels in the well.

Using these notations we have I_{max} (expression (9.b.22)) given by $I_{max}=N\hbar$, and thus we can define the dimensionless action J in units of I_{max} as

$$J=I/I_{max}=I/N\hbar. \qquad (9.c.3)$$

We define as ω_0 the bouncing frequency at the ground quantum level E_1, i.e. the frequency at which a particle with energy E_1 visits the turning points in the unperturbed system. Thus ω_0 is twice the libration frequency Ω_0, for that energy, and is given by $\omega_0=2\pi^2 I(E_1)/Md^2=(2\pi/Md)(2ME_1)^{1/2}$. Using expression (7.d.14) for E_n we have ω_0 given by

$$\omega_0 = 2\pi\hbar A_1/Md^2, \qquad (9.c.4)$$

where A_1 is as defined in section 7.d.

Using this definition for ω_0, we replace the laser frequency ω by the dimensionless parameter η given by

$$\eta = \omega/\omega_0, \qquad (9.c.5)$$

and the laser field E_L by the dimensionless parameter λ given by

$$\lambda = eE_L/Md\omega_0^2. \qquad (9.c.6)$$

Finally we change the time t to the dimensionless parameter τ given by

$$\tau = \omega t/2\pi, \qquad (9.c.7)$$

i.e. we express the time in units of the period of the oscillating laser field.

Using these dimensionless parameters the equations of motion (expression (9.c.1)) become

$$d\theta/d\tau = (N\pi^2/\eta A_1)J ;$$

$$dJ/d\tau = -(4\pi\lambda A_1/N\eta)S(\theta)\cos(2\pi\tau). \qquad (9.c.8)$$

A close look at expression (9.c.8) shows us, that if we replace J by the new variable $K = (N\pi^2/\eta A_1)J$, then we are left with only one parameter, namely λ/η^2, in the second equation. This parameter is proportional to E_L/ω^2, which occurs in the expression for the Chirikov criterion (expression (9.b.21)). This means that actually it is sufficient to carry out the numerical study for one

particular choice of N and η. Numerical studies for other values, however, can be helpful for estimating the accuracy of the estimates for the onset of stochasticity in the system.

As far as one remains in the range $0\leq\theta\leq\pi$ or in the range $\pi\leq\theta\leq 2\pi$, the equations of motion can be solved analytically. The solution is found by integrating the equation for $dJ/d\tau$ first, in order to obtain an expression for $J(\tau)$, and then integrating the equation for $d\theta/d\tau$, using this expression, in order to obatin an expression for $\theta(\tau)$.

The results are

$$\theta(\tau)=\mp(\pi\lambda/\eta^2)\cos(2\pi\tau)+(N\pi^2/\eta A_1)J_1\tau+\theta_1$$

$$J(\tau)=\pm(2\lambda A_1/N\eta)\sin(2\pi\tau)+J_1, \qquad (9.c.9)$$

where θ_1 and J_1 are initially given by

$$\theta_1=\theta_0\mp\pi\lambda/\eta^2 \; ; \; J_1=J_0. \qquad (9.c.10)$$

The lower signs are for $0\leq\theta\leq\pi$, and the upper signs are for $\pi\leq\theta\leq 2\pi$. θ_0 and J_0 are the values of θ and J respectively at $\tau=0$.

This solution, with the initial values of θ_1 and J_1 (as given by expression (9.c.10)), is used from the time $\tau=0$ until the time when $\theta=0$ or $\theta=\pi$ in the case $0\leq\theta_0\leq\pi$, or when $\theta=\pi$ or $\theta=2\pi$ in the case $\pi\leq\theta_0\leq 2\pi$, for the first time. We denote the value of τ, where this happens, by τ_0. The solution for values of $\tau>\tau_0$ (sufficiently close to τ_0) is given by

$$\theta(\tau)=\pm(\pi\lambda/\eta^2)\cos(2\pi\tau)+(N\pi^2/\eta A_1)J_2+\theta_2$$

$$J(\tau)=\mp(2\lambda A_1/N\eta)\sin(2\pi\tau)+J_2, \qquad (9.c.11)$$

where θ_2 and J_2 are constants, which are yet to be determined.

We know that $\theta(\tau)$ and $J(\tau)$ are continuous variables, and that θ is periodic, i.e. $\theta \pm 2\pi$ is equivalent to θ. Therefore we have the continuity conditions

$$\pm(\pi\lambda/\eta^2)\cos(2\pi\tau_0)+(N\pi^2/\eta A_1)J_2\tau_0+\theta_2 =$$

$$2\pi-[\mp(\pi\lambda/\eta^2)\cos(2\pi\tau_0)+(N\pi^2/\eta A_1)J_1\tau_0+\theta_1]$$

$$\mp(2\lambda A_1/N\eta)\sin(2\pi\tau_0)+J_2=\pm(2\lambda A_1/N\eta)\sin(2\pi\tau_0)+J_1. \qquad (9.c.12)$$

The right hand side of the first expression is equal to 2π, π, or 0, if $\theta(\tau_0)$ is equal to 0, π, or 2π respectively, and thus the continuity of $\theta(\tau)$ (modulus 2π) is guaranteed. Using (9.c.12), J_2 can be obtained (from the second equation), and then θ_2 can be obtained (from the first equation).

The numerical solution of the equations of motion proceeds thus as follows. Given the initial conditions, i.e. the values of τ_0 and J_0, the solution is given by expression (9.c.9) (with θ_1 and J_1 given by expression (9.c.10)), as long as $\theta(\tau)$ remains within the range $[0,\pi]$ or $[\pi,2\pi]$, according to θ_0. τ_0, the value of τ, where $\theta(\tau)$ reaches 0, π, or 2π, for the first time, is found numerically (by bisection), and then expression (9.c.12) is used in order to obtain the constants θ_2 and J_2 for the solution in the new range, $[\pi,2\pi]$ or $[0,\pi]$ respectively. The solution itself is given by expression (9.c.11). This solution is now used, as long as $\theta(\tau)$ remains within the above range. When $\theta=0$, $\theta=\pi$, or $\theta=2\pi$ is reached again, expression (9.c.12) is used once more, but this time with θ_2 and J_2 given, in order to find the

new values of θ_1 and J_1. The solution is now again given by expression (9.c.9), but with the new values of θ_1 and J_1. The above procedure is repeated again and again, until the desired final value of τ is reached.

We have seen thus how the equations of motion (in action-angle space) can be solved in a semi-analytical way, with the only numerical procedure required being the numerical solution of transcendental equations by bisection. Thus the error introduced in the computation of $\theta(\tau)$ and $J(\tau)$ is minimal. We should also point out, that the usual Runge-Kutta methods for solving differential equations are inadequate in this case due to the singular nature of the function $S(\theta)$ (expression (9.c.2)).

9.d. Comparison between the Chirikov criterion predictions for the onset of stochasticity and the results and conclusions

In order to compare the numerical results with the theoretical predictions for the onset of stochasticity, we first have to express the Chirikov criterion prediction (expression (9.b.21)) in terms of our dimensionless parameters. Using expressions (9.c.5) and (9.c.6) we obtain

$$\lambda_n=\eta^2/8(n+1)^2 \quad (n \text{ odd}), \tag{9.d.1}$$

where λ_n is the value of λ for which the n^{th} resonance is expected to become stochastic (the equivalent of $E_L^{(n)}$).

We also note, that the restriction on V_0 (expression (9.b.23)) now becomes a restriction on N (the number of quantum levels in the square well), given by

$$N>2\eta A_1/\pi. \tag{9.d.2}$$

The numerical study of the onset of stochasticity is carried out as follows. In order to study the n^{th} resonance the equations of motion (9.c.1) are numerically solved (using the semi-analytical procedure discussed in the previous section) with the initial value of ϑ, θ_0, chosen anywhere between 0 and 2π, and the initial value of J, J_0, given by

$$J_0=I_n/N\hbar=2\eta A_1/\pi nN \tag{9.d.3}$$

(obtained by using expressions (9.b.17), (9.c.4), and (9.c.5)).

The results $\vartheta(\tau)$ and $J(\tau)$ are displayed in a stroboscopical manner, with $J(\tau)$ shown as a function of $\theta(\tau)$ for integer values

of τ, i.e. for integer multiples of the period of the oscillating laser field.

If there is no perturbing field present, i.e. $\lambda=0$, then the solution to the equations of motion (expression (9.c.9)) simply becomes

$$\theta(\tau)=[(N\pi^2/\eta A_1)J_0\tau+\theta_0](\text{mod } 2\pi) \; ; \; J(\tau)=J_0. \qquad (9.d.4)$$

If we are at the n^{th} resonance, then J_0 is given by expression (9.d.3), and thus $\theta(\tau)=[(2\pi/n)\tau+\theta_0](\text{mod } 2\pi)$. Thus, in the above mentioned stroboscopic display of the results, n points show up for the n^{th} resonance, located at (θ_k,J_0), $k=1,2,\ldots,n$, where

$$\theta_k=(2\pi k/n+\theta_0)(\text{mod } 2\pi). \qquad (9.d.5)$$

When the perturbing laser field, i.e. the parameter λ, is introduced, the n points of the n^{th} resonance turn into a chain of n "islands" (Chirikov 1979, Richards 1982). When the perturbation parameter λ is further increased, the "islands" grow wider, and finally, when stochasticity sets in, they are destroyed, and the motion becomes random-like (see also section 8.b). This way, by observing the "islands" for the n^{th} resonance, for different values of λ, and estimating the point where they disappear, an estimate for λ_n, the value of λ for which the n^{th} resonance becomes stochastic, can be obtained. This value can be then compared with the Chirikov criterion prediction for λ_n (expression (9.d.1)).

We present here the results for the case of a square well with 4 quantum energy levels (N=4). The values of η (the frequency parameter) which have been used were $\eta=0.5$, $\eta=1.0$, and $\eta=1.5$. The

requirement (9.d.2) is satisfied for these values. For each value of η we have found the value of λ (the laser field parameter), for which the n=7, the n=5, the n=3, and the n=1 resonances disappear, by following the procedure outlined above.

As an example, we show the results, in the form of "island chains", of $J(\tau)$ as a function of $\theta(\tau)$ (note that J is marked as "I" in the diagrams) for the case η=1.0, once with λ=0.0052, in Figure 52, and once with λ=0.0054, in Figure 53. We see that in Figure 52, where λ=0.0052, the n=5 "island chain" (for the n=5 resonance) is clearly visible, whereas in Figure 53, where λ=0.0054, the n=5 "island chain" has already disappeared, as the random-like distribution of points indicates. Thus λ_5 in this case is about 0.0053. The n=1 and n=3 "island chains" (for the n=1 and n=3 resonances) are clearly visible in both figures, as they are going to disappear only for much larger values of λ.

The accuracy with which the value of λ_n can be obtained from the numerical results depends on n. For lower lying "island chains", i.e. larger n, the accuracy is better than 5%. For the n=1 and n=3 "island chains", however, the uncertainty in estimating λ_n is quite large - as much as 20-30%.

The results of our study are summarised in Table 3. For each value of η, the theoretical value of λ_n (for n=1,3,5,7), as obtained from expression (9.d.1), is shown, as well as the corresponding "experimental" value, as obtained from the numerical study.

As in other numerical investigations of the Chirikov criterion (Jensen 1984, Galvão et al 1984), the agreement between the

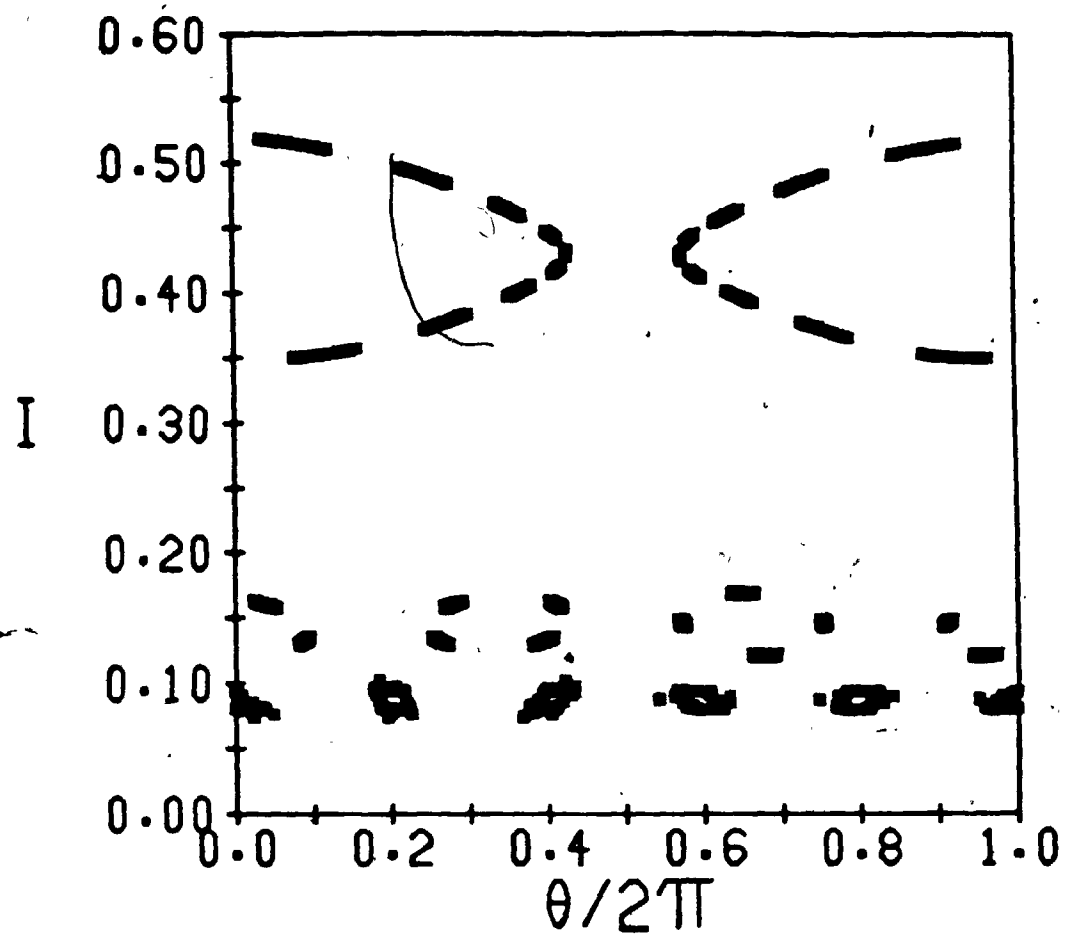

Figure 52

The resonances n=1, n=3, and n=5 for the square well with N=4 levels, perturbed by a laser field with frequency parameter η=1.0 and field strength parameter λ=0.0052. The resonances appear as "island chains". The n^{th} resonance has n "islands" in it.

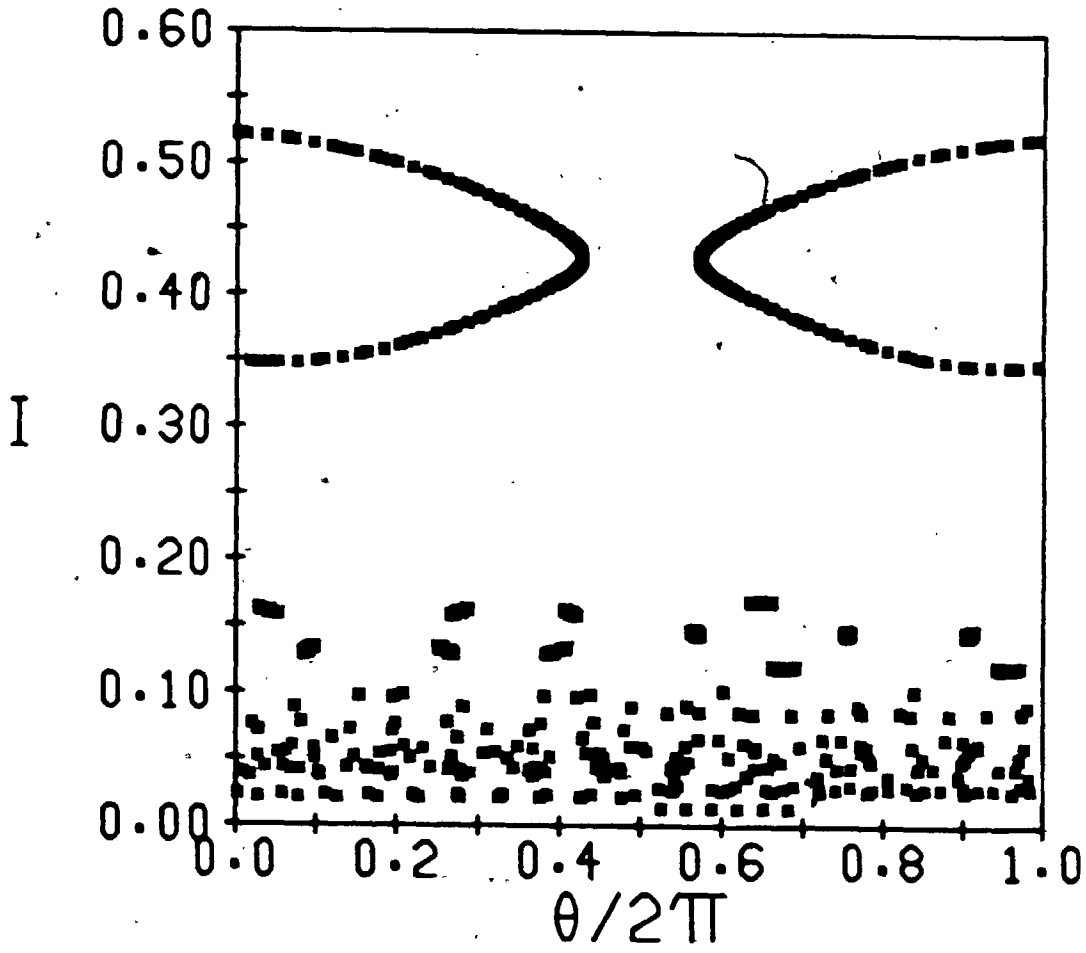

Figure 53

The resonances n=1, n=3, and n=5 for the square well with N=4 levels, perturbed by a laser field with frequency parameter η=1.0 and field strength parameter λ=0.0054. The resonances n=1 and n=3 still appear as "island chains", but the resonance n=5 has already become stochastic.

Table 3

Comparison between the λ_n, the values of the laser electric field parameter λ for the onset of stochasticity at the n^{th} resonance, as theoretically predicted by the Chirikov criterion, and as numerically obtained, for the case of a square well with 4 quantum energy levels (N=4), with the laser frequency parameter η equal to 0.5, 1.0, and 1.5.

η	n	λ_n (theoretical)	λ_n (numerical)
0.5	1	0.0078	0.025
	3	0.0020	0.0042
	5	0.00087	0.0013
	7	0.00049	0.0011
1.0	1	0.031	0.11
	3	0.0078	0.016
	5	0.0035	0.0053
	7	0.0020	0.0049
1.5	1	0.070	0.27
	3	0.018	0.032
	5	0.0078	0.0117
	7	0.0044	0.0107

values of λ_n, as obtained from the analytical expression, and the ones obtained numerically, is only a rough one. The agreement is the best (a difference by a factor of 1.5) in the case of n=5. For the higher lying resonances, i.e. n=1 and n=3, the difference is larger (up to a factor of roughly 4). This is due to the fact, that the Chirikov criterion is valid only for sufficiently small perturbations, and in the higher lying resonances rather large values of λ are involved. For the lower lying resonances, i.e. n=7,9,..., the difference is larger again (e.g. a factor of roughly 2.5 in the n=7 cases). This is due to the fact, that for large values of n the adjacent values of I_n (expression (9.b.17)) lie closer and closer to each other, and in such a case the assumption, that the motion near a given resonance is not affected by the other resonances (see section 9.b), is not valid any more. We also note that the numerical values of λ_n are always larger in our case, than the theoretical ones.

Ionisation can be expected to occur only for values of the laser field strength, for which motion in the entire system has become stochastic, as stochasticity is the mechanism which enables a particle, which is originally found near the bottom of the potential well, to reach the top of the well and leave it all together. Thus our results indicate, that ionisation is expected in our case, and they give us a rough idea, for what values of the laser field strength it should occur.

Chapter 10

The square well potential in an oscillating laser field - the study of ionisation

10.a. The equations of motion and compensated energy for the study of ionisation

Our study of the laser driven square potential well has shown us, so far, that stochasticity is present in this system, and thus ionisation can be expected. We are now ready to carry out the study of the ionization process, which is our main topic in this work. In order to study the ionisation process, we have to know the energy of the particle as a function of time. The latter is obtained from the position and momentum of the particle, which are found by solving the equations of motion in momentum-position space.

In order to make our model more realistic, we turn the laser field on and switch it off adiabatically. We follow previous workers in this field, and use an exponential switching function (Leopold and Percival 1979), given by

$$f(t)=\begin{cases}\exp[\gamma(t-t_i)] & \text{if } 0\leq t\leq t_i \\ 1 & \text{if } t_i\leq t\leq t_f \\ \exp[-\gamma(t-t_f)] & \text{if } t_f\leq t\leq t_0 .\end{cases} \qquad (10.a.1)$$

The value of γ is chosen so that $f(t)$ increases from an initial value $\varepsilon<<1$, at $t=0$, to 1, at $t=t_i$, over many periods of the oscillating laser field, remains constant (with the value of 1) over many more periods, until $t=t_f$ is reached, and finally decreases again, over many periods of the laser field, until it

reaches the initial small value ε at $t=t_0$.

Thus our Hamiltonian now changes to

$$H(p,x,t)=p^2/2M+V(x)+eE_L x\ f(t)\cos(\omega t), \qquad (10.a.2)$$

and the equations of motion (see expression (8.a.8)) thus become

$$dx/dt=p/M$$

$$dp/dt=-eE_L f(t)\cos(\omega t). \qquad (10.a.3)$$

We have omitted here the delta-functions located at x=0 and x=d (obtained from differentiating V(x)). We account for those by demanding that the momentum p changes sign whenever x=0 or x=d is reached.

Now we want to change our variables to dimensionless parameters, as we have done in the case of the numerical study of stochasticity. We use the dimensionless parameters introduced in section 9.c, with the addition of the dimensionless momentum

$$P=dp/\hbar \qquad (10.a.4)$$

and the dimensionless position

$$Z=x/d. \qquad (10.a.5)$$

Using these dimensionless parameters, the equations of motion become

$$dZ/d\tau=(1/\eta A_1)P$$

$$dP/d\tau=-(4\pi^2\lambda A_1/\eta)f(\tau)\cos(2\pi\tau). \qquad (10.a.6)$$

The delta-functions are now accounted for by requiring that the dimensionless momentum P changes sign whenever Z=0 or Z=1 is reached.

The switching function $f(\tau)$ is now given by

$$f(\tau)=\begin{cases}\exp[\Gamma(\tau-\tau_i)] & \text{if } 0\leq\tau\leq\tau_i \\ 1 & \text{if } \tau_i\leq\tau\leq\tau_f \\ \exp[-\Gamma(\tau-\tau_f)] & \text{if } \tau_f\leq\tau\leq\tau_0.\end{cases} \qquad (10.a.7)$$

Here $\Gamma=2\pi\gamma/\omega$, $\tau_i=\omega t_i/2\pi$, $\tau_f=\omega t_f/2\pi$, and $\tau_0=\omega t_0/2\pi$. The switching on and switching off times are normally chosen to be equal, and thus $\tau_i=\tau_0-\tau_f$. If ε is given, we can find Γ from the relation

$$\Gamma=-(\ln.\varepsilon)/\tau_i. \qquad (10.a.8)$$

As mentioned before, we are interested in the behaviour of the energy of the particle as a function of time. For this purpose we use the compensated energy (Leopold and Percival 1979, Galvão et al 1984), given by

$$E_C(t)=[p+eA_L(t)]^2/2M+V(x), \qquad (10.a.9)$$

where $A_L(t)$ is the vector potential of the laser field (including the switching function), given by

$$A_L(t)=-E_L\int_0^t f(t')\cos(\omega t')dt'. \qquad (10.a.10)$$

In order to switch to dimensionless parameters we express the energy in units of $\hbar^2/2Md^2$. In these units the depth of the square well is $N^2\pi^2$ (see section 7.d). The compensated energy in these units is denoted by $\varepsilon_C(\tau)$, and is given by

$$\varepsilon_C(\tau)=[P-(4\pi^2\lambda A_1/\eta)F(\tau)]^2+V(Z), \qquad (10.a.11)$$

where $F(\tau)$ is given by

$$F(\tau)=\int_0^{\tau} f(\tau')\cos(2\pi\tau')d\tau', \qquad (10.a.12)$$

and $V(Z)$ is given by

$$V(Z)=\begin{cases}0 & \text{if } 0<Z<1\\ N^2\pi^2 & \text{if } Z<0 \text{ or } Z>1.\end{cases} \qquad (10.a.13)$$

Using expression (10.a.7) for $f(\tau)$, $F(\tau)$ is found to be given by the following expressions:

For $0\leq\tau\leq\tau_i$:

$$F(\tau)=\{\exp[\Gamma(\tau-\tau_i)][\Gamma\cos(2\pi\tau)+2\pi\sin(2\pi\tau)]-$$
$$\Gamma\exp(-\Gamma\tau_i)\}/(\Gamma^2+4\pi^2). \qquad (10.a.14)$$

For $\tau_i\leq\tau\leq\tau_f$:

$$F(\tau)=\sin(2\pi\tau)/2\pi+\Gamma[\cos(2\pi\tau_i)-\exp(-\Gamma\tau_i)]/(\Gamma^2+4\pi^2)-$$
$$\Gamma^2\sin(2\pi\tau_i)/2\pi(\Gamma^2+4\pi^2). \qquad (10.a.15)$$

For $\tau_f\leq\tau\leq\tau_0$:

$$F(\tau)=\exp[-\Gamma(\tau-\tau_f)][2\pi\sin(2\pi\tau)-\Gamma\cos(2\pi\tau)]/(\Gamma^2+4\pi^2)+$$
$$\Gamma[\cos(2\pi\tau_i)+\cos(2\pi\tau_f)-\exp(-\Gamma\tau_i)]/(\Gamma^2+4\pi^2)-$$
$$\Gamma^2[\sin(2\pi\tau_i)-\sin(2\pi\tau_f)]/2\pi(\Gamma^2+4\pi^2). \qquad (10.a.16)$$

We have obtained thus all the equations and expressions required for the study of ionisation, in terms of our dimensionless variables and parameters.

10.b. The numerical solution of the equations of motion

The procedure we use in order to solve the equations of motion in momentum-position space (expression (10.a.6)) is very similar to the one we have used in section 9.c in order to solve the equations of motion in action-angle space. The main difference is, that because of the switching function $f(\tau)$ we have to treat the periods $0\leq\tau\leq\tau_i$, $\tau_i\leq\tau\leq\tau_f$, and $\tau_f\leq\tau\leq\tau_0$ separately. Each time we integrate the equation for $dP/d\tau$, and then, using the resulting expression for $P(\tau)$, integrate the equation for $dZ/d\tau$, and obtain an expression for $Z(\tau)$.

In the case of $0\leq\tau\leq\tau_i$ we obtain the expressions

$$Z(\tau,P_1,Z_1)=-4\pi^2\lambda\exp[\Gamma(\tau-\tau_i)][(\Gamma^2-4\pi^2)\cos(2\pi\tau)+4\pi\Gamma\sin(2\pi\tau)]/\eta^2(\Gamma^2+4\pi^2)^2+(P_1/\eta A_1)\tau+Z_1$$

$$P(\tau,P_1)=-4\pi^2\lambda A_1\exp[\Gamma(\tau-\tau_i)][\Gamma\cos(2\pi\tau)+2\pi\sin(2\pi\tau)]/\eta(\Gamma^2+4\pi^2)+P_1. \qquad (10.b.1)$$

Z_1 and P_1 are initially given by

$$Z_1=Z_0+4\pi^2\lambda(\Gamma^2-4\pi^2)\exp(-\Gamma\tau_i)/\eta^2(\Gamma^2+4\pi^2)^2$$

$$P_1=P_0+4\pi^2\lambda A_i\Gamma\exp(-\Gamma\tau_i)/\eta(\Gamma^2+4\pi^2), \qquad (10.b.2)$$

where Z_0 and P_0 are the initial conditions, i.e. the values of $Z(\tau)$ and $P(\tau)$ at $\tau=0$.

These expressions can be used with the initial values of Z_1 and P_1, as long as Z remains within the range $[0,1]$. Let us denote the value of τ, for which $Z(\tau,P_1,Z_1)$ becomes 0 or 1 for the first time, as τ_b, and let us denote the value of $Z(\tau_b,P_1,Z_1)$

as Z_b (i.e. $Z_b=0$ or $Z_b=1$). The value of Z_b (0 or 1) is determined by inspecting the analytical solution, as given by expression (10.b.2), and the value of τ_b is then found by solving the equation $Z(\tau,P_1,Z_1)=Z_b$ numerically, by bisection.

We know that $Z(\tau)$ is continuous at $\tau=\tau_b$, whereas $P(\tau)$ changes its sign there. For $\tau>\tau_b$ (sufficiently close to τ_b) the solution is still given by expression (10.b.1), but with Z_1 and P_1 replaced by Z_2 and P_2 respectively. Z_2 and P_2 are found from the matching of the two solutions at $\tau=\tau_b$, and they are thus given by the expression

$$Z_2=Z_1-Z(\tau_b,P_2,0) \quad , \quad P_2=P_1-2P(\tau_b,P_1), \qquad (10.b.3)$$

which is obtained from expression (10.b.1), when the above mentioned matching rules for Z and P are applied. First P_2 is found, and then, using P_2, Z_2 is found.

Z_2 and P_2 now become the new Z_1 and P_1 in expression (10.b.1), and this is now the solution, as long as Z remains within the range [0,1]. This process is repeated again and again, until $\tau=\tau_1$ is reached, unless the particle becomes ionised first (see below).

In the case of $\tau_1<\tau<\tau_f$ we obtain the expressions

$$Z(\tau,P_1,Z_1)=(\lambda/\pi^2)\cos(2\pi\tau)+(P_1/\pi A_1)\tau+Z_1$$

$$P(\tau,P_1)=-(2\pi\lambda A_1/\pi)\sin(2\pi\tau)+P_1. \qquad (10.b.4)$$

Z_1 and P_1 are initially given by

$$Z_1=Z_0-(\lambda/\pi^2)\cos(2\pi\tau_i)-(P_1/\pi A_1)\tau_i$$

$$P_1=P_0+(2\pi\lambda A_1/\eta)\sin(2\pi\tau_1), \qquad (10.b.5)$$

where Z_0 and P_0 are the values of $Z(\tau)$ and $P(\tau)$ at $\tau=\tau_1$, which have been found in the previous step.

These solutions, with the initial values of Z_1 and P_1, can be used, as long as Z remains within the range [0,1]. Then Z_2 and P_2, which become the new Z_1 and P_1, are calculated as before, using expression (10.b.3). This process is repeated until $\tau=\tau_f$ is reached, unless the particle becomes ionised first (see below).

In the case of $\tau_f<\tau<\tau_0$ we obtain the expressions

$$Z(\tau,P_1,Z_1)=-4\pi^2\lambda\exp[-\Gamma(\tau-\tau_f)][((\Gamma^2-4\pi^2)\cos(2\pi\tau)-$$
$$4\pi\Gamma\sin(2\pi\tau)]/\eta^2(\Gamma^2+4\pi^2)^2+(P_1/\eta A_1)\tau+Z_1$$
$$P(\tau,P_1)=4\pi^2\lambda A_1\exp[-\Gamma(\tau-\tau_f)][\Gamma\cos(2\pi\tau)-2\pi\sin(2\pi\tau)]/\eta(\Gamma^2+4\pi^2)+P_1. \qquad (10.b.6)$$

Z_1 and P_1 are initially given by

$$Z_1=Z_0+4\pi^2\lambda[(\Gamma^2-4\pi^2)\cos(2\pi\tau_f)-4\pi\Gamma\sin(2\pi\tau_f)]/\eta^2(\Gamma^2+4\pi^2)^2-(P_1/\eta A_1)\tau_f$$
$$P_1=P_0-4\pi^2\lambda A_1[\Gamma\cos(2\pi\tau_f)-2\pi\sin(2\pi\tau_f)]/\eta(\Gamma^2+4\pi^2), \qquad (10.b.7)$$

where Z_0 and P_0 are the values of $Z(\tau)$ and $P(\tau)$ at $\tau=\tau_f$, which have been found in the previous step.

These solutions, with the initial values of Z_1 and P_1, can be used, as long as Z remains within the range [0,1]. Then Z_1 and P_1 are recalculated as before, using expression (10.b.3). This process is repeated until $\tau=\tau_0$ is reached, unless the particle becomes ionised first.

With $Z(\tau)$ and $P(\tau)$ known, we can also calculate the dimensionless compensated energy $\epsilon_c(\tau)$ (expression (10.a.11)). Its average value over a cycle of the oscillating laser field is checked. If it becomes greater than the dimensionless well depth, namely $N^2\pi^2$, this means that the particle becomes ionised. It does not bounce back then, when Z=0 or Z=1 is reached, but rather moves on, away from the well.

As we are mainly interested in finding the time, where ionisation takes place, we are not interested in the evolution of $Z(\tau)$ and $P(\tau)$ beyond the ionisation point. Practically all the particles get ionised in the period $\tau_i \leq \tau \leq \tau_f$, i.e. when the laser field has its maximum amplitude. The average compensated energy remains constant after ionisation in that case, and therefore the particle is not expected to return into the well after it had become ionised.

We have seen thus how the equations of motion can be solved in a semi-analytical way. The only numerical procedure involved is the determination of τ_b by bisection. Thus the error introduced in the computation of $Z(\tau)$ and $P(\tau)$ is minimal.

10.c. The ionisation rate and its dependence on the laser intensity and frequency

We are now ready to make use of our results, and carry out the study of the ionisation rate as a function of the laser field strength (the parameter λ) and the laser frequency (the parameter η). We shall do that by means of a "numerical experiment", as has been done by other workers in this field, for similar problems (Leopold and Percival 1979, Galvão et al 1984).

We use for this purpose a large ensemble of particles (100 particles in our case). All the particles are given the same initial energy E_1, equal to the ground quantum level in the well. Thus, in our units the initial energy is A_1^2 (see section 7.d), and the initial momentum is thus $P_0=A_1$. Each particle is given an initial position located at random between the turning points, i.e. between x=0 and x=d. This means that in our units the initial position, Z_0, is given a random value between 0 and 1.

For each particle we solve now the equations of motion, using the semi-analytical procedure outlined in the previous section, and check the compensated energy during the process, as well, in order to see whether the particle becomes ionised, and if it does, at what time this happens. This way we obtain, for the ensemble as a whole, the percentage (or probability) of ionisation as a function of time (the latter in units of the period of the oscillating laser field).

We have studied this way the square wells with 4, 8, 10, and 12 quantum energy levels. In each case we have chosen several values of the laser frequency parameter η, and for each value we

have varied the laser field strength parameter λ, in order to see when ionisation sets in; and when it does, to see how the ionisation rate, i.e. the time derivative of the ionisation probability, in the region where it is nearly constant, varies as a function of λ. This way we have obtained the ionisation rate as a function of both λ and η.

We have used for our laser pulse a switching on/off time of 20 periods of the laser field, whereas the pulse duration (at maximum strength, i.e. between τ_i and τ_f) was 100 periods of the laser field. The parameter Γ (see expression (10.a.7)) was 0.23, corresponding to ε=0.01 as the relative strength of the laser field before switching on and after switching off.

In Figures 54 and 55 we see the dimensionless compensated energy $\varepsilon_C(\tau)$ as a function of the dimensionless time τ, for the square well with N=12 levels, with η=19.0 and λ=4.5. In Figure 54 we see $\varepsilon_C(\tau)$ in the case of a particle which does not ionise. In Figure 55 we see $\varepsilon_C(\tau)$ in the case of a particle which does ionise (around τ=80). The initial energy (in our units) is approximately 8.90. The well depth, i.e. the ionisation energy, is $144\pi^2$, i.e. approximately 1420, and it is indicated by the horizontal line in these figures.

In Figures 56 and 57 we see the ionisation probability (shown as ionisation percentage) as a function of the dimensionless time τ, again for the well with N=12 levels, with η=19.0. In Figure 56 λ=4.5, and in Figure 57 λ=6.5. From τ=0 to τ=20 the laser field is being switched on, and thus no ionisation occurs there. Ionisation starts only at some value of τ above 20; closer to 20 if λ is higher. First we see a linear increase, from which the ionisa-

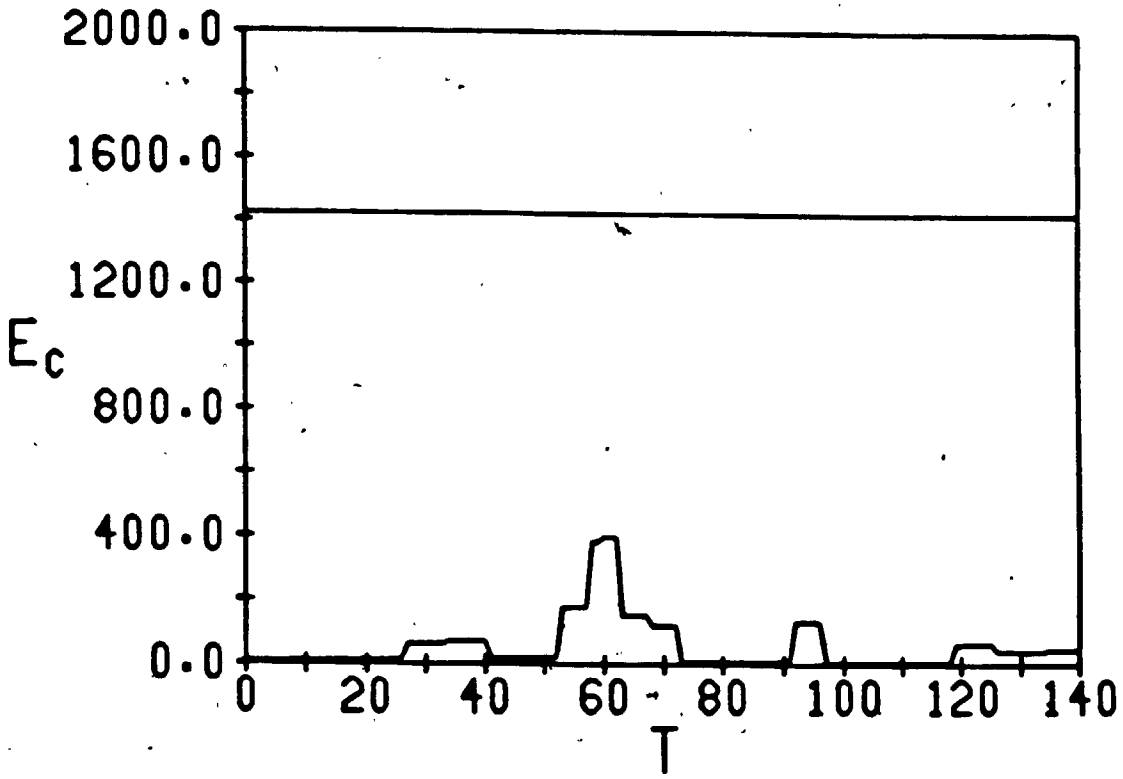

Figure 54

The compensated energy (in units of $\hbar^2/2Md^2$) as a function of time (in units of the period of the oscillating laser field) for a particle which does not ionise, in the case of the N=12 level well with η=19.0 and λ=4.5. The horizontal line at $144\pi^2$ denotes the ionisation threshold $E_c=V_0$.

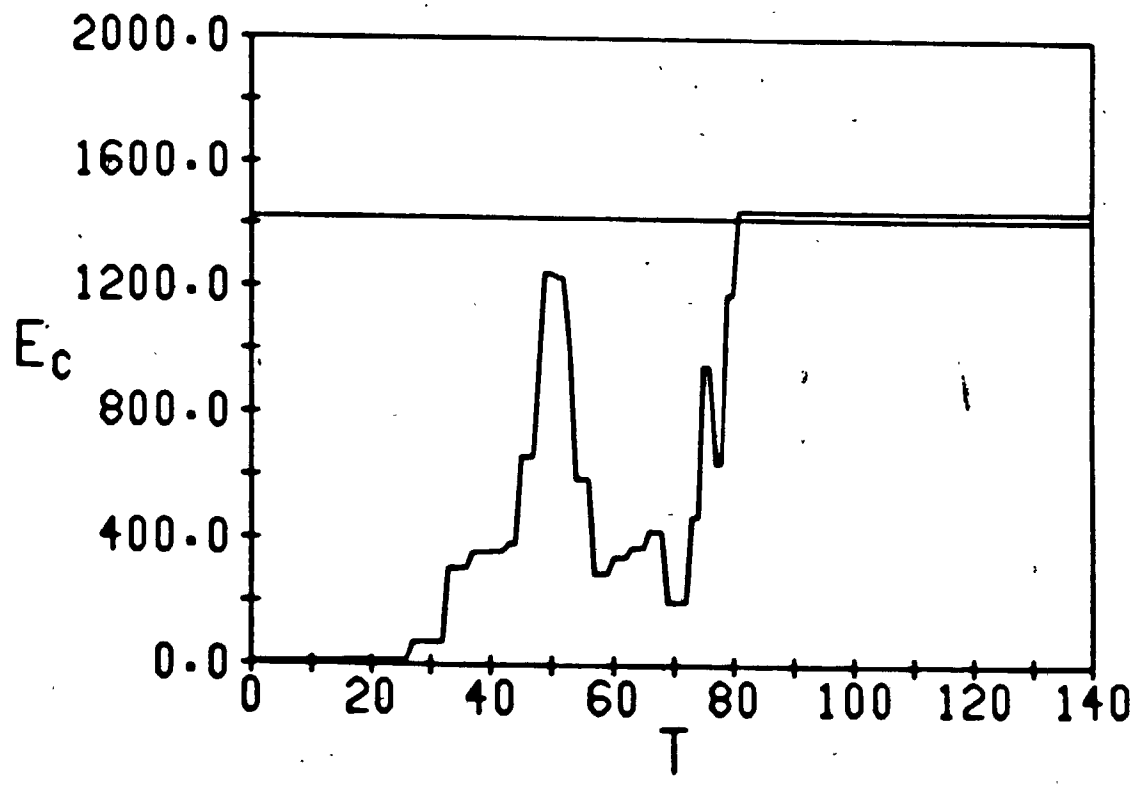

Figure 55

The compensated energy (in units of $\hbar^2/2Md^2$) as a function of time (in units of the period of the oscillating laser field) for a particle which does ionise, in the case of the N=12 level well with η=19.0 and λ=4.5. The horizontal line at $144\pi^2$ denotes the ionisation threshold $E_c=V_0$.

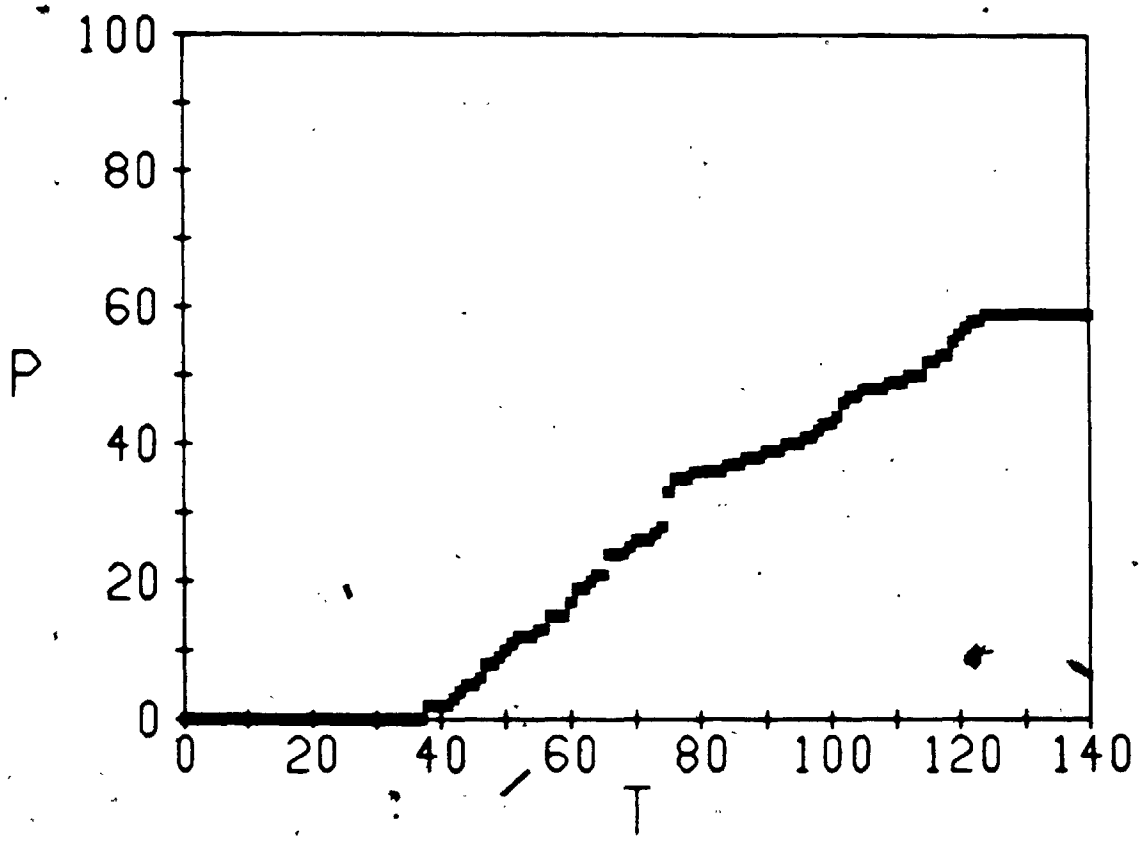

Figure 56

The ionisation probability P (in percents) as a function of time (in units of the period of the oscillating laser field) for an ensemble of 100 particles in the N=12 level well with η=19.0 and λ=4.5

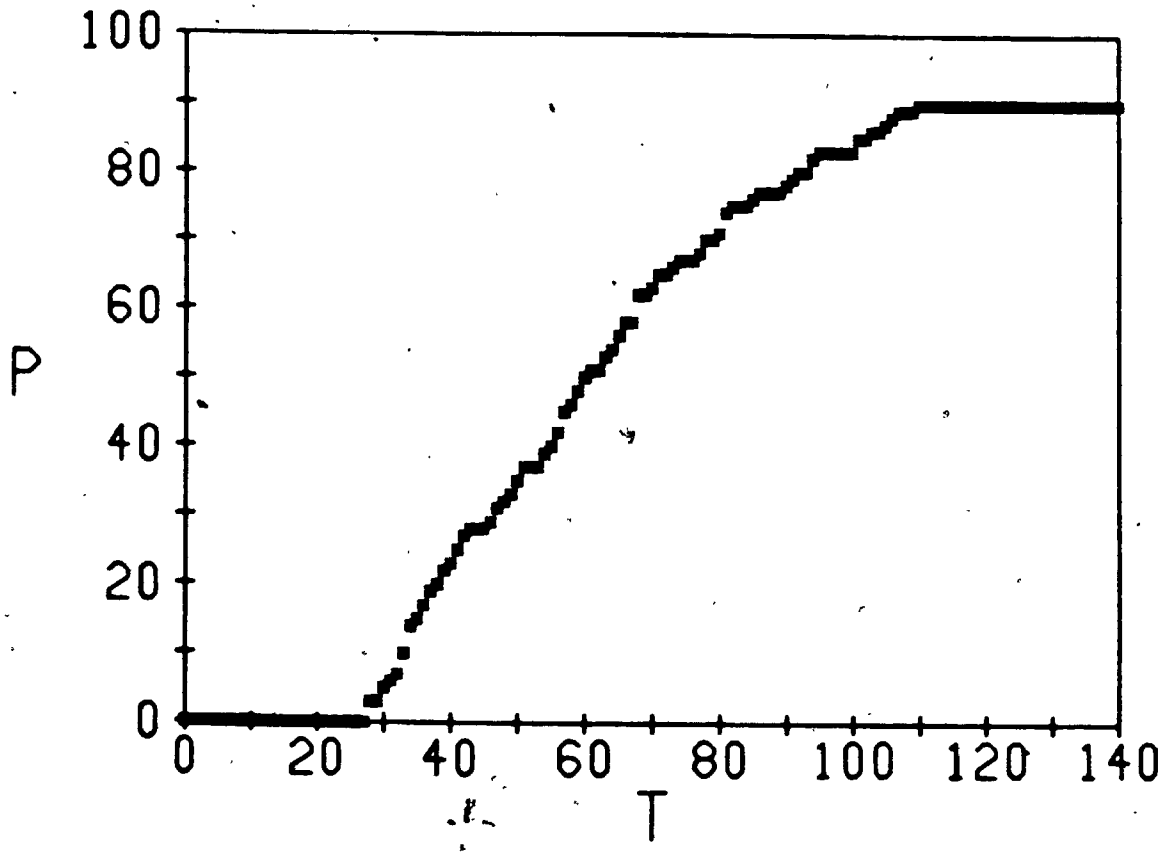

Figure 57

The ionisation probability P (in percents) as a function of time (in units of the period of the oscillating laser field) for an ensemble of 100 particles in the N=12 level well with η=19.0 and λ=6.5.

tion rate W (in our units, simply the slope) is found. Then the increase in the ionisation probability gradually declines, and if the laser pulse is long enough, as it is here in the λ=6.5 case (Figure 57), saturation is eventually reached, i.e. the ionisation probability reaches a nearly constant value (seen in Figure 57 to occur around τ=105). At τ=120, the laser field is switched off. Thus no ionisation occurs there any more, as well. This is not to be confused with the saturation mentioned above. This behaviour is typical to the ionisation process in all the cases we have studied.

For each square well potential, we have studied the behaviour of the ionisation rate W as a function of the laser field strength parameter α for several values of the laser frequency parameter γ. We have seen, in each case, that ionisation starts to take place only when α exceeds some threshold value, which we denote by α_t, and then increases with increasing α. In Figure 58 we see W as a function of α for the N=12 level square well, for two values of γ, γ=9.5 and γ=30.0. We see that the behaviour of log W as a function of log α is distinctly linear. This means that if we denote the slope as 2ν, then W is proportional to $\alpha^{2\nu}$. We have observed this power law behaviour of W as a function of α in all the cases we have studied.

We can thus summarise our results so far by stating, that for any of the square wells we have studied, we observe ionisation only when the laser field strength parameter α exceeds some threshold value α_t, which depends on the laser frequency parameter γ, and that for values of α above this threshold value we

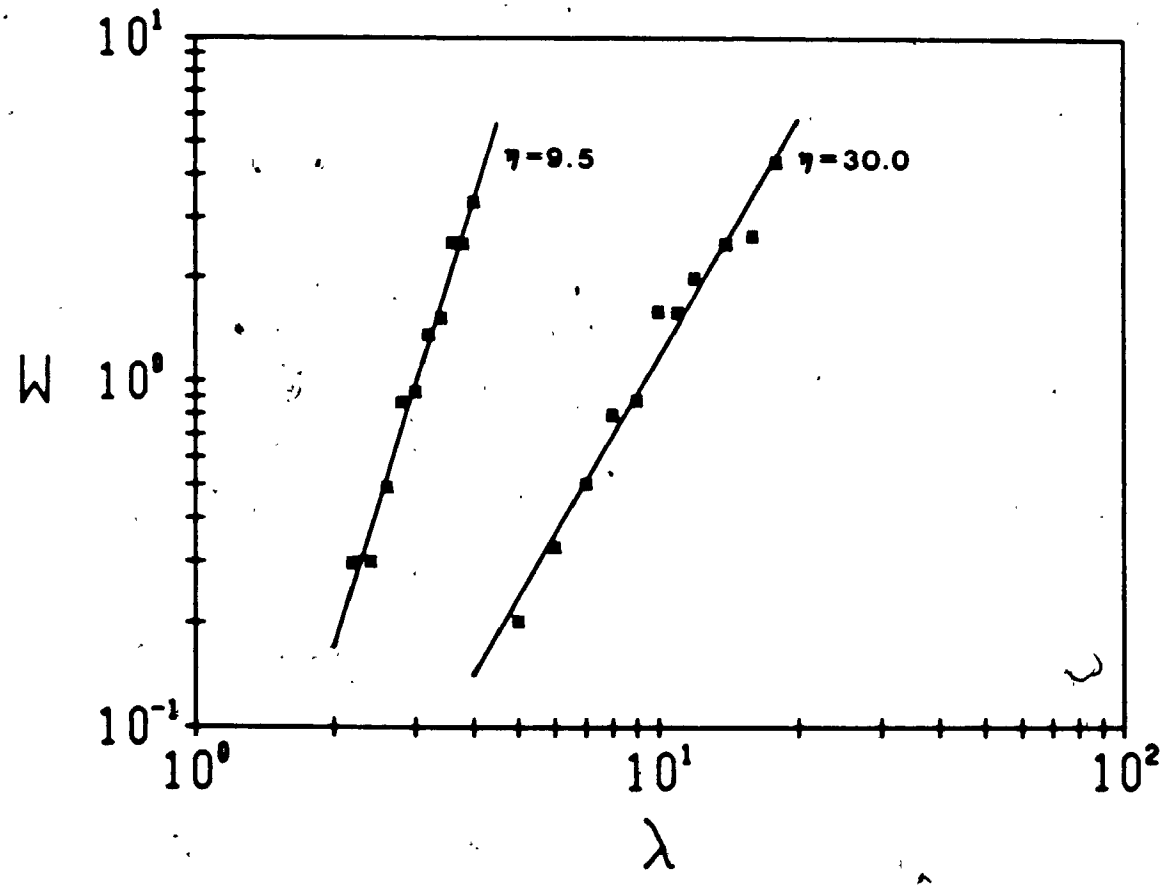

Figure 58

The ionisation rate W as a function of the laser field strength parameter λ for a N=12 level well. The straight lines indicate a $W \propto \lambda^{2\nu}$ behaviour. For η=9.5 the value of ν is 2.2, and for η=30.0 it is 1.2.

have $W \alpha \lambda^{2\nu}$, where ν depends on the laser frequency parameter η. As the laser intensity I_L is proportional to λ^2, we can state our result also as

$$W \alpha I_L^{\nu}. \qquad (10.c.1)$$

This kind of behaviour, with an integer ν, is typical to multiphoton processes; the ionisation probability is equal to the product of the ν transition probabilities involved, each of those being, in turn, proportional to the photon density, i.e. proportional to λ^2 (or to I_L).

For each of the four square wells we have studied, we have looked now at the behaviour of the coefficient ν as a function of the laser frequency parameter η. For high frequencies, i.e. large values of η, we find that ν is approximately inversely proportional to η, i.e. we have

$$\nu = A/\eta, \qquad (10.c.2)$$

where A is a constant. We have observed this kind of behaviour for all the square wells we have studied

If we look at the most basic quantum picture for the ionisation of an electron from the ground level of the quantum well by a laser field with frequency ω, then the number of photons required for the ionisation to occur is the first integer above ν_Q, where

$$\nu_Q = (V_0 - E_1)/\hbar\omega, \qquad (10.c.3)$$

where V_0 and E_1 have the same meanings as before. In our units expression (10.c.3) becomes

$$\nu_Q = B/\eta \; ; \; B = (N^2\pi^2 - A_1^2)/4\pi A_1 . \qquad (10.c.4)$$

The results of our study of ν as a function of η can be seen in Figures 59, 60, 61, and 62, which are for the square wells with 4, 8, 10, and 12 levels respectively. The error bars represent the statistical error in our results, and the bold lines represent ν_Q, the quantum mechanical estimate for ν, as given by expression (10.c.4). We can clearly see in each case, that at the high frequency range, i.e. for high values of η, our results fall rather close to the values expected from the quantum mechanical picture, especially in the 12 level case.

We also represent our results in the form of a table (Table 4). For each of the four wells we have studied, we list the values of γ we have examined, and for each value of η we list λ_t, the threshold value of λ for the onset of ionisation, our numerically obtained value for ν, and the corresponding quantum mechanical estimate ν_Q (as defined in expression (10.c.4)) for multiphoton ionisation.

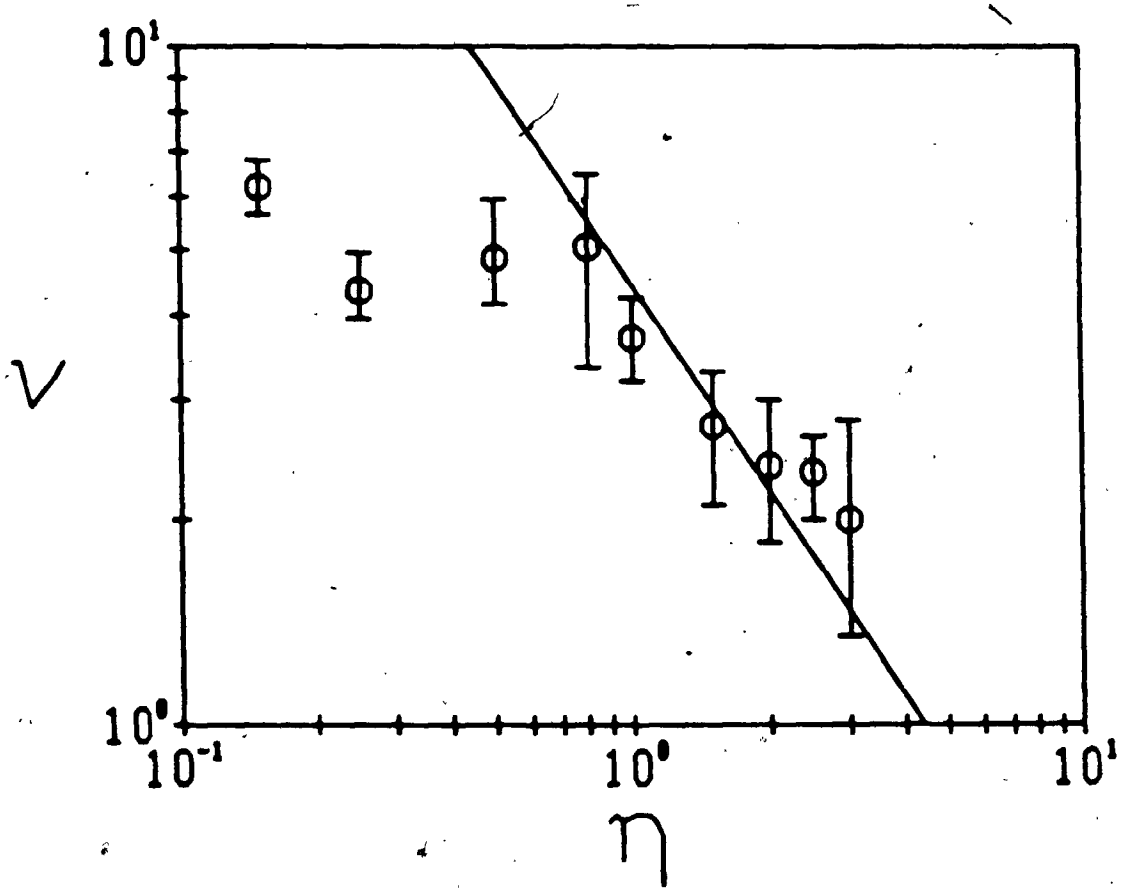

Figure 59

The power law exponent ν as a function of the frequency parameter η for the N=4 level well. The straight solid line corresponds to the quantum expression for ν as a function of η.

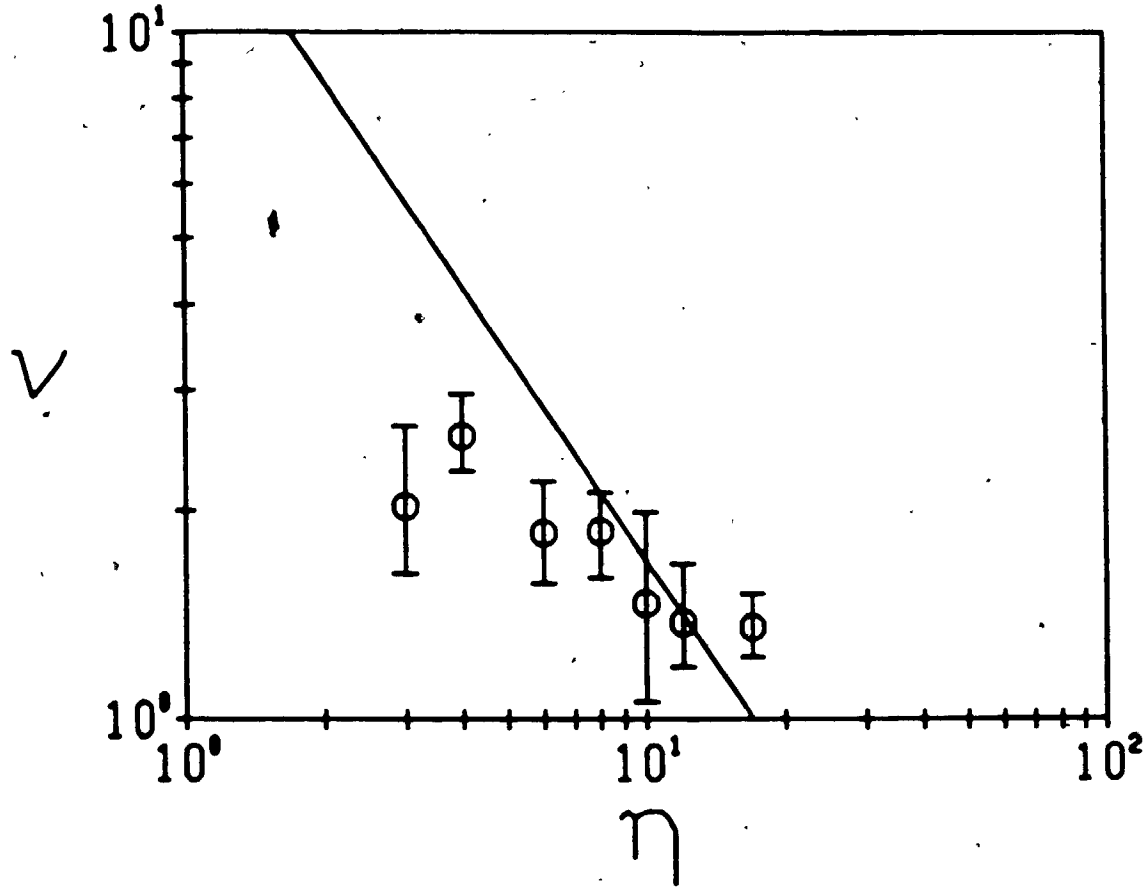

Figure 60

The power law exponent ν as a function of the frequency parameter η for the N=8 level well. The straight solid line corresponds to the quantum expression for ν as a function of η.

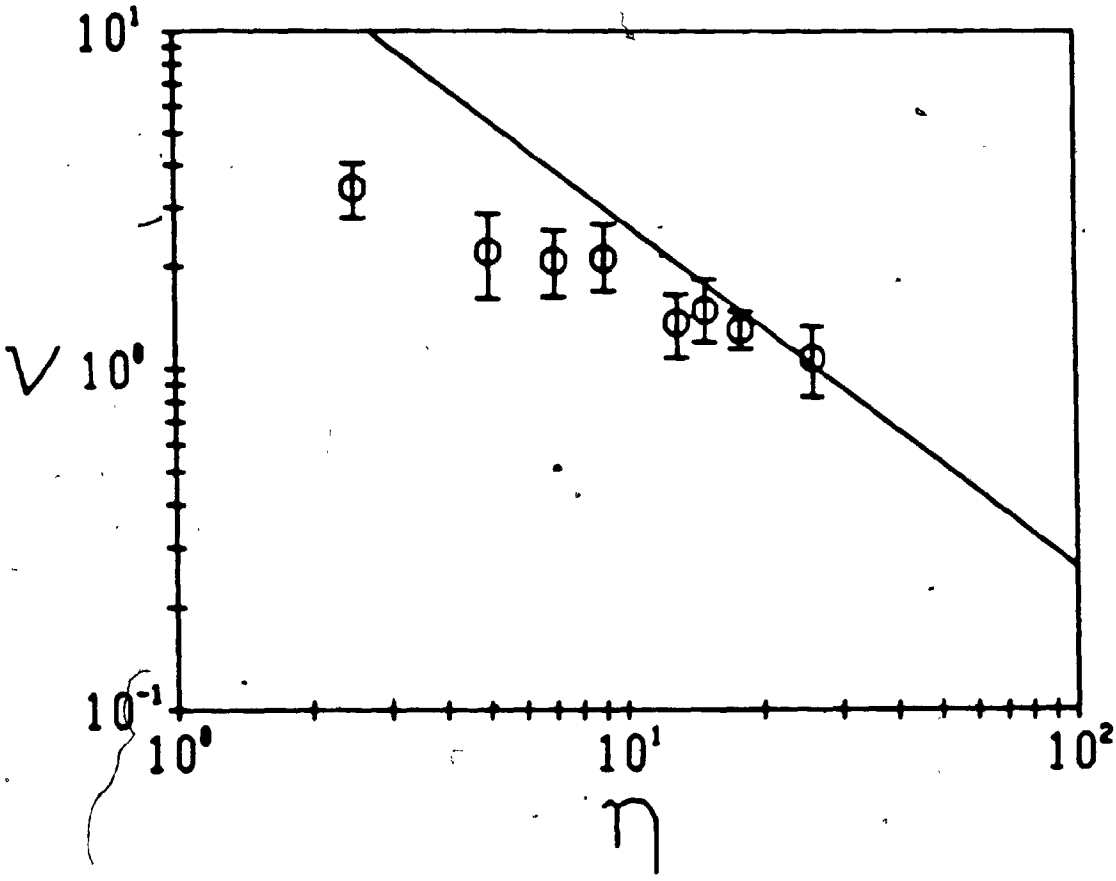

Figure 61

The power law exponent ν as a function of the frequency parameter η for the N=10 level well. The straight solid line corresponds to the quantum expression for ν as a function of η.

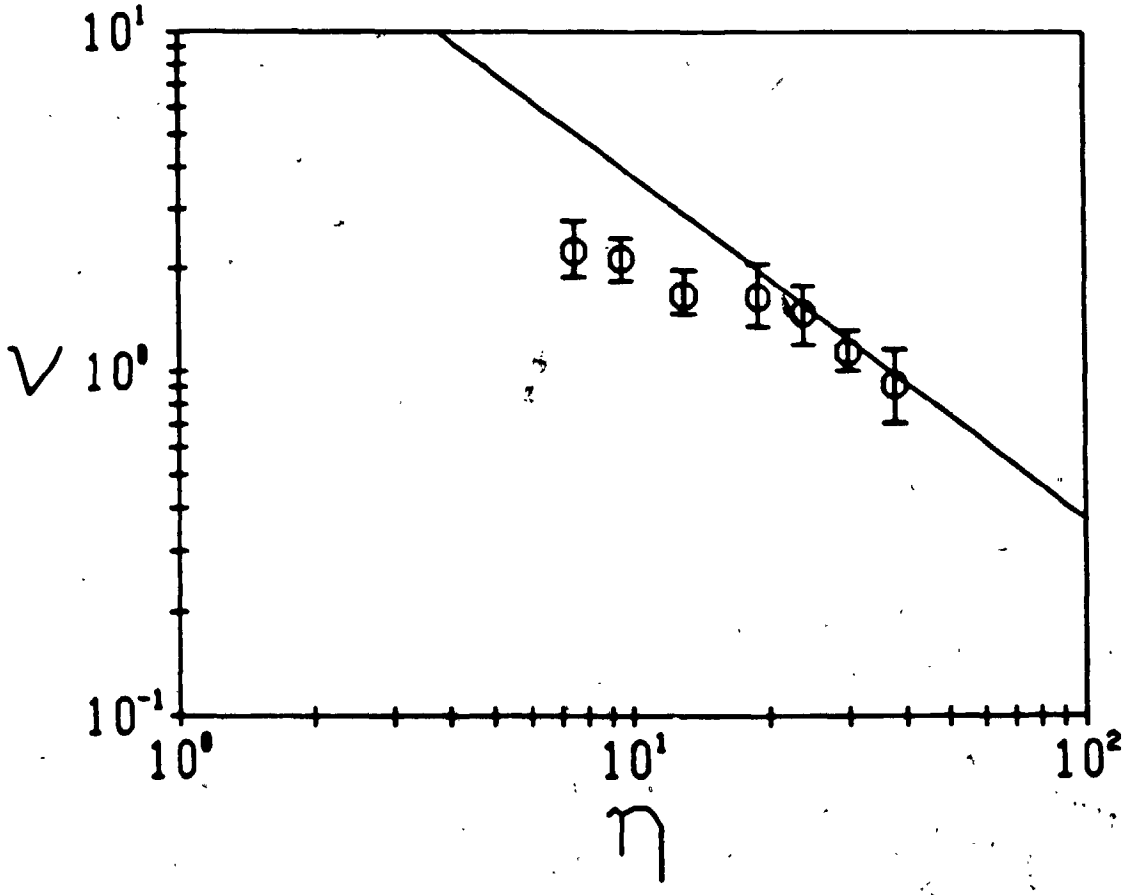

Figure 62

The power law exponent ν as a function of the frequency parameter η for the N=12 level well. The straight solid line corresponds to the quantum expression for ν as a function of η.

Table 4

Summary of the results of the numerical experiments on the ionisation rate for electrons in the square wells with 4, 8, 10, and 12 energy levels. For each well several values of η (the laser frequency parameter) are presented. For each value of η the corresponding values of λ_t (the threshold value of λ for the onset of ionisation), the numerically obtained ν (for the power law dependence $W \alpha \lambda^{2\nu}$), and the corresponding quantum mechanical estimate ν_Q are shown.

N	η	λ_t	ν	ν_Q
4	0.15	0.40	6.2	29.5
	0.25	0.34	4.4	17.7
	0.5	0.25	4.8	8.85
	0.8	0.20	5.0	5.53
	1.0	0.16	3.7	4.43
	1.5	0.07	2.7	2.95
	2.0	0.10	2.4	2.21
	2.5	0.17	2.3	1.77
	3.0	0.24	2.0	1.48
8	3.0	0.24	2.0	5.68
	4.0	0.40	2.6	4.26
	6.0	0.80	1.9	2.84
	8.0	1.0	1.9	2.13
	10.0	0.95	1.5	1.70
	12.0	1.2	1.4	1.42
	17.0	1.8	1.4	1.00

Table 4 (continued)

N	n	λ_t	ν	ν_Q
10	2.5	0.8	3.4	10.5
	5.0	0.7	2.2	5.27
	7.0	1.2	2.1	3.77
	9.0	1.7	2.0	2.93
	13.0	1.5	1.4	2.03
	15.0	2.0	1.5	1.76
	18.0	2.4	1.3	1.46
	26.0	3.5	1.1	1.01
12	7.5	1.5	2.3	5.02
	9.5	2.0	2.2	3.97
	13.0	2.4	1.7	2.90
	19.0	3.2	1.7	1.98
	24.0	4.0	1.5	1.57
	30.0	5.0	1.2	1.26
	38.0	7.0	0.92	0.99

10.d. Discussion of the numerical results for the ionisation rate in the high frequency region

The numerical results for the ionisation rate, that we have obtained by means of our classical model, bear the characteristics of a multiphoton process, when we are at the high frequency range. We have seen that our classical ionisation rate W is proportional to I_L^{ν}, where I_L is the laser intensity, and that ν, in the high frequency range, is quite close to ν_Q, the estimate obtained from the basic quantum model (expression (10.c.3)).

From the quantum mechanical point of view, ionisation from a potential well, in the presence of an oscillating electric field, can occur either through tunnelling or through a multiphoton process. The type of ionisation process that actually occurs depends on the ratio of the mean energy of the bound electron and the average energy of oscillation of the free electron in the oscillating field (Keldysh 1965, Geltman 1977). This ratio can be expressed in the form of the "adiabaticity parameter" γ, given by

$$\gamma=\omega[2M(V_0-E_1)]^{1/2}/eE_L. \qquad (10.d.1)$$

When $\gamma<<1$, tunnelling is dominant, and when $\gamma>>1$, multiphoton processes are dominant. Generally speaking, this means, that multiphoton processes can be expected to be dominant in the high frequency range.

In our units the expression for the parameter γ becomes

$$\gamma=\eta(N^2\pi^2-A_1^2)/2\pi\lambda A_1. \qquad (10.d.2)$$

Using this expression we have verified, that in our high frequen-

cy range, in each case, multiphoton processes are really expected to be dominant.

Our results, which show a multiphoton-like behaviour of the ionisation rate as a function of the laser intensity in the high frequency range, may be puzzling. Our calculation of the ionisation rate was purely classical, and it is a common understanding that multiphoton processes are quantum mechanical in nature. This apparent contradiction may be resolved by explaining these results in terms of higher harmonics of the effect the oscillating laser field has on the square well poteptial.

We use as our starting point the usual Hamiltonian in momentum-position space (without the switching function f(t)), given by (cf. expression (10.a.2))

$$H(p,x,t)=p^2/2M+V(x)+eE_L x\cos(\omega t). \qquad (10.d.3)$$

The only change we introduce here is in the reference points for measuring the position and energy. Thus V(x) is now given by

$$V(x)=\begin{cases} -V_0 & \text{if } |x|<d/2 \\ 0 & \text{if } |x|>d/2. \end{cases} \qquad (10.d.4)$$

The term $(1/2)eE_L d\cos(\omega t)$, implicitly added this way to the Hamiltonian, does not cause any change in the equations of motion, and thus is of no consequence in this case.

Now we apply the canonical transformation

$$\pi=p-eA_L(t) \; ; \; \xi=x, \qquad (10.d.5)$$

which is obtained from the generating function

$$F(\pi,x,t)=[\pi+eA_L(t)]x, \qquad (10.d.6)$$

where

$$A_L(t)=-E_L\int_0^t \cos(\omega t')dt'=-(E_L/\omega)\sin(\omega t). \qquad (10.d.7)$$

When p and x are replaced by π and ξ respectively, and the term $\partial F/\partial t=-eE_L x\cos(\omega t)$ is added, we obtain the new Hamiltonian

$$H(\pi,\xi,t)=[\pi+eA_L(t)]^2/2M+V(\xi). \qquad (10.d.8)$$

We have obtained thus the Hamiltonian in terms of the magnetic vector potential, from the original Hamiltonian, which was in terms of the electric potential.

Now we introduce a second canonical transformation, given by

$$P=\pi \; ; \; X=\xi+\delta(t), \qquad (10.d.9)$$

which is obtained from the generating function

$$F(P,\xi,t)=P[\xi+\delta(t)]+\varepsilon(t), \qquad (10.d.10)$$

where

$$\delta(t)=-(e/M)\int_{\pi/2\omega}^t A_L(t')dt'=-(eE_L/M\omega^2)\cos(\omega t)=-a\cos(\omega t) \qquad (10.d.11)$$

and

$$\varepsilon(t)=-(e^2/2M)\int_0^t A_L^2(t')dt'=-(e^2E_L^2/8M\omega^3)[2\omega t-\sin(2\omega t)]. \qquad (10.d.12)$$

Here $\partial F/\partial t=-(eP/M)A_L(t)-(e^2/2M)A_L^2(t)=P^2/2M-[P+eA_L(t)]^2/2M$, and thus the Hamiltonian becomes

$$H(P,X,t)=P^2/2M+V(X-\delta(t))=P^2/2M+V(X+a\cos(\omega t)). \qquad (10.d.13)$$

a, which is defined by expression (10.d.11), is the amplitude of the electron's oscillation in the electric field $E_L\cos(\omega t)$.

We have thus switched to a frame of reference which oscillates with the electron. In this new frame of reference the square well potential is seen as oscillating back and forth. In the high frequency range the electron sees the square well potential distorted, due to the average effect of these oscillations. The canonical transformation we have used here is the classical equivalent of the unitary transformation (Gerck and Miranda 1984, Mayer et al 1985), which is used in the quantum mechanical treatment of the Hamiltonian for the same purpose.

The Fourier transform of V(x) (expression (10.d.4)) is given by

$$V(k)=\int_{-\infty}^{\infty} V(x)\exp(-ikx)dx=-V_0\int_{-d/2}^{d/2}\exp(-ikx)dx=$$

$$-(2V_0/k)\sin(kd/2), \qquad (10.d.14)$$

and thus, using the inverse Fourier transform, we have

$$V(X+a\cos(\omega t))=(1/2\pi)\int_{-\infty}^{\infty} V(k)\exp(ikX)\exp[ika\cos(\omega t)]dk. \qquad (10.d.15)$$

By making use of the expansion (Gradshteyn and Ryzhik 1980)

$$\exp[ika\cos(\omega t)]=\sum_{n=-\infty}^{\infty} i^n J_n(ka)\exp(-in\omega t), \qquad (10.d.16)$$

where $J_n(x)$ denotes the Bessel function of the first kind, we can rewrite expression (10.d.15) as

$$V(X+a\cos(\omega t))=(1/2\pi)\sum_{n=-\infty}^{\infty} i^n\left[\int_{-\infty}^{\infty} V(k)J_n(ka)\exp(ikX)dk\right]\exp(-in\omega t). \qquad (10.d.17)$$

a is a function of E_L, and thus also a function of our dimension-

less parameter λ. Therefore we define

$$V_n(X;\lambda)=(1/2\pi)i^n\int_{-\infty}^{\infty}V(k)J_n(ka)\exp(ikX)dk, \qquad (10.d.18)$$

and, using this definition, our Hamiltonian becomes

$$H(P,X,t)=P^2/2M+\sum_{n=-\infty}^{\infty}V_n(X;\lambda)\exp(-in\omega t). \qquad (10.d.19)$$

Using (10.d.14), expression (10.d.18) can be rewritten as

$$V_n(X;\lambda)=\begin{cases}-(2V_0/\pi)i^n\int_0^{\infty}(1/k)\sin(kd/2)J_n(ka)\cos(kX)dk & \text{if n is even}\\ -(2V_0/\pi)i^{n+1}\int_0^{\infty}(1/k)\sin(kd/2)J_n(ka)\sin(kX)dk & \text{if n is odd}\end{cases} \qquad (10.d.20)$$

We define now new variables:

$$\sigma=2a/d\ ;\ s=2x/d\ ;\ t=kd/2. \qquad (10.d.21)$$

Using these, the last expression becomes

$$V_n(X;\lambda)=\begin{cases}-(V_0/\pi)i^n\int_0^{\infty}[J_n(\sigma t)/t]\{\sin[(1+s)t]+\sin[(1-s)t]\}dt\\ -(V_0/\pi)i^{n+1}\int_0^{\infty}[J_n(\sigma t)/t]\{\cos[(1-s)t]-\cos[(1+s)t]\}dt.\end{cases} \qquad (10.d.22)$$

The top expression on the right hand side is for even n and the bottom expression is for odd n.

Now we introduce the integration formulae (Gradshteyn and Ryzhik 1980; for a general ν)

$$\int_0^{\infty}[J_\nu(\sigma t)/t]\sin[(1\pm s)t]dt=\begin{cases}\sin(\nu\arcsin[(1\pm s)/\sigma])/\nu\\ \sigma^\nu\sin(\nu\pi/2)/\nu\{1\pm s+[(1\pm s)^2-\sigma^2]^{1/2}\}^\nu\end{cases} \qquad (10.d.23)$$

and

$$\int_0^\infty [J_\nu(\sigma t)/t]\cos[(1\pm s)t]dt = \begin{cases} \cos(\nu \arcsin[(1\pm s)/\sigma])/\nu \\ \sigma^\nu \cos(\nu\pi/2)/\nu(1\pm s+[(1\pm s)^2-\sigma^2]^{1/2})^\nu \end{cases} \quad (10.d.24)$$

The top expression on the right hand side, in each case, is for $|1\pm s|\leq\sigma$, and the bottom expression is for $|1\pm s|\geq\sigma$.

Using these we have (for $\sigma<1$)

$$V_0(X;\lambda) = \begin{cases} -V_0 & \text{if } |s|\leq 1-\sigma \\ -(V_0/\pi)\{\pi/2+\arcsin[(1-|s|)/\sigma]\} & \text{if } 1-\sigma\leq|s|\leq 1+\sigma \\ 0 & \text{if } |s|\geq 1+\sigma. \end{cases} \quad (10.d.25)$$

If the laser field is not too strong, i.e. σ is small enough, then $V_0(X;\lambda)$ is approximately given by expression (10.d.4) for $V(x)$. We denote this approximation for $V_0(X;\lambda)$ as $V_0(X)$.

We also have, for non-zero even n,

$$V_n(X;\lambda) = \begin{cases} -(V_0/n\pi)(-1)^{n/2}\sin(n \arcsin[(1-|s|)/\sigma]) \\ 0, \end{cases} \quad (10.d.26)$$

and, for odd n,

$$V_n(X;\lambda) = \begin{cases} -(V_0/n\pi)(-1)^{(n+1)/2}\mathrm{sgn}(s)\cos(n \arcsin[(1-|s|)/\sigma]) \\ 0. \end{cases} \quad (10.d.27)$$

The top expression on the right hand side, in each case, is for $1-\sigma\leq|s|\leq 1+\sigma$, and the bottom expression is for $|s|\leq 1-\sigma$ or $|s|\geq 1+\sigma$.

We note, from the aboye expressions, that $V_{-n}(X;\lambda)=V_n(X;\lambda)$ for all n, and thus we can rewrite the Hamiltonian (expression (10.d.19)), for small enough values of σ, as

$$H(P,X,t)=H_0(P,X)+2\sum_{n=1}^{\infty}V_n(X;\lambda)\cos(n\omega t), \qquad (10.d.28)$$

where $H_0(P,X)$ is the unperturbed Hamiltonian for the square well, given by

$$H_0(P,X)=P^2/2M+V_0(X), \qquad (10.d.29)$$

and the $V_n(X;\lambda)$ are given by expressions (10.d.26) and (10.d.27). $V_n(X;\lambda)$ is the contribution of the n^{th} harmonic of the laser frequency ω to the distortion of the square well potential, as seen by the electron.

Now we perform the usual transformation to action and angle variables. Using expression (9.a.3) we have

$$I(E)=(1/\pi)\int_{-d/2}^{d/2}[2M(E+V_0)]^{1/2}dX=(d/\pi)[2M(V_0+E)]^{1/2}, \qquad (10.d.30)$$

and thus we have

$$H_0(I)=\pi^2I^2/2Md^2-V_0, \qquad (10.d.31)$$

and, using expression (9.a.4), we also have

$$\Omega_0(I)=\pi^2I/Md^2. \qquad (10.d.32)$$

Using expression (9.a.5), we have now

$$\theta(I,X)=M\Omega_0(I)\int_{X_0}^{X}(2M[H_0(I)+V_0])^{-1/2}dX'=$$
$$\pm(\pi/d)(X-X_0)=\pm(\pi/2)(s-s_0) \qquad (10.d.33)$$

In order to have $\theta(s)$ uniquely defined, we choose the signs and X_0, so that we have (cf. section 9.a)

$$\theta(s)=\begin{cases}(\pi/2)s & \text{if } P>0 \text{ and } S>0\\ (\pi/2)(2-s) & \text{if } P<0\\ (\pi/2)(s+4) & \text{if } P>0 \text{ and } s<0,\end{cases} \qquad (10.d.34)$$

and thus we have

$$s(\theta)=\begin{cases}(2/\pi)\theta & \text{if } 0\leq\theta\leq\pi/2\\ (2/\pi)(\pi-\theta) & \text{if } \pi/2\leq\theta\leq3\pi/2\\ (2/\pi)(\theta-2\pi) & \text{if } 3\pi/2\leq\theta\leq2\pi.\end{cases} \qquad (10.d.35)$$

The Fourier series expansion of $V_n(X;\lambda)$ is given by (cf. expressions (9.a.16) and (9.a.17))

$$V_n(X;\lambda)=\sum_{m=-\infty}^{\infty} V_n^m(\lambda)\exp(im\theta), \qquad (10.d.36)$$

where

$$V_n^m(\lambda)=(1/2\pi)\int_0^{2\pi} V_n(X;\lambda)\exp(-im\theta)d\theta. \qquad (10.d.37)$$

Using expressions (10.d.34) and (10.d.35) we can rewrite this as

$$V_n^m(\lambda)=(1/4)[\int_0^1 V_n(X;\lambda)\exp(-im\pi s/2)ds+(-1)^m\int_{-1}^1 V_n(X;\lambda)\exp(im\pi s/2)ds+$$
$$\int_{-1}^0 V_n(X;\lambda)\exp(-im\pi s/2)ds], \qquad (10.d.38)$$

and thus we have

$$V_n^m(\lambda)=\begin{cases}(1/2)\int_{-1}^1 V_n(X;\lambda)\cos(m\pi s/2)ds & \text{if } m \text{ is even}\\ -(i/2)\int_{-1}^1 V_n(X;\lambda)\sin(m\pi s/2)ds & \text{if } m \text{ is odd.}\end{cases} \qquad (10.d.39)$$

Using expressions (10.d.26) and (10.d.27) we have thus, for non-zero even n

$$V_n^m(\lambda)=\begin{cases}-(V_0/n\pi)(-1)^{n/2}\int_{1-\sigma}^{1}\sin(\pi\arcsin[(1-s)/\sigma])\cos(m\pi s/2)ds\\ 0,\end{cases} \qquad (10.d.40)$$

and, for odd n,

$$V_n^m(\lambda)=\begin{cases}0\\ i(V_0/n\pi)(-1)^{(n+1)/2}\int_{1-\sigma}^{1}\cos(n\arcsin[(1-s)/\sigma])\sin(m\pi s/2)ds.\end{cases} \qquad (10.d.41)$$

The top expression on the right hand side, in each case, is for even m, and the bottom expression is for odd m.

By using the change of variables $\xi=(1-s)/\sigma$ (i.e. $s=1-\sigma\xi$), we obtain now

$$V_n^m(\lambda)=\begin{cases}-(V_0\sigma/n\pi)(-1)^{(n+m)/2}\int_{0}^{1}\sin(n\arcsin\xi)\cos(m\pi\sigma\xi/2)d\xi\\ i(V_0\sigma/n\pi)(-1)^{(n+m)/2}\int_{0}^{1}\cos(n\arcsin\xi)\cos(m\pi\sigma\xi/2)d\xi.\end{cases} \qquad (10.d.42)$$

The top expression on the right hand side is for even m and n, and the bottom expression is for odd m and n. If m+n is odd, then $V_n^m(\lambda)=0$.

Now we are ready to apply the Chirikov criterion to our results. For a given value of n, the m^{th} resonance occurs at the value of the action I_n^m, given by (cf. expression (9.b.3))

$$n\omega=m\Omega_0(I_n^m). \qquad (10.d.43)$$

Using expression (10.d.32) we obtain

$$I_n^m=Md^2\omega n/\pi^2 m. \qquad (10.d.44)$$

We have $\Omega_0'(I)=\pi^2/Md^2$, and thus we have

$$(\Delta I)_n^m=(2d/\pi)|2MV_n^m(\lambda)|^{1/2}=(2d/\pi)(2MV_0\sigma/n\pi)^{1/2}|F(n,m)|^{1/2} \quad (10.d.45)$$

where $F(n,m)$ is given by

$$F(n,m)=\begin{cases}\int_0^1 \sin(n\arcsin\xi)\cos(m\pi\sigma\xi/2)d\xi & \text{if } m,n \text{ are even}\\ \int_0^1 \cos(n\arcsin\xi)\cos(m\pi\sigma\xi/2)d\xi & \text{if } m,n \text{ are odd.}\end{cases} \quad (10.d.46)$$

The Chirikov criterion (for a given value of n) is given by (cf. expression (9.b.14))

$$(\Delta I)_n^m+(\Delta I)_n^{m+2}\geq|I_n^m-I_n^{m+2}|, \quad (10.d.47)$$

which becomes here

$$(2MV_0\sigma/n\pi)^{1/2}[|F(n,m)|^{1/2}+|F(n,m+2)|^{1/2}]\geq Md\omega n/\pi m(m+2). \quad (10.d.48)$$

Now we switch to our dimensionless parameters (see section 9.c), and obtain

$$(\sigma/n\pi)^{1/2}[|F(n,m)|^{1/2}+|F(n,m+2)|^{1/2}]\geq 2\eta A_1 n/N\pi m(m+2) \quad (10.d.49)$$

and

$$\sigma\cong 2\lambda/\eta^2. \quad (10.d.50)$$

From expression (10.d.30) we see, that I is limited to the range

$$I\leq(d/\pi)(2MV_0)^{1/2}. \quad (10.d.51)$$

Using our dimensionless parameters and expression (10.d.44) we obtain thus, for a given n, the requirement

$$m\geq 2\eta A_1 n/N\pi. \quad (10.d.52)$$

The n^{th} harmonic is thus expected to become fully stochastic, when the Chirikov criterion (expression (10.d.49)) is satisfied for the smallest possible value of m for this value of n (expression (10.d.52)).

For a given square well potential (a given value of N) and a given value of η, we can thus check, using expressions (10.d.49) and (10.d.50), for what value of λ the n^{th} harmonic becomes fully stochastic. We have found out, that for all the square wells we have studied, for high frequencies (high values of η); if our numerical experiments yielded the relation $W \propto \lambda^{2\nu}$ (see section 10.c), then the value of λ for which the n^{th} harmonic, with n being the integer closest to ν, becomes fully stochastic, is quite close to the threshold λ_t for the onset of ionisation, as found from the numerical experiments. The results for the 4 level and 12 level wells are summarised in Table 5.

The results of this study show, that the multiphoton-like behaviour, which we have observed in our classical results, is due to the higher order harmonics of the oscillating laser field, through their contribution to the distortion of the square well potential, as seen by the electron in the high frequency range. The similarity between these results and multiphoton transition probabilities probably implies, that multiphoton processes are important in laser induced ionisation, as expected from quantum mechanical ideas. A full quantum mechanical study of this system, however, has not been performed yet.

Table 5

Comparison between λ_n, the value of λ (the laser field strength parameter) for the onset of full stochasticity in the n^{th} harmonic of the oscillating potential, as seen by the electron in the high frequency range; and the threshold value λ_t for the onset of ionisation, as found from the numerical experiments. The results for the N=4 and N=12 level wells are shown here.

N	η	ν	λ_t	n	λ_n
4	1.0	3.7	0.16	4	0.21
	1.5	2.7	0.07	2 / 3	0.07 / 0.26
	2.0	2.4	0.10	2	0.23
	2.5	2.3	0.17	2 / 3	0.06 / 0.43
	3.0	2.0	0.24	2	0.12
12	7.5	2.3	1.5	2 / 3	0.65 / 4.1
	9.5	2.2	2.0	2	1.7
	13.0	1.7	2.4	2	1.5
	19.0	1.7	3.2	2	2.4
	24.0	1.5	4.0	1 / 2	3.4 / 6.2
	30.0	1.2	5.0	1	8.3
	38.0	0.92	7.0	1	6.6

Chapter 11

Prospects for further study of the problem

11.a. The reasons for carrying out the classical study and the difficulties in carrying out the quantum mechanical study of the problem

The study of the square well potential in the oscillating laser field, that we have carried out in this work, was purely classical. Strictly speaking, a quantum mechanical treatment, based upon the solution of the time dependent Schrödinger equation, should be carried out here. However, on one hand, there are justifications for carrying out the classical calculation, and on the other hand, the quantum caculation is very difficult to perform, as we shall see below.

As a general rule, the more quantum energy levels we have in the well, and the closer together they are, the more reliable a classical treatment of the problem will be. We can obtain a kind of rough estimate for the validity of the classical treatment, by comparing the quantum energy levels with the semiclassical ones, obtained by using the Sommerfeld quantisation rule

$$(1/\pi)\int_{x_1}^{x_2}\{2M[E_n-V(x)]\}^{1/2}dx=n\hbar, \qquad (11.a.1)$$

where x_1 and x_2 are the values of x which satisfy $V(x_1)=V(x_2)=E_n$.

In our case V(x) is given by expression (7.d.2), $x_1=0$, and $x_2=d$, and thus we obtain

$$E_n=n^2\pi^2\hbar^2/2Md^2 \; ; \; n=1,2,\ldots,N, \qquad (11.a.2)$$

where N is the same as for the quantum case (defined by expres-

sion (7.d.10)). The value of N is determined by the width and depth of the well.

We can now compare the quantum levels (expression (7.d.14)) with the semiclassical ones (expression (11.a.2)). The comparison shows that in the case of the 4 level well (N=4) the difference varies between 35% (for the ground level) and 41% (for the top level). In the case of the 8 level well the difference varies only between 17% and 21%, and for the 12 level well it is down to the range between 11% and 14%. We can therefore expect that, with the possible exception of the 4 level case, our classical treatment of this system (with 4, 8, 10, and 12 levels) should be reasonable.

As we have seen in section 8.c, similar classical studies of stochasticity and ionisation have been carried out for other physical systems in the past, with the results showing good agreement with the experimental data. The success of the classical approach in this previous work suggests, that it has a good chance of yielding reasonable results in our case as well.

We now direct our attention to the quantum mechanical study of the problem. The full time dependent Schrödinger equation is given by the expression

$$-(\hbar^2/2M)(\partial^2\psi/\partial x^2)+V(x)\psi+eE_L x\, f(t)\cos(\omega t)\psi=i\hbar(\partial\psi/\partial t), \qquad (11.a.3)$$

where $\psi=\psi(x,t)$ is the time dependent wave function. All the other symbols and notations have the same meaning as in the previous sections. Carrying out the straight numerical solution of this equation turns out to be unpractical due to numerical instability

problems and unfeasible computation times. Such a calculation has been carried out only for the considerably simpler case of a delta-function potential (Geltman 1977). Therefore some kind of an approximate method has to be used instead.

The first approximate method, which we have looked into, is the usual perturbation theory. The ionisation rate for a multi-photon process involving n photons is given, to first approximation, by an expression which is derived from the n^{th} order perturbation theory (Bunkin and Tugov 1973, Gontier et al 1975). The evaluation of this expression in our case can be carried out analytically, and thus does not present a problem for itself. However, perturbation theory turns out to be invalid in our case, as the effect of the oscillating laser potential is much larger than the separation between the unperturbed energy levels near the bottom of the square well. This is especially true in the cases with 8 or more levels in the well, where the classical treatment is expected to be rather reliable, and which were of main interest in our study.

Another approximate method, which we have looked into, is the S-matrix method (Keldysh 1965, Reiss 1971). The S-matrix gives the transition probabilities from initial states to final states, and the transition rate (ionisation rate) can be calculated from it. The S-matrix element $S_{f,i}$ is given by

$$S_{f,i}=\delta_{f,i}-(i/\hbar)\int_{-\infty}^{\infty}\langle\psi_f(x,t)|H'|\phi_i(x,t)\rangle dt, \qquad (11.a.4)$$

where H' is the interaction causing term (perturbation term) in the Hamiltonian ($eE_L x\, f(t)\cos(\omega t)$ in our case), $\phi_i(x,t)$ is the initial state of the unperturbed Hamiltonian, and $\psi_f(x,t)$ is the

final state of the perturbed Hamiltonian. $S_{f,i}$ is the transition probability from the initial state i to the final state f. So far everything is exact. The approximation is introduced in the choice of some approximate expression for $\psi_f(x,t)$, which is usually unknown, as in our case. Making the proper choice of the approximate expression for $\psi_f(x,t)$ is of critical importance here. When we have followed the choice made by Keldysh (using the expression for a free electron in the oscillating electric field), we got a zero ionisation rate, which indicates that this choice is inadequate in our case. Another choice for the approximate $\psi_f(x,t)$ (an expression derived from the final state for the square well potential, when the oscillating electric field is not present) yielded results for the ionisation rate, which were too small to be reasonable. This indicates, that the S-matrix method is not reliable in our case, due to the lack of an adequate approximation for the final state $\psi_f(x,t)$.

As the perturbation term in our case is periodic in time (if the switching function f(t) is omitted), we also looked into the use of the Floquet theorem for dealing with the perturbed Hamiltonian (Shirley 1965). However, the use of this method becomes practical only when the physical system in question can be approximated by a two level system (plus the continuum), i.e. a system with a single quasi-resonant intermediate state. In our case this is generally not the case. In order to deal with the continuum a perturbation theory based treatment needs to be used (Maquet et al 1983, Holt et al 1983), and, as mentioned above, perturbation theory is not valid in our case.

There are other available methods, like the resolvent method (Beers and Armstrong 1975), and rate equation based methods (de Meijere and Eberly 1978, Eberly and ONeil 1979). However, again, these methods are mainly useful for systems which can be reduced to two levels, with a perturbation theory based treatment of the continuum, and thus are not suitable for our case.

In the spirit of the previous work in this field, we suggest an experimental study of the ionisation from square potential wells in semiconductors, driven by a laser field. As the ionisation rate is an experimentally measurable quantity, such a study will be able to check our somewhat unusual classical predictions for it, and especially its multiphoton-like character in the high frequency range. The experimental study is discussed in the following two sections.

11.b. The experimental study of ionisation from a square well potential in an oscillating laser field

As we have seen in section 7.b, present day technology makes it possible to fabricate potential well structures, of desired shape and dimensions, in semiconductors, and square well potentials in particular. Thus the effectively one dimensional square well potentials we have discussed in this work can be fabricated in practice, and made available for experimental study.

The experimental study of the square well potential in an oscillating laser field is of special interest, as it serves as a test for the extent of validity of our classical study of the onset of ionisation and the ionisation rate. As we shall see below, both the threshold value of the laser field strength for the onset of ionisation, and the ionisation rate itself, can be experimentally measured, and compared with the classical predictions.

The tunable laser system, as discussed in section 7.c, can serve as the basic system for the experimental study. By proper choice of the dimensions of the square well potential, the desired number of levels can be obtained. The frequency of the laser can be varied by using different laser sources, to correspond to the several different values of the frequency parameter η, used in the theoretical study of each square well potential. Finally, the laser intensity can be varied, thus varying the laser field strength, to correspond to the field strength parameter λ in the theoretical study.

The study itself basically consists of the application of a

pulse of the driving laser, and the measurement of the resulting ionisation. The duration of the pulse is chosen so that it corresponds to the duration used in the theoretical study (see section 11.c for further discussion of this point). The intensity is chosen as outlined above.

The presence of ionisation can be experimentally detected in two ways. The first method is based upon the measurement of the intensity of the tunable laser output. The lasing of the tunable laser itself, as we have seen in section 7.c, occurs due to the recombination of electrons in the square well with holes in the valence band. When ionisation occurs, the number of electrons, which are left in the potential well, and are thus available for recombination, decreases according to the extent of the ionisation, and this results in a corresponding decrease in the intensity of the tunable laser beam, which can be measured.

The second method is based upon the measurement of the electric conductivity of the conduction band. When ionisation occurs, electrons leave the square well and move into the conduction band. Their number varies according to the extent of the ionisation. This increase in the number of electrons in the conduction band, results in a corresponding increase in the electrical conductivity of the latter, which is the quantity that is experimentally measured in this case.

Using this experimental system, and either one of the two measurement methods, the experimental study can now be carried out. By varying the driving laser intensity, and looking for the decrease in the tunable laser beam intensity, or the increase in the electric conductivity of the conduction band, the threshold

value for the onset of ionisation can be found.

By increasing the driving laser intensity beyond the threshold value and carrying out a quantitative measurement of the tunable laser intensity, or the conduction band's electric conductivity, an experimental value for the ionisation rate can be obtained. This can be carried out for several values of the driving laser intensity, and thus the scaling of the ionisation rate with the driving laser intensity can be experimentally obtained, and compared with the results of the theoretical study.

11.c. Suggested experimental system for the performance of the study

As we have seen in the previous section, the ionisation of electrons from a square well potential in an oscillating laser field can be experimentally studied. Here we suggest a possible system for the conduction of such a study. The system is the combination of GaAs and $Al_xGa_{1-x}As$ in multilayer Heterojunctions (Dingle et al 1978; see section 7.b for further explanations).

The square well potential is fabricated by having a layer of GaAs between two layers of $Al_xGa_{1-x}As$. By varying the concentration x of the Al, the depth of the square well can be controlled. The width of the square well is equal to the thickness of the GaAs layer, and thus it can be controlled as well. This way square well potentials can be fabricated with a width d between 100Å and 800Å, and a depth V_0 between 0.20eV and 0.55eV. This corresponds to a range of 2 to 25 quantum levels in the well, as the effective mass of the electrons is equal to $0.07m_e$ in this case.

As an example we discuss here in detail the N=4 level case. A 4 level well is obtained, for example, when d=130Å and V_0=0.505eV. Using expression (9.c.4) we find, that the bouncing frequency in this case is given by $\omega_0=1.66\times10^{14}s^{-1}$

If we use in our system a CO_2 laser, which has a frequency of $\omega=1.78\times10^{14}s^{-1}$, we find that our frequency parameter is $\eta=1.07$ in this case. From table 4 we see, that the value of λ_t (the value of the laser strength parameter for the onset of ionisation) for this frequency should be around 0.14. By using expression (9.c.6)

and the relation

$$I_L=(1/2)\epsilon_0 cE_L^2, \qquad (11.c.1)$$

we find that the above value of λ_t corresponds to a laser intensity of 53MW/cm^2, which is well within the experimentally available range. A pulse duration of 100 periods of the CO_2 laser turns out to be about 3.5ps, which is again experimentally available.

The rise in temperature in the semiconductor crystal due to the laser pulse is given by (Gerck and Miranda 1984)

$$\Delta T=\alpha I_L t_p/\rho C, \qquad (11.c.2)$$

where α is the absorption coefficient, I_L is the laser intensity, t_p is the laser pulse duration, ρ is the density, and C is the specific heat. For GaAs these parameters are given by (Grave 1967, Pankove 1971) $\alpha=9cm^{-1}$ (for a carrier density of $3x10^{17}cm^{-3}$), $\rho=5.32g/cm^3$, and $C=0.35J/g°K$. Thus, in our case, the rise in temperature is only about $10^{-3}°K$, and thus totally negligible.

We see thus, that the laser pulse intensity and duration involved in the experimental study, in this case, are well within the current experimental capabilities. The heating of the sample is negligible, and thus causes no problem here. This is true for the 8, 10, and 12 level wells as well. The example for the 4 level well, discussed here, as well as similar examples of possible experimental parameters for the 8, 10, and 12 level square wells, are summarised on Table 6.

We should note that the dimensions given here for the various

Table 6

List of possible values for the physical parameters for some selected GaAs quantum wells driven by a CO_2 laser (ω=1.78x10^{14} s^{-1}) for possible experimental investigation. The pulse duration for 100 periods of the oscillating laser field is 3.5ps.

N	V_0 (eV)	d (Å)	ω_0 (s^{-1})	η for CO_2 laser	λ_t for this η	I_L/λ^2 (GW/cm^2)	$I_L(\lambda_t)$ (MW/cm^2)
4	0.505	130	1.66x10^{14}	1.07	0.14	2.7	53
8	0.47	270	4.15x10^{13}	4.29	0.45	0.045	9.2
10	0.44	350	2.51x10^{13}	7.11	1.3	0.010	17
12	0.40	440	1.60x10^{13}	11.1	2.2	0.0027	13

square wells are only examples, and the same number of levels can also be obtained with other combinations of width and depth within the above mentioned ranges. Using the relation (cf. expression (7.d.10))

$$V_0 = N^2 \pi^2 \hbar^2 / 2Md^2, \qquad (11.c.3)$$

we obtain

$$V_0 d^2 / N^2 = 537 \qquad (11.c.4)$$

where V_0 is given in eV and d in Å.

By varying V_0 and d so that $V_0 d^2$ remains constant, the number of levels in the well (N) is not changed. The bouncing frequency ω_0 changes, however, and thus η changes, even when the driving laser frequncy ω remains the same. Thus η can be varied this way, as an alternative to using different types of lasers. For example, in the 4 level case, η can be varied this way, with the CO_2 laser, between 0.99 and 2.7 - a range similar to the one we have used in the theoretical study.

References

Ambartsumyan R V, Gorokhov Y A, Letokov V S and Makarov G N (1976) Sov. Phys. JETP 42 993.

Arnold V I (1978) "Mathematical Methods of Classical Mechanics", Springer-Verlag, Berlin.

Bayfield J E and Koch P M (1974) Phys. Rev. Lett. 33 258.

Beers B L and Armstrong L (1975) Phys. Rev. A 12 2447.

Belobrov P I, Berman G P, Zaslavskiĭ G M and Slivinskiĭ A P (1979) Sov. Phys. JETP 49 993.

Berry M V (1983) in "Chaotic Behaviour of Deterministic Systems", Iooss G, Helleman R H G and Stora R editors, North-Holland, Amsterdam, pp. 171-271.

Bunkin F V and Tugov I I (1973) Phys. Rev. A 8 601.

Chirikov B V (1979) Phys. Rep. 52 263.

de Meijere J L F and Eberly J H (1978) Phys. Rev. A 17 1416.

Dingle R, Störmer H L, Gossard A C and Wiegmann W (1978) Appl. Phys. Lett. 33 665.

Eberly J H and ONeil S V (1979) Phys. Rev. A 19 1161.

Esaki L and Tsu R (1969) IBM Research Report No RC-2418.

Galvão R M O, Miranda L C M and Mendonça J T (1984) J. Phys. B: Atom. Molec. Phys. 17 L577.

Geltman S (1977) J. Phys. B: Atom. Molec. Phys. 10 831.

Gerck E and Miranda L C M (1984) Appl. Phys. Lett. 44 837.

Gontier Y, Rahman N K and Trahin M (1975) J. Phys. B: Atom. Molec. Phys. 8 L179.

Gradshteyn I S and Ryzhik J M (1980) "Tables of Integrals, Series and Products; Corrected and Enlarged Edition", Academic Press, New York.

Grimes C C, Brown T R, Burns M L and Zipfel C L (1976) Phys. Rev. B 13 140.

Grove A S (1967) "Physics and Technology of Semiconductor Devices", Wiley, New York, p. 102.

Hogg T and Huberman B A (1982) Phys. Rev. Lett. 48 711.

Holonyak N, Kolbas R M, Dupuis R D and Dapkus P D (1980) IEEE J. Quantum Electron. QE16 170.

Holt C R, Raymer M G and Reinhardt W P (1983) Phys. Rev. A 27 2971.

Jensen R V (1982) Phys. Rev. Lett. 49 1365.

Jensen R V (1984) Phys. Rev. A 30 386.

Jones D A and Percival I C (1983) J. Phys. B: Atom. Molec. Phys. 16 2981.

Kasemset D, Hong C S, Patel N B and Dapkus P D (1982) Appl. Phys. Lett. 41 912.

Keldysh L V (1965) Sov. Phys. JETP 20 1307.

Korsch H J and Berry M V (1981) Physica 3D 627.

Lamb W E (1977) in "Laser Spectroscopy III", Hall J L and Carlsten J L editors, Springer-Verlag, Berlin, pp. 116-120.

Leopold J G and Percival I C (1979) J. Phys. B: Atom. Molec. Phys. 12 709.

Ley-Koo E and Cruz S A (1981) J. Chem. Phys. 74 4603.

Maquet A, Chu S I and Reinhardt W P (1983) Phys. Rev. A 27 2946.

Mayer I L, Miranda L C M and Galvão R M O (1985) Can. J. Phys. (to be published).

McGervey J D (1971) "Introduction to Modern Physics", Academic Press, New York, pp. 141-154.

Meerson B I, Oks E A and Sasarov P V (1978) JETP Lett. 29 72.

Narayanamurti V (1984) Physics Today, October issue, pp. 24-32.

Pankove J I (1971) "Optical Processes in Semiconductors", Prentice-Hall, Englewood Cliffs, NJ, p. 75.

Percival I C and Richards D (1982) "Introduction to Dynamics", Cambridge University Press, Cambridge.

Reiss H R (1971) Phys. Rev. D 4 3533.

Richards D (1982) J. de Physique 43 C2-63.

Shirley J H (1965) Phys. Rev. 138 B979.

Shuryak E V (1976) Sov. Phys. JETP 44 1070.

Zaslavsky G M (1981) Phys. Rep. 80 157.

Zimmermann M L, Kash M M and Welch G R (1982) J. de Physique 43 C2-113.

END

12·03·86

FIN